Host Guest Chemistry of a Photoactive Coordination Cage

The University Of Sheffield.

Jerico Richard Piper

A thesis submitted to the University of Sheffield in partial fulfilment of the requirements for the Degree of Doctor of Philosophy

April 2018

Department of Chemistry, University of Sheffield

Author's Declaration

Except where specific reference has been made to other sources, the work within this thesis is the original work of the author. It has not been submitted, in whole or part, for any other degree.

Jerico Richard Piper

April 2018

Chapter Abstracts

Chapter 1 introduces the area of supramolecular chemistry and then how it evolved to include coordination cages. The host-guest functionality of coordination cages is explained, leading to a discussion on the application of coordination cages and other supramolecular structures in photochemistry – dubbed "supramolecular photochemistry". Finally, previous work conducted by the Ward group, that forms the foundation of this thesis, is discussed.

Chapter 2 describes the synthesis of a fluorescent and water soluble $[Cd_8L_{12}]^{16+}$ cubic coordination cage, with a revised synthetic route. The effect of guest encapsulation on the fluorescence of the cage is then explored, both the quenching and enhancement of fluorescence is observed. Transient absorption studies and various photophysical experiments showed that guest molecules were able to undergo host-to-guest photoinduced energy- or electron-transfer following encapsulation.

Chapter 3 explores the ability of $[M_8L_{12}]^{16+}$ cubic coordination cages to bind metal complexes. The encapsulation of a number of metal complexes was confirmed by fluorescence and ^{1}H NMR, it was discovered that metal complexes that were too big to fit in the cage cavity still had a quenching effect on the fluorescence of the $[Cd_8L_{12}]^{16+}$ cage, ascribed to either aggregation or collisional quenching mechanisms.

Chapter 4 explores the idea of using $[Cd_8L_{12}]^{16+}$ cubic cage in a two-step energy transfer to a Eu(III) guest, affording sensitisation of red Eu(III) emission. The synthesis of the "rod like" pyrene based chelate – Eu(III) complex **Py-Che-Eu** is described. Fluorescence and ^{1}H NMR experiments indicated binding of **Py-Che-Eu** within $[Cd_8L_{12}]^{16+}$ and consequential two-step energy-transfer was observed.

Acknowlegdements

Firstly, I would like to thank Mike Ward for allowing me to undertake this project. His continuous support is what has allowed me to get this far and I am truly grateful. I now understand why people say Mike is one of the best supervisors you could ask for.

I would like to name and thank some members of the Ward groups: Will, for whom without I probably wouldn't be writing this thesis in the first place. He was my mentor at the beginning and continued to be an inexhaustible fountain of knowledge when it came to NMR and host-guest chemistry. And then Methers, our shared music tastes has made working in the lab' so much more enjoyable and his help with volume calculations, x-ray crystallography and NMR experiments is greatly appreciated. And a big thanks to Jamie and Beth, my gossip buddies and providers of copious amounts of tea. Also thanks the rest of the group: Ash, AJ, Chris, Dillan, Jenny, Liz, Suad and Zainab for imparting their knowledge upon me and making life generally enjoyable. Thanks to the Brammer, Conte and Foster groups for sharing an office and providing the banter.

Thanks to the MChem students that I looked after (Jonny and Holly) and also those I didn't. Hopefully I wasn't too bad at providing help… Oh, and Laura I've known you seen you were a fresh faced chemical engineer; I converted you to chemistry, but never expected you to do your masters in the Ward group!

Thanks to the staff of the University of Sheffield chemistry department, without your help none of us would be able to do anything. Thanks to Igor at the Central Laser Facility.

Also to everyone in the University of Sheffield Singers' Society thank you for providing a much needed respite for the last 6 years. I've made some fantastic friends, especially Rachel and Lucy may we have many more wine and lasagne evenings! Thanks to the Computer Gaming Society for letting me be the geek I know I am in public! Thank you to Kat and Maria, you may be biologists but you're still pretty cool. And thanks to all my past housemates, I blame you guys for my drinking habits.

Finally I'd like to thank my family for 26 years of unwavering support; I might repay you at some point. We'll see…

List of Publications

1) C. G. P. Taylor, **J. R. Piper** and M. D. Ward, "*Binding of chemical warfare agent simulants as guests in a coordination cage: contributions to binding and a fluorescence-based response*" , *Chem. Commun.*, 2016, **52**, 6225-6228

2) **J. R. Piper**, L. Cletheroe, C. G.P. Taylor, A. J. Metherell, J. A. Weinstein, I. V. Sazanovich and M. D. Ward, "*Photoinduced energy- and electron-transfer from a photoactive coordination cage to bound guests*", *Chem. Commun.*, 2017, **53**, 408-411

Table of Contents

Abbreviations

acac	acetyl acetone
AIBN	azobisisobutyronitrile
a.u.	arbitrary units
nBuLi	n-butyl lithium
COSY	correlation spectroscopy
DMF	N,N'-dimethylformamide
DEEP	diethyl ethylphospinate
DEMP	diethyl methylphospinate
DIMP	diisopropyl methylphospinate
DMMP	dimethyl methylphospinate
DMSO	dimethyl sulphoxide
EI-MS	electron ionisation mass spectrometry
ES-MS	electrospray mass spectrometry
EtOH	ethanol
fac	facial
FI	Fluorescence Intensity
G	guest
H	host
K	binding constant
L	ligand
$Lw^{1,5\text{-naph}}$	hydroxymethyl pendant
M	metal
M	molarity (mol dm^{-3})
m-	meta
mCPBA	*meta*-chloroperoxybenzoic acid

MeCN	acetonitrile
MeOH	methanol
mer	meridional
MeCN	acetonitrile
MLCT	metal-to-ligand charge transfer
naph	naphthalene
NBS	N-bromosuccinimide
NMR	nuclear magnetic resonance
o-	ortho
OD	Optical Density
PEnT	Photoinduced energy-transfer
PET	Photoinduced electron-tranfer
ph	Phenyl
PyPz	pyridine pyrazole
TA	transient absorption
TBAF	tetrabutylammonium fluoride
TBDMS	*tert*-butyldimethylsilyl
TFA	trifluoroacetic acid
THF	tetrahydrofuran
TMSA	tetramethylsilylacetylene
TMV	Tobacco Mosaic Virus
Tp	tris(pyrazolyl)borate
UV	ultraviolet
ε	molar extinction coefficient
τ	lifetime
λ	wavelength

Chapter 1

Introduction

1.1 Self-Assembly

The field of chemistry that focuses primarily on non-covalent interactions between molecules and structures is called supramolecular chemistry, described as the "chemistry beyond the molecule".[1] As is well known by most chemists, molecules are held together by covalent interactions; structures in supramolecular chemistry however, are held together by relatively weak and reversible forces.[2] The process by which these supramolecules are formed is known as self-assembly, which is the spontaneous and reversible interaction of smaller components to form a larger, higher-ordered system. The intermolecular forces used in self-assembly include electrostatic interactions, hydrogen bonding, dispersion forces, π-π stacking interactions and hydrophobic effects,[3–5] as well as ligand coordination to metal ions provided the interaction is labile.

1.2 Self-Assembly in Nature

Examples of self-assembly are abundant in nature, and as is case for so many aspects of chemistry, nature has perfected the art. The archetypal example of self-assembly within nature is the tobacco mosaic virus (TMV).[6] Comprising a single RNA strand and 2130protein subunits, the virus spontaneously self-assembles from its constituent parts when subjected to physiological conditions (Fig. 1.2.1). The TMV virus shows *in vitro* self-assembly; changing external factors, for example temperature and pH, leads to the dissociation of the TMV into its constituent parts. Upon restoring the original conditions the TMV spontaneously reassembles into the fully functional virus, with no loss of capability.[7]

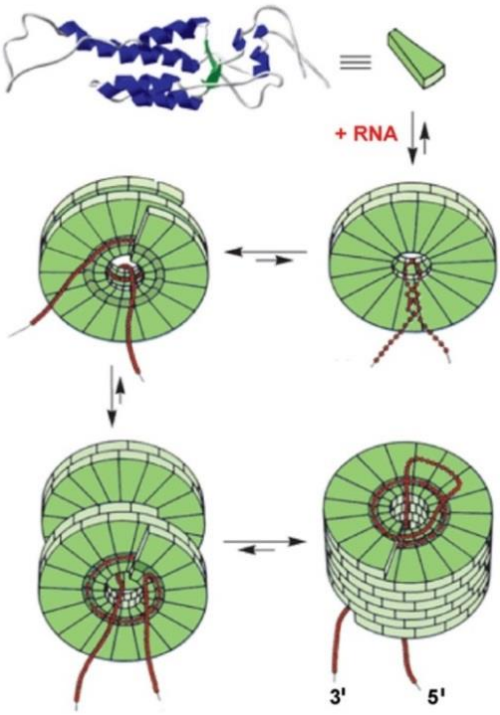

Figure 1.2.1 - Self-assembly of the tobacco mosaic virus, reproduced from Ref. 7.

1.3 Supramolecular Chemistry

1.3.1 Origins of Supramolecular Chemistry

The roots of synthetic supramolecular chemistry are grounded in serendipity; Pedersen's macrocyclic ethers were formed due to an impurity found in a reaction mixture.[8] These cyclic 'crown' ethers were found to bind alkali metal ions within a binding site or cavity. This is significant as the metal ion templated formation of the macrocycle, preorganisation of the organic substrate lowers the entropic cost of reaction. It was also noted that the metal salts were soluble in organic solvents such as benzene and as such the ions were poorly solvated which enhanced the reactivity of the anion.[9]

As we move forward in time, supramolecular chemistry as a field begins to blossom. More complex systems began to emerge. Examples include Sauvage's knots and interlinked rings,[10] Stoddart's catenanes,[11] and Lehn's cryptands.[12] The 1987 Nobel Prize for Chemistry was to Lehn, Pedersen and Cram for their pioneering work in this field.

From the 1980s Lehn's work was directed towards the self-assembly of helicates and grids. His worked showed that taking different oligobipyridine type ligands and combining them

with 4-coordinate Cu(I) or 6-coordinate Ni(II) ions allowed for the selective formation of double or triple helicates (Fig. 1.3.1).13

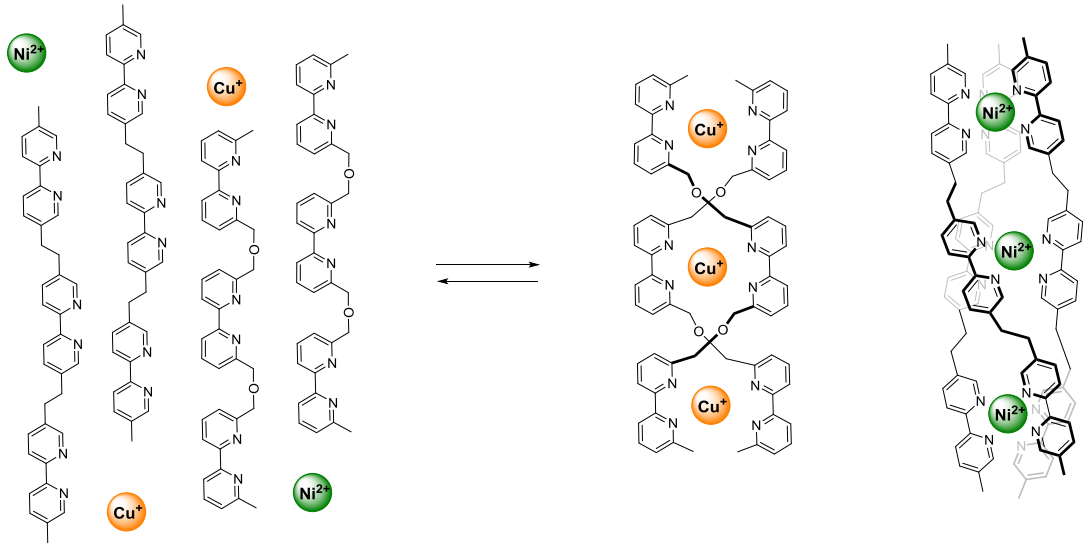

Figure 1.3.1 - Parallel formation of a double helicate and a triple helicate by self-selection.[13]

1.3.2 Two-dimensional Supramolecular Structures

Stang and co-workers realised the idea of using well known coordination chemistry to perform rational design of symmetrical shapes from metal ions and rigid linking ligands.[14] This work used the predictable coordination geometries of metal ions and rigid bridging ligands to create 2D polygons and eventually 3D Platonic and Archimedean solids (Fig. 1.3.2). This work is a prime example of how the utilization and combination of different ligand bond angles and specific metal ion coordination geometries can create a myriad of different structures.[15]

Fujita and co-workers used a square planar $\{Pd(en)\}^{2+}$ ion in combination with linear 4,4'-bipyrdine ligands to form a 2D square (Fig. 1.3.3). The Pd(II) ions lie at the vertices of the square allowing for the creation of 90^{o} corners, with the bipyridine units bridging the ions to complete the square. The ethylenediamine ligands are tightly bound due to formation of 5-membered chelate rings, ensuring that the remaining Pd(II) coordination sites are both kinetically labile towards the bipyrdine and that they are 90^{o} from each other.16 It was shown that replacing the Pd(II) ions with Pt(II) did not readily afford the square at room temperature but instead required heating to 100 ^{o}C, the difference in lability of the metals

ions meant that the Pt(II) based square was much more stable than the Pd(II) based square at room temperature.[17]

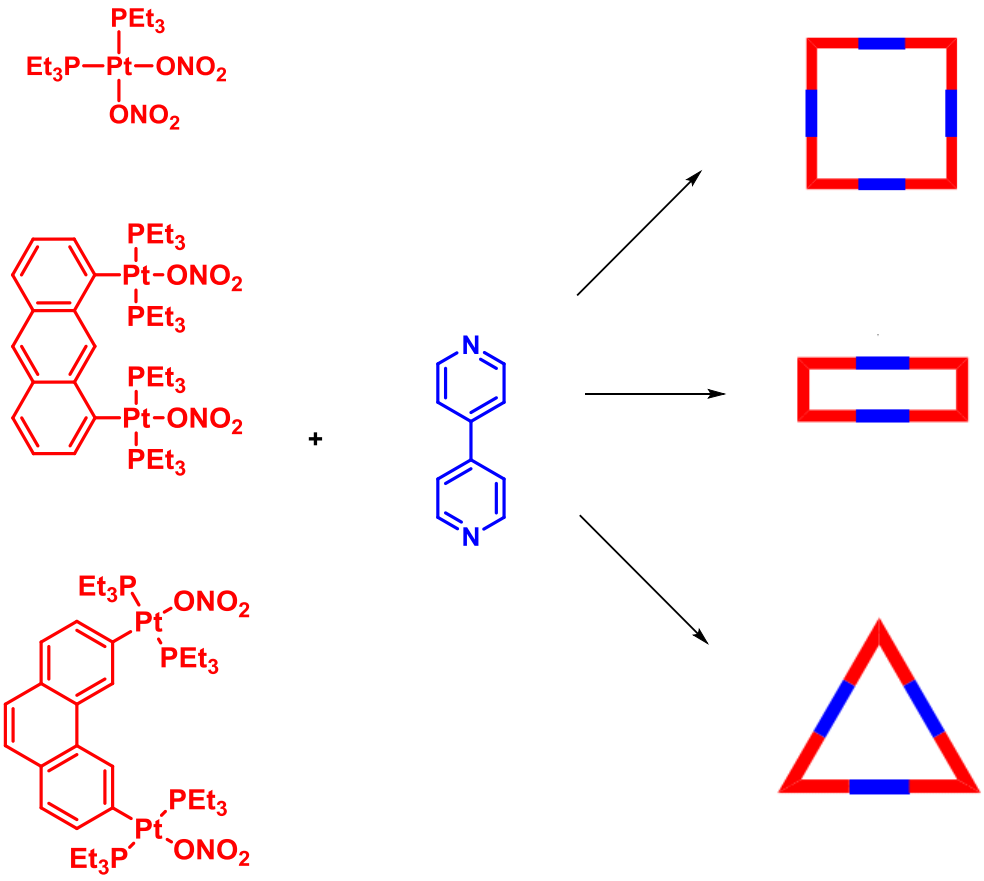

Figure 1.3.2 - Examples of Stang's work on 2D polygons by predesign.

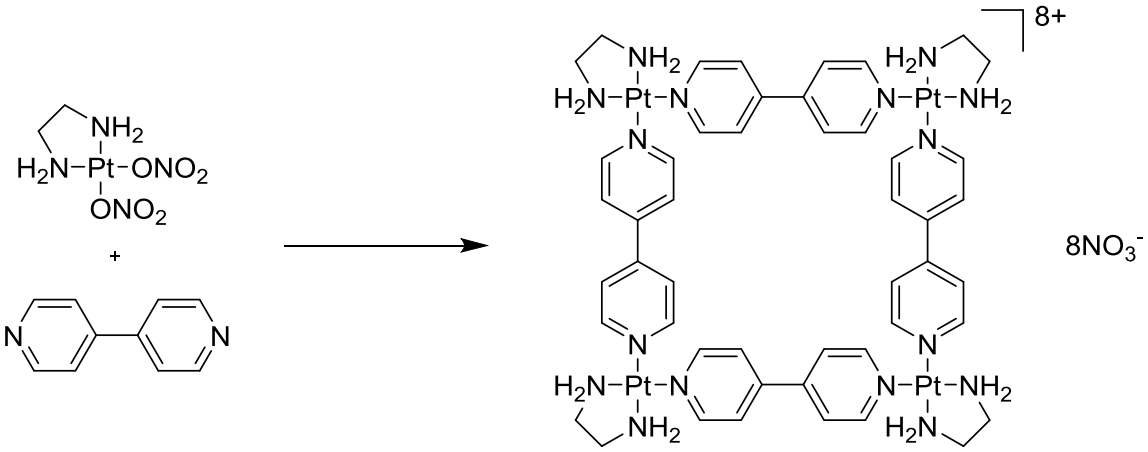

Figure 1.3.3 - Fujita's coordination square.[16]

1.3.3 Three-dimensional Supramolecular Structures: Coordination Cages

The logical progression from two-dimensional structures would be to exploit the interactions between metal ions and organic ligands to form three-dimensional structures, these are known as 'coordination cages'. Some of the initial examples were relatively simple tetrahedral assemblies; four metal ions and six bridging ligands were arranged with the metal ions at each of the vertices and the ligands forming the six edges – such as those from Saalfrank and co-workers (Fig. 1.3.4).[18,19] More recent examples show the ability to rationally design structures by the manipulation of the component parts' properties; Fujita showed that his Pd_nL_{2n} based 'nanospheres' varied in size by changing the curvature of the bis-pyridyl bridging ligands – these have ranged in sizes from Pd_6L_{12} to an impressive $Pd_{60}L_{120}$.[20–22]

These cages provide an interesting synthetic challenge, as with careful control over the choice of metal ion used and the ligand structure, highly complex and aesthetically pleasing structures can be created from a mixture of simple component parts. For example the $Pd_{24}L_{48}$ nanospheres contain 70 components of two different types which self-assemble into a distinct structure with no other species present.[21]

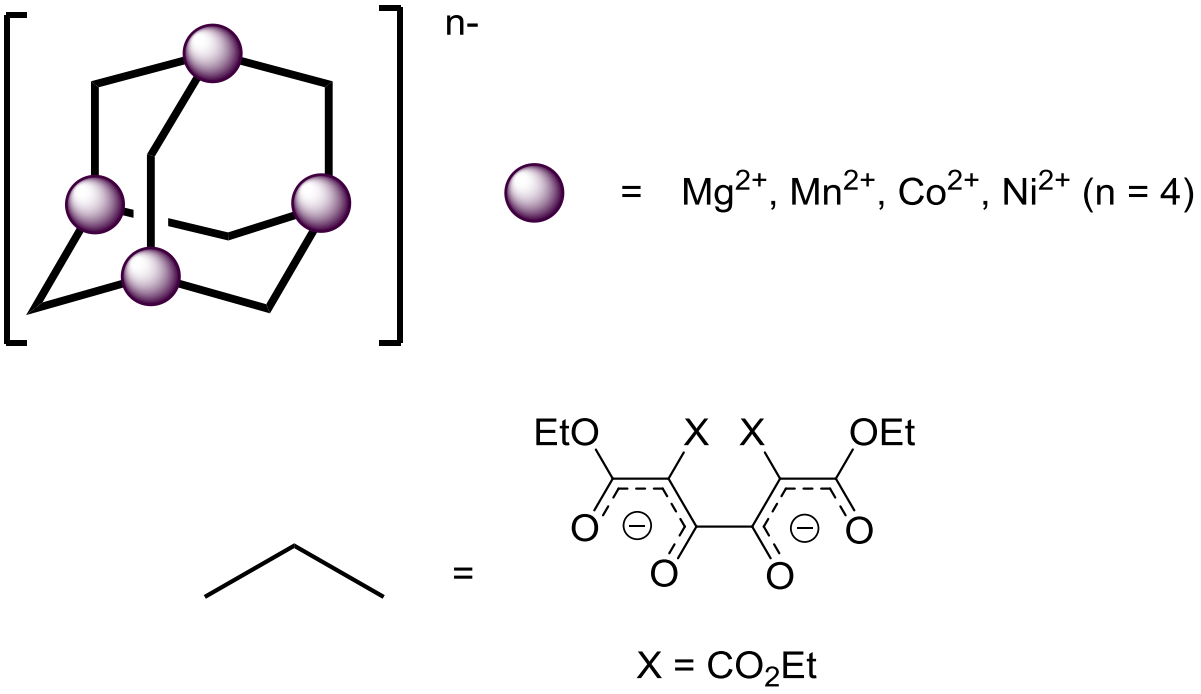

Figure 1.3.4 - Saalfrank's M_4L_6 adamantanoid cage.

Probably the most enticing aspect of coordination cages is the fact many of them contain a central cavity, which often are large enough to encapsulate guest molecules. Encapsulation of guests can provides a unique environment for the molecule, separate from that of the bulk solvent. As such applications of these cages in host-guest chemistry has become a huge driving force in their research. A famous example from Nitschke and co-workers is an anionic Fe_4L_6 cage - in the presence of Fe(II), 4,4'-diaminobiphenyl-2,2'-disulfonic acid and 2-formylpyridine condense to form a water soluble tetrahedral cage (Fig. 1.3.5).[23] This cage is able to uptake the pyrophoric P_4 molecule in aqueous solution and as a result stabilizes it from air, then when a competing guest such as benzene is introduced the P_4 is displaced from the cavity and oxidized to phosphoric acid.[24] The cage is also able to encapsulate SF_6, a greenhouse gas, which under specific conditions can be released.[25]

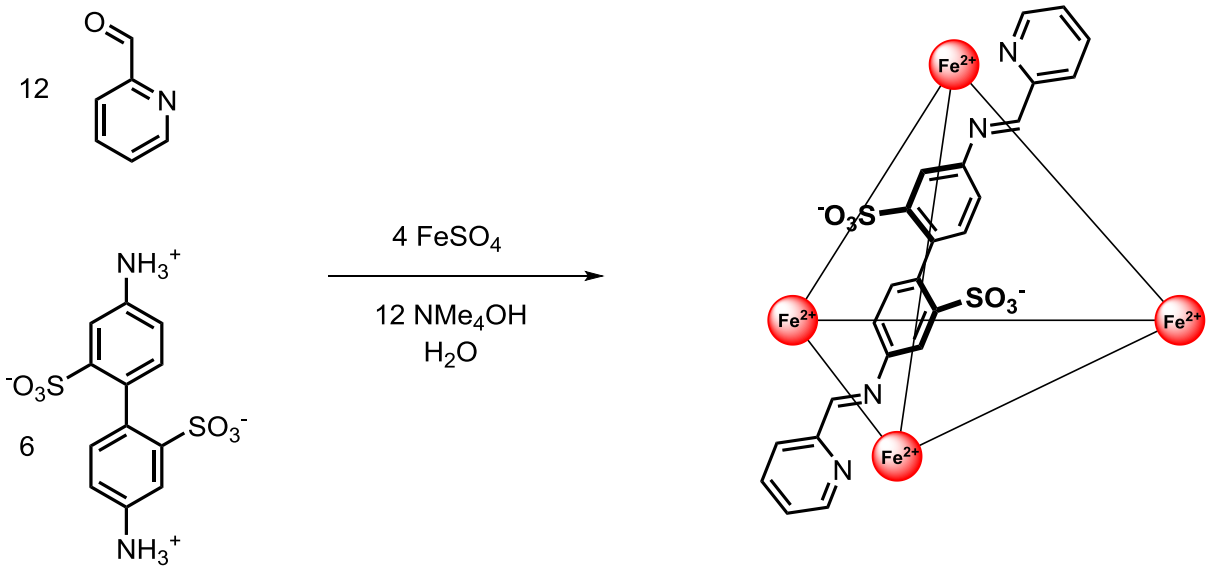

Figure 1.3.5 - Subcomponent self-assembly of a Fe_4L_6 tetrahedral cage.[23]

1.4 Supramolecular Photochemistry

A recent area focus of substantial interest is the development of coordination cages which are in some way photophysically active – in which the ligand and/or the metal exhibits luminescence. Drawing on ideas from other areas of chemistry immediately suggests opportunities for applying such systems to the sensing and photocatalysis of guest molecules bound in the cavity. The structures of self-assembled coordination cages provide an environment in which a large number of photoactive centres surround an encapsulated guest. The high local concentration of these photoactive centres may unlock potential interactions with excited state species unavailable to other systems.

1.4.1 Ligand based Cage Luminescence

Luminescence in cages can arise due to the incorporation of emissive organic fluorophores into the ligand structures. Stang, Huang and co-workers have combined a tetraphenyl-ethylene fluorophore with pyridyl moieties (L1) to form a prismatic cage with Pt(II) ions at the vertices. Two Pt_4(Ligand) panels are held together by dicarboxylate 'pillars'. Tetraphenyl ethylene moieties show aggregation-induced augmentation of luminescence due to conformational change. The rigidity the cage structure imposes restrictions on conformational change, allowing luminescence at low concentration. When allowed to aggregate at higher concentrations the cage shows a concentration controlled tunability of emission across the visible region as well as white light emission in tetrahydrofuran.[26]

Recently Pt(II)-tetraphenylethylene-based organometallic ligands (L3) have combined with the previously used pyridyl-pendant tetraphenylethylene ligands (L1, L2); these result in either a metallacycle or a "drum-shaped" metallacage (Fig. 1.4.1). In dilute solution weak emission is observed from the metallacycle, whereas the cage exhibits strong emission, likely due to the rigidity imposed by the formation of the cage. Both structures, at higher concentrations, display aggregation-induced enhanced emission - typical of structures incorporating tetraphenylethylene moieties. A counterion effect was also observed, stronger emission was seen as anion was changed: PF_6^- > OTf^- > NO_3^-.[27]

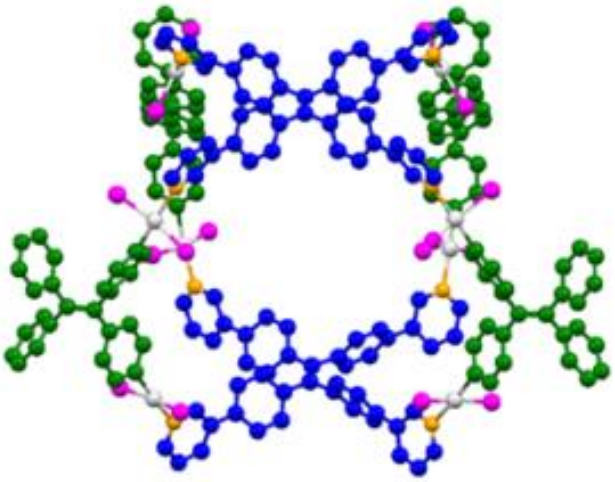

Figure 1.4.1 - Simulated molecular model of Stang's Pt(II) based drum-shaped metallacage. Reproduced with permission from reference 27, copyright 2016 American Chemical Society.

M_4L_6 tetrahedral cages reported by Würthner and co-workers are based on ligands which incorporate perylene-(bis)imide spacers between two chelating bispyridine units. (L 4) These ligands span the edges of the cage, producing edges roughly 4 nm in length.[28,29] The properties of the perylene-(bis)imide units are unaffected by formation of the cage, therefore show the characteristic electrochemical and spectroscopic behaviour typical of such units. When the cage is formed using Fe(II) the perylene emission is quenched.[28] However using Zn(II) instead restored the perylene emission which may now be partially quenched upon binding of coronene and perylene within the cavity in MeCN, affording a luminescent sensor for these guest molecules.[29]

Nitschke and co-workers reported tetrahedral cages consisting of 'bodipy' fluorophore containing ligands in a M_4L_6 structure (L5); red fluorescence is observed from these cages which can be modulated by the binding of anions or amino acids within the cavity, resulting in a fluorescent sensor for these guests.[30] Additionally it was shown that the ligands could be altered to include a pyrene fluorophore at each terminus, this results in 12 pyrene units in the cage structure with green emission at ligand ends and red emission from the 6 bodipy centres. When the blue-emitting perylene was introduced as a guest, white light was produced from the combination of the three fluorophores.[30]

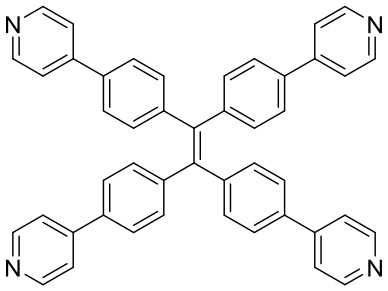

L1

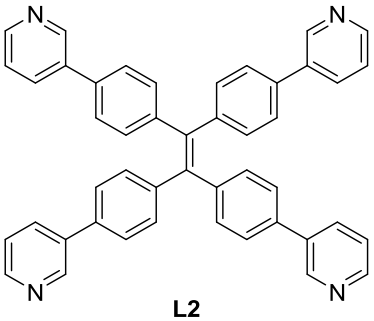

L2

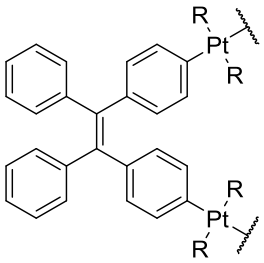

L3 (R = PEt_3)

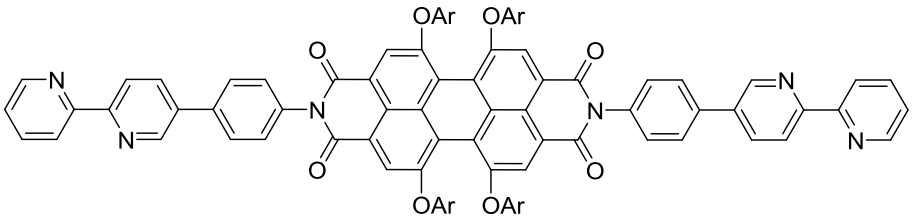

L4

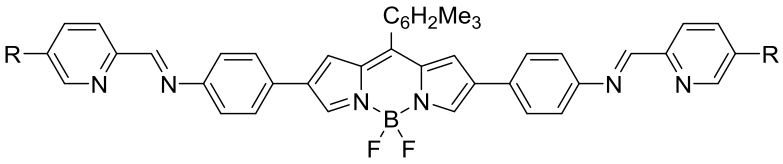

L5 (R = H / Ph)

Cages utilizing bent, 'banana-shaped' bis-pyridine ditopic ligands have been reported by a number of groups:[31] incorporation of suitable moieties into the ligands results in fluorescence from these cage structures. For example, Hooley and co-workers reported a Pd_2L_4 cage where inclusion of amine moieties (which point into the central cavity) into the ligand affords strong fluorescence.[32] Yoshizawa and co-workers reported a series of cages based on bis-pyridine ligands, such as Fig 1.4.2, where two anthracene groups have been employed.[33–37] The resulting eight anthracene groups surround a large, roughly spherical cavity, *ca.* 1 nm in diameter, which can accommodate a variety of organic guests which are protected from the external bulk environment by the anthracene groups. When the metal ion is Pd(II), emission from the cage is not seen but the anthracene groups still perform a structural role by allowing the binding of aromatic guest molecules.[33,34] However, when the metal ion is non-quenching [i.e. Zn(II)] the cage exhibits strong, anthracene-like,

fluorescence with quantum yields of up to 0.8.[35] Varying the metal ion gave varying results; Mn(II) and Ni(II) both yielded cages that presented weak luminescence. Cu(II) however, displays strong solvent-dependent luminescence, with quantum yields varying from 0.76 in DMSO to 0 in MeCN. This is due to the varying extent to which solvent molecules coordinate to the axial sites of the Cu(II) ions.[36]

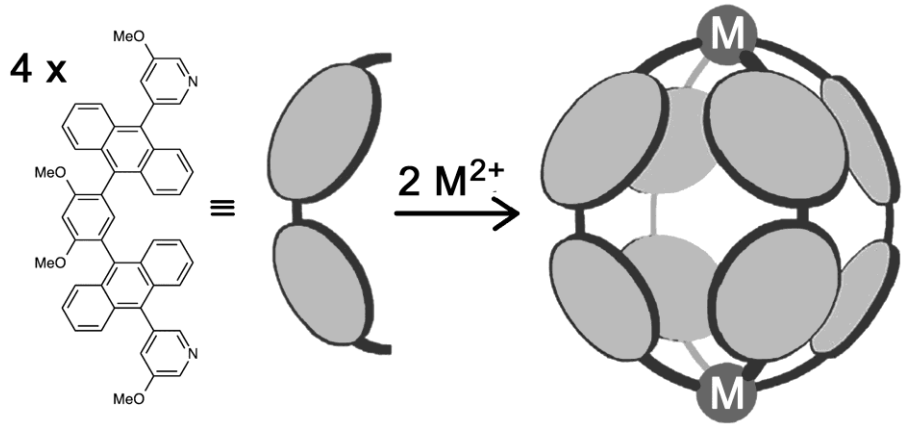

Figure 1.4.2 - M2L4 complexes based on M^{2+} ions with square planar geometry with bent anthracene containing ligands. Reproduced, with permission, from reference 35.

Duan and co-workers have reported M_6L_4 luminescent cages that incorporate quinoline groups that are pendant from a N,N,O-chelating moiety (L6).[38,39] The amide groups facilitate the strong binding of glucosamine[38] and cytidine[39] in organic solvents *via* hydrogen-bonding interactions. As seen before, use of the non-quenching Zn(II) ions allows for strong quinoline fluorescence, which is further enhanced by the binding of guest molecules.[38,39] Four quinoline units connected via amide spacers to an aromatic centre affords a Pd_3L_3 macrocyclic assembly whose cavity exhibits selectivity for uridine over other nucleosides, with enhancement of luminescence upon binding. Three quinoline units act as monodentate N-donor termini, opposed to tridentate chelating termini, linked to a central aromatic unit via amide groups to afford a triangular ligand (L7). When combined with Pd(II) ions, this affords the luminescent Pd_6L_8 truncated octahedral cage. The amide groups again allow for the binding of RNA nucleosides in the cavity by hydrogen-bonding, with uridine showing the strongest binding affinity.[40]

Coincidently the same luminescent Pd_6L_8 cage has been reported, both with amides and also using ester linkers, showing applications in C-C coupling catalysis.[41]

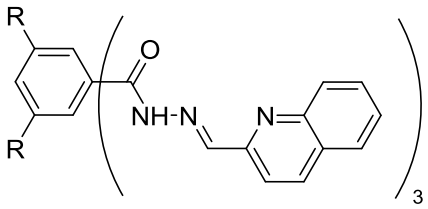

L6

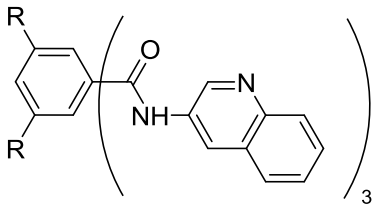

L7

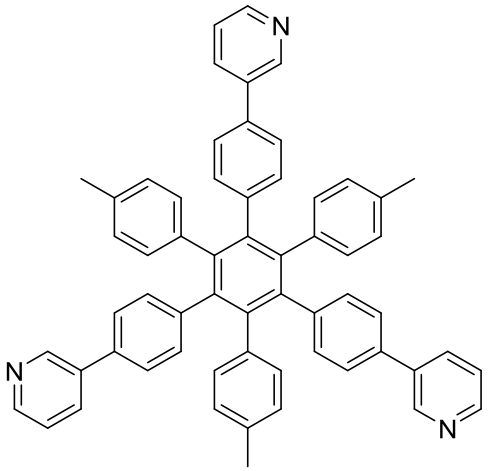

L8

Mukherkee *et. al.* have reported use of the fluorescent ligands in Pt(II)-based cages for the sensing the uptake of electron-deficient nitroaromatic guests, which has application in the detection of vapours from certain types of explosives.[42–45] The cages are synthesised from Pt-alkyne units and multi-topic, bis-/tris-pyridine ligands. The cavity of these cages can accommodate planar, electron-deficient aromatic guest molecules; charge-transfer complexes are formed between the electron rich walls of the cavity and the electron-deficient guest molecule. These charge-transfer complexes with nitro-aromatics such as TNT cause fluorescence quenching of the cage emission both in solution and as a thin film.[42,43]

An example of switching between fluorescent and non-fluorescent cage structures in solution was reported by Shionoya and co-workers. The two cages are built upon on the same metal ion and ligand scaffold only in different proportions. Tris-pyridyl tritopic ligand L8 forms a Hg_6L_8 capsule with ligands over each face of the Hg_6 octahedron with each Hg(II)

ion being 4-coordinate; ligand-based fluorescence is observed at 360 nm. However upon doubling of the metal to ligand ratio, a more open Hg_6L_4 cage forms where only alternate faces of the octahedron are capped and each Hg(II) ion is 2-coordinate; this cage does not show any fluorescence. This structural change can be triggered by adding additional Hg(II) ions to the Hg_6L_8 cage in solution to generating two equivalents of the Hg_6L_4 cage. Removing half of the Hg(II) ions using a cryptand ligand to regenerates the Hg_6L_8 cage.[46]

1.4.2 Luminescent cages: second- or third-row transition metals

To achieve photoactive cages, one can take advantage of either metal complexes within the cage structure, *i.e.* at the vertices, or organic bridging units which connect the metal complex vertices. When considering luminescent metal complexes and then looking at the literature it is obvious that of the d-block metals, it is the second and third row metal ions [Ru(II), Ir(III), Pt(II), Re(I), Os(II)] (those with low-spin d^6/d^8 electron configurations) that can be most easily identified with strong luminescence. Such metal centres however show kinetic inertness that does not match particularly well the requirements of self-assembly under mild conditions. The heavier metal ions often require harsher conditions to prepare them.

In spite of this, Lusby and co-workers reported preparation of an octahedral coordination cage in which six $\{Ir(ppy)_2\}^+$ moieties (ppy = N,C – cyclometalating anion of 2-phenylpyridine) at each vertex of the cage – connected by four 1,3,5,-tricyanobenzene ligands (Fig. 1.4.3).[47] The phosphorescence shown by the cage is characteristic of that shown by $[Ir(ppy)_2X_2]^+$ units ($\lambda_{em} \approx 570$ nm, $\phi = 0.04$). The cavity plays hosts to four triflate anions which, when exchanged for other anions, alter the luminescence intensity.

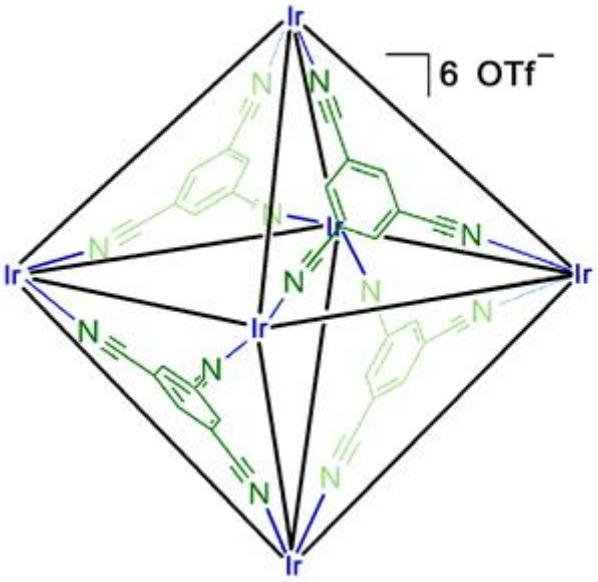

Figure 1.4.3 - Octahedral coordination cage based on six Ir(III)/phenylpyridine vertices capped with four 1,3,5-tricyanobenzene ligands. Reproduced with permission from reference 47, copyright 2012 American Chemical Society.

A method used to circumvent problems with synthesising cages based on inert metal centres such as Ru(II) and Os(II), was to take a stepwise approach. By employing typical preparation methods it is possible to produce a mononuclear complex of an inert metal, with a pendant vacant binding site. This can then be combined with a second more kinetically labile metal (which bind to the pendant sites) to complete the assembly of the cage structure.

Beves and co-workers have prepared such a structure based on the $[Ru(terpy)_2]^{2+}$ complex: four pendant bipy units coordinate Pd(II) ions to afford cages where three or four Ru(II) complex units combine with six or eight $[Pd(dppp)]^{2+}$ units (Fig. 1.4.4). The characteristic luminescence of $[Ru(terpy)_2]^{2+}$ persists though assembly of the cage.[48]

Similarly, a Ru(II) complex with three pendant pyridyl groups as a complexing ligand has been reported by Pan, Su and co-workers; combination with square planar Pd(II) ions affords a $Pd_6(RuL_3)_8$ octahedral cage, where each triangular face is capped by a $[RuL_3]^{2+}$ unit. [49] The cage cavity has volume of >5000 $Å^3$ and can encapsulate a variety of aromatic guest molecules. Photosensitive guests are shielded from UV degradation due to the high

absorptivity of the cage – encapsulated guests undergo photo-degradation at a slower rate than ones in free solution.

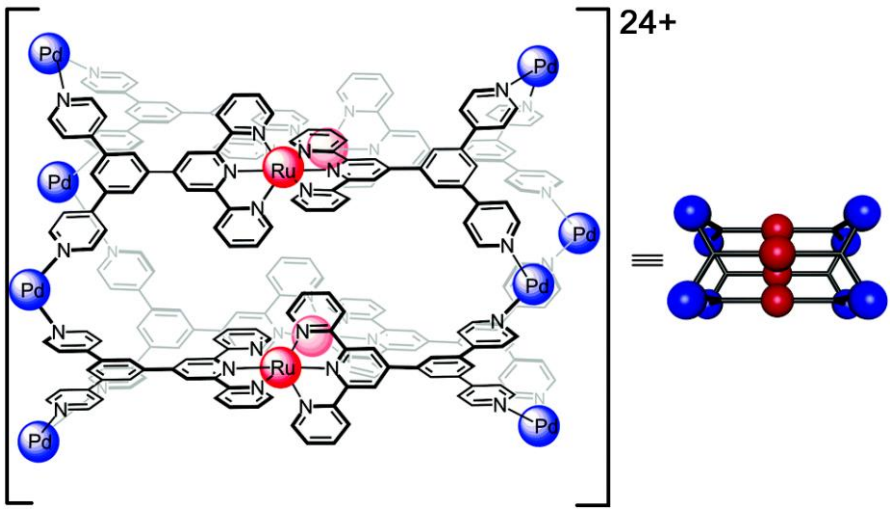

Figure 1.4.4 – A coordination cage containing four $[Ru(terpy)_2]^{2+}$ units connected by eight cis-protected Pd(II) units. Reproduced with permission from ref. 48.

Unlike the previous examples, Kühn and co-workers have reported a Pd_2L_4 cage where L has been exo-functionalised – i.e. the substituents are not part of the main cage scaffold - to incorporate $[Ru(terpy)_2]^{2+}$ or $[Ru(bipy)_3]^{2+}$ complexes (L9, L10). There is no emission observed from the $[Ru(terpy)_2]^{2+}$ based cage, however addition of an alkyl bridge to separate the Ru(II) unit from the Pd(II) coordinating bis-pyridyl moiety affords an emission in region that is typically observed for $[Ru(bipy)_3]^{2+}$, showing enhanced emission at 640 nm with a quantum yield of 0.66.[50]

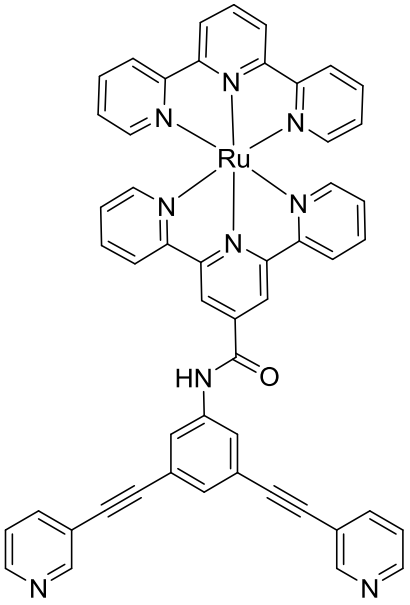

L9

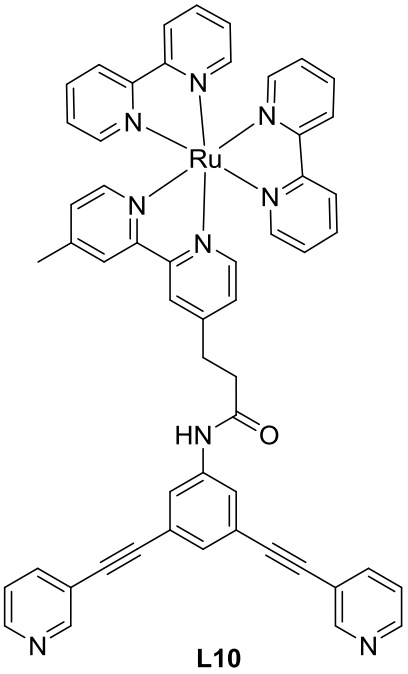

L10

Ward and co-workers have prepared $[OsL_3]^{2+}$ complexes in which the ligand based on two pyrazolyl-pyridine termini. The $[OsL_3]^{2+}$ complex has three vacant bidentate binding sites: combining these with labile Co(II) or Cd(II) ions affords a $Os_4M_4L_{12}$ cubic cages. The metal ions compose the vertices with each ligand bridging one Os(II) ion and one M(II) ion which alternate around the vertex positions.[51] An interesting point to note is that the $[Os(L2)_3]^{2+}$ mononuclear complex component is conveniently synthesised as a statistical 3:1 mixture of *mer* and *fac* isomers, the prerequisite ratio that is also coincidentally required for total assembly of the cage (Fig. 1.4.5). The Os(II) units display long-lived – up to hundreds of nano seconds – red ^{3}MLCT luminescence, and the excited state exhibits good photo-electron donor properties (superior to that of $[Ru(bipy)_3]^{2+}$). This offers potential for photoinduced electron-transfer from the array of Os(II) chromophores to a bound guest within the cage's cavity.

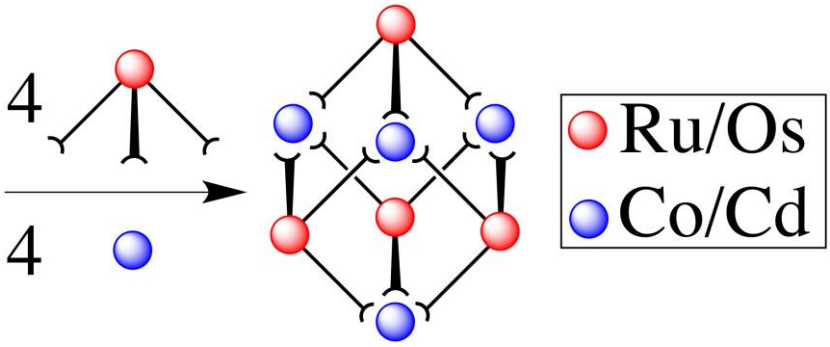

Figure 1.4.5 - Heteronuclear cubic coordination cages containing kinetically inert [Ru(II) or Os(II)]and kinetically labile [Co(II) or Cd(II)] ions at alternating sites. Reproduced with permission from ref. 51.

1.4.3 Luminescent cages based on lanthanide ions

Metal ions from the lanthanide (Ln) series combine high lability (single step assembly of cages is possible) with highly luminescent properties. The majority of the luminescent cage structures formed are Ln_4L_4 tetrahedra – metal ions lie at each of the vertices, and triply-bridging ligands cover each triangular face coordinating to three metal ions. Hamacek and co-workers have synthesised a series of these Ln_4L_4 tetrahedral cages using tripodal ligands (L11, 12) utilising tridentate dicarbonyl-pyridine O,N,O-chelating arms (Fig. 1.4.6); coordination of three of these to each metal ion means that each Ln(III) ion is nine-coordinate.[52–54] A number of these cages lack a central cavity for the encapsulation of guests;[52] others however have cavities with the capacity to play host to a variety of anions.[54,55] Utilising Eu(III) or Tb(III) to assemble the cages results in a strong red or green luminescence respectively, which is characteristic of these cations.[52–54]

Similar chiral O,N,O-chelating units afford Ln_4L_4 tetrahedra with face-capping ligands, but the inherent chirality about the metal centres induced by the chirality of the ligands means that a single diastereoisomer is formed. When L13 is used as a racemic mixture, the two enantiomers of the ligand afford Ln_4L_4 tetrahedral cages in which the ligands have undergone a homochiral self-sorting during the assembly of the cage. A chiral bridging ligand (L14) affords an enantiopure Ln_4L_6 tetrahedral cage based on the same principle. Combination of chiral cages with luminescent properties of lanthanides provides potential applications as chiroptical probes.

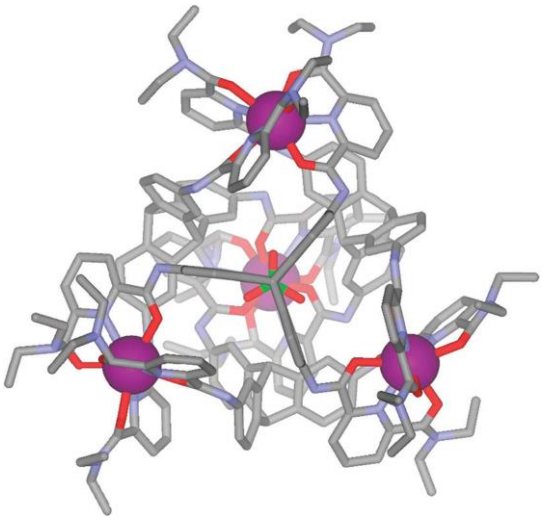

Figure 1.4.6 - A tetrahedral europium-based cage complex $[Eu_4(L12)_4]^{12+}$ with a bound perchlorate anion Reproduced with permission from ref. 52, published by the Royal Society of Chemistry.

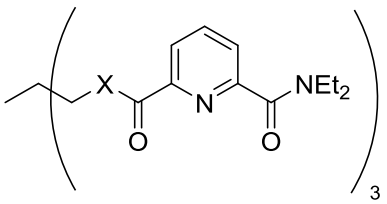

L11 X = NH
L12 X = O

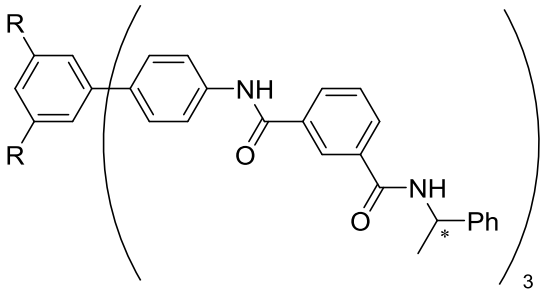

L13 (* = chiral centre)

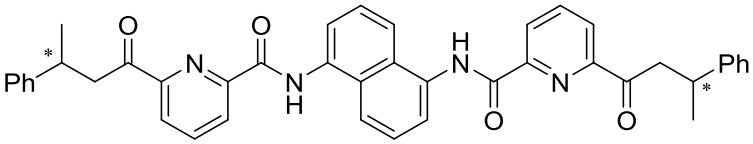

L14 (* = chiral centre)

Dong and co-workers reported a family of Ln_2L_4 complexes with tetragonal prismatic structures, in which the central cavity is occupied by a $[Ln(H_2O)_8]^{3+}$ guest ion hydrogen-bonded to the cavity surface which is highly polar (Fig. 1.4.7). The restriction of the octa-aqua lanthanide(III) cation significantly enhances its luminescence intensity and lifetime. If the Ln(III) ion in the Ln_2L_4 cage (M_1 in Fig. 1.4.7) and the guest $[Ln(H_2O)_8]^{3+}$ species (M_2) are different, luminescence from both host and guest can be observed.[56]

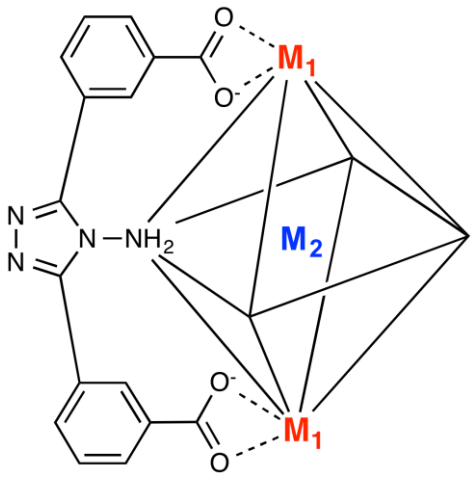

Figure 1.4.7 - A heteronuclear lanthanide complex where a guest complex $[M_2(H_2O)_n]^{3+}$ lies inside the cavity of the cage (see ref. 56).

He, Duan and co-workers have reported a series of luminescent cages based on Ce(III) or Ce(IV), utilising O,N,O-chelating ligands with anionic termini. These have been shown to function as luminescent sensors for a variety of guest molecules.[57–65] Each lanthanide cation is in a 9-coordinate environment provided by three tridentate binding sites. The luminescence based on the Ce(III) 4f-5d transition is more sensitive to environmental changes than that of the luminescence arising from the Eu(III) and Tb(III) 4f-4f transitions, therefore Ce(III)-based luminescent cages are more sensitive to environmental changes imposed by the binding of guest molecules. Where Ce(IV) based cages are concerned the luminescence arises from an organic fluorophore incorporated into the ligands, and these cages act as luminescent sensors for the binding of guest molecules.

Ce_4L_4 and Ce_4L_6 tetrahedral cages based on face-capping (L15) and edge-bridging (L16) ligands show an enhancement of luminescence intensity upon the binding of saccharides.[58] Recognition is due to hydrogen-bonding interactions between the bound saccharides and the amide groups in the ligands. More extravagant bridging ligands such as L17 – L19 lead to larger octanuclear polyhedra.[59,61] These display a similar luminescence response when the guest is complementary to the cage cavity; these cages therefore act as size/ shape selective sensors for a number of saccharides.

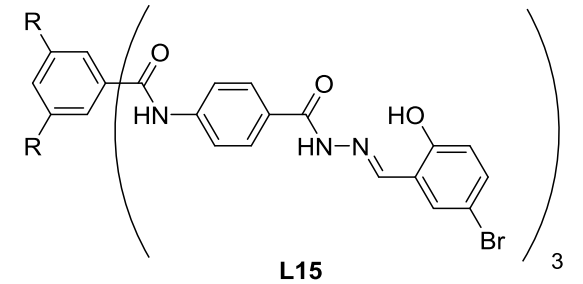

L15

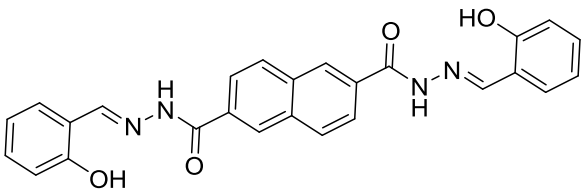

L16

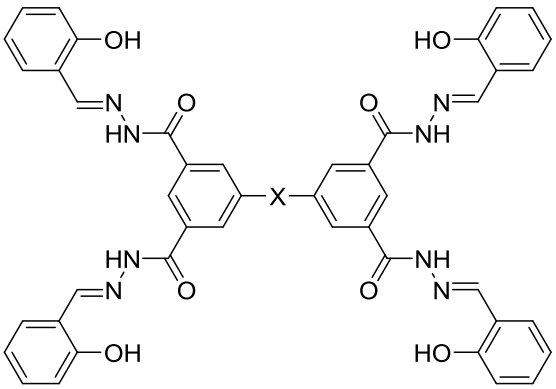

L17: X = NH-C(O)-(p-C_6H_4)-C(O)-NH
L18: X = OCH_2CH_2O
L19: X = OCH_2-(p-C_6Me_4)-CH_2O

Introducing a triphenylamine moiety into the face-capping ligand L22 results in Ce_4L_4 cages with ligand-based, strong blue fluorescence.[62,63] The organic radical 4,4,5,5-tetra-methylimidazolineyloxyl-3-oxide, which is a spin-trapping agent for NO, is strongly bound by the cage. Upon binding this guest the cage fluorescence is significantly quenched. Trace amounts of NO lead to the restoration of cage fluorescence as the typical reaction with the 4,4,5,5-tetra-methylimidazolineyloxyl-3-oxide occurs. Therefore the combination of cage, spin-trap and guest acts as a sensitive luminescent reporter of NO with a detection limit much lower than that of the more commonly-used EPR spectroscopic assay.[63] The same cage has shown selectivity for binding of tryptophan over other amino acids, providing the

basis of a luminescent assay for tryptophan in serum.[64] Again, using the same cage, selective binding of 5-hydroxyindole-3-acetic acid (5-HIAA), an important marker for the diagnosis of tumours, was observed. The encapsulation (through weak interactions and spatial selectivity) leads to an enhancement of luminescence resulting in a sensor capable of detecting 5-HIAA in urine over other relevant species, with high sensitivity.[66]

Incorporating a dihydropyridine-amido group into the tritopic bridging ligand L20 results in a Ce_4L_4 tetrahedral cage that selectively binds the explosive RDX; a strong luminescent response is observed compared to other explosive molecules.[62] Similarly, incorporation of hydrogen-bonding triamino-triazine units, as in L21, affords a Ce_4L_4 tetrahedral cage which selectively binds guanosine, with significant luminescence enhancement, over nucleosides in organic solvents.[39]

Building upon the capabilities of these cages is to utilise them as sensors to report on the progress of a reaction: the luminescence change can be used to monitor substrate concentration as the reaction progresses. Tritopic-face capped Ce_4L_4 tetrahedra from this family, such as those using ligands L22 and L23 which facilitate binding of guests by hydrogen bonding to the amide groups, have to been studied for this role. The Knoevenagel condensation and cyanosilylation of aromatic aldehydes had their reaction rates accelerated in the cage cavities, progress of which was monitored by restoration of the cage luminescence.[65,67]

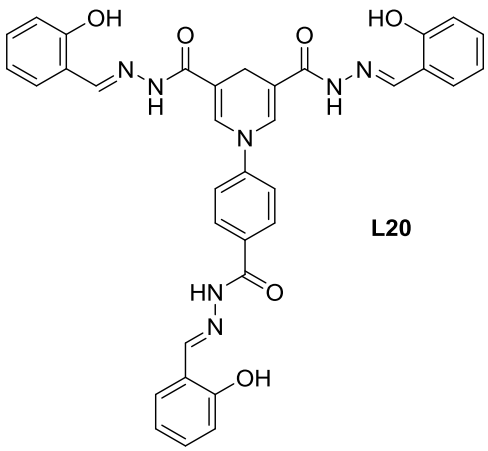

L20

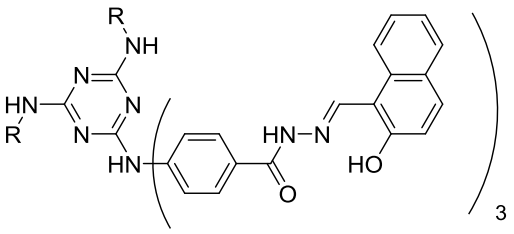

L21

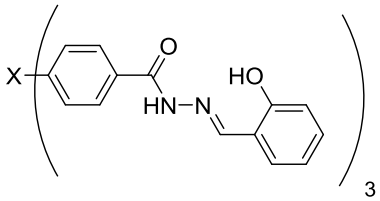

L22: X = N
L23: X = 1,3,5-C_6H_3

1.4.4 Photochromic / photo-switchable cages

A number of examples of cages exist which do not exhibit luminescence but which however do incorporate photosensitive functional groups: these form the basis for photo-induced switching of structure and/or properties. Clever and co-workers have reported the photo-induced conformational change of a cage based on a photochromic group built into the ligands. The resulting opening and closing of the cage affords the light-triggered uptake and release of guest molecules. The Pd_2L_4 cage is based on the 'banana-shaped' bis-pyridyl ligands spanning two Pd(II) centres.[31] The photo-induced opening/closing mechanism is due to the incorporation of the dithienyl-ethylene group (L24), and the changes in conformation lead to the altering of the Pd-Ligand termini distances. This process can be viewed as a reversible swelling or contraction of the cage, modulating the cavity volume and resulting in the strength of guest binding changing in such a way that the guest binding is indeed photo-switchable.[68]

A $Pd_{12}L_{24}$ 'nanosphere' reported by Fujita and co-workers is based on bent, rigid bis-pyridyl ligands incorporating azobenzene groups (L25), such that there are 24 azobenzene groups pointing into the central cavity. Upon irradiation by light a number of the azobenzene groups converted from *trans* to *cis* form; the *cis* form is inherently more polar than the trans form and such reduced the hydrophobicity of the cavity and consequently decreased the capacity to bind hydrophobic guest molecules. Reversion of the conformational change is achieved by heating the cage, resulting in the increase of hydrophobicity of the cavity and the restoration of guest binding.[69]

Mukherjee and co-workers attempted to synthesise a trigonal prismatic cage by combining three cis-[Pd(diamine)]$^{2+}$ units with two triangular tris-pyridyl units. The result was two Pd_3L_2 cages which were triply interlocked to give a Pd_6L_4 species with no chemical bonds existing between the two Pd_3L_2 components (Fig. 1.4.8). The crystal structure shows that the proximity of the carbon double bonds between adjacent Pd_6L_4 assemblies facilitates a 2+2 photocyclisation bridging the two Pd_6L_4 assemblies to give a cyclobutane unit. The cyclisation could be reversed thermally, isolating the two Pd_6L_4 assemblies. [70]

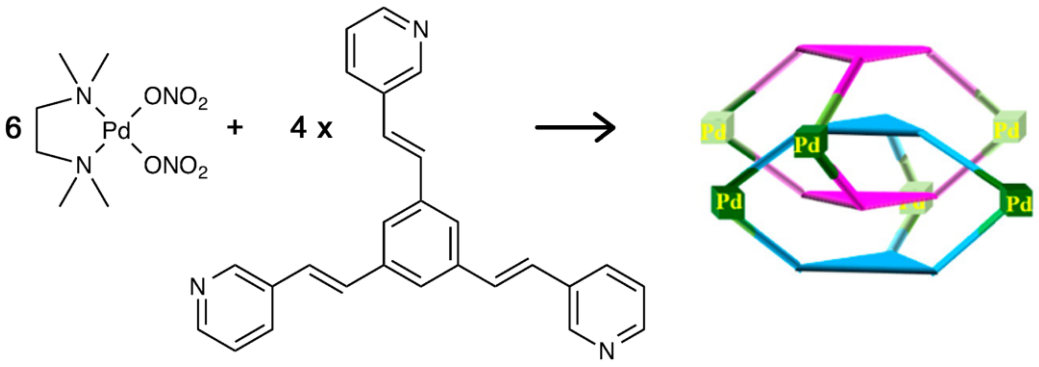

Figure 1.4.8 - The assembly of two interlocked Pd_3L_2 trigonal prismatic cages. Adapted with permission from ref. 55.

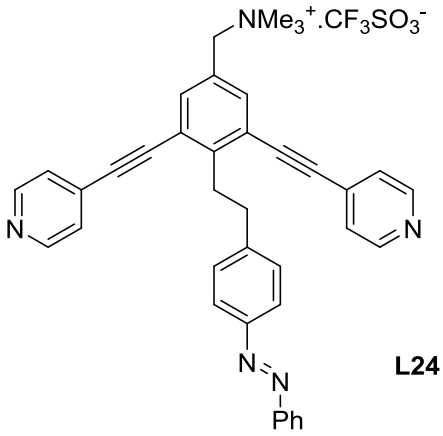

L24

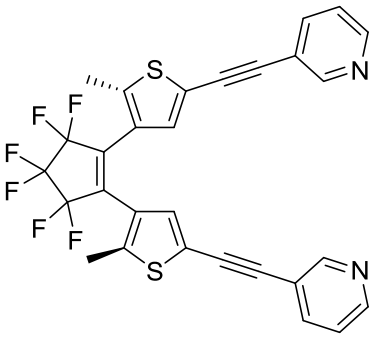

L25

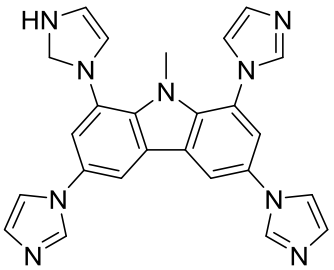

L26

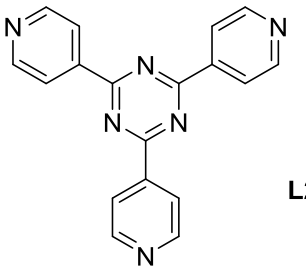

L27

1.4.5 Optical properties of bound guests

If one looks beyond the cages as the photophysically active species, there are several examples in which it is the guest molecules, rather than the host cages, which possess useful photophysical behaviour and properties. Binding of these guest molecules within the cavity of cages may result in the modulation of their photophysical behaviour or just simply allow for transport inside the host.

Therrien and co-workers have utilised a similar idea in the use of prismatic cages to transport photosensitisers across cell membranes for use in photodynamic therapy (Fig. 1.4.9). The planar aromatic ligand panels within the cage structure afford strong binding of planar guest molecules such as porphines, metalloporphyrins and substituted pyrenes due to stacking interactions. Encapsulation of the guests provides protection from light as well as enabling transport to cancer cells.[71,72]

Similarly, Mukherjee and co-workers reported the preparation of a Pd_8L_4 barrel-like cages, consisting roughly of a cubic arrangement of Pd(II) ions with four tetra-topic ligands L26 arranged about four of the six faces with the top and bottom faces of the cube remaining open. This allows the cage to bind fluorescent aromatic guests, such as coronene and perylene, in water *via* π-stacking interactions with the walls of the cavity. The cage is able to permeate cell membranes allowing the transport of perylene into the cells where it could be visualised by fluorescence microscopy.[73]

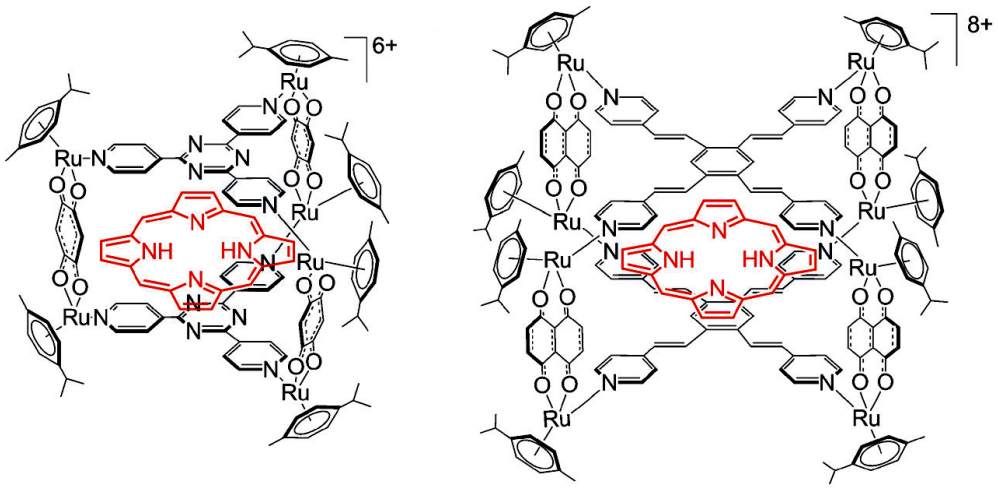

Figure 1.4.9 – Uptake of porphine photosensitisers into prismatic Ru-based cages (see ref. 71).

Binding of guest molecules within cages isn't limited to simply to being protected from photodamage. Tetraaza-porphine is a poorly/non-fluorescent molecule in solution due to aggregation based quenching effects and/or the effects of solvent-based quenching. The binding of tetraaza-porphine, in the cavity of a trigonal prismatic cage containing two L27-based $Pt_3(L)_2$ units in water inhibits both of these quenching pathways, and its red fluorescence is restored. There is no emission quenching due to charge-transfer interactions between the L35 chromophore and the guest, which has been a common case for other fluorescent guests in cages.[74] Yoshizawa's Pt_2L_4 cages containing anthracene groups around the central cavity[33–36] were used to bind a variety of coumarin and BODIPY derivatives. The anthracene ligands are not fluorescent themselves in the Pt(II) cages: the bound guests however retain their fluorescence, due to the energy of their excited states being low enough to avoid being quenched by the anthracene π-π* states. Co-binding of different organic guests has been found to modulate the colour of emission of the bound BODIPY guests – stacking of the BODIPY with a second planar aromatic guest affords a bathochromic shift in the fluorescence from BODIPY – providing an interesting method for tuning the fluorescence of the bound BODIPY. [75]

Fujita and co-workers showed that the binding of phthalein type dyes in a cage cavity can affect the equilibrium between different structural forms of the dye – which convert from coloured quinone dianions at high pH to colourless lactones at low pH. A Pt_6L_4 octahedral cage containing L27 on four faces selectively binds the colourless lactone form of phenolphthalein and stabilises the structure even at high pH, due to the size and shape complementarity between the cage cavity and the lactone. This provides a method of visualising the binding of other guests, phenolphthalein being displaced and hence allowing the rearranging to the coloured quinone form.[76]

1.4.6 Photoinduced reactions of bound guests

There are several examples exist where photoinduced reactions of bound guests in cages take place in which the cage acts solely as a "box", restricting the available space for the reaction and thereby altering the possible reaction pathways of guests, resulting in novel products from these reactions. Fujita's series of octahedral $[Pd(NN)]_6L_4$ cages (where L = L35 and 'NN' represents either ethylenediamine or 2,2'-bipyridine, see Fig. 1.4.10), have been well studied for these types of reactions by numerous groups.[77–82] Confinement of an *N*-substituted maleimide and a variety of polyaromatics such as pyrene, triphenylene or acenaphthylene afforded facile [2+2] cross-photoadditions between the two substrates. High regioselectivity was observed, with the *syn*-isomers being exclusively formed. The suggested reason for this was due to the close proximity of the typically unreactive aromatic guest to the maleimide enforcing an orientation that would favour that particular reaction pathway. [77,78] If the terminal capping ligands on the Pd(II) ions were exchanged for chiral diaminoethane ligands, the [2+2] photocyclisation reaction in the cavity – between the same maleimide derivative and some substituted fluoranthenes – yields chiral products with a significant enantiomeric excess.[79]

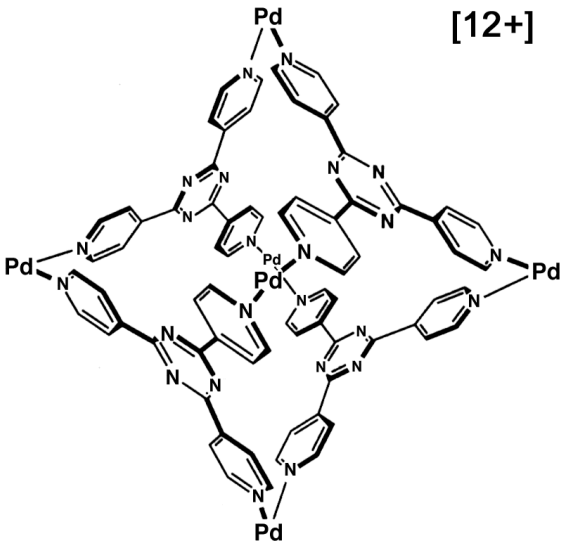

Figure 1.4.10 - General structure of a family of a Pd_6L_4 cages (see ref. 77-82).

The typical photolysis of an α-diketone results in a photo-cleavage reaction to give two acyl radicals. However when diphenylethanedione is bound inside a $[Pd(NN)]_6L_4$ cage, photolysis results in a range of cyclised products being formed instead. The suppression of the photo-cleavage reaction allows for normally kinetically unfavourable reaction pathways to occur instead to give different products. [83]

The photo-irradiation of a system in which an *ortho*-quinone and a substituted arene are co-bound results in a product formed from combination a photo-generated semiquinone and benzylic radicals (Fig. 1.4.11). This again displays how the cage cavity can afford control of reactivity, allowing stabilisation of transition states and therefore products that are otherwise kinetically unfavourable.[84]

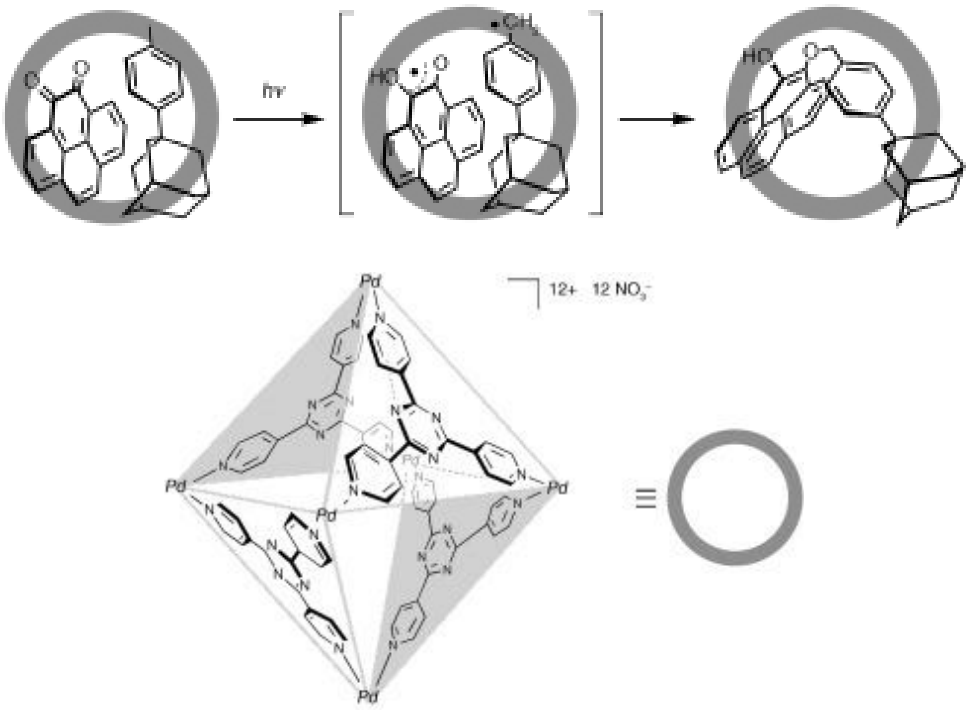

Fig. 1.4.11 – Photoreaction of a quinone within the cavity of a coordination cage. Reproduced with permission from ref. 84.

Work done with Fujita's $[Pd(NN)]_6L_4$ cage by Ramamurthy and co-workers has noted that not all substrates that undergo the [2+2] photodimerisation do so with high *syn*–regioselectivity. The results of photodimerisation for a range of substituted anthracenes were more complex – only 9-formyl-anthracene gave the expected 'head-to-tail' dimer. No evidence of photodimerisation was observed for the rest of the substituted anthracene guests, even if they do undergo photodimerisation in free solution.[80] Expanding the study to coumarins[81] and *trans*-cinnamic acid esters[82] gave better results, as these underwent [2+2] photodimerisation with higher stereoselectivity than seen in free solution. In these cases the wavelength at which the substrates absorb light is lower in energy than that of the cage (strongly absorbing in the UV, $\lambda < 330$ nm) meaning that is possible to directly excite the guest molecules.

1.4.7 Photoinduced processes involving both cage and guest

The ability of self-assembled cage structures to provide a unique environment to the encapsulated guest molecules, which is different from the bulk solution, provides the potential for use in photo-catalysis. This is because the structures of photophysically active cages provide an array of chromophoric units surrounding a central cavity where a guest is bound, thereby providing a very high local concentration of chromophoric units around a guest which would be difficult to achieve in any other way.

The first example is from Duan and co-workers, who have utilising the photophysical properties of a Ce_4L_6 cage/guest assembly for light-driven H_2 production. The Ce_4L_6 complex is based on an array of Ce(IV) ions bridged by bis-tridentate ligands L28 spanning the edges of a square shape. Though the structure is closer to that of a metallacycle, a cavity exists that encapsulates a $Fe_2(CO)_6$(dithiolate) complex which is known as a catalyst in the production of H_2. The carbazole units in the briding ligands are quenched by the $Fe_2(CO)_6$(dithiolate) guest, and a $[Fe^{I}\text{-}Fe^{0}]$ species is generated as a result which has the capacity to reduce protons to H_2.[85] Similar work from the same group involves the use of a $Co^{III}{}_4L_4$ tetrahedral cage assembled using a face-capping tritopic ligand with bidentate thiosemicarbazone *N,S*-donor termini L29. In this system the photosensitiser fluorescein is bound in the cage cavity: excitation of the photosensitiser leads to a cobalt (III) ion – these redox sites (involving Co(I) species) proceed to reduce protons from water molecules.[86]

Toste, Raymond and Bergman have reported a cage-to-guest photoinduced electron transfer following UV excitation resulting rearrangement of an encapsulated cinnamylammonium cation guest. The Ga_4L_6 cage is based on Ga(III) tris-catecholate, with the ligand L30 incorporating a naphthyl group as the photosensitiser. The photoinduced electron-transfer facilitates an allylic 1,3-rearrangement generating a higher-energy branched isomer, and this process does not occur unless the guest is bound.[87]

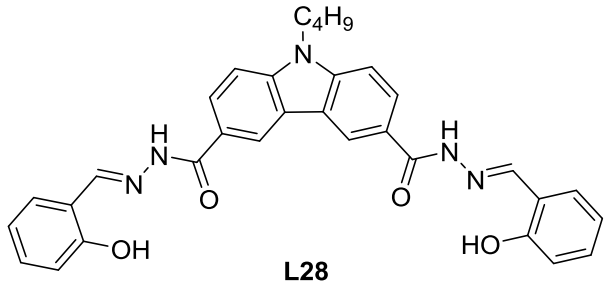

L28

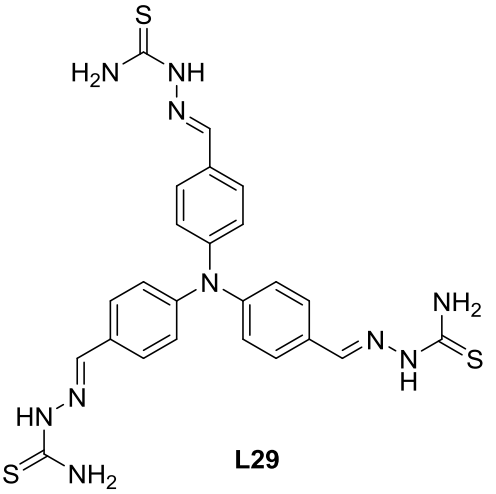

L29

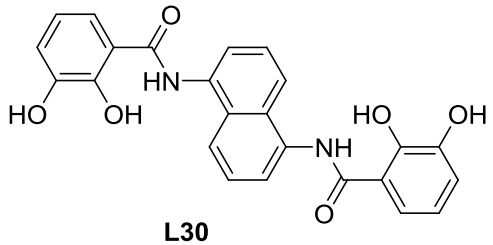

L30

In the previous examples the Pd_6 cage merely fulfils a role as a sterically confining container which changes the kinetic pathway of reactions. Fujita and co-workers have shown that these cages can be actual participants in photoinduced processes, interacting with the substrates. Oxidation of a bound adamantane guest gives 1-adamantanol and 1-adamantylhyroperoxide. Since adamantane itself does not absorb the excitation radiation, the mechanism was proposed to be a photo-excitation of the ligand to generate a π-π* excited state, with subsequent photoinduced electron-transfer from the adamantane to the excited state of the triazine group. The resulting triazine radical anion is oxidised by O_2, and the adamantyl radical reacts irreversibly with O_2 to afford the observed products.[88,89] The

same photoinduced electron-transfer process results in photo-oxidation of bound triquinacene to 1-hydroxy-triquinacene, and of arylalkynes to benzyl-ketones in an anti-Markovnikov hydration reaction.[90] An example of photoinduced energy transfer between host and guest using the same family of $[Pd(NN)_6]L_4$ cages was observed when the guest 9,9'-bis-anthracene was bound inside the cavity. The proximity of two anthracene groups and the four triazine groups resulted in a low-energy absorption band in the UV/Vis spectrum at roughly 450 nm which is associated with a charge-transfer transition between the guest's electron-rich and the host's electron-deficient aromatic panels. The excited state of the bis-anthracene guest is quenched by rapid energy-transfer to this low-lying charge-transfer state resulting in weak fluorescence at 650 nm.[91]

Dasgupta and co-workers used a $[Pd(NN)]_6L_4$ cage to study the excited-state dynamics of a charge-separated host-guest pair, particularly the proton transfer process of guest to solvent which follows an initial photoinduced electron transfer. Upon irradiation of 4-hydroxy-diphenylamine, as the guest, guest-to-ligand photoinduced electron transfer is observed converting the guest into a radical cation. Rapid loss of a proton to water gives a neutral bound radical and H_3O^+. The ligand radical anion, the guest radical cation and the neutral guest radical could be detected using ultrafast spectroscopy techniques with measurement of the timescales on which the processes occur in the confined space.[92]

1.5 Cages of the Ward Group

1.5.1 The Cages

For the past two decades Ward and co-workers have been studying coordination cages. An interest in polydentate ligands resulted in the studying tris(pyrazolyl)borate $[Tp^{Py}]^-$ a hexadentate ligand (Fig. 1.5.1).[93] It would be expected that a six coordinate metal ion would sit within the cavity in a trigonal prismatic coordination geometry, which in the case of Co(II) is true – affording the mononuclear complex $[Co(Tp^{Py})]^+$.[94] However, if the metal is replaced with either Mn(II) or Zn(II), the ligand adopts a different coordination mode in which it spans three metal ions capping a triangular face of a tetrahedral cage $[M_4(Tp^{Py})_4]^{4+}$ (Fig. 1.5.1).[94,95]

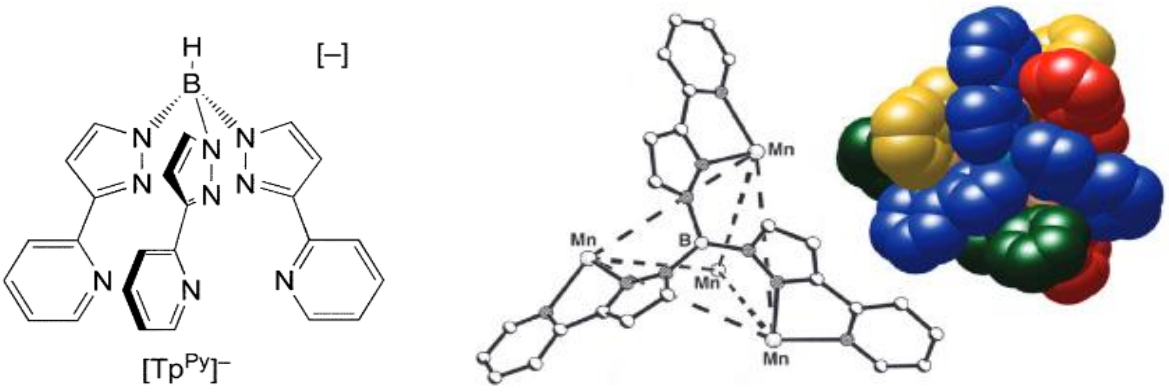

Figure 1.5.1 – $[Tp^{Py}]^-$ ligand and the M_4L_4 tetrahedron. Reproduced with permission from Ref. 93.

Following these results, ligands containing the bidentate pyrazolyl-pyridine unit became the focus of further study. This led to the development of a family of ligands incorporating two pyrazolyl-pyridine units separated by aromatic spacer groups linked via flexible methylene hinges. The synthesis of these ligands was relatively simple - the reaction of 3-(2-pyridyl)pyrazole with a bis(bromomethyl)aromatic compound under basic conditions.

The first of these ligands, $L^{o\text{-}Ph}$, contains an *ortho*-phenylene spacer. Reaction of $L^{o\text{-}Ph}$ with 4-coordinate Cu(I) afforded the double helical structure $[Cu_2(L^{o\text{-}Ph})_2]^{2+}$ and reaction with Ni(II) afforded a dinuclear complex $[Ni_2(L^{o\text{-}Ph})_3]^{2+}$ where one ligand bridges the two Ni(II) centres and the remaining two ligands coordinate in a tetradentate manner.[96] This 2M:3L ratio is a perquisite for all complexes containing bis-bidentate ligands and six-coordinate metal ions to achieve coordinative saturation.

Reaction of $L^{o\text{-}Ph}$ with $Co(BF_4)_2$ yielded an unexpected tetrahedral coordination cage $[Co_4(L^{o\text{-}Ph})_6](BF_4)_8$ (Fig. 1.5.2). This cage fulfils the 2M:3L stoichiometric requirement; each ligand spans an edge of the tetrahedron with a Co(II) ion occupying each vertex and having a *fac* tris-chelate geometry. X-ray crystallography revealed a single BF_4 anion encapsulated within the cavity, orientated in way that suggested that hydrogen bonding interactions with internally-directed CH protons from the ligands present. An attempt as synthesising the cage with a non-fitting anion failed, providing evidence that the cage formation is templated by suitable anions.[97] Another important point is the extensive π-stacking that exists

between the pyrazolyl-pyridine and phenylene units of different ligands, which helps to stabilise of the cage structure.

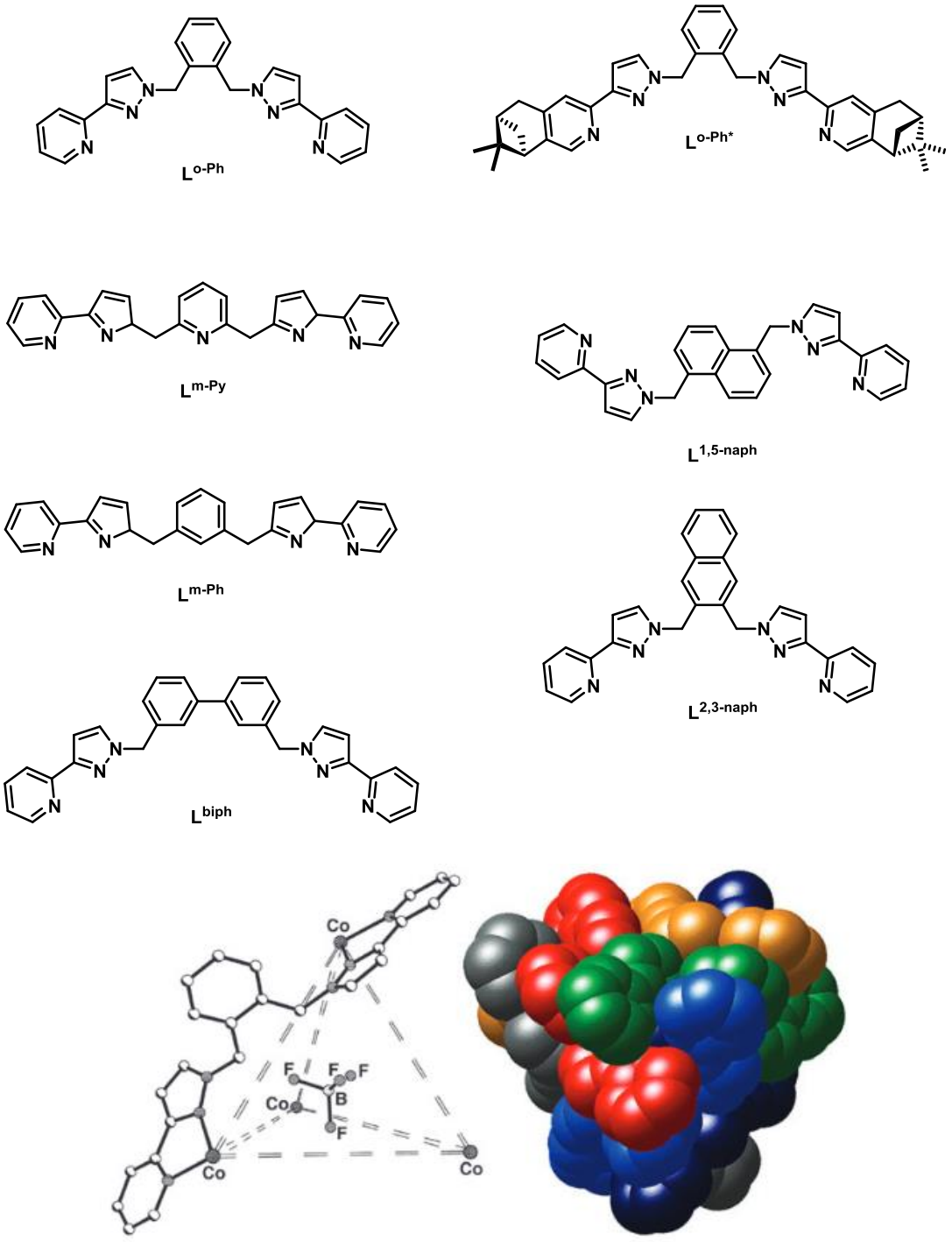

Figure 1.5.2 *- The tetranuclear cage complex* $[Co_4(L^{o\text{-}Ph})_6](BF_4)_8$ *showing only the internal anion (left) and a space-filling model (right). Reproduced from Ref. 97 with permission from The Royal Society of Chemistry.*

Structures analogous to that of $[Co_4(L^{o\text{-}Ph})_6]^{8+}$ tetrahedron were synthesised with the ligands $L^{2,3\text{-}naph}$ and L^{biph}. Cages utilizing $L^{2,3\text{-}nap}$ are isostructural with those of $L^{o\text{-}Ph}$, whereas the cage utilizing L^{biph} affords a larger tetrahedral cage where one metal vertex has a *fac* tris-chelate coordination geometry and the other three have *mer* geometries. The larger cavity allow for the encapsulation of larger anions such as hexafluorophosphate which can exchange rapidly with external anions according to NMR measurements.[97]

Variations on the structure of the bridging ligand, but maintaining the 2M:3L, ratio has resulted in more complex coordination cages beyond tetrahedra (the simplest member of the family). The ligand $L^{m\text{-}Ph}$ when combined with Co(II), Zn(II) or Ni(II), results in a an $[M_6L_9]^{12+}$ 'open book' , a $[M_8L_{12}]^{16+}$ slanted molecular cube or a $[M_4L_6]^{8+}$ square.[98] $L^{1,5\text{-}naph}$ also forms M_8L_{12} cubic cages when paired with Cu(II), Zn(II), or Co(II).[99] In the crystal structures of the $[Co_8(L^{1,5\text{-}naph})_{12}](BF_4)_{16}$ cube the extensive π-stacking interactions can clearly be seen; stacking of electron-rich naphthyl groups between the electron-poor pyridyl-pyrazole units is also again apparent (Fig. 1.5.3).

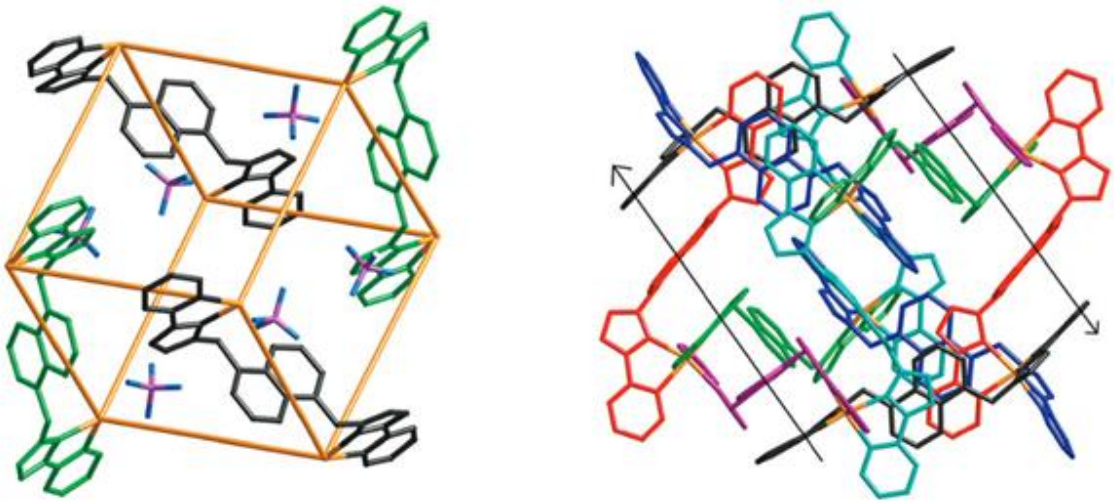

Figure 1.5.3 – Left: Simplified structure of $[Co_8(L^{1,5\text{-}naph})_{12}][BF_4]_{16}$. Right : Same structure orientated to show π-stacking. Reproduced with permission from Ref. 99.

Utilizing the ligand $L^{1,8\text{-naph}}$ with a variety of of M(II) ions yielded a $[M_{12}(L^{1,8\text{naph}})_{18}]^{24+}$ truncated tetrahedral cage.[100] A truncated tetrahedron is a tetrahedron where each vertex has been sliced off, generating four new triangular faces and the original four faces becoming hexagonal. Again this cage exhibits the extensive array of π-stacking interactions between the alternating electron-rich/poor aromatic units contributing to the cage's formation and stability in solution.

Work with the ligand $L^{p\text{-Ph}}$ in combination with different M(II) ions resulted in the formation of three different coordination cage structures.[101,102] $L^{p\text{-Ph}}$ with Ni(II) afforded a $[Ni_8L_{12}](BF_4)_{12}(SiF_6)_2$ cube, whereas reaction with Cu(II) afforded the formation of a $[Cu_6L_9](BF_4)_{12}$ trigonal prism. Finally, the reaction with either Zn(II) or Cd(II) resulted in the largest homoleptic cage seen in this series, an elaborate $[M_{16}L_{24}]^{32+}$ tetra-capped truncated tetrahedron. ESMS studies showed that this cage exists in equilibrium with a hexanuclear trigonal prismatic cage in solution, but upon crystallisation only the M_{16} cage is afforded (Figure 1.5.4).[102] Replacing $L^{p\text{-Ph}}$ with $L^{1,4\text{-naph}}$ and then reacting with Cd(II) again affords an $[M_{16}L_{24}]^{32+}$ tetra-capped truncated tetrahedron, isostructural to that of resulting from $L^{p\text{-Ph}}$, however no interconversion to a hexanuclear prism is observed. This is likely due to the improved π-stacking interactions that is afforded by use of a naphthyl group in $L^{1,4\text{-naph}}$ rather than the phenyl group seen in $L^{p\text{-Ph}}$, which stabilises the larger assembly and prevents rearrangements.[103]

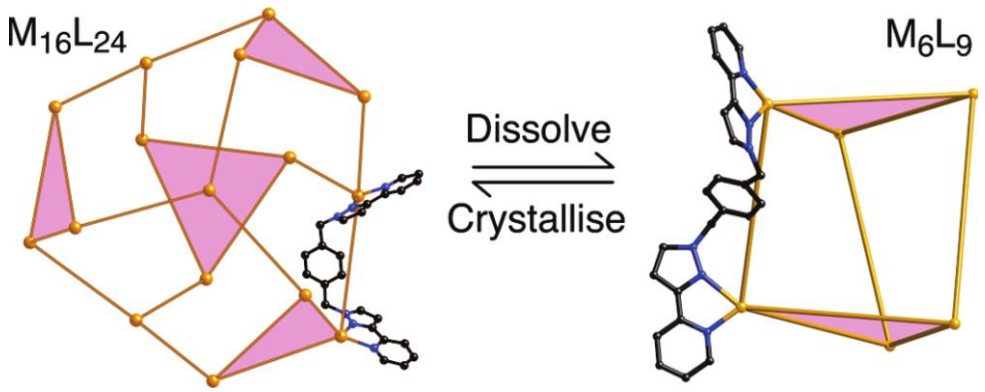

Figure 1.5.4 – Illustration of the $M_{16}L^{p\text{-ph}}{}_{24}$ cage rearrangement in solution. Reproduced with permission from Ref. 103

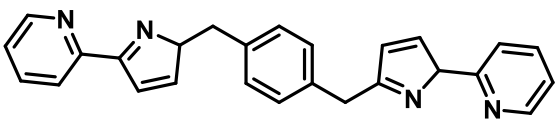

$L^{p\text{-}Ph}$

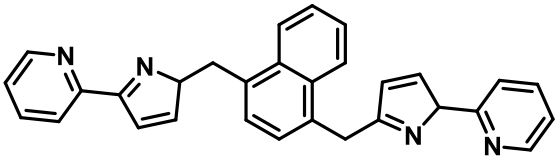

$L^{1,4\text{-}naph}$

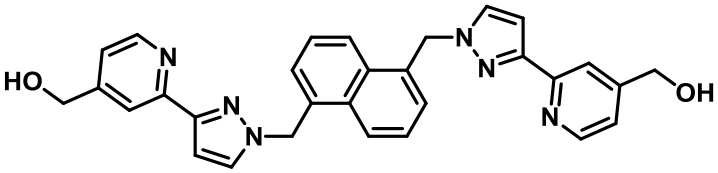

$Lw^{1,5\text{-}naph}$

1.5.2 Host-Guest Chemistry

The large majority of the host-guest chemistry investigated by the Ward group utilizes the $[M_8L_{12}]^{16+}$ cubic cages. The $[Co_8(L^{1,5\text{-}naph})_{12}]^{16+}$ cubic cage was found bind coumarin-type guests within the cavity, more specifically they bind at the *fac* metal positions (at opposite corners of the cube). Two components are involved in this guest binding; non-polar van der Waals' interactions between the coumarin and the interior surface of the cage, and an electrostatic hydrogen bonding interaction between the coumarin carbonyl oxygen and the acidic methylene protons within the vicinity of the *facial* Co(II) ions.[104] This has work has been expanded upon to involve various guests (Fig. 1.5.5), each possessing a polar hydrogen-bond accepting group.[105]

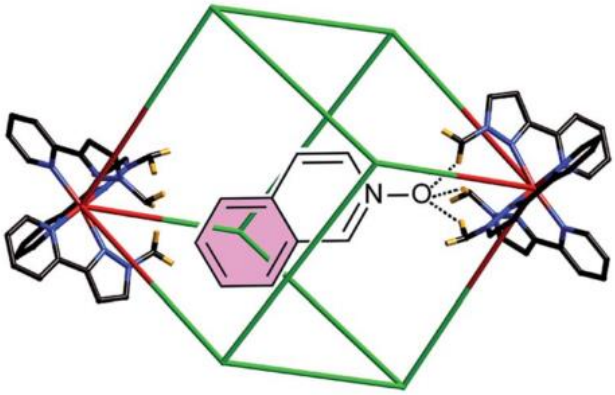

Figure 1.5.5 – X-ray crystallographic structure of the $L^{1,5\text{-naph}}$ cube showing the CH_2 groups pointing into the cavity generating a hydrogen bonding binding pocket. Reproduced with permission from Ref. 105.

Recently the Ward group have rendered their existing cages water soluble; as the hydrophobic effect will enable many new possibilities for host-guest chemistry. The ligand $L_w^{1,5\text{-naph}}$, which was synthesised to incorporate two pendant methylhydroxy groups, forms cages isostructural to the M_8L_{12} cages prepared with $L^{1,5\text{-naph}}$ (Figure 1.5.6).[105] This cage was found to bind hydrophobic guest molecules in water very strongly due to the hydrophobic effect. The binding constants of these were orders of magnitudes higher than that measured previously for the same guests in MeCN. Crystal structures of many host/guest complexers have been determined, including one with the strongly-bonding guest cycloundecanone ($K > 10^6$ M^{-1}) in the cage cavity.[106]

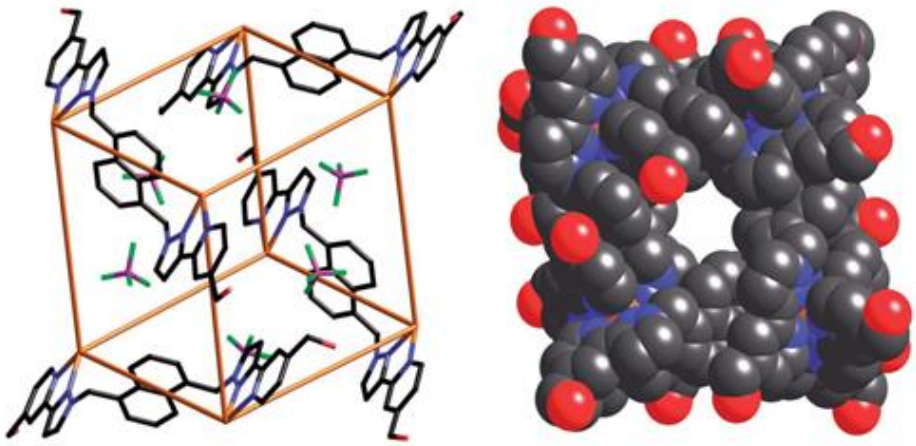

Figure 1.5.6 – left: Simplified X-ray crystallographic structure of the $[Co_8L_w{}^{1,5\text{-naph}}{}_{12}](BF_4)_{16}$ cube, right: space-filling model of the same structure. Reproduced, with permission, from Ref. 106.

Recent work has shown that the $[Co_8L_{12}]^{16+}$ cubic cage is an effective catalyst for the Kemp elimination reaction of benzisoxazole in water.[107] The reaction produces an anionic product which does not bind and therefore is ejected from the cage to be replaced by more substrate, thus bringing about catalytic turnover (fig. 1.5.7). The catalysis is based on two independent interactions: the hydrophobic binding of the guest molecule inside the cage cavity, and the binding of hydroxide ions to sites on the cage's cationic exterior surface by ion-pairing. The binding of these anions generates a high local concentration of the hydroxide ion around the cage surface in close proximity to the bound substrate; this produces an observed reaction rate enhancement of 2×10^5, significantly greater than observed for other supramolecular structures such as vesicles and micelles.

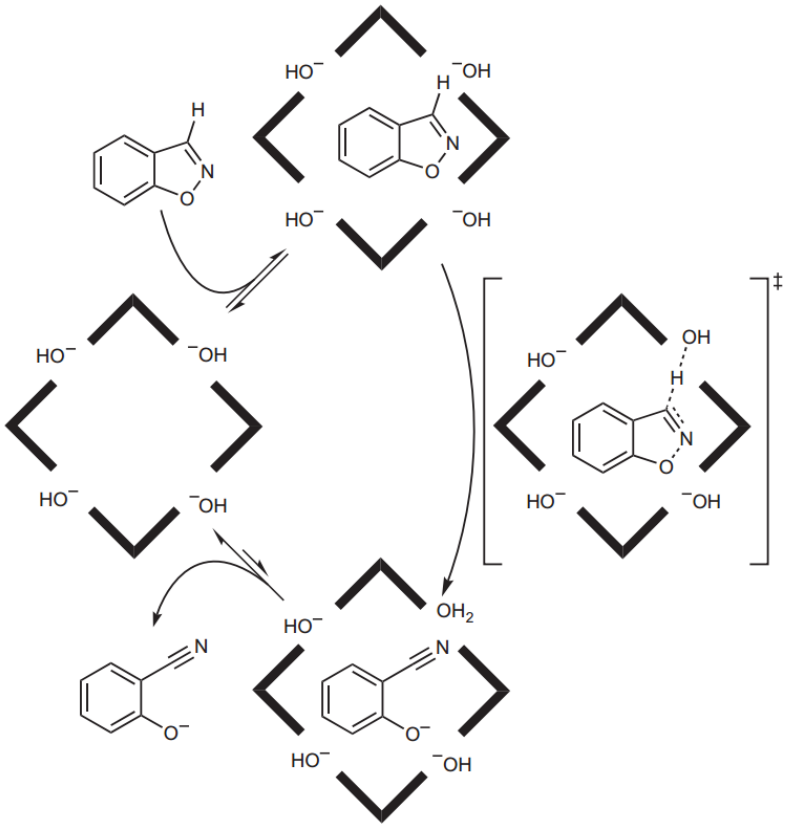

Figure 1.5.7 - A representation of the Kemp elimination catalytic reaction cycle catalysed by $[Co_8L_{12}]^{16+}$. Reproduced permission from Ref. 107.

1.6 References

1 J-M. Lehn, *Angew. Chem. Int. Ed.*, 1988, **27**, 89–112.

2 G. R. Desiraju, *Nature*, 2001, **412**, 397–400.

3 C. A. Hunter, J. K. M. Sanders, G. S. Beddard and S. Evans, *J. Chem. Soc. Chem. Commun.*, 1989, 1765.

4 C. T. Seto and G. M. Whitesides, *J. Am. Chem. Soc.*, 1993, **115**, 905–916.

5 J. W. Steed and J. L. Atwood, *Supramolecular Chemistry*, Wiley, 2nd Edition, 2009.

6 A. Klug, *Philos. Trans. R. Soc. B*, 1999, **354**.

7 S. Toksöz and M. O. Guler, *Nano Today*, 2009, **4**, 458–469.

8 C. J. Pedersen, *J. Am. Chem. Soc.*, 1967, **89**, 7017–7036.

9 C. J. Pedersen, *Angew. Chem. Int. Ed*, 1988, **27**, 1021–1027.

10 J. P. Sauvage and M. Ward, *Inorg. Chem.*, 1991, **30**, 3869–3874.

11 J. P. Mathias, E. E. Simanek, J. A. Zerkowski, C. T. Seto and G. M. Whitesides, *J. Am. Chem. Soc.*, 1994, **116**, 4316–4325.

12 B. Dietrich, J. M. Lehn and J. P. Sauvage, *Tetrahedron Lett.*, 1969, **10**, 2885–2888.

13 J.-M. Lehn, *Supramol. Chem. Self-Assembly*, 2002, **295**, 2400–2403.

14 P. J. Stang and B. Olenyuk, *Acc. Chem. Res.*, 1998, **30**, 502–518.

15 S. R. Seidel and P. J. Stang, *Acc. Chem. Res.*, 2002, **35**, 972–983.

16 M. Fujita, O. Sasaki, T. Mitsuhashi, T. Fujita, J. Yazaki, K. Yamaguchi and K. Ogura, *Chem. Commun.*, 1996, **20**, 1535.

17 F. Makoto, Y. Jun and O. Katsuyuki, *Chem. Lett.*, 1991, 1031–2.

18 R. W. Saalfrank, A. Stark, K. Peters and H. G. von Schnering, *Angew. Chem. Int. Ed*, 1988, **27**, 851–853.

19 R. W. Saalfrank, A. Stark, M. Bremer and H. U. Hummel, *Angew. Chem. Int. Ed.*, 1990, **29**, 311–314

20 K. Harris, D. Fujita and M. Fujita, *Chem. Commun.,* 2013, **49**, 6703–12.

21 Q.-F. Sun, J. Iwasa, D. Ogawa, Y. Ishido, S. Sato, T. Ozeki, Y. Sei, K. Yamaguchi and M. Fujita, *Science*, 2010, **328**, 1144–1147.

22 D. Fujita, Y. Ueda, S. Sato, H. Yokoyama, N. Mizuno, T. Kumasaka and M. Fujita, *Chem*, 2016, **1**, 91–101.

23 P. Mal, D. Schultz, K. Beyeh, K. Rissanen and J. R. Nitschke, *Angew. Chem. Int. Ed*, 2008, **47**, 8297–8301.

24 P. Mal, B. Breiner, K. Rissanen and J. R. Nitschke, *Science*, 2009, **324**, 1697–1699.

25 I. A. Riddell, M. M. J. Smulders, J. K. Clegg and J. R. Nitschke, *Chem. Commun.*, 2011, **47**, 457–459.

26 X. Yan, T. R. Cook, P. Wang, F. Huang and P. J. Stang, *Nat. Chem.*, 2015, **7**, 342–348.

27 X. Yan, M. Wang, T. R. Cook, M. Zhang, M. L. Saha, Z. Zhou, X. Li, F. Huang and P. J. Stang, *J. Am. Chem. Soc.*, 2016, **138**, 4580–4588.

28 K. Mahata, P. D. Frischmann and F. Würthner, *J. Am. Chem. Soc.*, 2013, **135**, 15656–15661.

29 P. D. Frischmann, V. Kunz and F. Würthner, *Angew. Chem. Int. Ed.*, 2015, **54**, 7285–7289.

30 P. P. Neelakandan, A. Jiménez and J. R. Nitschke, *Chem. Sci.*, 2014, **5**, 908–915.

31 M. Han, D. M. Engelhard and G. H. Clever, *Chem. Soc. Rev.*, 2014, **43**, 1848.

32 A. M. Johnson, O. Moshe, A. S. Gamboa, B. W. Langloss, J. F. K. Limtiaco, C. K. Larive and R. J. Hooley, *Inorg. Chem.*, 2011, **50**, 9430–9442.

33 N. Kishi, Z. Li, K. Yoza, M. Akita and M. Yoshizawa, *J. Am. Chem. Soc.*, 2011, **133**, 11438–11441.

34 N. Kishi, Z. Li, Y. Sei, M. Akita, K. Yoza, J. S. Siegel and M. Yoshizawa, *Chem. - Eur. J.*, 2013, **19**, 6313–6320.

35 Z. Li, N. Kishi, K. Hasegawa, M. Akita and M. Yoshizawa, *Chem. Commun.*, 2011, **47**, 8605.

36 Z. Li, N. Kishi, K. Yoza, M. Akita and M. Yoshizawa, *Chem. - Eur. J.*, 2012, **18**, 8358–8365.

37 N. Kishi, M. Akita and M. Yoshizawa, *Angew. Chem. Int. Ed.*, 2014, **53**, 3604–3607.

38 C. He, Z. Lin, Z. He, C. Duan, C. Xu, Z. Wang and C. Yan, *Angew. Chem. Int. Ed*, 2008, **47**, 877–881.

39 Y. Liu, X. Wu, C. He, Z. Li and C. Duan, *Dalt. Trans.*, 2010, **39**, 7727.

40 Y. Liu, X. Wu, C. He, R. Zhang and C. Duan, *Dalton Trans.*, 2008, 5866–5868.

41 T. H. Noh, W. Hong, H. Lee and O.-S. Jung, *Dalton Trans.*, 2015, **44**, 787–794.

42 S. Ghosh, B. Gole, A. K. Bar and P. S. Mukherjee, *Organometallics*, 2009, **28**, 4288–4296.

43 S. Shanmugaraju, H. Jadhav, Y. P. Patil and P. S. Mukherjee, *Inorg. Chem.*, 2012, **51**, 13072–13074.

44 M. Wang, V. Vajpayee, S. Shanmugaraju, Y.-R. Zheng, Z. Zhao, H. Kim, P. S. Mukherjee, K.-W. Chi and P. J. Stang, *Inorg. Chem.*, 2011, **50**, 1506–1512.

45 S. Shanmugaraju and P. S. Mukherjee, *Chem. Eur. J.*, 2015, **21**, 6656–6666.

46 K. Harano, S. Hiraoka and M. Shionoya, *J. Am. Chem. Soc.*, 2007, **129**, 5300-5301

47 O. Chepelin, J. Ujma, X. Wu, A. M. Z. Slawin, M. B. Pitak, S. J. Coles, J. Michel, A. C. Jones, P. E. Barran and P. J. Lusby, *J. Am. Chem. Soc.*, 2012, **134**, 19334–19337.

48 J. Yang, M. Bhadbhade, W. A. Donald, H. Iranmanesh, E. G. Moore, H. Yan and J. E. Beves, *Chem. Commun.*, 2015, **51**, 4465–4468.

49 K. Li, L. Y. Zhang, C. Yan, S. C. Wei, M. Pan, L. Zhang and C. Y. Su, *J. Am. Chem. Soc.*, 2014, **136**, 4456–4459.

50 A. Schmidt, M. Hollering, J. Han, A. Casini and F. E. Kühn, *Dalton Trans.*, 2016, **45**, 12297-126300.

51 A. B. Wragg, A. J. Metherell, W. Cullen and M. D. Ward, *Dalton Trans.*, 2015, **44**, 17939–17949.

52 J. Hamacek, G. Bernardinelli and Y. Filinchuk, *Eur. J. Inorg. Chem.*, 2008, **2008**, 3419-3422

53 B. El Aroussi, L. Guénée, P. Pal and J. Hamacek, *Inorg. Chem.*, 2011, **50**, 8588–8597.

54 L. L. Yan, C.H. Tan, G. L. Zhang, L. P. Zhou, J. C. Bünzli and Q. F. Sun, *J. Am. Chem. Soc.*, 2015, **137**, 8550–8555.

55 J. Hamacek, D. Poggiali, S. Zebret, B. El Aroussi, M. W. Schneider and M. Mastalerz, *Chem. Commun.*, 2012, **48**, 1281–1283.

56 P. Wang, J.-P. Ma and Y.-B. Dong, *Chem. - Eur. J.*, 2009, **15**, 10432–10445.

57 Y. Liu, Z. Lin, C. He, L. Zhao and C. Duan, *Dalton Trans.*, 2010, **39**, 11122.

58 Y. Liu, X. Wu, C. He, Y. Jiao and C. Duan, *Chem. Commun.*, 2009, **38**, 7554.

59 L. Zhao, S. Qu, C. He, R. Zhang and C. Duan, *Chem. Commun.*, 2011, **47**, 9387.

60 J. Zhang, C. He and C. Duan, *Inorg. Chem. Commun.*, 2014, **49**, 140–142.

61 Y. Jiao, J. Zhang, L. Zhang, Z. Lin, C. He and C. Duan, *Chem. Commun.*, 2012, **48**, 6022.

62 L. Zhao, Y. Chu, C. He and C. Duan, *Chem. Commun.*, 2014, **50**, 3467.

63 J. Wang, C. He, P. Wu, J. Wang and C. Duan, *J. Am. Chem. Soc.*, 2011, **133**, 12402–12405.

64 C. He, J. Wang, P. Wu, L. Jia, Y. Bai, Z. Zhang and C. Duan, *Chem. Commun.*, 2012, **48**, 11880.

65 Y. Jiao, J. Wang, P. Wu, L. Zhao, C. He, J. Zhang and C. Duan, *Chem. - A Eur. J.*, 2014, **20**, 2224–2231.

66 Y. Jiao, H. He, J. Yin, L. Zhou, C. He and C. Duan, *Inorg. Chem. Commun.*, 2016, **73**, 129–133.

67 J. Zhang, H. Yu, C. Zhang, C. He and C. Duan, *New J. Chem.*, 2014, **38**, 3137.

68 M. Han, R. Michel, B. He, Y. S. Chen, D. Stalke, M. John and G. H. Clever, *Angew. Chem. Int. Ed*, 2013, **52**, 1319–1323.

69 T. Murase, S. Sato and M. Fujita, *Angew. Chem. Int. Ed*, 2007, **46**, 5133–5136.

70 D. Samanta and P. S. Mukherjee, 2014, 1–4.

71 F. Schmitt, J. Freudenreich, N. P. E. Barry, L. Juillerat-Jeanneret, G. Süss-Fink and B. Therrien, *J. Am. Chem. Soc.*, 2012, **134**, 754–757.

72 B. Therrien, *Chem. - Eur. J.*, 2013, **19**, 8378–8386.

73 B. Roy, A. K. Ghosh, S. Srivastava, P. D'Silva and P. S. Mukherjee, *J. Am. Chem. Soc.*, 2015, **137**, 11916–11919.

74 K. Ono, J. K. Klosterman, M. Yoshizawa, K. Sekiguchi, T. Tahara and M. Fujita, *J. Am. Chem. Soc.*, 2009, **131**, 12526–12527.

75 M. Yamashina, M. M. Sartin, Y. Sei, M. Akita, S. Takeuchi, T. Tahara and M. Yoshizawa, *J. Am. Chem. Soc.*, 2015, **137**, 9266–9269.

76 H. Takezawa, S. Akiba, T. Murase and M. Fujita, *J. Am. Chem. Soc.*, 2015, **137**, 7043–7046.

77 Y. Nishioka, T. Yamaguchi, M. Yoshizawa and M. Fujita, *J. Am. Chem. Soc.*, 2007, **129**, 7000–7001.

78 M. Yoshizawa, Y. Takeuchi, T. Okano and M. Fujita, *J. Am. Chem. Soc.*, 2003, **125**, 3243–3247.

79 Y. Nishioka, T. Yamaguchi, M. Kawano and M. Fujita, *J. Am. Chem. Soc.*, 2008, **130**, 8160–8161.

80 S. Karthikeyan and V. Ramamurthy, *Tetrahedron Lett.*, 2005, **46**, 4495–4498.

81 S. Karthikeyan and V. Ramamurthy, *J. Org. Chem.*, 2006, **71**, 6409–6413.

82 S. Karthikeyan and V. Ramamurthy, *J. Org. Chem.*, 2007, **72**, 452–458.

83 T. Furusawa, M. Kawano and M. Fujita, *Angew. Chemie Int. Ed.*, 2007, **46**, 5717–5719.

84 T. Yamaguchi and M. Fujita, *Angew. Chem. Int. Ed.*, 2008, **47**, 2067–2069.

85 C. He, J. Wang, L. Zhao, T. Liu, J. Zhang and C. Duan, *Chem. Commun.*, 2013, **49**, 627–629.

86 X. Jing, C. He, Y. Yang and C. Duan, *J. Am. Chem. Soc.*, 2015, **137**, 3967–3974.

87 D. M. Dalton, S. R. Ellis, E. M. Nichols, R. A. Mathies, F. Dean Toste, R. G. Bergman and K. N. Raymond, *J. Am. Chem. Soc.*, 2015, **137**, 10128–10131.

88 M. Yoshizawa, S. Miyagi, M. Kawano, K. Ishiguro and M. Fujita, *J. Am. Chem. Soc.*, 2004, **126**, 9172–9173.

89 Y. Furutani, H. Kandori, M. Kawano, K. Nakabayashi, M. Yoshizawa and M. Fujita, *J. Am. Chem. Soc.*, 2009, **131**, 4764–4768.

90 T. Murase, H. Takezawa and M. Fujita, *Chem. Commun.*, 2011, **47**, 10960.

91 J. K. Klosterman, M. Iwamura, T. Tahara and M. Fujita, *J. Am. Chem. Soc.*, 2009, **131**, 9478–9479.

92 R. Gera, A. Das, A. Jha and J. Dasgupta, *J. Am. Chem. Soc.*, 2014, **136**, 15909–15912.

93 M. D. Ward, *Chem. Commun.*, 2009, 4487–4499.

94 R. L. Paul, A. J. Amoroso, P. L. Jones, S. M. Couchman, Z. R. Reeves, L. H. Rees, J. C. Jeffery, J. A. McCleverty and M. D. Ward, *J. Chem. Soc. Dalt. Trans.*, 1999, 1563–1568.

95 R. L. Paul, S. M. Couchman, J. C. Jeffery, J. A. McCleverty, Z. R. Reeves and M. D. Ward, *J. Chem. Soc. Dalt. Trans.*, 2000, 845–851.

96 J. S. Fleming, K. L. V Mann, E. Psillakis, J. C. Jeffery, M. D. Ward, J. A. McCleverty and C.-A. Carraz, *Angew. Chem. Int. Ed.*, 1998, **1**, 1279.

97 R. L. Paul, Z. R. Bell, J. S. Fleming, J. C. Jeffery, J. A. McCleverty and M. D. Ward, *Heteroat. Chem.*, 2002, **13**, 567–573.

98 A. M. Najar, I. S. Tidmarsh, H. Adams and M. D. Ward, *Inorg. Chem.*, 2009, **48**, 11871–11881.

99 I. S. Tidmarsh, T. B. Faust, H. Adams, L. P. Harding, L. Russo, W. Clegg and M. D. Ward, *J. Am. Chem. Soc.*, 2008, **130**, 15167–15175.

100 S. P. Argent, H. Adams, T. Riis-Johannessen, J. C. Jeffery, L. P. Harding, O. Mamula and M. D. Ward, *Inorg. Chem.*, 2006, **45**, 3905–3919.

101 S. P. Argent, H. Adams, T. Riis-Johannessen, J. C. Jeffery, L. P. Harding and M. D. Ward, *J. Am. Chem. Soc.*, 2006, **128**, 72–73.

102 A. Stephenson, S. P. Argent, T. Riis-Johannessen, I. S. Tidmarsh and M. D. Ward, *J. Am.*

Chem. Soc., 2011, **133**, 858–870.

103 A. Stephenson, D. Sykes and M. D. Ward, *Dalt. Trans.*, 2013, **42**, 6756.

104 S. Turega, M. Whitehead, B. R. Hall, M. F. Haddow, C. A. Hunter and M. D. Ward, *Chem. Commun.*, 2012, **48**, 2752.

105 M. Whitehead, S. Turega, A. Stephenson, C. A. Hunter and M. D. Ward, *Chem. Sci.*, 2013, **4**, 2744.

106 S. Turega, W. Cullen, M. Whitehead, C. A. Hunter and M. D. Ward, *J. Am. Chem. Soc.*, 2014, **136**, 8475–8483.

107 W. Cullen, M. C. Misuraca, C. A. Hunter, N. H. Williams and M. D. Ward, *Nature Chem.*, 2016, **8**, 231–236.

Chapter 2

Synthesis and Host-Guest Chemistry of a Fluorescent Coordination Cage

2.1 Introduction

2.1.1 Past Methods of Binding Constant Determination

The most utilised cage for host guest studies from the Ward group cage family is the M_8L_{12} cubic cage, based on the paramagnetic Co(II) ion. The paramagnetism facilitates the measurement of binding constants by NMR spectroscopy experiments; the large dispersion of peaks (over a 200 ppm range) allows for the easy assessment of spectral changes. However the use of NMR spectroscopy has its limitations: a good signal to noise ratio requires a large number of scans which can lead to a single measurement taking up to 30 minutes. While this is reasonable for a high concentration of guest molecules, higher binding constants require lower concentrations to be accurately measured resulting in longer NMR experiment times.[1]

A viable alternative that overcame these limitations is fluorescence spectroscopy. Typical concentrations are much lower than used for NMR, as such allowing for higher binding constants to be reliably measured. Additionally fluorescence measurements generally take less time than NMR measurements, allowing for a higher throughput of experiments.

Performing fluorescence measurements with the Co(II) based cage is a problem: the low energy d-d transitions associated with Co(II) quenches the naphthalene-based emission and consequently the Co(II) cage is not luminescent itself. This limitation was overcome by the utilisation of the organic fluorophore coumarin as a guest in a displacement assay. Coumarin is able to bind in the cage cavity, where upon encapsulation, its fluorescence is quenched by the Co(II) ions. Addition of a competing guest leads to the displacement of the coumarin restoring its fluorescence: by knowing the binding constant of the coumarin, and measuring the changes in fluorescence on addition of the competing guest, it is possible to measure the binding affinity of a competing guest.[2] In this way fluorescence methods could be exploited for binding constant measurements even though neither the host cage nor the guest in question is fluorescent.

2.1.2 A Luminescent Host

While the fluorescence displacement assay worked very well for the determination of binding affinities for guest molecules, the need for an additional organic fluorophore to act as the luminescent reporter added another layer of complexity to the system. In addition, the low energy d-d transitions associated with Co(II) limit any potential photo-induced naphthalene / guest interactions by acting as a quencher for the naphthyl excited state.

The solution to this was to replace the Co(II) ions with non-quenching metal ions – those with a d^{10} electronic configuration and hence no low-energy d-d transitions. It has been shown that M_8L_{12} cages based on Zn(II) and Cd(II) are structurally analogous to those based on Co(II).[3] However the use of d^{10} metals ion meant the naphthalene excited state was not quenched and the cages themselves were revealed to be luminescent. This means we can potentially use cage fluorescence directly for the measurement of guest binding, by observing changes in cage luminescence induced by guest uptake. We can also exploit the naphthyl-based excited state for potential photo-induced interactions with bound guests.

As the host-guest chemistry of this cage is primarily studied in water, the Cd(II)-based M_8L_{12} cage needed to be made water soluble. This was achieved via the same method used for the Co_8L_{12} cages – using the hydroxymethyl-substituted ligand, $Lw^{1,5\text{-naph}}$.

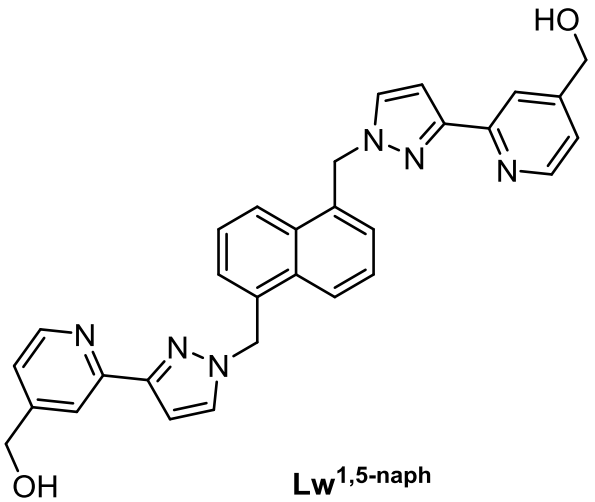

$Lw^{1,5\text{-naph}}$

2.2 Results and Discussion

2.2.2 Synthesis of the $Lw^{1,5\text{-naph}}$ ligand

Synthesis of OTBDMS-PyPz (4)

The first step towards the synthesis of $L_w{}^{1,5\text{-naph}}$ was the synthesis of the pyridyl-pyrazole (PyPz) unit, since the target cage is water soluble the PyPz unit required a CH_2OH substituent at the 4-postion of the pyridyl group.

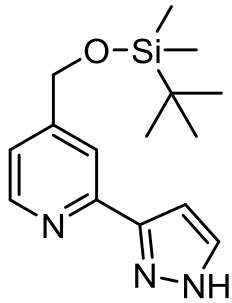

OTBDMS-PyPz (**4**)

Previous to this work, the acylation of **1** (Scheme 1) at the 2-postion to afford **2** was originally performed in 3 steps: generation of a pyridine N-oxide with *m*-chloroperoxybenzoic acid, conversion to the pyridine-2-carbonitrile with dimethylcarbamoyl chloride and trimethylsilylcyanide, and then a Grignard reaction with methylmagnesium bromide to convert the nitrile to an acetyl group (Scheme 1). However the poor and inconsistent yield from the Grignard reaction step prompted a search for a better yielding route to **2**.

This search resulted in a procedure that allowed for the formation of **2** directly from **1**. This was achieved by reacting N,N'-dimethylaminoethanol with n-BuLi in toluene at 0 ^{o}C: addition of **1** generated a cyclic intermediate which directed lithiation to the 2-position of the pyridine ring. N,N'-dimethylacetamide then acted as the electrophile and source of acyl group, subsequent hydrolysis then afforded **2.** This new method not only improved upon the yield obtained from the Grignard reaction (30% instead of 11%), but also removed two steps from the synthetic route, enhancing the global yield and reducing the amount of time needed for the synthesis.

The remaining transformations are the same as the previously carried out by the group.[4] **2** was reacted with N,N'-dimethylformamide-dimethylacetal to form **3,** then reaction of **3** with hydrazine monohydrate in a ring closing reaction yielded the pyrazole **4,** OTBDMS-PyPz (Scheme 2).

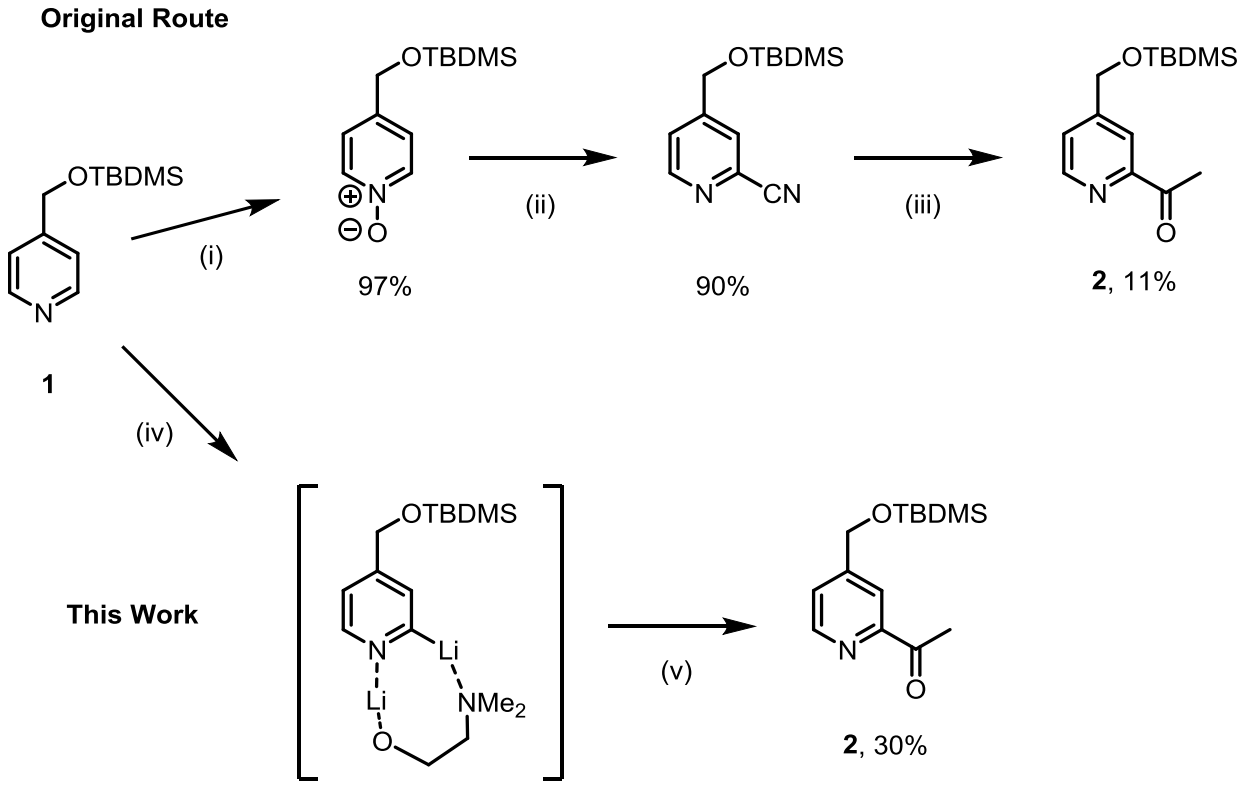

Scheme 1 – Synthetic routes, original and new, to **2**; i) mCPBA, CH_2Cl_2; ii) dimethylcarbamoyl chloride, trimethylsilylcyanide, CH_2Cl_2; iii) MeMgBr, aq. ammonium chloride, 0 °C; iv) N,N'-dimethylaminoethanol, nBuLi, Toluene, 0 °C; v) dimethylacetamide, H_2O.

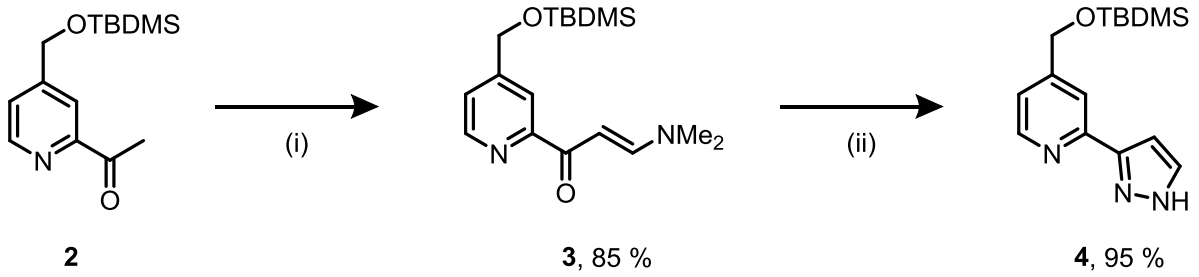

Scheme 2 - Synthetic route from **2** to **4**: i) DMF-DMA, 90 °C; ii) $N_2H_4 \bullet H_2O$, EtOH, 60 °C.

Synthesis of 1,5-bis(bromomethyl)naphthalene (6)

The $L_w^{1,5\text{-naph}}$ ligand consists of a naphthalene aromatic spacer with PyPz units attached at the 1 and 5 positions via methylene links. This uses 1,5-dimethylnapthalene as the source of the spacer group. However, the cost of purchasing 1,5-dimethylnapthalene had become relatively expensive (approx. £125 /g), the requirement for sizeable amounts of 1,5-dimethylnapthalene led to a need for a cheaper synthetic approach to obtaining the compound.

A potential starting material was 1,5-dimethyltetralin, it is both similar in structure in to 1,5-dimethylnaphthalene and much cheaper to buy from suppliers. It is known that CH_2 groups adjacent to carbocations can be deprotonated to form alkenes, typically this is a dehydration - loss of a $–OH_2$ using H_2SO_4. Lack of a hydroxyl group means this will not work for 1,5-dimethylnaphthalene, but a similar reaction should occur if a hydride ion were able to be abstracted.

The triphenylmethyl (trityl) cation is a known hydride abstracter, so this was used in an effort to generate a carbocation on 1,5-dimethyltetralin. The trityl cation was generated by reacting triphenyl methanol with triflouoroacetic acid, affording a deep yellow solution characteristic of the trityl cation (Fig. 2.2.1). Reaction with 1,5-dimethyltetralin and a basic work up yielded the desired 1,5-dimethylnapthalene in 90% yield (Scheme 3) and importantly at a lower cost than purchasing the product directly from suppliers.

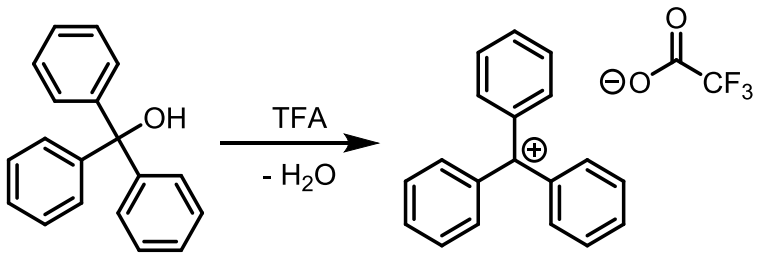

Figure 2.2.1 – Generation of the trityl cationby reaction of TFA with triphenyl methanol.

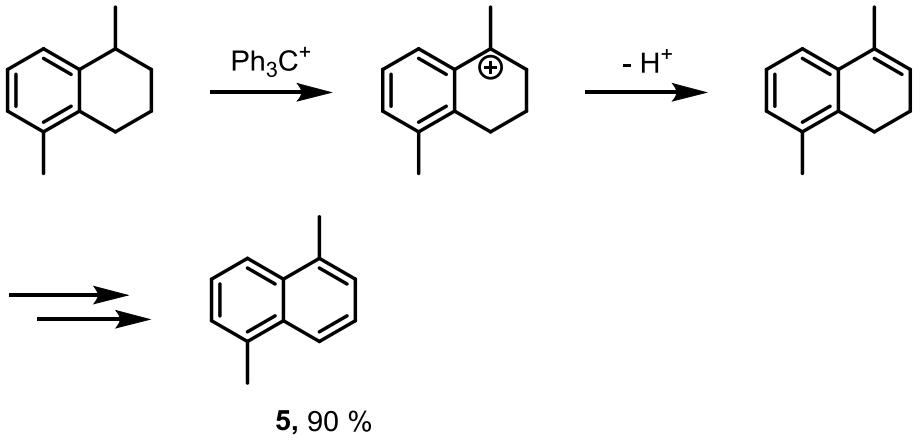

5, 90 %

Scheme 3 – Proposed mechanism for the synthesis of **5** from 1,5-dimethyltetralin

1,5-dimethylnaphthalene was then brominated via a radical reaction using N-bromosuccinimide, AIBN, in CH_2Cl_2 under irradiation by a tungsten lamp. Irradiation was applied for two hours to avoid "over-brominating" one or both methyl groups (Scheme 4).

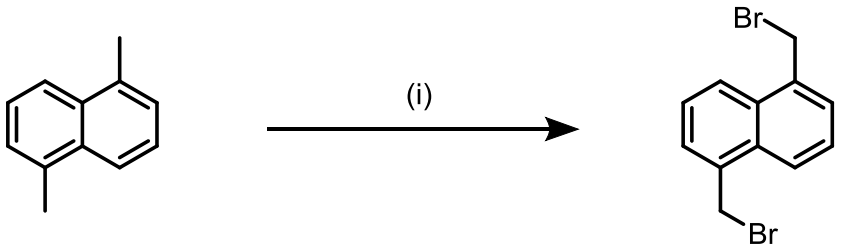

5 **6**

Scheme 4 – Synthesis of **6** from **5**; i) n-bromosuccinimide, AIBN, CH_2Cl_2, hv, 95%.

Synthesis of $L_w^{1,5\text{-naph}}$

The remaining steps towards the synthesis of $L_w^{1,5\text{-naph}}$ remained unchanged from that previously reported. Two equivalents of **4** was reacted with a single equivalent of **6** in a nucleophilic substitution reaction, with THF as the solvent and NaH as base, to give **7** with a yield of 60% (Scheme 5) . This is followed by deprotection of the silyl ether groups by tetrabutylammonium fluoride in THF at room temperature to afford the target ligand, $\mathbf{L_w^{1,5\text{-naph}}}$.

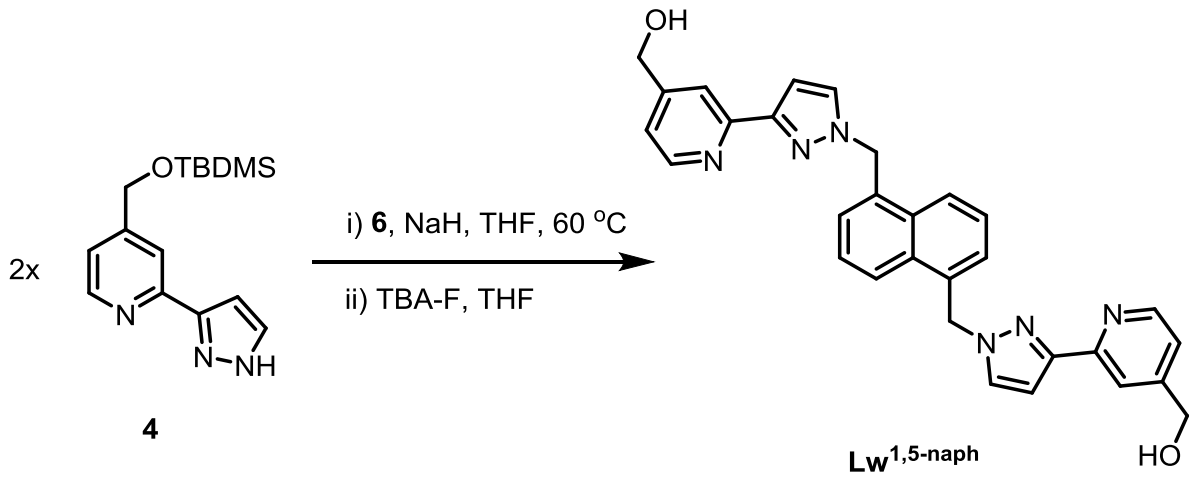

Scheme 5 – Synthesis of Lw1,5-naph from **4** and **6**: i) NaH, THF, 60°C; ii) tetrabutylammonium fluoride, THF.

2.2.2 Assembly of the $[Cd_8(L_w^{1,5\text{-naph}})_{12}](X)_{16}$ cages

The assembly of the cages was performed by either refluxing the components in methanol for 24 hours or by solvothermal synthesis in a Teflon-lined autoclave. The ligand ($L_w^{1,5\text{-naph}}$) and the Cd(II) salt (either BF_4^- or NO_3^-) were combined in a L3:M2 ratio to fully satiate the available coordination sites of both ligand and the metal.

The solvothermal synthesis was performed with an added amount of methanol, acetonitrile or nitromethane; the sealed autoclave was then heated to and held at 100 ^oC for 12 hours after which it was cooled slowly (0.1 $^oC\ min^{-1}$) in an attempt to promote crystallisation - unfortunately this method yielded no crystals. The resulting cloudy solutions from both methods were evaporated to dryness and the residue the washed with DCM, chloroform, diethyl ether and sparing amounts of cold methanol to remove any unreacted starting materials.

The formation of the cage was confirmed by a number of NMR experiments and mass spectrometry studies.

2.2.3 Characterisation of $[Cd_8(L_w^{1,5\text{-naph}})_{12}](NO_3)_{16}$

A 500 MHz ^{1}H NMR spectrum of $[Cd_8(L_w^{1,5\text{-naph}})_{12}][NO_3]_{16}$ (Fig. 2.2.2) shows the presence of two independent ligand environments each showing no internal symmetry, as expected of the S_6 symmetric structure – resulting in 48 independent ^{1}H signals. The diastereotopic CH_2 groups adjacent to the naphthyl units are expected to rise to a set of four pairs of doublets, and this is confirmed by a COSY spectrum; the pairs of doublets are labelled on the 500 MHz spectrum.

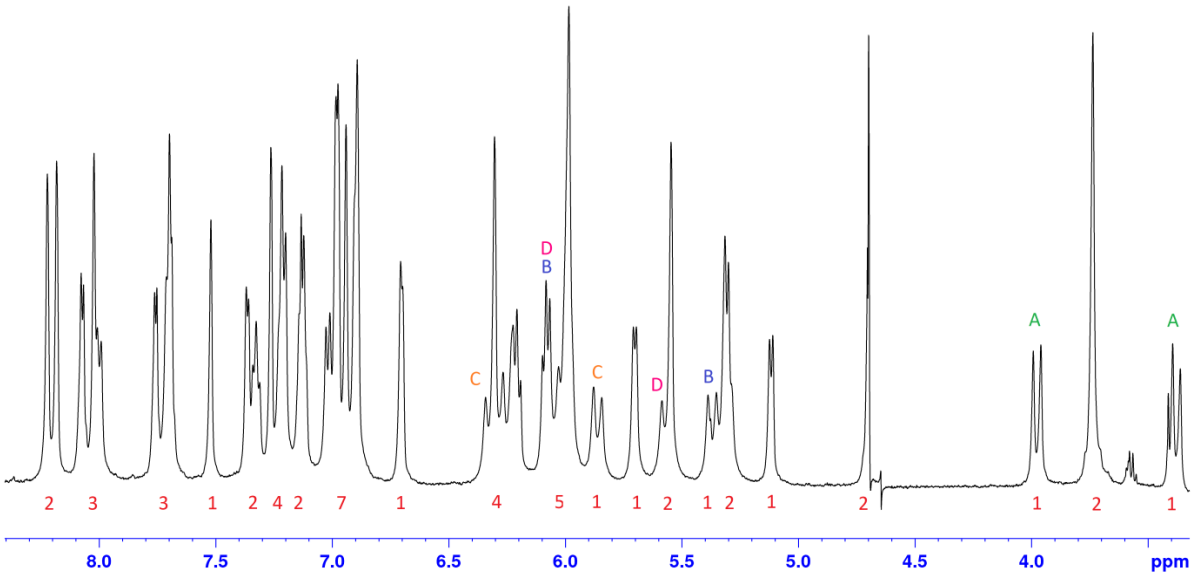

Figure 2.2.2 – 500 MHz ^{1}H NMR spectrum of $[Cd_8(L_w^{1,5\text{-naph}})_{12}](NO_3)_{16}$ in D_2O at 298 K, integrals are included under the signals. Letters refer to pairs of the diastereotopic CH_2 groups.

The S_6 symmetric structure of the cage also results in the presence of two equivalent *fac* tris-chelate Cd(II) centres, and six equivalent *mer* tris-chelate Cd(II) centres. This generates a 3:1 *mer* to *fac* relationship that can be seen in the ^{113}Cd NMR spectrum of $[Cd_8(L_w^{1,5\text{-naph}})_{12}](NO_3)_{16}$ which shows two signals in an approximately 3:1 ratio (Fig. 2.2.3).

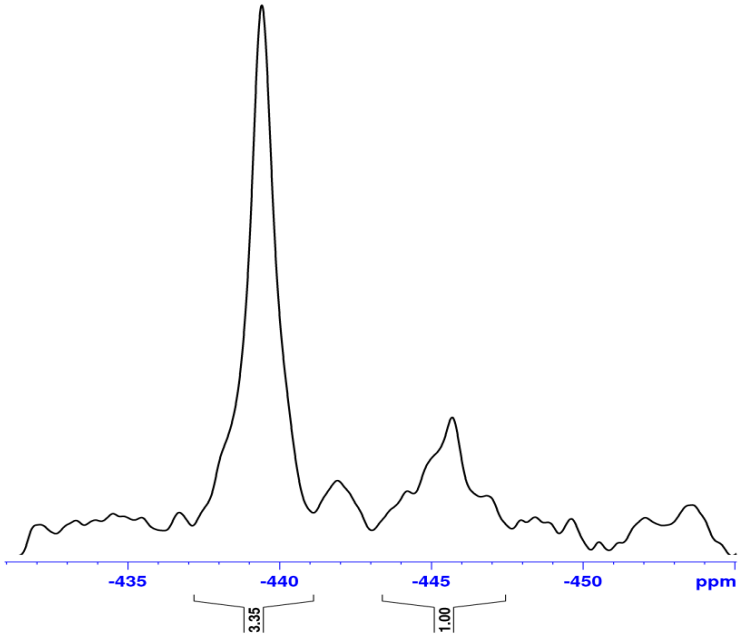

Figure 2.2.3 – ^{113}Cd NMR spectrum of $[Cd_8(L_w^{1,5\text{-naph}})_{12}](NO_3)_{16}$ in D_2O at 298K, signals are referenced to $Cd(ClO_4)_2$.

X-ray quality crystals were grown by the vapour diffusion of di(isopropyl) ether into a solution of $[Cd_8(L_w^{1,5\text{-naph}})_{12}](NO_3)_{16}$ in DMF. The crystal structure (Fig. 2.2.4a) is, as expected, basically identical to that of the Co(II) analogue.[4] Regardless of slightly longer metal–N distances as a result of the larger ionic radius of Cd(II) compared to Co(II), the Cd–Cd separations along the edges of the cage are comparable to the Co–Co separations in the Co(II)-based cubes. Two DMF guest molecules can be seen within the central cavity, whose carbonyl groups are directed into the H-bond donor pockets associated with the internal surface of the cage around the two facial tris-chelate metal sites (Fig. 2.2.4b).[5] Every face of the cube has a nitrate anion associated with the window in the face centre, with the anion forming a set of CH•••O interactions with the surface of the cage (Fig. 2.2.4c).

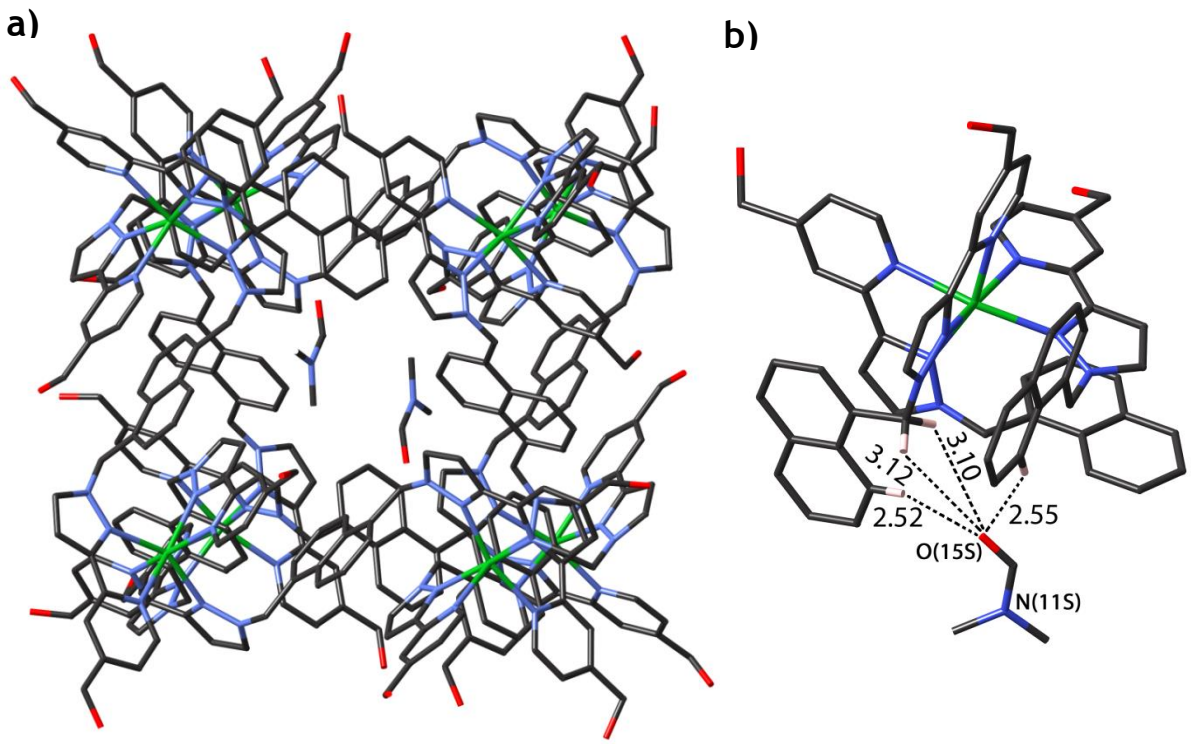

Figure 2.2.4 – Three representations of the crystal structure of $[Cd_8(L_w^{1,5\text{-naph}})_{12}](NO_3)_{16}$ •13(DMF)•2(H_2O). a) A wire-frame view of the cage showing the occupation of the central cavity by two DMF molecules. b) An enhanced view of one of the facial tris-chelate vertices showing one bound DMF guest molecules, with the four shortest CH•••O contacts shown, distances are shown in Å. (Cd, green; O, red; N, blue; C, black).

The UV/vis absorption and steady-state fluorescence spectra are shown in figures 2.2.5 and 2.2.6 respectively. The fluorescence spectrum of $[Cd_8(L_w^{1,5\text{-naph}})_{12}][NO_3]_{16}$ shows a weak maximum at *ca.* 330 nm which is attributed to 'normal' fluorescence of the naphthalene unit; the more intense lower energy, broad peak is ascribed to a exciplex-like emission from an excited state which involves the extensive π-stacking between the alternating electron-rich naphthyl units and the electron-deficient pyridyl-pyrazole units.[6] This phenomenon has previously been observed for $[Cd_8(L^{1,5\text{-naph}})_{12}]$ (BF_4) in MeCN,[3] however the exciplex-like signal is much more apparent in aqueous solution. The lifetime of the peak centred at 400 nm fits a two-exponential decay with values of 4 ns and 10 ns with a quantum yield of 8 % (aerated H_2O, vs. $[Ru(bipy)_3]Cl_2$). 10 ns is about what is expected for the decay of a naphthalene singlet state, which leaves the shorter decay as a characteristic of the exciplex-like emission.

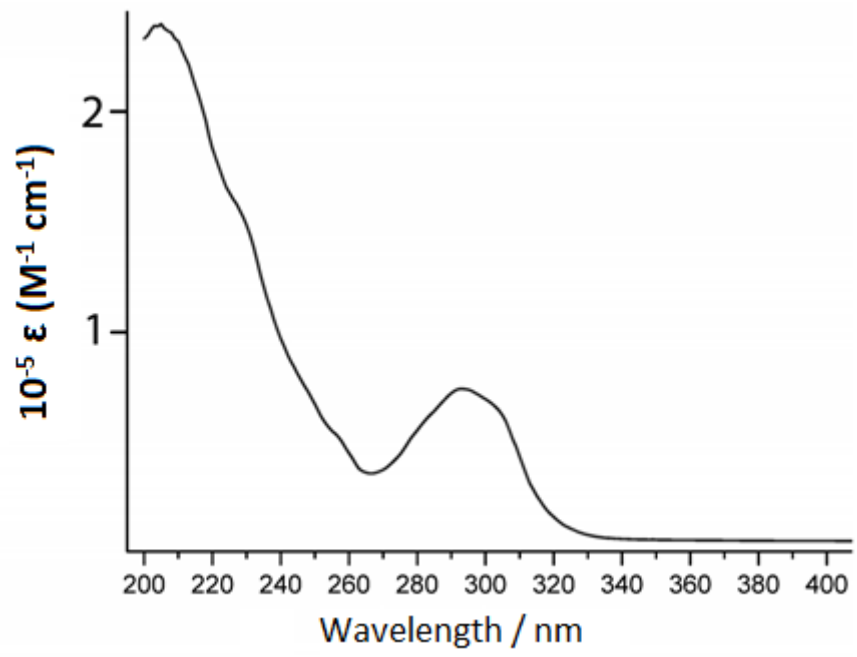

Figure 2.2.5 - UV/Vis absorption spectrum of $[Cd_8(L_w^{1,5\text{-naph}})_{12}](NO_3)_{16}$ in H_2O

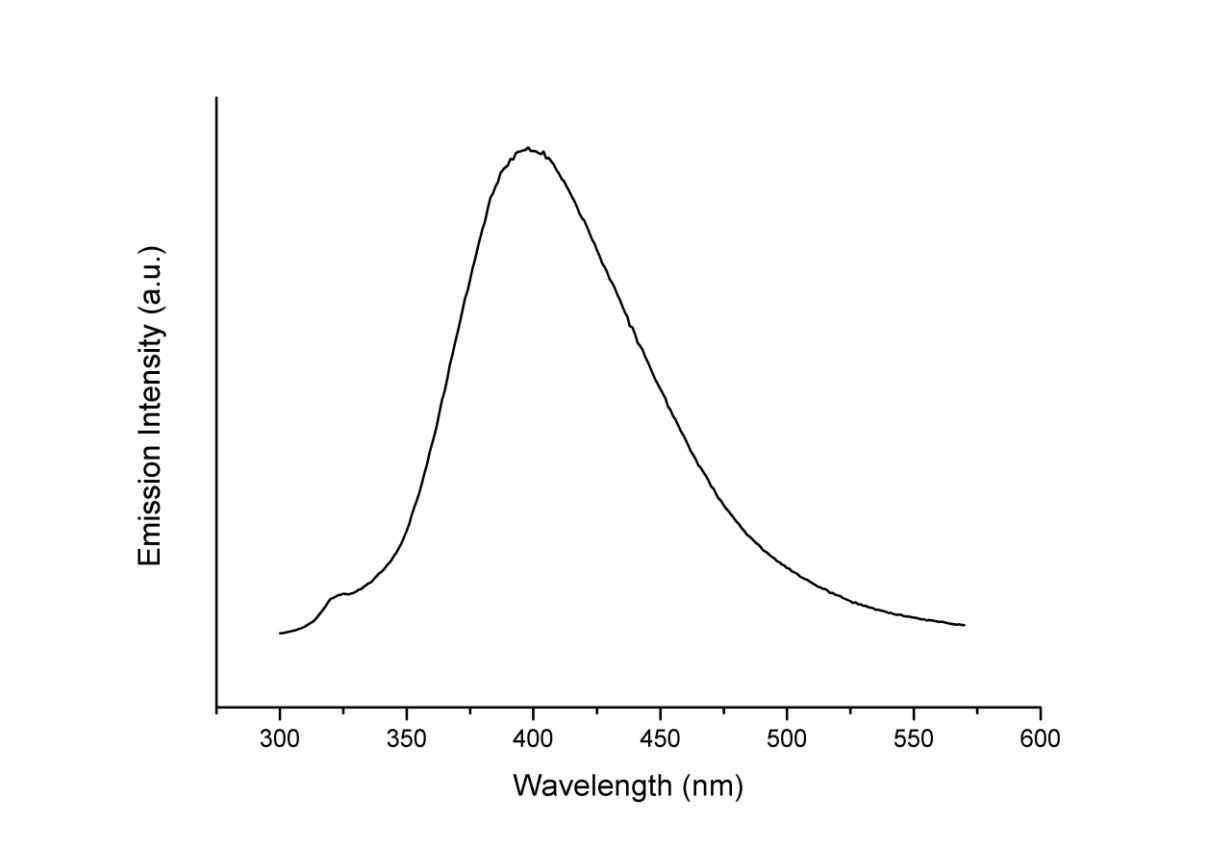

Figure 2.2.6 - Luminescence spectrum of $[Cd_8(L_w^{1,5\text{-naph}})_{12}](NO_3)_{16}$ in H_2O at 298 K with excitation wavelength set at 290 nm.

2.3 Effects of guest binding on cage photophysics.

2.3.1 Photo-innocent guest molecules

A number of organic molecules are known to bind within the cavity of the isostructural $[Co_8(Lw^{1,5\text{-naph}})_{12}]^{16+}$ cage, measured by ^1H NMR titrations. Therefore, to determine whether guests bound in the same manner within the Cd(II) cage and whether there was any change in the photophysical properties of the cage, it was prudent to study guest molecules from these same studies.

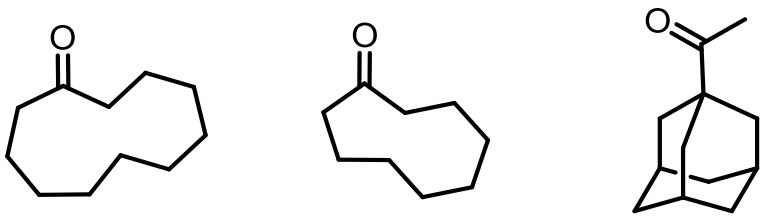

G1 **G2** **G3**

Initially to investigate the potential effects that guest binding would have on the luminescence of the $[Cd_8Lw^{1,5\text{-naph}}{}_{12}](NO_3)_{16}$ cage (from now on referred to as **H**), non-chromophoric and non-redox-active guests were studied as they would provide no or little complications to any results obtained. The first guest studied was cycloundecanone **G1** (an aliphatic cyclic ketone); titration of small amounts of **G1** into an aqueous solution of the **H** afforded the partial loss of **H** luminescence intensity (fig. 2.3.1). The sequential loss of the luminescence was fitted to a 1:1 binding isotherm allowing for the calculation of a binding constant, the determined value showed good agreement with what has previously been reported for the Co(II) cage (Table 1).

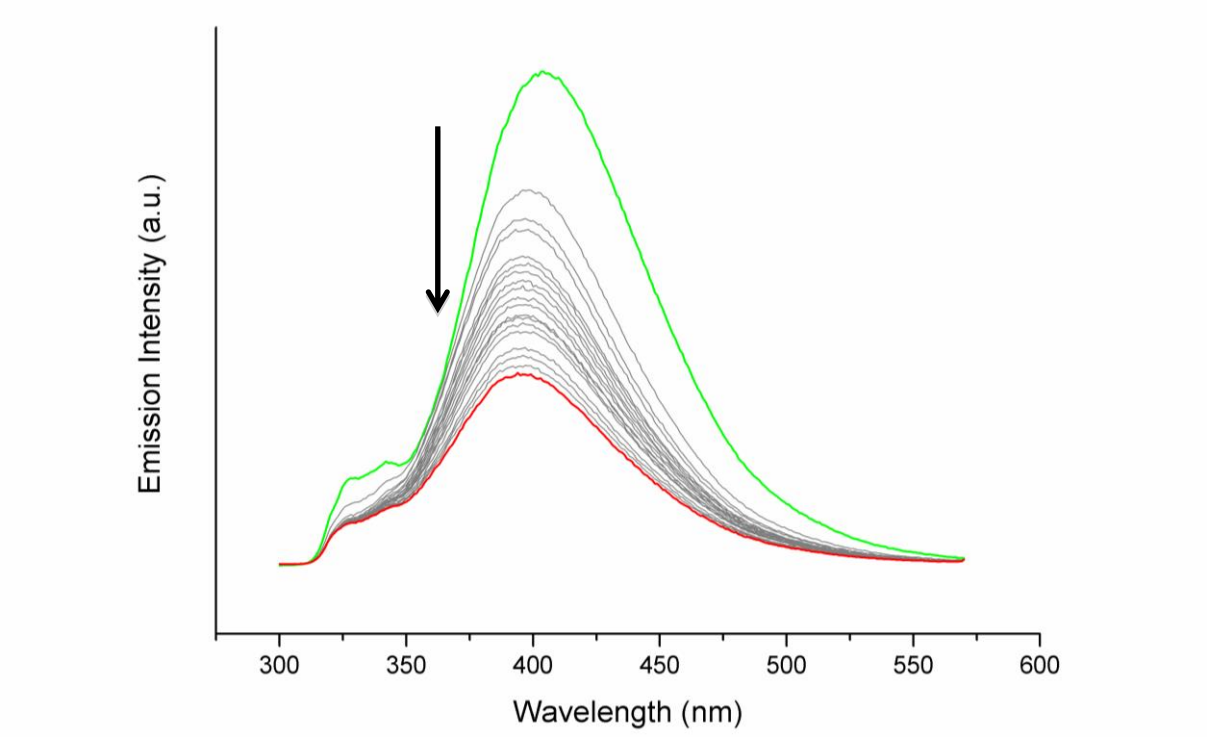

Fig. 2.3.1 – Luminsecence spectra recorded during the addition of 0 - 2000 µL **G1** (0.01 mM) into a solution of **H** (1 µM) in H_2O, excitation at 290 nm.

Cyclononanone **G2** is another cyclic ketone previously studied by the Ward group, structurally similar to **G1**. It has been shown that the number of methylene units in an alkyl chain has an effect on the binding constant of the guest molecules, therefore it was expected, should binding of **G2** be observed, that the binding constant lower than that of **G1.** Titration of **G2** (fig. A1.2.1 in appendix 1) into a solution of **H**, partial loss of **H** luminescence was again observed and fitting to a 1:1 binding isotherm showed, expectedly, a binding constant less than that of **G1** and is in agreement with the previously determined value for the Co(II) cage.

Guest	K / M^{-1}
Cycloundecanone (G1)	1.1×10^6
Cyclononanone (G2)	2.8×10^4
1-Adamantylmethylketone (G3)	3×10^4
1-hydroxypyrene (G4)	1.3×10^6
4-chloro-7-nitrobenzofurazan (G5)	1.4×10^4
4-amino-7-nitrobenzofurazan (G6)	4.4×10^3
4-(N,N'-dimethyl)amino-7-nitrobenzofurazan (G7)	6.0×10^3
4-nitro-2,1,3-benzothiadiazole (G8)	2.2×10^4
2-amino-6-nitrobenzothiazole (G9)	2×10^3
1,2,4,5-tetracyanobenzene (G10)	1.3×10^4
1,4-naphthoquinone (G11)	1.5×10^4
3,4,5,6-tetrachloro-1,2-benzoquinone (G12)	2.9×10^4

Table 1 – Binding constants (M^{-1}) at 298 K for the host/guest complexes studied. Binding isotherms for guest can be found in herein or in appendix 1.

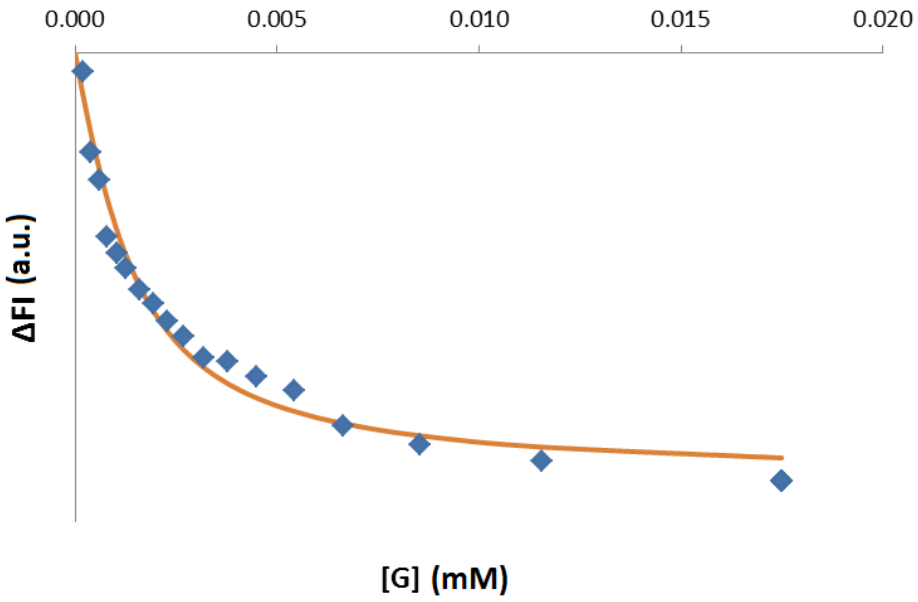

Fig. 2.3.2 – Plot of the changes in cage **H** fluorescence vs. the concentration of added guest **G1**, fitted to a 1:1 binding isotherm.

To study the effects of more rigid guest molecules on the luminescence of **H**, 1-adamanytlmethylketone **G3** was studied. Conversely, rather than observing a quenching of **H** luminescence, titration of **G3** into a solution of **H** resulted in the enhancement of **H** luminescence (Fig. 2.3.3). Nevertheless, the fitting of this luminescence change to a binding isotherm produced a binding constant again comparable to one measured previously. This means that the luminescence enhancement is directly related to the binding of **G3.**

The changes in **H** luminescence upon binding of the guests **G1, G2** and **G3** can be ascribed to the mechanical effects that each guest imparts to the system. The flexibility of **G1** and **G2** provide additional vibrational modes, facilitating an increased number of non-radiative deactivation pathways, whereas the much more rigid **G3** has the opposite effect; inducing additional rigidity in the cage structure and hence making non-radiative deactivation less likely. These non-chromophoric and photophysically inactive guests could not be participating in photoinduced energy- or electron-transfer with the cage so such mechanical effects are the only way to explain the luminescence intensity changes.

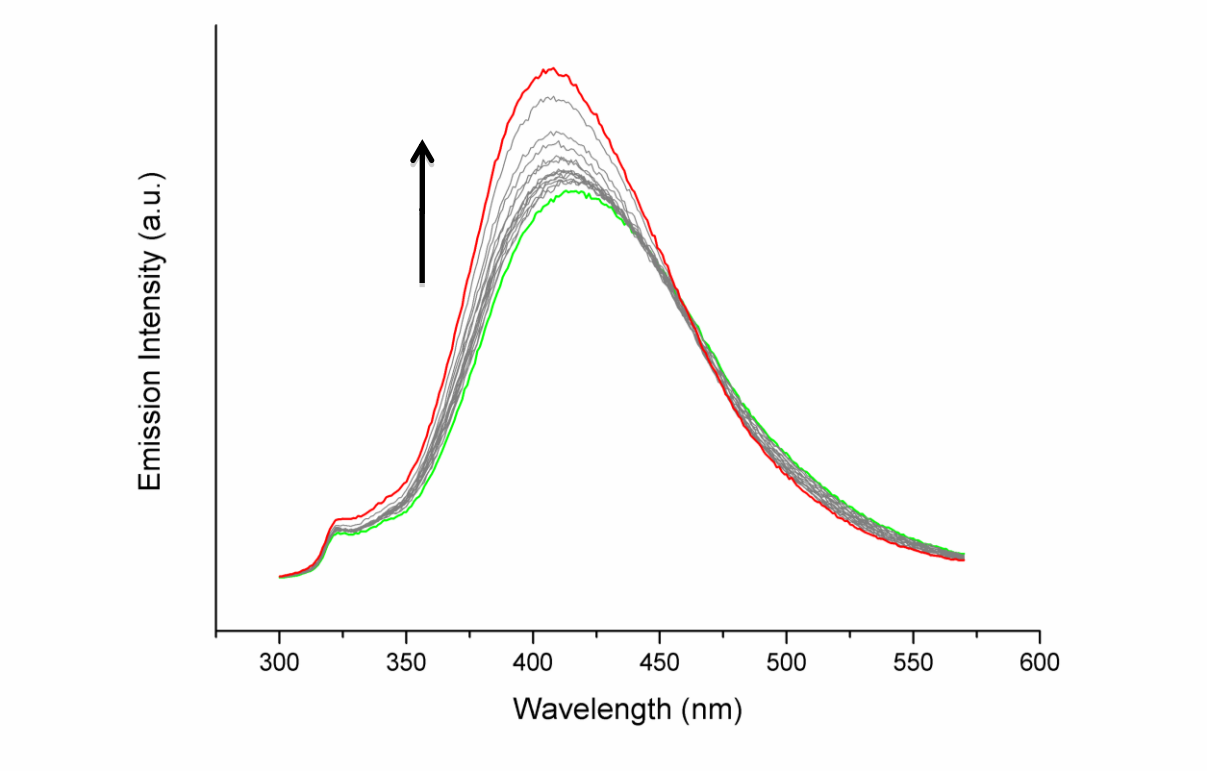

Fig. 2.3.3 - Luminescence spectra recorded during the addition of 0 - 2000 µL **G3** (0.1 mM) into a solution of **H** (0.01 mM) in H_2O, excitation at 290 nm.

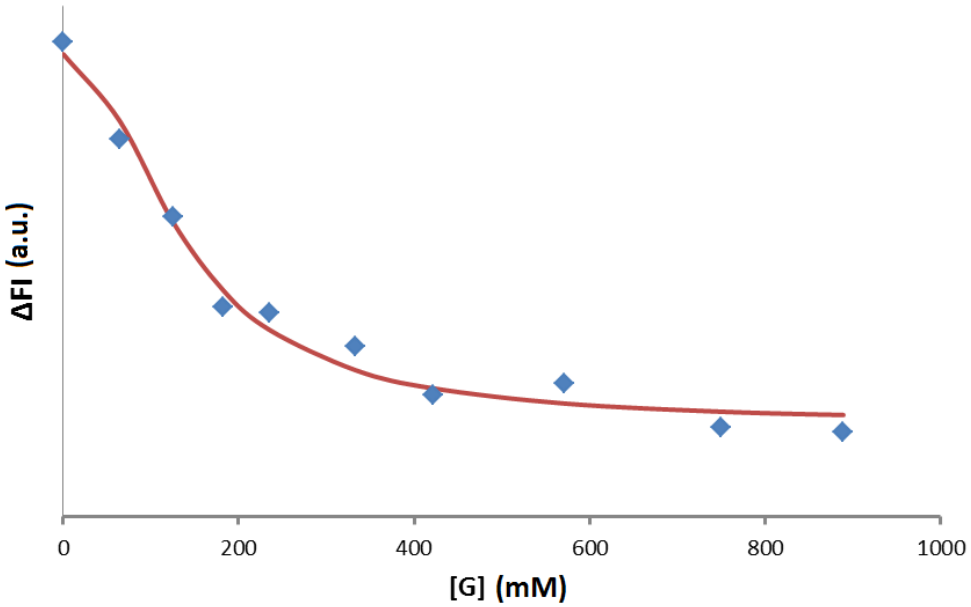

Fig. 2.3.4 - Plot of the changes in cage **H** fluorescence vs. the concentration of added guest **G3**, fitted to a 1:1 binding isotherm.

2.3.2 Photoactive guest molecules

Now that it had been shown that **H** could reliably signal the binding constants of guest molecules by change in **H** fluorescence, study moved to the effect of binding more "photo-interesting" molecules. **H** has the capacity to act as an energy or electron donor from its excited state. The singlet excited state of naphthalene has energy of roughly 4 eV[7–9] and consequently can act as an energy donor to any species possessing lower energy excited states. The excited state of naphthalene is also oxidised to its radical cation relatively easily meaning the excited state is also a strong electron donor, known to undergo PET to various electron-acceptor quenchers.[10–12]

At room temperature **H** displays a broad fluorescence at *ca.* 400, but at 77K in EtOH/MeOH glass this shifted blue-shifted to 350 nm, indicating that an excited-state energy of about 28 500 cm^{-1} is available (Fig. 2.3.5).

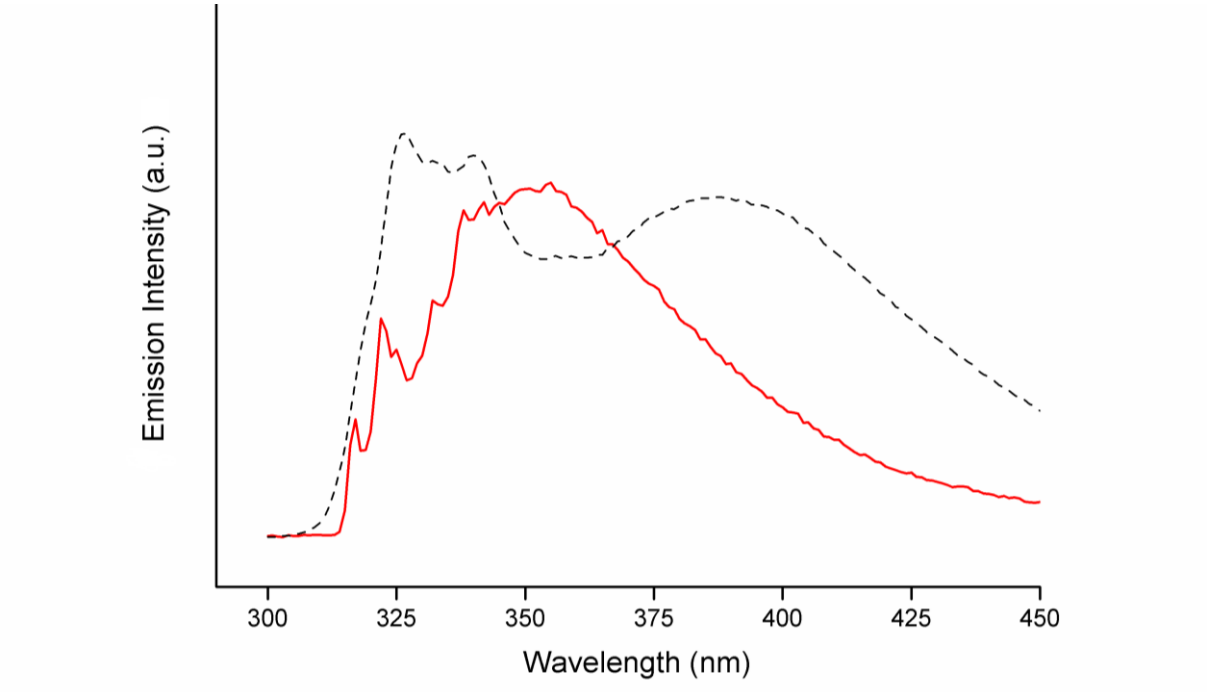

Fig. 2.3.5 – Luminescence spectra of cage **H**: 77 K in 4:1 EtOH/MeOH glass (red), and 298 K in 4:1 EtOH/MeOH(Black).

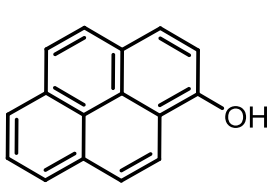

G4

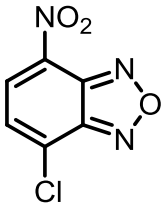

G5

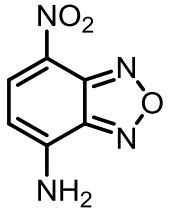

G6

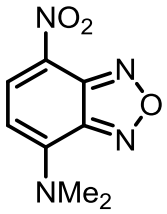

G7

G8

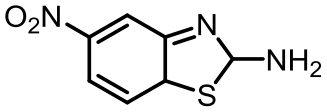

G9

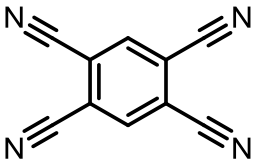

G10

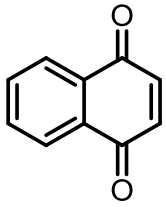

G11

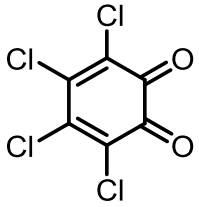

G12

The next guest, **G4**, is a substituted pyrene. Since it is known that naphthyl to pyrenyl photoinduced energy transfer can occur,[13] it was expected that the uptake of **G4** into **H** would provide an example of PEnT from the array of naphthyl chromophores of the host to the bound pyrene guest, potentially resulting in sensitised emission from the pyrene. The titration of **G4** in to a solution **H** provided a change in **H** luminescence that when plotted gave a high binding constant of $1.3 \times 10^6\ M^{-1}$, where again is in good agreement with previous observations. Upon binding of **G4** the standard broad fluorescence centred at 400 nm diminished in intensity and was replaced by growing sharp, structured features which are characteristic of pyrene fluorescence (Fig. 2.3.6).

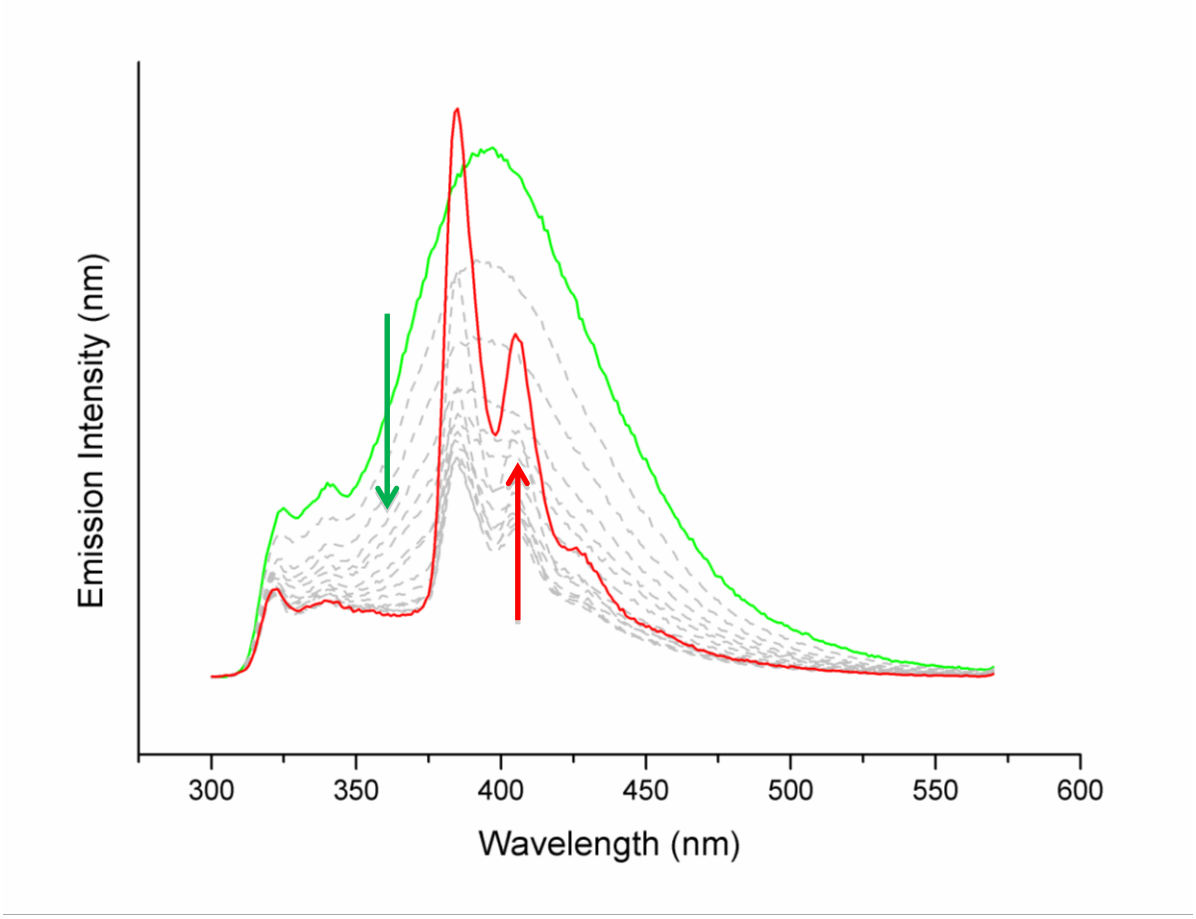

Figure 2.3.6 – Luminsecence spectra recorded during the addition of 0 - 2000 µL **G4** (0.01 mM) into a solution of **H** (1 µM) in H_2O, excitation at 290 nm.

The question was now whether the **G4** based emission arises due to PEnT from the host or via direct excitation of **G4** as the concentration of the guest increases throughout the titration. The first piece of evidence was the progressive quenching of the naphthyl-based fluorescence, associated with free **H**, throughout the titration. The second piece of evidence arose from the fact that the excitation wavelength during the titration was 290 nm, if we compare the absorption spectra for both **H** and **G4** (fig. 2.3.7) we see that at 290 nm: the array of **H** naphthyl fluorophores absorb strongly (ε = 55 000 M^{-1}) but 1-hydroxypyrene absorbs comparatively weakly (ε = 1400 M^{-1}). The fact that **H** is roughly 39 times more absorbing at 290 nm than **G4** and that the level of intensity of the fluorescence from **G4** is so large that it is unlikely to be accounted for by direct excitation.

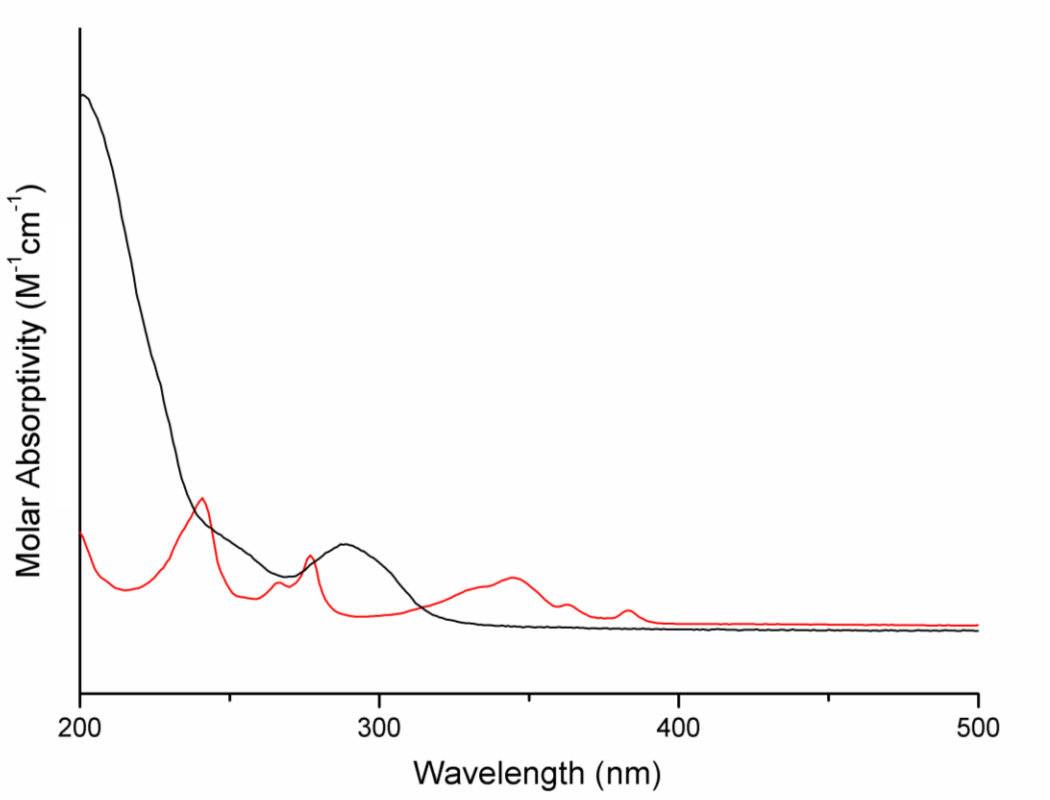

Figure 2.3.7 – Absorbance spectra of **H** (black) and 1-hydroxypyrene **G4** (red) in H_2O.

Subsequently, if we look at the excitation spectrum of **G4** (fig. 2.3.8) at 385 nm, the emission maximum, we can see that there is very little emission as result of excitation at 290 nm – the same wavelength at which the titrations were excited. Then if an excitation spectrum is measured of the **H•G4** host-guest complex at the end of the titration we can see that there is now a significant amount of emission at 385 nm due to excitation at 290 nm. Since a significant amount of emission at 385 nm is only observed while there is the presence of **H,** this provides evidence for PEnT occurring between host and guest resulting in the sensitisation of fluorescence from **G4**.

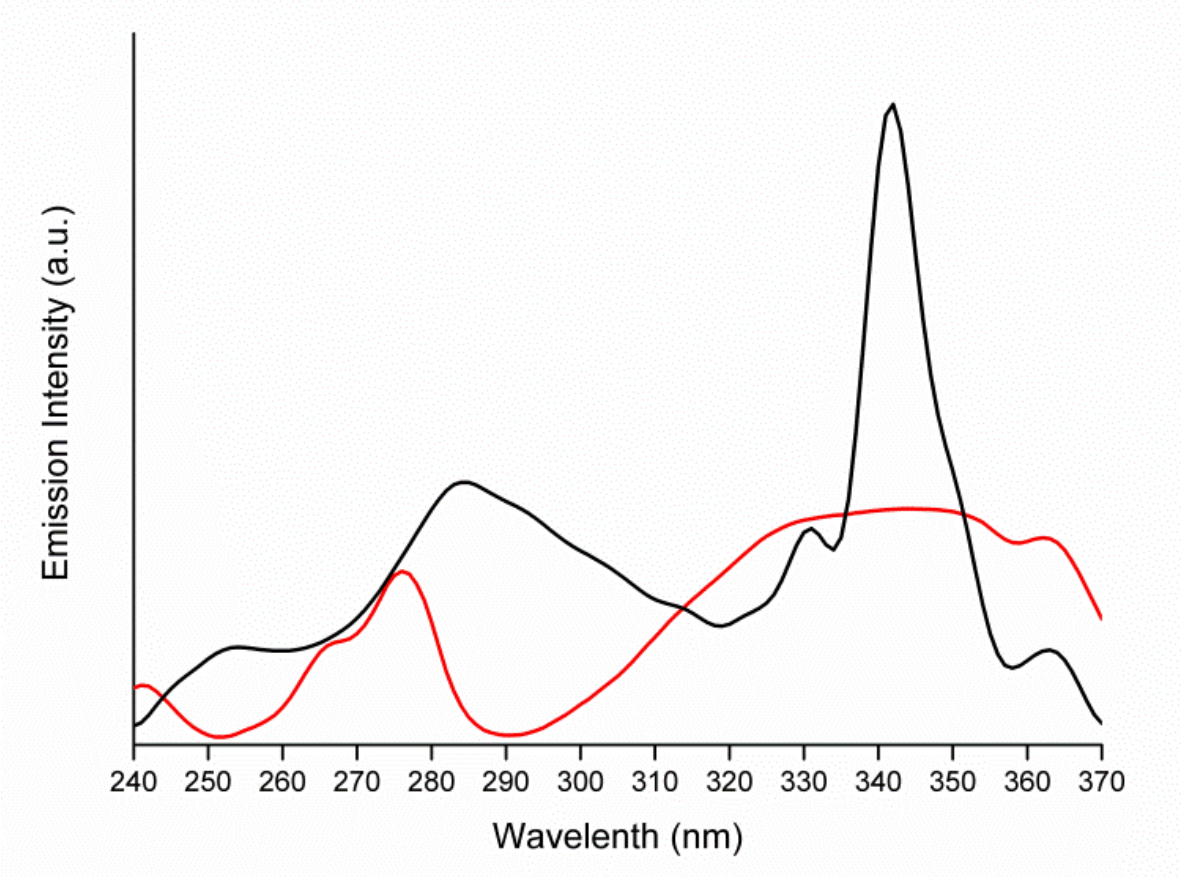

Fig. 2.3.8 – Excitation spectra of the **H•G4** cage/guest complex (black) and **G4** in the absence of cage (red). Emission measured at 385 nm in H_2O.

The final piece of evidence, and perhaps the most definitive, is a competition experiment, the addition of a new guest to a solution of **H•G4**. Adding a competing guest will displace an amount of **G4** from the host cavity and if there is PEnT occurring between **H** and **G4** there should be a diminishing of the **G4** fluorescence intensity. The guest that was utilised for the experiment was cycloundecanone (**G1**) – which is photophysically innocent under the experimental conditions and possesses a high binding constant. Addition of **G1** does indeed result in the loss of sensitised pyrene-based fluorescence as well as a slight restoration of cage-based fluorescence as **G1** displaces **G4** from the cage cavity (fig. 2.3.9). This provides definite confirmation that cage-to-guest PEnT is occurring in the **H•G4** assembly.

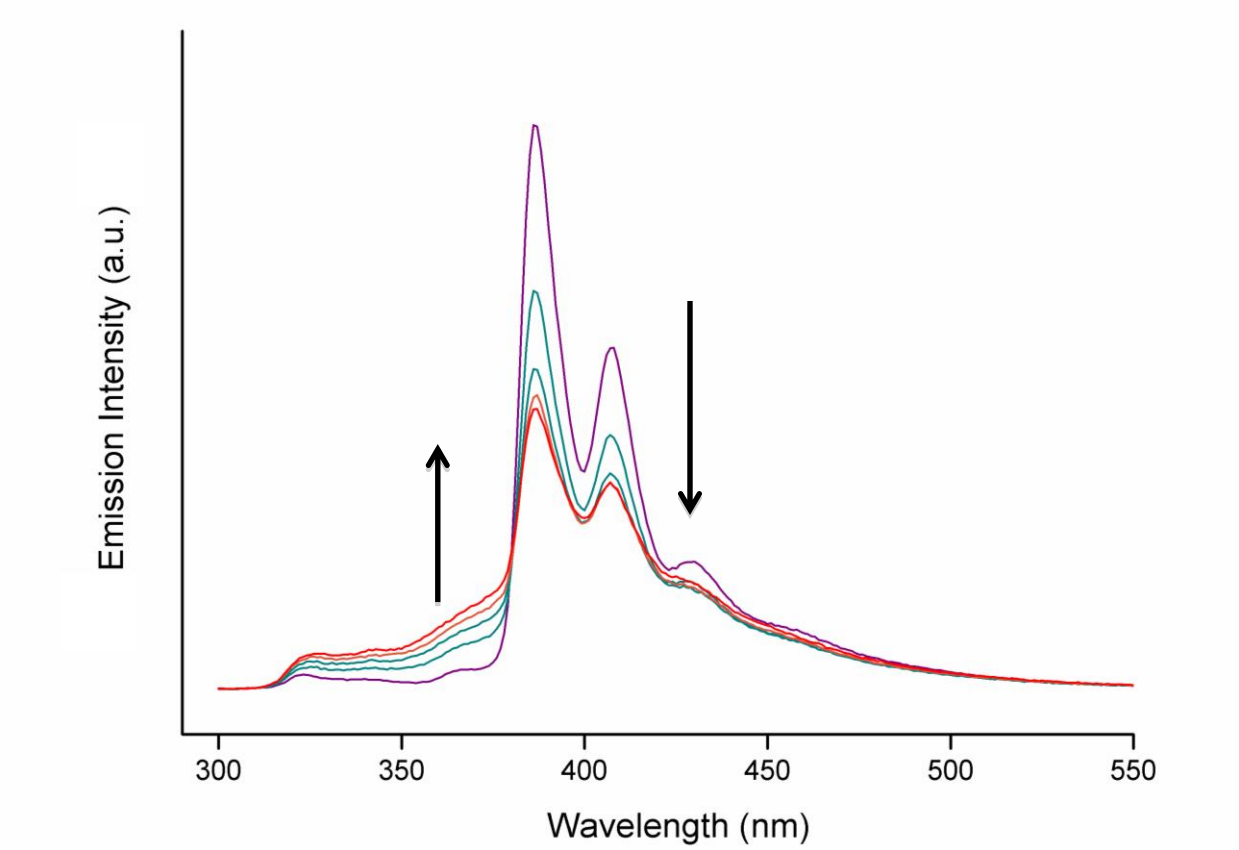

Fig. 2.3.9 – Loss of sensitised fluorescence from **G4** and restoration of **H** fluorescence following the addition of increasing equivalents (0.5 – 3.0 equivalents) of cycloundecanone to the **H•G4** complex in water.

Next, a series of benzofurazan-type structures were studied, these derivatives have been studied mostly as fluorescent sensors. This along with their size match for the host cavity provides a perfect set of photoactive molecules in which to study the effects of uptake of these molecules.

Titration of **G5** into **H** resulted in the complete quenching of the cage fluorescence (fig. A1.2.2 in appendix 1). Fitting the fluorescence change to a 1:1 binding isotherm yields a modestly strong binding constant (1.4×10^4), comparable to previously measured guests of similar molecular weight. Binding of **G5** was confirmed by a ^{1}H NMR binding study using the isostructural $[Co_8(Lw^{1,5\text{-naph}})_{12}]^{16+}$ cage. In comparison to the "photo-innocent" guests discussed earlier, the extent of quenching of the host's fluorescence suggests that the

mechanism of excited state deactivation is beyond that of simple mechanical effects. PEnT is the expected cause of the observed quenching effect as one of the requirements for PEnT is good amount of spectral overlap in donor emission and acceptor absorbance. As can be seen in fig. 2.3.10 there is an overlap between the **H** (donor) fluorescence and the absorbance of **G5** (acceptor), this shows there is the capacity for PEnT to occur. It is typically found that if PEnT occurs there is a reduction in the donor's emission lifetime, however the value of **H** lifetime at the end of the titration remained unchanged at 10 ns, though this was mostly due to residual luminescence from free **H** whose life will remain at 10 ns.

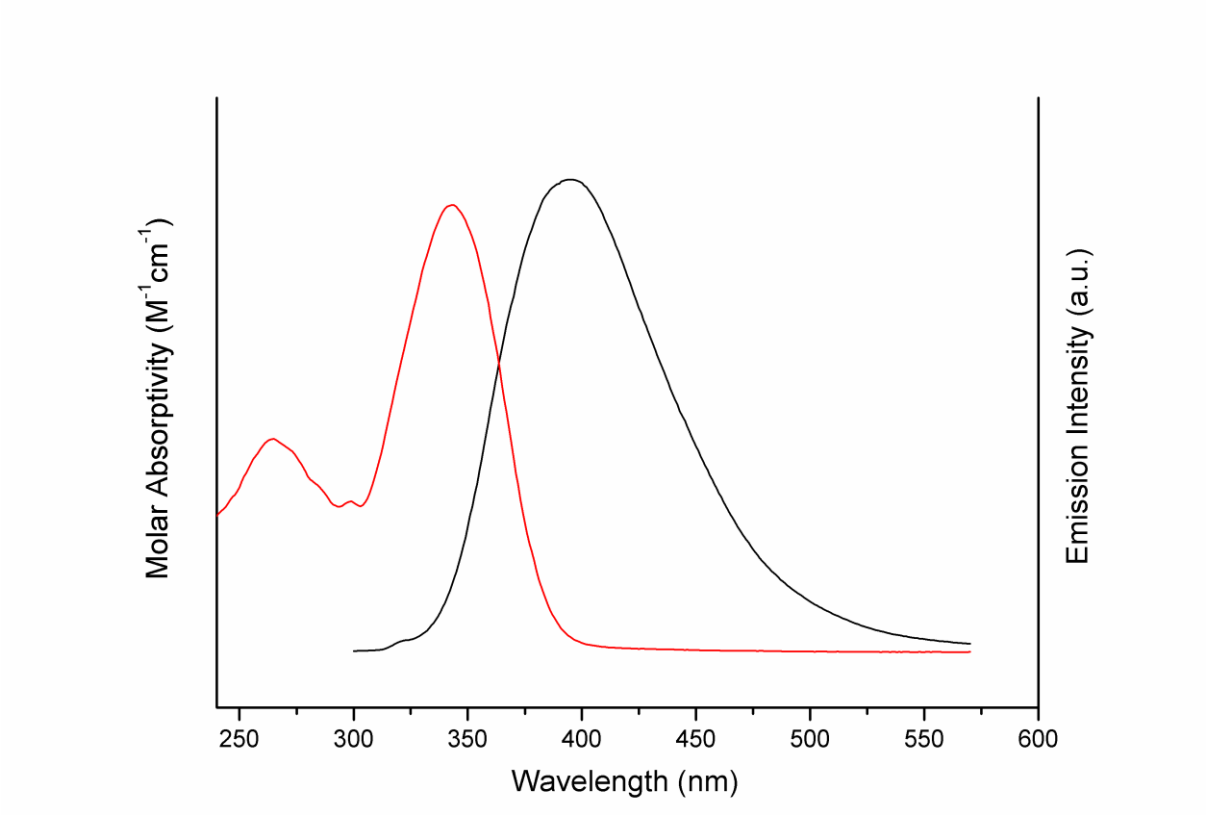

Fig. 2.3.10 – Spectral representation illustrating the spectral overlap of **G5** absorption (red) and **H** fluorescence (black).

Exchanging the Cl group on **G5** to an NH_2 group affords **G6** which is emissive, unlike **G5.** The fluorescence of **G6** lies in the green-yellow region (*ca.* 550 nm) in the visible spectrum; this should be easily distinguishable from the cage fluorescence. If PEnT from **H** to **G6** results in sensitised emission from the guest it is also likely that PEnT also occurred in the previous experiments between **H** and **G5**.

Fig. 2.3.11 shows the fluorescence spectra recorded during titration of **G6** into a solution of **H**, the expected quenching of cage fluorescence can be seen as well as the appearance of an emission at centred at 560 nm associated with the fluorescence of the guest. The measured (from cage quenching) binding constant is similar to that of **G5** (4.4×10^3) suggesting that **G6** is binding within the cage. Furthermore plotting the increase in fluorescence of **G6** at 560 nm to the binding isotherm affords the same binding constant value as obtained for the quenching of cage fluorescence, this suggests that emission of the guest is a result of it binding inside the cage. To prove whether the emission from **G6** is sensitised by the cage or not, a competition experiment was again performed, utilising **G1** as the competing guest. The addition of **G1** results in a decrease in fluorescence at 560 nm (fig. 2.3.12) meaning that emission from the bound guest is indeed undergoing sensitisation as a result of PEnT from the cage.

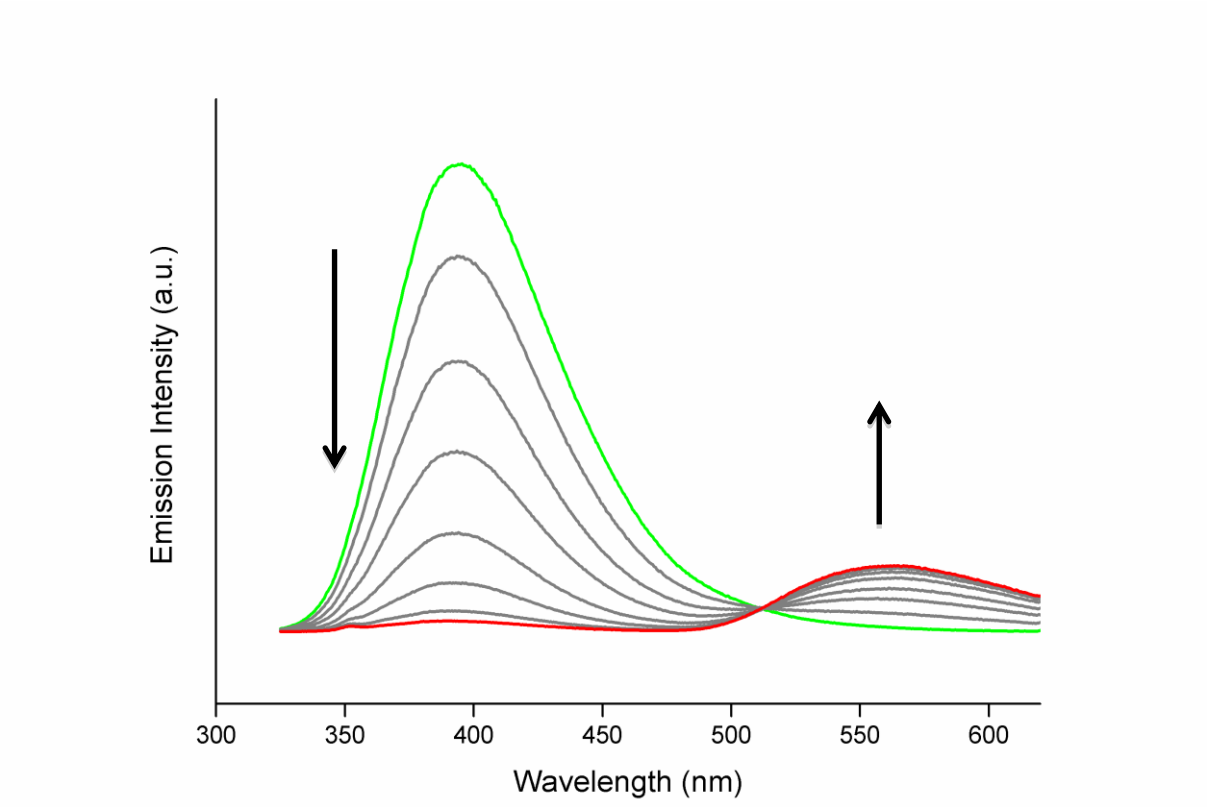

Fig. 2.3.11 - Luminsecence spectra recorded during the addition of 0 - 1500 µL **G6** (0. 1 mM) into a solution of **H** (0.01 µM) in H_2O, excitation at 290 nm.

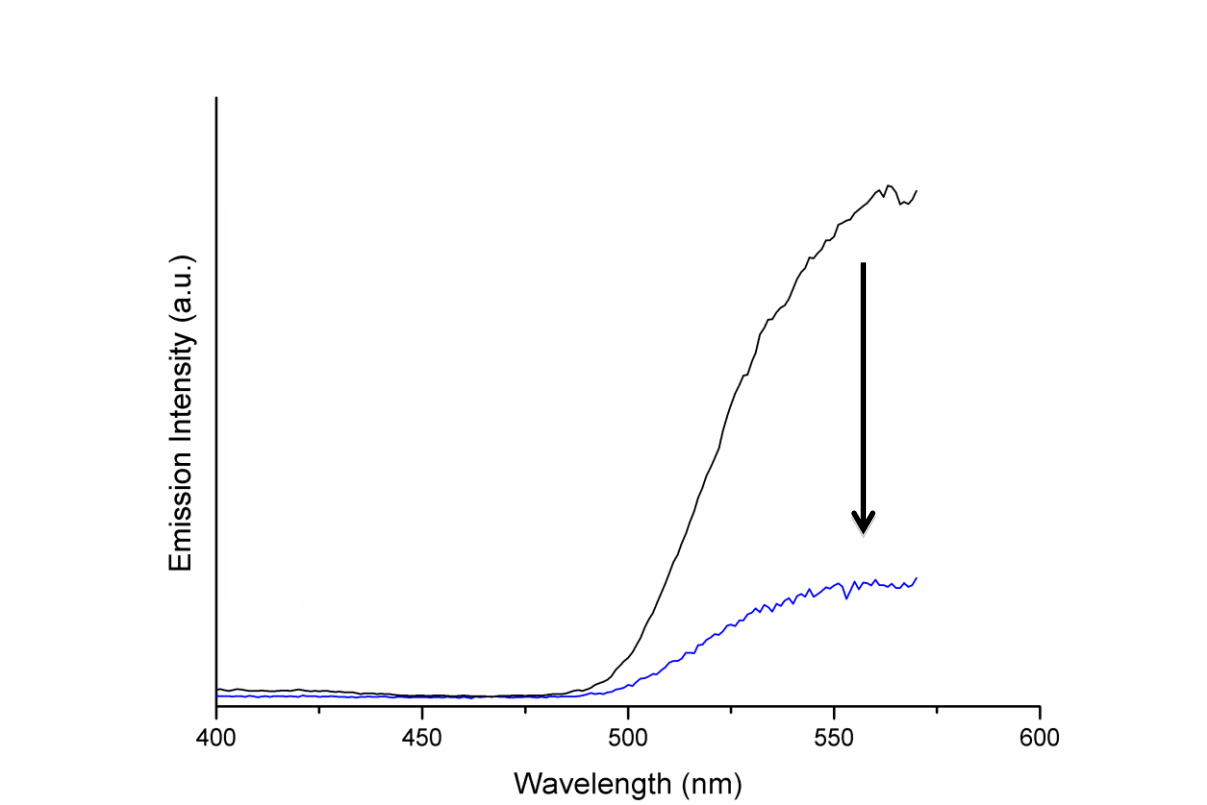

Figure 2.3.12 – Loss of **G6**-based fluorescence from the **H•G6** cage/guest complex (0.01 mM) upon the addition of 3 equivalents of cycloundecanone in H_2O, excitation at 290 nm.

As the quenching mechanism of the cage's fluorescence in the presence of **G6** can be accredited to photo-induced energy transfer it is reasonable to deduce that the quenching caused by **G5** is also most likely due to cage-to-guest PEnT.

G7 is structurally identical that of **G6** except that the amino group has been replaced by a dimethylamino group; the addition of methyl groups increases the hydrophobicity of the molecule, as shown by an increased binding constant when compared to **G6** ($7.7 \times 10^4\ M^{-1}$). Due the structural and photophysical similarities of **G7** with **G6**, the binding of **G7** likely results in cage-to-guest PEnT with consequent sensitised emission from the guest.

G8 and **G9** are both structurally similar to the series of benzofurazans, both also possess similar absorption spectra with maxima at 343 nm and 357 nm respectively. Both guests quench cage fluorescence when titrated into a solution of **H** (figures A1.2.3 and A1.2.4 in

appendix 1**)** most likely due to cage-to-guest PEnT, but due to both guests being non-emissive this could be proved directly.

The binding constant of **G8** is similar to that of **G5** and the binding constant for **G9** lies below that of **G6.** This allows for an order of binding strength for **G5 – G9: G5** > **G8** > **G7** > **G6** > **G9**. This order can be rationalised by comparing the effect of the functional groups on the hydrophobicity of the guests. The amino groups on **G6** and **G7** allow for some degree of hydrogen bonding with the solvent whereas **G5** and **G8** lack this capacity and consequently have a larger affinity for the hydrophobic environment of the cage cavity. In the case of **G9** there is no resonance structure that allows for the interaction of the NH_2 lone pair with the nitro group (results in unfavourable carbanions) whereas in **G6** and **G7** the lone pair and nitro group are conjugated (Fig. 2.3.13). As a result the lone pair in **G6** and **G7** is less available for hydrogen bonding with the bulk solvent, hence the stronger binding affinities compared to **G9.**

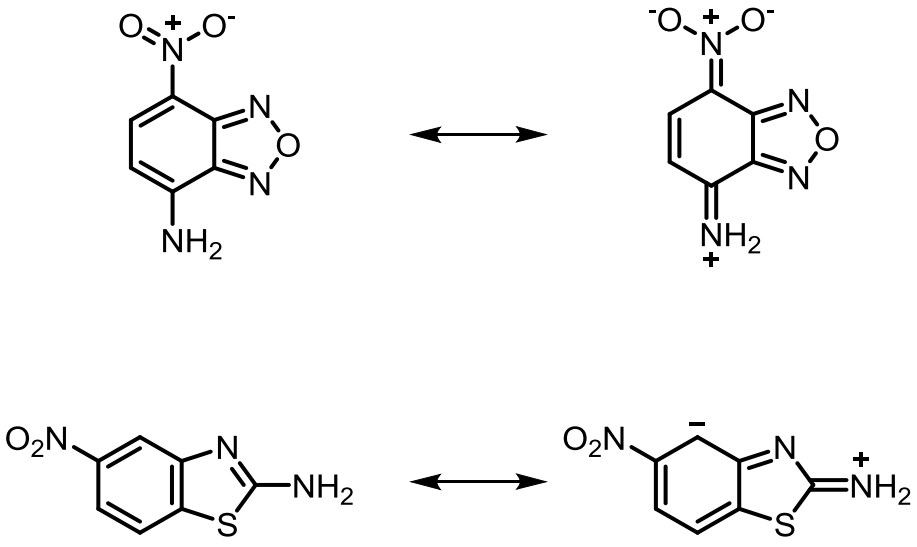

Figure 2.3.13 – Resonance forms of guests **G6** and **G9,** representing favourable delocalisation in **G6** and generation of an unfavourable carbanion in **G9**.

2.3.3 Photoinduced electron-transfer

To explore the potential of photoinduced *electron* transfer occurring between host and guest three strong electron acceptors **G10** - **G12** were studied. Each guest caused substantial quenching of the cage luminescence upon binding (Fig. 2.3.14); titration of **G10**, **G11** and **G12** yielded comparable binding constants of 1.3 x 10^4 M^{-1}, 1.5 x 10^4 M^{-1} and 2.9 x 10^4 M^{-1} respectively. Given the ease with which these guests can undergo a one electron reduction, the quenching can be tentatively ascribed to PET from the array of naphthalene groups to the guest bound in the cage cavity. PET would facilitate the generation of a charge-separated H^+/G^- pair. Utilising transient absorption spectroscopy should allow for detection of the characteristic spectroscopic signatures of radical species with measurement of the formation and decay kinetics of such charge-separated states.

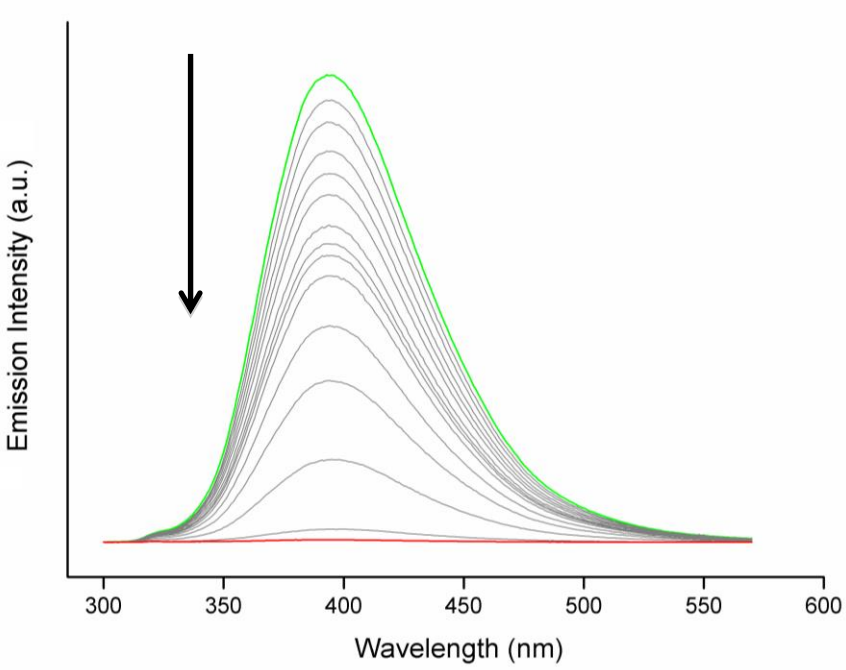

Figure 2.3.14 – Luminsecence spectra recorded during the addition of 0 - 2000 µL **G11** (0. 1 mM) into a solution of **H** (0.1 mM) in H_2O, excitation at 290 nm.

Femtosecond TA spectroscopy measurements[14] were performed on a system consisting of **H** and **G10** in water, the concentrations of which were 0.01 mM and 4.0 mM respectively. Based on the earlier reported binding constant of **G10**, the large excess of guest should

guarantee that the host is *ca.* 99% bound – the concentration of the host complex should be close to 0.01 mM. Control experiments of **H** on its own and of **G10** on its own were run under the same conditions.

Excitation of the aqueous solution of **H** at 290 nm with a 40 fs pulse, followed by measurement of the absorption spectra at a sequence of time delays up to 3 ns, generated differential TA spectra shown in Fig. 2.3.15. A broad positive signal appears across the region of interest, 320 nm to 550 nm, with a distinct band with slight vibronic structuring at *ca.* 400 nm. The shape of the band resembles the singlet-singlet excited state absorption of naphthalene, with the broadness being a result of delocalisation of the π-stacked array seen in the cage structure. A distribution of environments for ^{1}naph* along with the influence from the π-stacking affords complex decay kinetics, which fit well to a bi-exponential decay with half-life values of 32 (11) ps, and 1130 (150) ps.

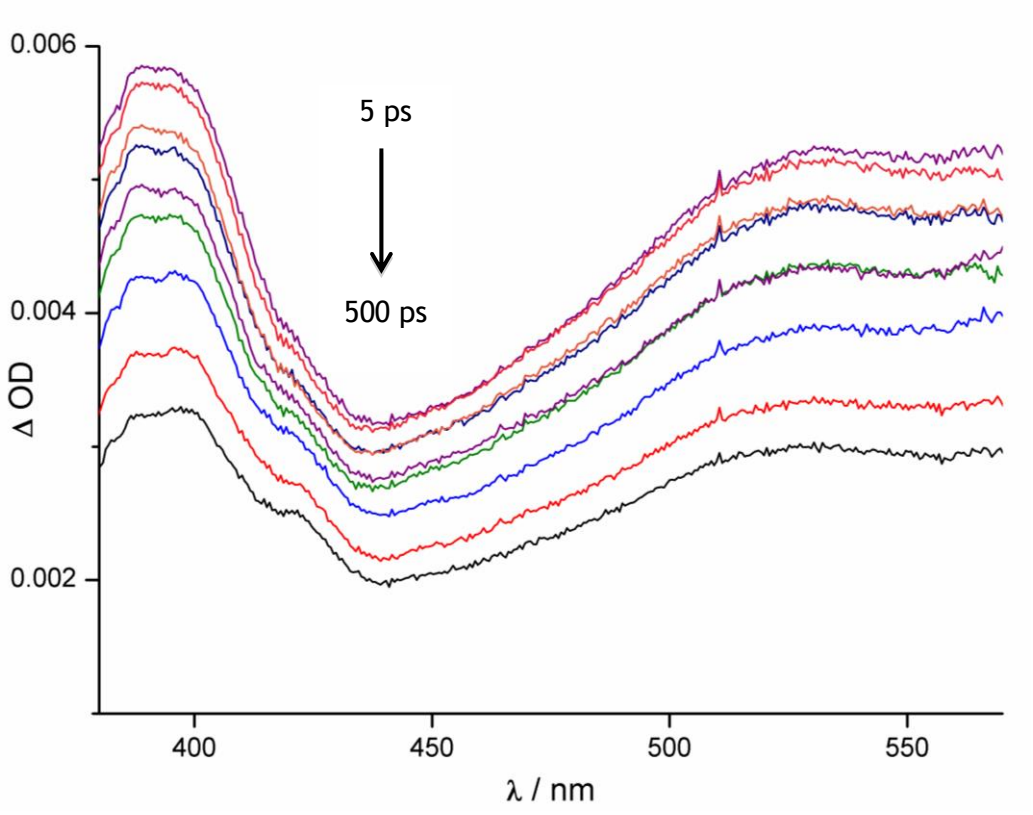

Figure 2.3.15 – Transient absorption spectra of **H** at a series of delays following a 40 fs excitation pulse at 290 nm.

Excitation of the complex **H•G10** under the same conditions produced the set of difference spectra that look similar to that measured for free **H**. These similarities are due to there being a single guest per 12 naphthalene units and the fact that there will be a small amount of free **H** in the equilibrium mixture at any one time. However, there are very visible differences in the shape of the TA spectra of **H•G10** when compared to **H**: an increased absorbance in the 380-460 nm region, the appearance of an additional narrow band at 450 nm and significant addition to the fine structure of the 400 nm band (fig. 2.3.16).

The new absorbance that appears at 380-410 nm matches what is expected for the presence of the tetracyanobenzene radical anion, **G10**$^{\bullet-}$,[15] and the naphthyl radical cation from **H**$^{\bullet+}$. The naphthyl radical cation possesses a comparatively sharp absorption band at 382 nm with a shoulder at 366 nm, explaining the increase in absorbance in the TA spectrum of **H•G10** when compared to **H**. The sharp feature that appears at 450 nm in TA spectrum of **H•G10** aligns with the most intense feature in the absorption spectrum of **G10**$^{\bullet-}$, the control TA spectrum of **G10** lacks this feature.

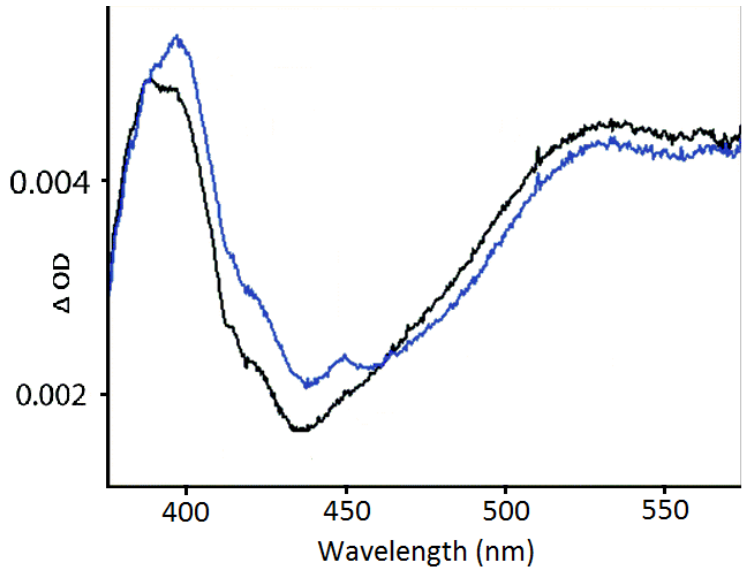

Figure 2.3.16 – Overlay of transient absorption spectra of **H** (black) and **H•G10** (blue) at the time delay of 20 ps. The spectra are normalised to OD at 385 nm (OD = optical density; the ability for a wave to propagate through solution, also known as absorbance).

The occurrence of features in the TA spectrum of **H•G10** that are missing from the spectrum of **H** on its own are consistent with the generation of the $\mathbf{H}^{+}/\mathbf{G10}^{-}$ charge-separated pair as a result of cage-guest PET. The excited state features accredited to $\mathbf{H}^{+}/\mathbf{G10}^{-}$ decay synchronously with the first-order time constant of 160(25) ps, which is a result of charge recombination from back electron transfer. The features of the transient spectrum of **G10** associated with ^{1}naph* continue over longer time scales, decaying with the same dynamics as the free cage.

TA experiments were performed on **G11** under similar conditions before: concentration of **G11** = 4.0 mM, and concentration of **H** = 0.01 mM. Again, under these conditions the host should be *ca.* 99% bound based on the measured binding constant of **G11**. Control experiments of **H** on its own and of **G11** on its own were also measured under the same conditions.

Excitation of a solution of **H•G11** at 290 nm, under the experimental conditions, yielded the difference spectra shown in fig. 2.3.17. As with **H•G10** there are a few similarities with the TA spectrum of **H** on its own, but in the case of **H•G11** an increased absorbance can be seen throughout the majority of the spectrum in addition to extra fine structure seen in the band *ca.* 400 nm.

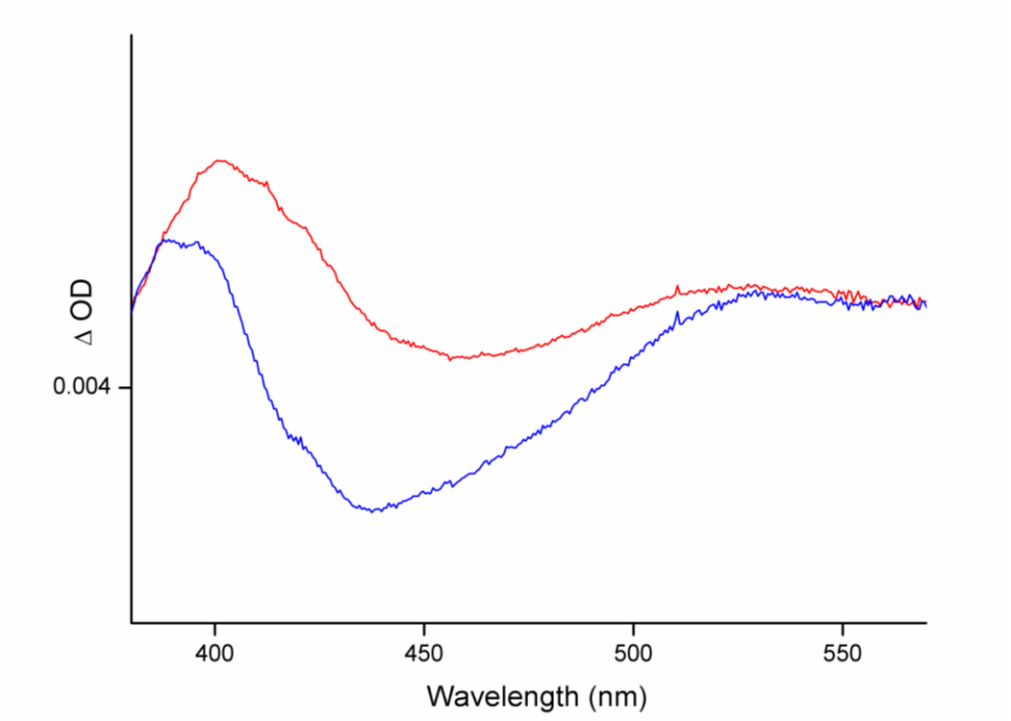

Figure 2.3.16 – Overlay of transient absorption spectra of **H** (Blue) and **H•G11** (Red) at the time delay of 20 ps. The spectra are normalised to OD at 385 nm.

The additional absorbance that appears in the region 380-410 nm again matches what is expected for the presence of the naphthyl radical cation from $\mathbf{H}^{\bullet+}$ as well as the presence of the naphthoquinone semiquinone radical anion $\mathbf{G11}^{\bullet-}$. The region of 425-500 nm has a notable increase in absorbance when compared to the **H**; this area of increased absorbance is expected from the semiquinone radical anion.[16] These differences in the TA spectra from that of **H** on its own provide evidence of the generation of the $\mathbf{H}^{+}/\mathbf{G10}^{-}$ charge separated state.

Under the same conditions, the same TA experiments were performed with **G12.** The TA spectrum for **H•G12** has some very noticeable differences compared to the TA spectrum for **H** alone. At delays up to 80 ps there is a negative signal centred at about 450 nm (fig. 2.3.17) this corresponds to the ground state absorbance of **G12**. A sharp feature also appears at 507 nm which decays before 80 ps, this is assigned to the formation of the **G12** triplet

state,[17] which decays with a first-order time constant of 13 (0.9) ps. This peak is observed in the TA spectrum for the control sample of **G12** also gives a decay value of 13 (0.3) ps which suggests the cage has no effect on the triplet state of **G12,** though it is possible the triplet state only arises as a result of guest not being bound by the cage.

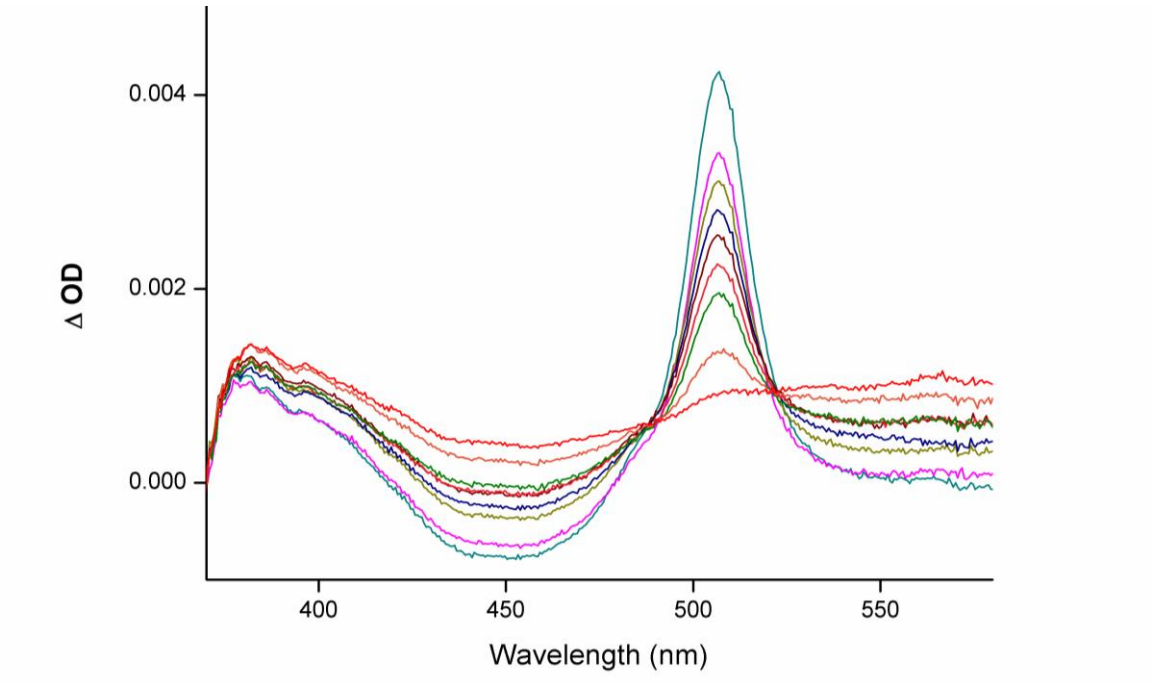

Figure 2.3.17 – Transient absorption spectra of **G12** at a series of delays following a 40 fs excitation pulse at 290nm.

As in both previous cases, a region of enhanced absorbance in the 380-410 nm region can be observed (fig. 2.3.18) However, this time there is much more pronounced absorbance at *ca.* 380 nm which coincides with the sharp absorbance at 382 nm expected for the presence of the naphthyl radical cation. The region of enhanced absorbance observed over the area of 425-475nm can be attributed to the generation of the **G12** semiquinone radical anion which has an absorbance over this region.[18] The excited state features decay with rate of 115(66) ps which suggests back electron transfer to restore the ground states of cage and guest. The appearance of spectroscopic signals suggesting the generation of both ^{1}naph* and **G12**$^{\bullet-}$, and then their synchronous decay, indicates that the **H**$^{+}$/**G12**$^{-}$ is formed; providing evidence that PET occurs in the **H•G12** system**.**

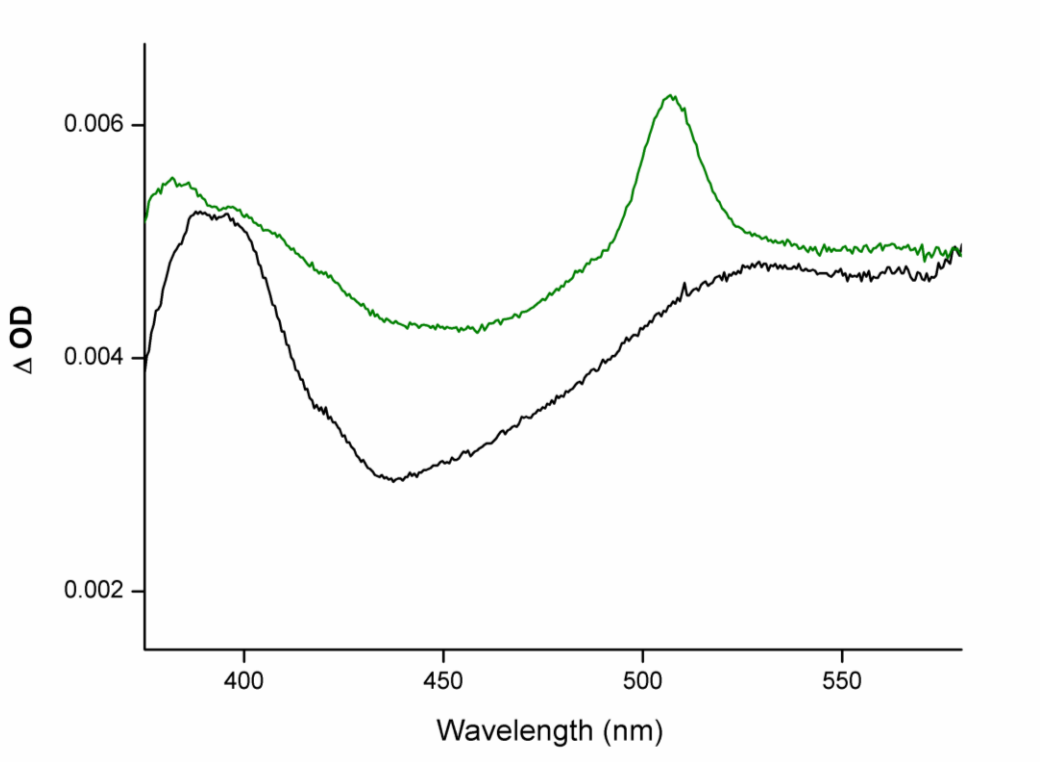

Figure 2.3.18 – Overlay of transient absorption spectra of **H** (Black) and **H•G12** (Green) at the time delay of 20 ps.

2.3.4 An Application of Cage Fluorescence Quenching

An appealing prospect for a photo-active coordination cage is generation of a fluorescence response following the uptake of a guest molecule. This could provide, for example, real-world application for detection of unwanted pollutants in the environment. Organophosphorus chemical warfare agents (CWAs) are examples of such pollutants in which the ability to detect them in the environment would be highly advantageous.

There has been recent use of supramolecular systems in the molecular recognition of CWAs; incorporation of reporter groups has laid the basis for the optical sensing of CWAs. Due to the requirement of specialist facilities for handling of CWAs, the majority of work is done on 'simulants', which include alkyl phosphonates that possess a similar size/shape to CWAs but with the absence of the highly reactive leaving group (**G13 – 16**).

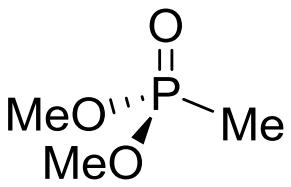

G13

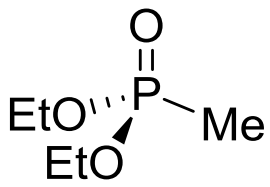

G14

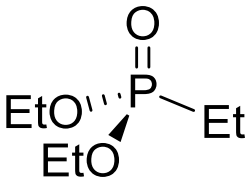

G15

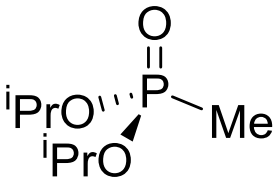

G16

These molecules are "photo-innocent" in the same way as **G1** – **G3**, possessing no chromophore that exhibits absorption in the UV region concerned and no cability to be involved in photoinduced energy- or electron-transfer with naphthyl chromophores. As such they are only expected to interact with the cage fluorescence in a similar or the same way as guests **G1** – **G3**. Indeed the binding of these alkyl phosphonate guests does result in partial quenching of the fluorescence of **H**.

The quenching of cage fluorescence upon titration of **G16** into **H** is shown in fig. 3.2.19; the changes in fluorescence intensity fitted well to a 1:1 binding isotherm (as did **G14** and **G15**) with the values shown in table 2 (Binding isotherms for **G14** – **G16** can be found in appendix 1). These values are, in some cases, somewhat different to those previously measured by NMR titration; given the different ionic radius of Cd(II) compared to Co(II), in addition to the presence of NO_3^- anions than BF_4^- anions, it is not surprising there exists some variation in the binding constants, though the general trend remains the same. Fluorescence intensity quenching on binding **G13** best fits a 2:1 host/guest model (fig. 3.2.20) which was also seen by NMR titration; the value given in table 2 represents the individual binding constant value per guest molecule. All other guests showed 1:1 binding.

	DMMP (G13) K / M^{-1}	DEMP (G14) K / M^{-1}	DEEP (G15) K / M^{-1}	DIMP (G16) K / M^{-1}
$[Cd_8Lw^{1,5naph}{}_{12}](NO_3)_{16}$ /H_2O [a]	7	20	31	46
$[Co_8Lw^{1,5naph}{}_{12}](BF_4)_{16}$ /D_2O [b]	7	26	160	390

Table 2 – Binding constants (K) at 298 K for the alkyl phosphonates cage/guest complexes. [a] Measured by luminescence titration. [b] Measured by NMR spectrosopic techinques.

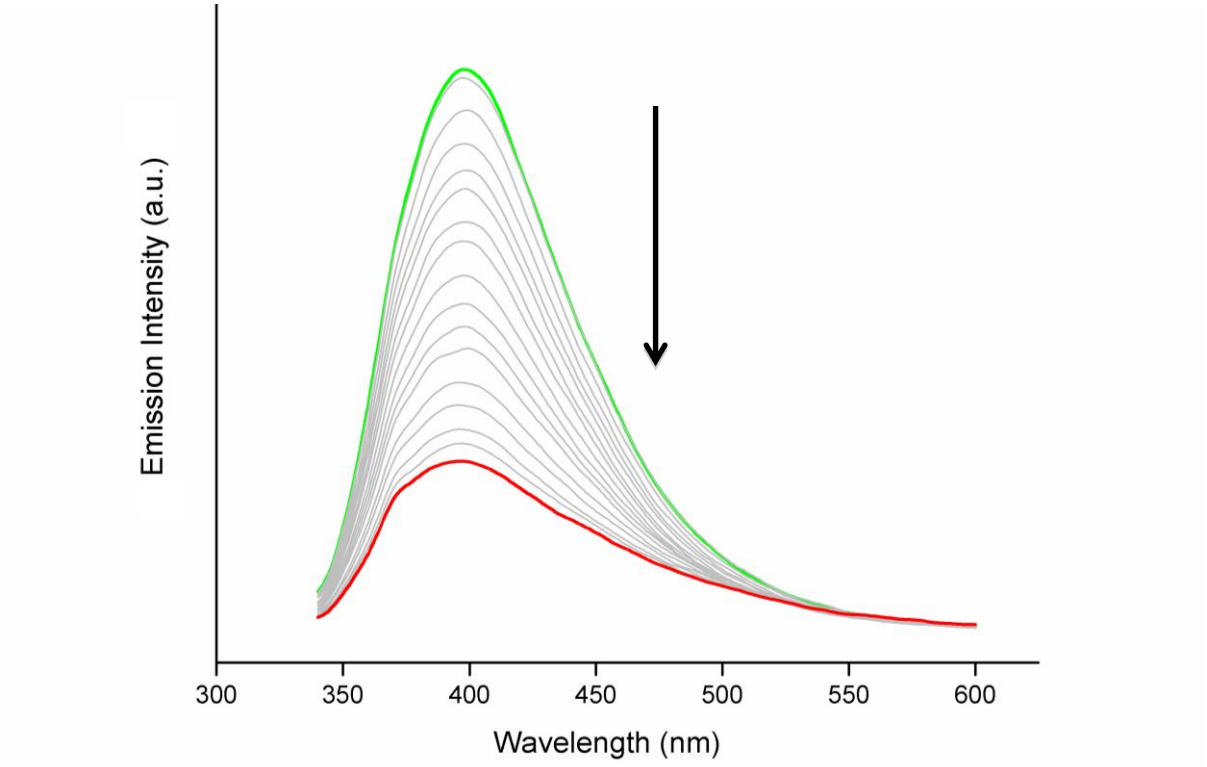

Figure 2.3.19 - Luminescence spectra representing the progressive decrease in fluorescence of cage **H** (0.01 mM) in water as a result of the sequential addition of a solution of DIMP (1 mM), **G16.**

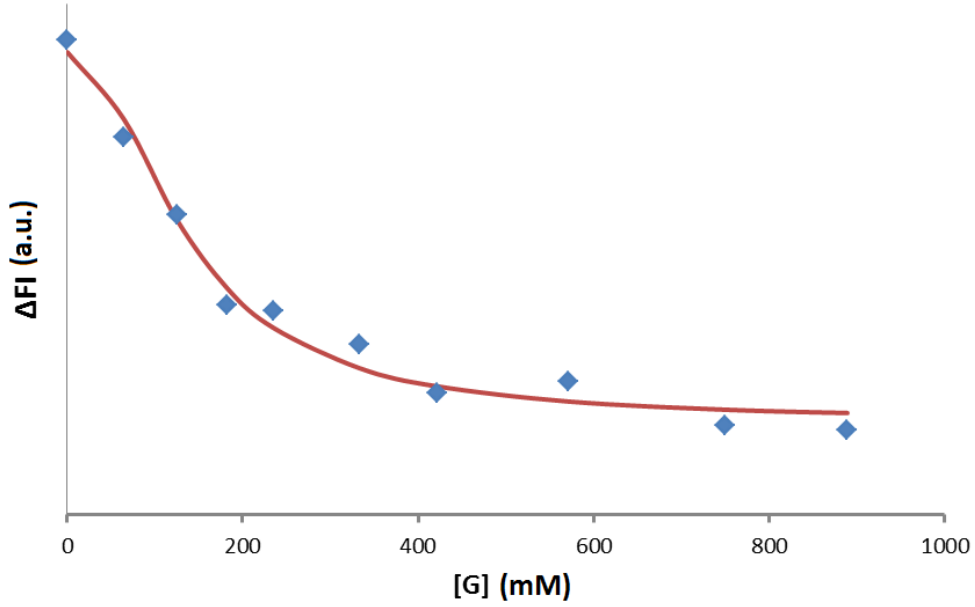

Fig. 2.3.20 - Plot of the changes in cage **H** fluorescence vs. the concentration of added guest **G13**, fitted to a 2:1 binding isotherm.

2.4 Conclusion

The target cage $[Cd_8(Lw^{1,5\text{-naph}})_{12}][NO_3]_{16}$ has been successfully synthesised which has led to a new route towards the synthesis of the ligand $Lw^{1,5\text{-naph}}$. This new route is both shorter and provides an improved overall yield compared to the previous route.

The ability to determine binding constants of guest uptake into the $[Cd_8(Lw^{1,5\text{-naph}})_{12}][NO_3]_{16}$ cage *via* luminescence titrations has been demonstrated, with good agreement with binding constants measured by NMR spectroscopic studies.

The cage has exhibited the capacity to act as both a photo-induced energy and electron donor to acceptor guest molecules, with various examples given and proved by guest competition experiments and transient absorption studies to characterise the charge-separated excited states and their dynamic behaviour.

A spectroscopic response is observed upon the binding of alkyl phosphonate chemical warfare simulants, demonstrating the potential for these cage/guest systems as fluorescent sensors for chemical warfare agents.

2.5 Experimental Techniques and Procedures

2.5.7 Synthetic procedures

4-[(*tert*-butyldimethylsilyl)hydroxymethyl]pyridine (1)

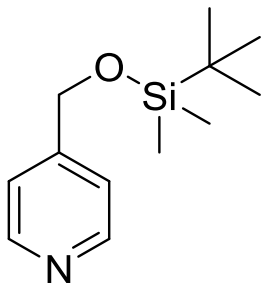

Imidazole (14.17 g, 0.235 mol) was dissolved in 90 ml dry DMF and 10 ml DCM under nitrogen atmosphere. *tert*-Butyldimethylsilyl chloride (24.9 g, 0.165 mol) was added proportion wise and was left to stir for 10 mins. 4-methanolpyridine (15.0 g, 0.137 mol) was added proportion wise and stirred at room temperature for 16 hours. The solvent was removed under reduced pressure; 100 ml of water was added and extracted with Ethyl Acetate and n-Hexanes (1:1 ratio) 4 x 100 ml. The organic phase was dried over $MgSO_4$ and the solvent was removed under reduced pressure to give **1** (29 g, 95%) a pale yellow oil.

ES-MS m/z (%) 224.14 $[M + H]^+$

^{1}H NMR (400 MHz, $CDCl_3$) δH 0.10 (s, 6H); 0.94 (s, 9H); 4.72 (s, 2H); 7.24 (d, J = 5.8 Hz, 2H); 8.52 (d, J = 5.8 Hz, 2H);

2-(acetyl)-4-[(*tert*-butyldimethylsilyl)oxymethyl]pyridine (2)

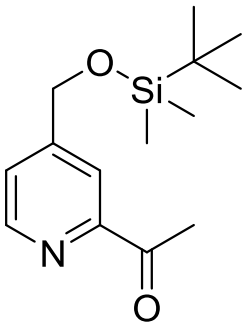

2-*N,N'*-dimethylamino-ethanol (2.7 ml, 27 mmol) was dissolved in 30 ml dry toluene under an atmosphere of N_2. The solution was cooled to 0 ^oC and n-butyl lithium (22ml, 2.5 M) was

added drop wise, this was left to stir at 0 ^{o}C for 30 mins. A solution of **1** (3.0 g, 13 mmol) in 10 ml toluene was added drop wise and left to stir at 0 ^{o}C for 1 hr. N,N'-dimethylacetamide (3.11 ml, 34 mmol) was then added and the reaction was left to reach room temperature. The reaction was then hydrolysed with 30 ml water and left to stir for 10 mins. The organic layer was separated and the aqueous was washed with 3 x 100 ml dichloromethane. The organic phases were combined and then dried with $MgSO_4$ and the solvent was removed under reduced pressure to give red/brown oil. Purification by column chromatography (Silica, ethyl acetate: petroleum ether 1:4) afforded **2** (1.07 g, 30%) a yellow oil.

ES-MS m/z (%) 266.15 $[M + H]^+$

^{1}H NMR (400 MHz, $CDCl_3$) δ 0.15 (s, 6H); 0.99 (s, 9H); 2.76 (s, 3H); 4.85 (s, 2H); 7.24 (d, J = 4.8 Hz, 1H); 7.97 (s, 1H); 8.66 (d, J = 4.8 Hz, 1H);

2-(acetyl-dimethylenamine)-4-[(tert-butyldimethylsilyl)oxymethyl]pyridine (**3**)

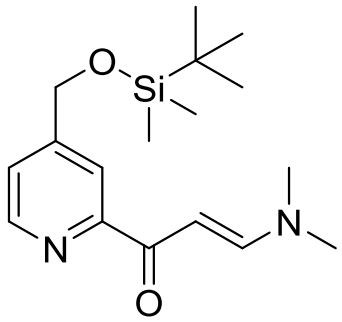

2 (7 g, 26 mmol) and DMF-DMA (6.7 cm3, 47 mmol) were stirred and heated to 110 oC for 16 hours. The solvent was then removed and the product was purified by column chromatography (Silica, 10% Methanol: Dichloromethane) to afford 3 (6.23 g, 73%) a yellow oil.

ES-MS m/z (%) 321.19 $[M + H]^+$

^{1}H NMR (400 MHz, $CDCl_3$) δ 0.13 (s, 6H); 0.98 (s, 9H); 3.01 (s, 3H, N-CH_3); 3.19 (s, 3H, N-CH_3); 4.82 (s, 2H); 6.26 (d, J = 12.3 Hz, 1H, C=CH); 7.44 (d,J = 5.4 Hz, 1H); 7.94 (d, J = 12.3 Hz, 1H, HC=C); 8.06 (s, 1H); 8.61 (d, J = 5.4 Hz, 1H);

4-[(*tert*-butyldimethylsilyl)-PyPz (4)

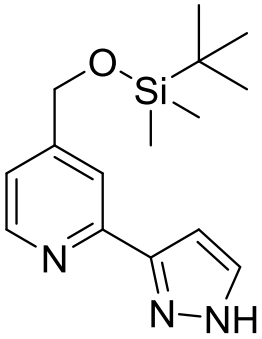

3 (6.23 g, 19 mmol) was dissolved in 40 ml of ethanol; hydrazine monohydrate (11.9 ml, 380 mmol) was then added. The mixture was then heated to 60 ^oC for 30 minutes and then allowed to cool to room temperature. The solvent was removed and the residue was dissolve in 50 ml dichloromethane and washed with water (3 x 50 ml) the organic phase was dried with $MgSO_4$ and the solvent removed *in vacuo.* Purification was afforded by column chromatography (Silica, 5% Methanol: Dichloromethane) to yield **4** (4.5 g, 82%) a yellow/orange oil that solidified on standing.

ES-MS m/z 290.16 $[M + H]^+$;

^{1}H NMR (400 MHz, $CDCl_3$) δH 0.16 (s, 6H); 1.00 (s, 9H); 4.83 (s, 2H); 6.84 (d, J = 2.0 Hz, 1H); 7.26 (d, J = 5.4 Hz, 1H); 7.70 (d, J = 2.0 Hz, 1H); 7.74 (s, 1H); 8.61 (d, J = 5.4 Hz, 1H);

1,5-dimethylnaphthalene (5)

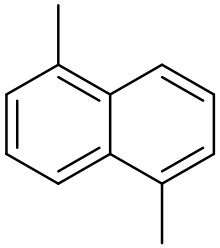

To triphenylmethanol (34.1 g, 125 mmol), 25 ml trifluoroacetic acid was added slowly and stirred for 15 mins. 1,5-dimethyltetralin (10 ml, 60 mmol) was added, the reaction was heated to 75 ^{o}C for 1 hour. The reaction was allowed to cool to room temp and 150 ml aqueous K_2CO_3 (2.5 M) was carefully added, the mixture was then extracted with diethyl ether (3 x 150 ml) and the organic phases collected and dried over $MgSO_4$ and the solvent removed *in vacuo.* Purification by column chromatography (silica, petroleum ether) affords **5** (8.6 g, 92%) a white solid.

EI-MS m/z: 156.01 $[M]^+$;

^{1}H NMR (400 MHz, $CDCl_3$); 2.73 (s, 6H); 7.35 (d, J = 6.9 Hz, 2H); 7.44 (t, J = 6.9 Hz, 2H); 7.90 (d, J = 8.2 Hz, 2H);

1,5-bis(bromomethyl)naphthalene (6)

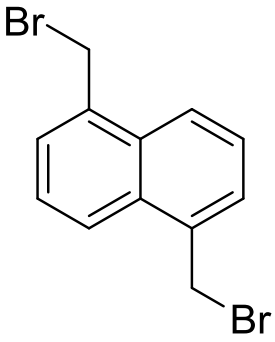

1,5-dimethylnaphthalene (**5**) (5.07 g, 32 mmol) was dissolved in 100 ml dry dichloromethane under an atmosphere of N_2. N-bromosuccinimide (12.7 g, 71 mmol) was added and the reaction mixture was heated to 40 ^{o}C and a catalytic amount of azobisisobutyronitrile was added. UV irradiation by tungsten lamp was applied for 2 hours.

The mixture was filtered and the solid was washed with water (3 x 100 ml) to yield 1,5-bis(bromomethyl)naphthalene (**5**) (7.055 g, 70%) a white solid.

EI-MS m/z: 313.91 $[M]^+$; 233.0 $[M - Br]^+$; 154.08 $[M - 2Br]^+$;

^{1}H NMR (400 MHz, $CDCl_3$); 4.98 (s, 2H); 7.60 (m, 4H); 8.21 (d, J = 8.5 Hz, 2H);

OTBDMS-$L_w^{1,5naph}$ (7)

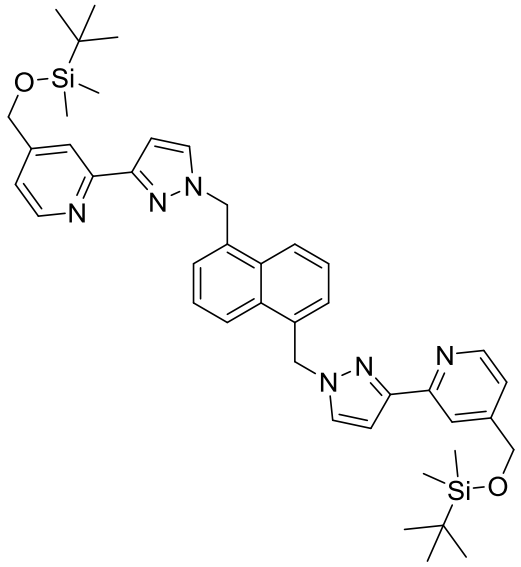

3 (1 g, 3.45 mmol) and sodium hydride (0.17 g, 7.2 mmol) were dissolved in 25 ml dry tetrahydrofuran under nitrogen atmosphere and was stirred until effervescence stopped. The reaction mixture was left to stir for a further 10 minutes. 1,5-bis(bromomethyl) naphthalene (**5**) (0.54 g, 1.73 mmol) was added and the reaction was heated to 70 ^oC for 16 hours. The reaction was quenched with 10 ml methanol and solvent was removed *in vacuo.* Purification by column chromatography (silica, 5% methanol: dichloromethane) yielded **6** (0.76 g, 60%) a yellow solid.

ES-MS m/z: 754. 732.1 $[M + Na]^+$; 732.1 $[M + H]^+$; 366.6 $[M + 2H]^{2+}$

^{1}H NMR (400 MHz, $CDCl_3$); 0.15 (s, 12H); 0.99 (s, 18H); 4.83 (s, 4H); 5.89 (s, 4H); 6.88(d, J= 2.3 Hz); 7.25-7.28 (m, 4H); 7.36 (d, J = 7.2 Hz, 2H); 7.50 (t, J = 7.2 Hz, 2H); 7.91 (s, 2H); 8.07 (d, J = 8.5 Hz, 2H); 8.62 (d, J = 5.1 Hz, 2H);

$L_w^{1,5naph}$ (8)

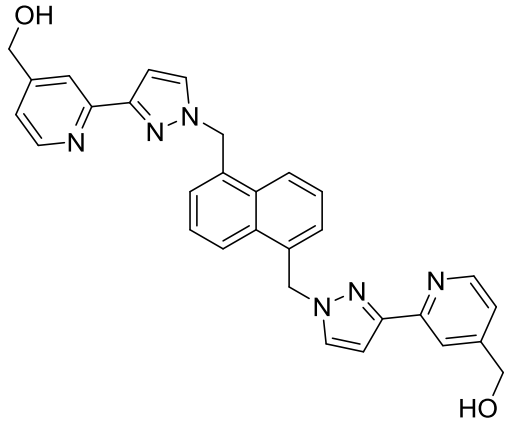

6 (0.76 g, 1 mmol) was dissolved in 30 ml THF, TBA-F (0.63, 2 mmol) was added and the reaction was left to stir for 24 hours. 20 ml DCM and 20 ml water were added to the reaction mixture and a white ppt. formed. The solid was filtered and washed with cold DCM and chloroform to give **7** (0.49 g, 98%) a yellow-white solid.

ES-MS m/z: 526.3 $[M + Na]^+$; 503.2 $[M + H]^+$ 252.1 $[M + 2H]^{2+}$

^{1}H NMR (400 MHz, $CDCl_3$) δH 2.50 (s, DMSO); 3.30 (s, H_2O); 4.56 (s, 4H); 5.94 (s, 4H); 6.85 (s, 2H); 7.20 (d, J = 5.0 Hz, 2H); 7.27 (d, J = 7.0 Hz, 2H); 7.58 (t, J = 7.6 Hz, 2H); 7.89 (m, 4H); 8.22 (d, J = 8.5, 2H); 8.47 (d, J = 5.0 Hz, 2H);

$[Cd_8(L_w^{1,5naph})_{12}](BF_4)_{16}$ (9)

To a suspension of **7** (30 mg, 0.06 mmol) in 20 ml MeOH,
cadmium tetrafluoroborate hexahydrate (15.6 mg, 0.04 mmol) was added, the mixture was refluxed for 24 hours. The reaction was mixture allowed to cool and a white ppt. formed. The solid was filtered off and washed with cold DCM and chloroform and sparingly with cold MeOH, to give **9** (38.2 mg, 92%) a white solid.

ES-MS m/z: 1588 $\{[Cd_8(L_w^{1,5naph})_{12}][BF_4]_{11}Na_2\}^{5+}$; 1309 $\{[Cd_8(L_w^{1,5naph})_{12}][BF_4)_{10}Na\}^{6+}$; 1110 $\{[Cd8(L_w^{1,5naph})_{12}][BF_4]_9Na_2\}^{7+}$; 953 $\{[Cd_8(L_w^{1,5naph})12][BF_4]_8\}^{8+}$.

$[Cd_8(L_w^{1,5naph})_{12}](NO_3)_{16}$ (10)

The procedure of **10** is same as for **9**, using cadmium nitrate tetrahydrate (12.3 mg, 0.04 mmol) to give a white solid (35.2 mg, 89%).

^{1}H NMR (500 MHz, D_2O) δH 3.40 (d, J = 16.6 Hz, 1H); 3.98 (s, 2H); 3.40 (d, J = 16.6 Hz, 1H); 4.70 (s, 2H); 5.12 (d, J = 7.39 Hz, 1H); 5.31 (d, J = 7.39 Hz, 2H); 5.37 (d, J = 16.6 Hz, 1H); 5.55-5.58 (m, 2H); 5.70 (d, J = 5.54 Hz, 1H); 5.86 (d, J = 16.6 Hz, 1H); 5.98 – 6.10 (m, 4H); 6.71(s, 1H); 6.89 – 7.03 (m, 7H); 7.13 (d, J = 5.5 Hz, 2H); 7.20 - 7.26 (m, 4H); 7.31 – 7.34 (m, 2H); 7.52 (s, 1H); 7.69 – 7.76 (m, 3H); 7.99 – 8.08 (m, 3H); 8.21 (d, J = 20.3 Hz, 2H);

4-amino-7-nitrobenzofurazan (G6)

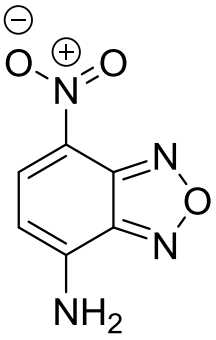

4-chloro-7-nitrobenzofurazan (0.50 g, 2.3 mmol) was dissolved in 10 ml MeOH, 10 ml of ammonia solution (7M in MeOH) was added and the reaction was stirred at room temperature for 2 hours. The solvent was removed *in vacuo* and purification was afforded by column chromatography (silica, 3:2 EtOAc: hexane) to give **10** (0.26 g, 62%) an orange solid.

ES-MS m/z: 179.03 $[M - H]^-$

^{1}H NMR (400 MHz, $CDCl_3$) δH 6.43 (d, J = 8 Hz, 1H); 8.50 (d, J = 8 Hz, 1H);

4-(N,N'-dimethyl)amino-7-nitrobenzofurazan (G7)

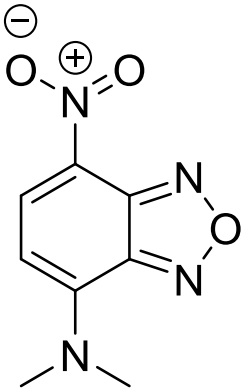

4-chloro-7-nitrobenzofurazan (0.50 g, 2.3 mmol) was dissolved in 20 ml MeCN, 10 ml of dimethylammonia solution (5.5M in EtOH) was added and the reaction was stirred at room temperature for 16 hours. The ppt. was filtered and washed with cold MeCN to give **11** (0.39 g, 80%) an orange solid.

ES-MS m/z: 209.06 $[M + H]^+$

^{1}H NMR (400 MHz, $CDCl_3$) δH 3.60 (s, 6H); 6.10 (d, J = 9 Hz, 1H); 8.50 (d, J = 9 Hz, 1H);

2.5.2 X-ray crystallography

The crystal structure data collection for $[Cd_8(L_w^{1,5naph})_{12}](NO_3)_{16}$ was performed at the EPSRC National Crystallography Service at the University of Southampton,UK.[19] The structure was solved and refined by Alex Metherell using the SHELX suite of programmes.[20]

All atoms were refined anisotropically excluding identifiable atoms of the, which were refined isotropically. SADI and FLAT commands were applied to disordered hydroxy methyl groups; several of which were modelled as two parts over different orientations. The aromatic rings were fixed with AFIX restraints: AFIX 56 for pyrazolyl rings; AFIX 66 for pyridine rings and AFIX 116 for naphthyl groups. Weak global restraints were applied to all C, N, O atoms of the ligands to achieve a more chemically reasonable model which refined stably (SIMU and DELU commands). Disordered anions and solvent molecules resided within the remaining undefined space. This region of diffuse electron density was removed with the SQUEEZE command on PLATON.

	$[Cd_8(L_w^{1,5naph})_{12}](NO_3)_{16}\bullet(dmf)_{13}\bullet(H_2O)_2$
Formula	$C_{399}H_{407}Cd_8N_{101}O_{87}$
Molecular Weight	8908.43
T, K	100(2)
Crystal system	Triclinic
Space Group	P-1
a, Å	23.1625(3)
b, Å	101.7820(1)
c, Å	24.2858(3)
α, °	108.5500(10)
β, °	101.7820(1)
γ, °	90.4160(10)
V, $Å^3$	12374.8(3)
Z	1
ρ, g cm^{-3}	1.195
Final R1, wR2	0.0925, 0.333

2.6 References

1 S. Turega, M. Whitehead, B. R. Hall, M. F. Haddow, C. A. Hunter and M. D. Ward, *Chem. Commun.*, 2012, **48**, 2752.

2 S. Turega, W. Cullen, M. Whitehead, C. A. Hunter and M. D. Ward, *J. Am. Chem. Soc.*, 2014, **136**, 8475–8483.

3 I. S. Tidmarsh, T. B. Faust, H. Adams, L. P. Harding, L. Russo, W. Clegg and M. D. Ward, *J. Am. Chem. Soc.*, 2008, **130**, 15167–15175.

4 M. Whitehead, S. Turega, A. Stephenson, C. A. Hunter and M. D. Ward, *Chem. Sci.*, 2013, **4**, 2744.

5 A. J. Metherell and M. D. Ward, *Dalt. Trans.*, 2016, **45**, 16096–16111.

6 P. D. Frischmann, V. Kunz and F. Würthner, *Angew. Chemie Int. Ed.*, 2015, **54**, 7285–7289.

7 R. Dabestani and I. N. Lvanov, *Photochem. Photobiol.*, 1999, **70**, 10–34.

8 G. A. George and G. C. Morris, *J. Mol. Spectrosc.*, 1968, **26**, 67–71.

9 E. S. Pysh and N. C. Yang, *J. Am. Chem. Soc.*, 1963, **85**, 2124–2130.

10 G. Accorsi, F. Barigelletti, A. Farrán, F. Herranz, R. M. Claramunt, M. Marcaccio, G. Valenti, F. Paolucci, E. Pinilla and M. R. Torres, *J. Photochem. Photobiol. A Chem.*, 2009, **203**, 166–176.

11 H. Kotani, K. Ohkubo and S. Fukuzumi, *Faraday Discuss.*, 2012, **155**, 89–102.

12 K. K. Mentel, R. M. D. Nunes, C. Serpa and L. G. Arnaut, *J. Phys. Chem. B*, 2015, **119**, 7571–7578.

13 D. F. Anghela, V. Alderson, F. M. Winnik, M. Mizusaki and Y. Morishima, *Polymer*, 1998, **39**, 3035–3044.

14 G. M. Greetham, P. Burgos, Q. Cao, I. P. Clark, P. S. Codd, R. C. Farrow, M. W. George, M. Kogimtzis, P. Matousek, A. W. Parker, M. R. Pollard, D. A. Robinson, Z. J. Xin and M. Towrie, *Appl. Spectrosc.*, 2010, **64**, 1311–1319.

15 M. Fagnoni, S. Protti, D. Ravelli and A. Albini, *Beilstein J. Org. Chem.*, 2013, **9**, 800–808.

16 G. Balakrishnan, A. Babaei, A. J. McQuillan and S. Umapathy, *J. Biomol. Struct. Dyn.*, 1998, **16**, 123–131.

17 D. R. Kemp and G. Porter, *J. Chem. Soc. Chem. Commun.*, 1969, 1029.

18 J. J. Andre and G. Weill, *Mol. Phys.*, 1968, **15**, 97–99.

19 S. J. Coles and P. A. Gale, *Chem. Sci.*, 2012, **3**, 683–689.

20 G. M. Sheldrick, *Acta Crystallogr. Sect. C Struct. Chem.*, 2015, **71**, 3–8.

Chapter 3

Encapsulation of Metal Complexes within a Coordination Cage

3.1 Introduction

Examples of host-guest systems involving coordination cages (or similar macrostructures) in which the guest molecule is a metal complex rather than an organic compound are relatively rare. One of the first examples of a transition metal complex within the cavity of a supramolecular structure came from Reek and co-workers. The 1:3 combination of a family of C_3-symmetric ligands and zinc porphyrins self-assembles into structure where the cavity formed by the porphyrins encapsulates a free phosphine which can act as a ligand for transition metal complexes (fig. 3.1.1).[1] The addition of $Rh(acac)(CO)_2$ results in the ligation of the phosphine to the Rh complex resulting in encapsulation of the metal complex inside the Zn-porphyrin cage.

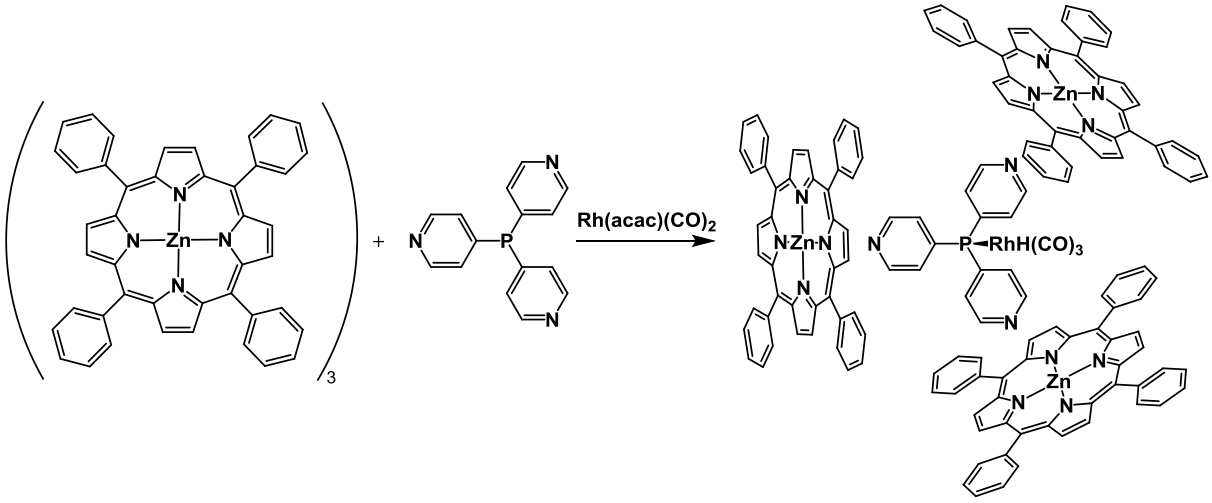

Figure 3.1.1 – Assembly of a supramolecular coordination complex.

The encapsulated $(R_3P)RhH(CO)_3$ complex shows catalytic activity towards the hydroformylation of alkenes, however this "supramolecular catalyst" displayed different activity and selectivity when compared to the behaviour of the non-encapsulated catalyst system, when 1-octene was used as a model hydroformylation substrate. Specifically, the encapsulated $RhH(CO)_3$ complex was found to be more active than unencapsulated rhodium species and also displays higher selectivity for the hydroformylation of internal alkenes.[2]

An examples of a transition metal complexes being encapsulated within a coordination cage using non-covalent interactions include iridium piano-stool complexes incorporated into a Ga_4L_6 tetrahedral cage by the Raymond group (fig. 3.3.2). These iridium complexes are known to act as catalysts for C-H bond activation for a number of organic substrates at low temperature. The encapsulated iridium complexes induce C–H bond activation and/or decarbonylation of aldehydes able that are able to fit within the cage cavity, also displaying shape selectivity.[3]

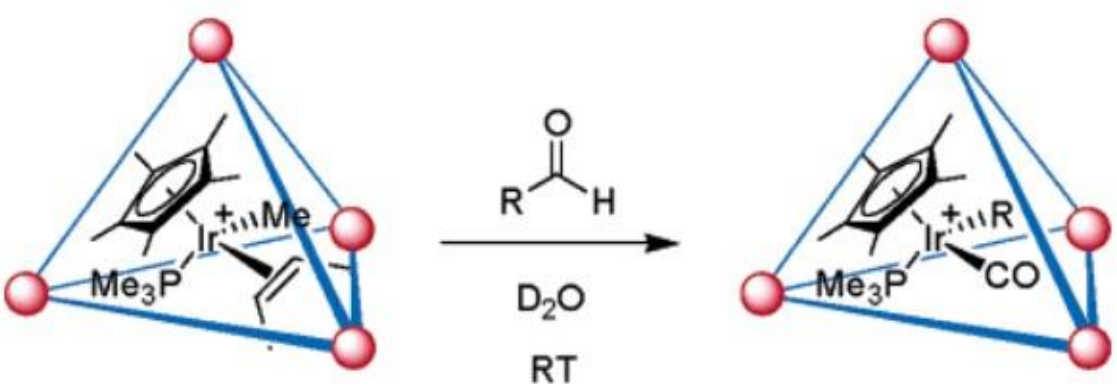

Figure 3.1.2 – Room temperature reaction of aldehydes with an encapsulated Ir half-sandwich complex. Reproduced with permission from reference 3, copyright 2006 American Chemical Society.

The same Ga_4L_6 tetrahedral cage was shown to encapsulate the ruthenium piano-stool complex $[RuCp(PMe_3)(MeCN)_2]^+$. The encapsulation protected the ruthenium complex from decomposition in water: a decomposition half-life of about one hour for the free complex turned into a lifetime of days after it was encapsulated.[4]

The Fujita group has demonstrated the uptake of ferrocene and its derivatives into the cavity of an octahedral $[Pd_6L_4]^{12+}$ cage. Uptake of ferrocene was driven by the hydrophobic effect, but after oxidation of ferrocene to the ferrocenium ion electrostatic repulsion lead to the expulsion of the guest from the cage cavity.[5]

Uptake of the anti-cancer drug molecule cisplatin into the cavity of a Pd_2L_4 cage has been performed by the Crowley group.[6] The central cavities of these cages have four inwardly-directed pyridine units which act as hydrogen bond acceptors, facilitating the encapsulation

of two molecules of cisplatin (Fig. 3.1.3). This host-guest system can be disassembled by the addition of a competing ligand affording the release of the cisplatin into solution – this forms the basis of potential use of coordination cages in targeted drug-delivery.

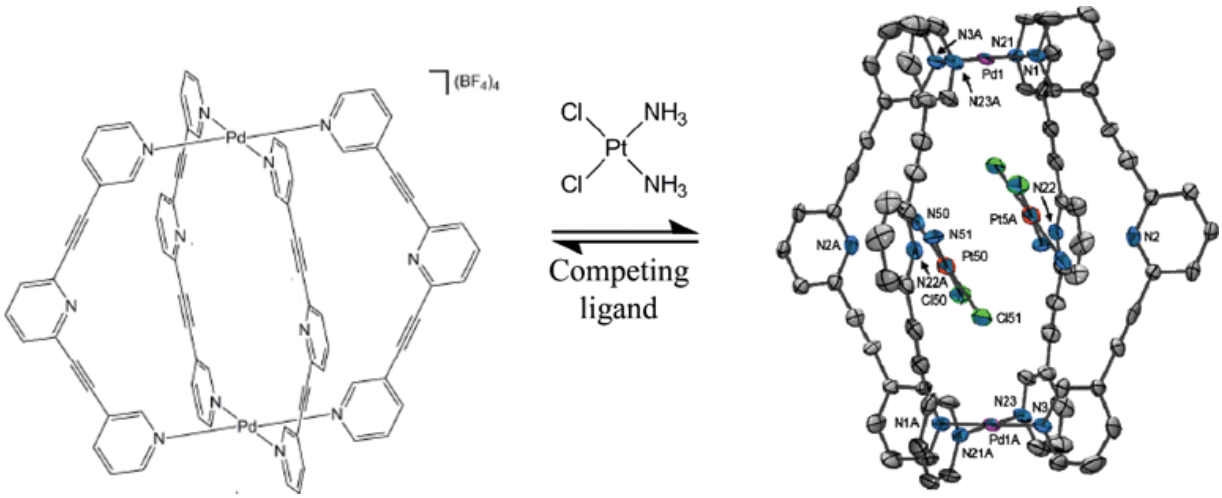

Figure 3.1.3 – Uptake of two molecules of cisplatin into the cavity of a coordination cage. Reproduced with permission from reference 6.

3.2 The Project

This project's aim was to explore the uptake of metal complexes into the cavity of the $[Cd_8(L_w^{1,5\text{-naph}})_{12}](NO_3)_{16}$ cubic cage **H** (described in a previous chapter) in water. As **H** is photoactive and has displayed the ability to interact photophysically with bound guest molecules it was thought that such interactions should be possible with a bound metal complex, potentially to lead to new photocatalytic systems. Cage-based photocatalytic systems in which the host cage acts as both host and photosensitiser, transferring energy or electrons to a bound guest, are almost unknown in the literature.

The constraints on the metal complexes chosen as potential guests are that (i) they fit within the cavity of **H** and (ii) are neutral and hydrophobic – earlier attempts by the group showed that there either postively or negatively charged species bind only weakly, as these are hydrophophilic and remain the bulk aquous phase, cations are also likely repelled by the overall 16+ charge of the cage.

3.2.1 Binding of neutral metal complexes

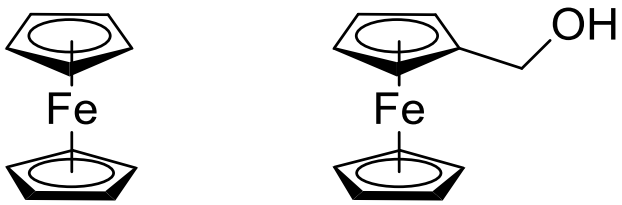

G17 **G18**

The first two guests that were studied were both ferrocene-based complexes. The first guest ferrocene **G17** was found to be too insoluble in water to attempt a titration which would allow determination of the binding constant. To resolve this insolubility issue**,** we used a ferrocene derivative, **G18,** which is functionalised with hydroxymethyl group which facilitates solubility in water. After **G18** was found to be suitably soluble in water a fluorescence titration of **G18** into a solution of **H** (fig. 3.2.1) showed partial quenching of the fluorescence of **H**. The modest amount of quenching however, suggests that photoinduced energy or electron transfer between cage and guest is not occurring: the mechanism of quenching is therefore probably just additional vibrational relaxation pathways, as was also seen for the non-chromophoric organic guest molecules seen in chapter 2. Nevertheless, fitting the change in fluorescence to a 1:1 binding isotherm produced a fairly high binding constant of 8.8 x 10^5 M^{-1} which is comparable to values shown by the stronger-binding organic guests. Uptake of **G18** has been previously confirmed by a ^{1}H NMR binding study using the $[Co_8(Lw^{1,5\text{-naph}}{}_{12})]^{16+}$ cubic cage $\mathbf{H_{Co}}$, structurally analogous to **H**.

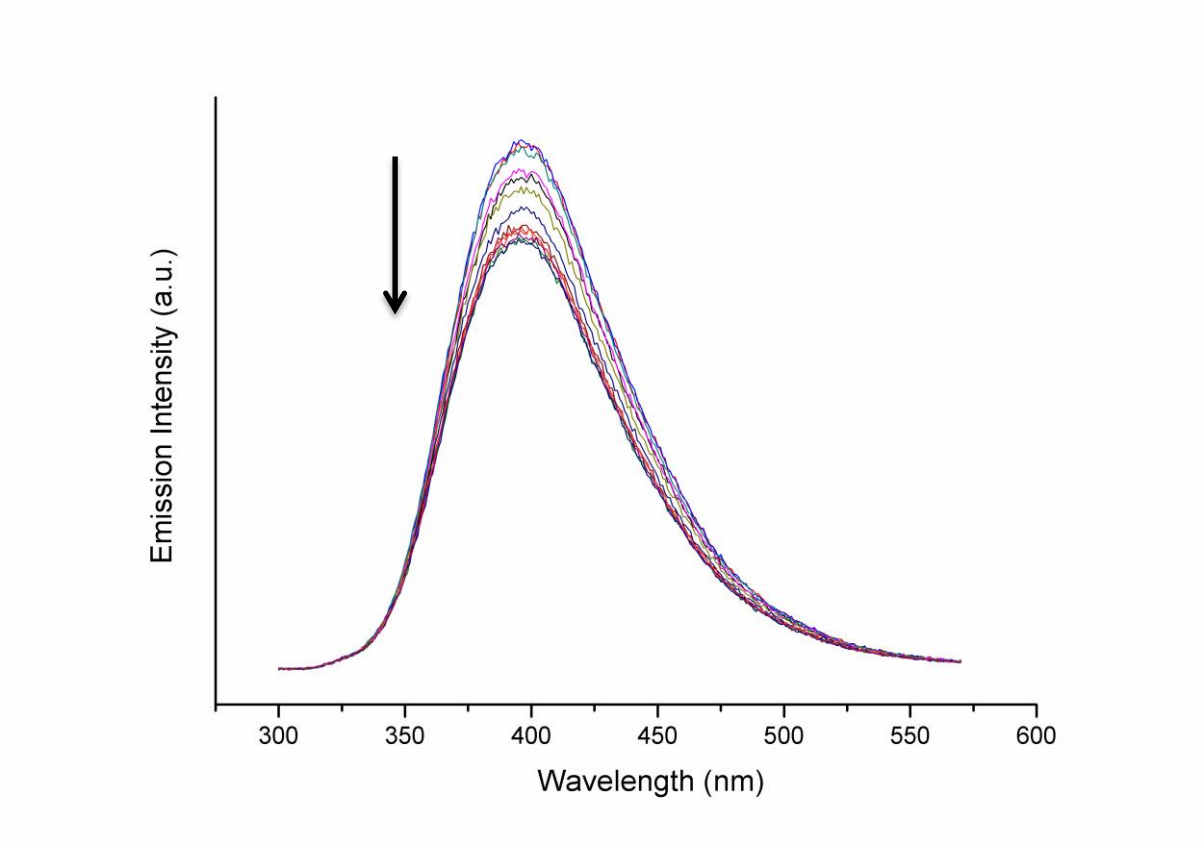

Figure 3.2.1 – Luminsecence spectra showing the addition of 0 - 1500 µL **G18** (0.1 mM) into a solution of **H** (10 µM) in H_2O, excitation at 290 nm.

The next two guests are "piano-stool" complexes, both containing an η^5-cylopentandienyl manganese tricarbonyl unit. These are structurally related to sandwich complexes like ferrocene, but offer more in terms of chemistry – specifically metal-carbonyls are known to undergo carbonyl substitution reactions at the metal centre, as well as the CO ligands themselves being susceptible to nucleophilic attack. The addition of **G19** into a solution of **H** afforded the quenching of **H** fluorescence (Fig. A2.1.2 in appendix 2), however **G19** has poor solubility in water, and therefore a binding constant could not be calculated as the actual amount of **G19** in solution was unknown. It is likely that the quenching of **H** fluorescence reflects an amount of **G19** that is able to enter into aqueous solution and then is up taken into the cage. Thus the cage might act in a way similar to a phase-transfer agent and transport the insoluble material **G19** into aqueous solution in the cage cavity, which may explain why any quenching is observed at all.

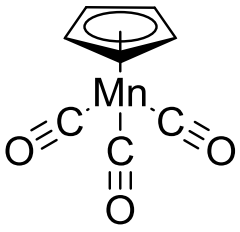

G19

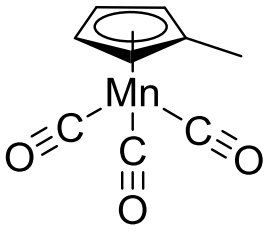

G20

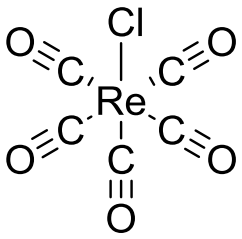

G21

Qualitative ^{1}H NMR experiments on both **G19** and **G20** provide good evidence for binding of these guests inside the cavity of $\mathbf{H_{Co}}$. The ^{1}H NMR experiment with **G20** (fig. 3.2.2) shows the shifting of peaks associated with $\mathbf{H_{Co}}$ after the addition of **G20**, which is expected to happen following the uptake of guests. Additionally in the -ve ppm range, new signals that are associated with, and indicative of, a bound guest can be seen at *ca.* -4.5, -5, and -7 ppm; these integrate to 2, 2, and 3 protons, matching what is expected for **G20**. This negative chemical shift is considered diagnostic of bound guests in the paramagnetic cavity; this shift is caused by the array of aromatic groups that form the cage's structure. Protons within the cavity lie perpendicular the aromatic ring current and are therefore shielded from the external magnetic field, resulting in the negative shift.

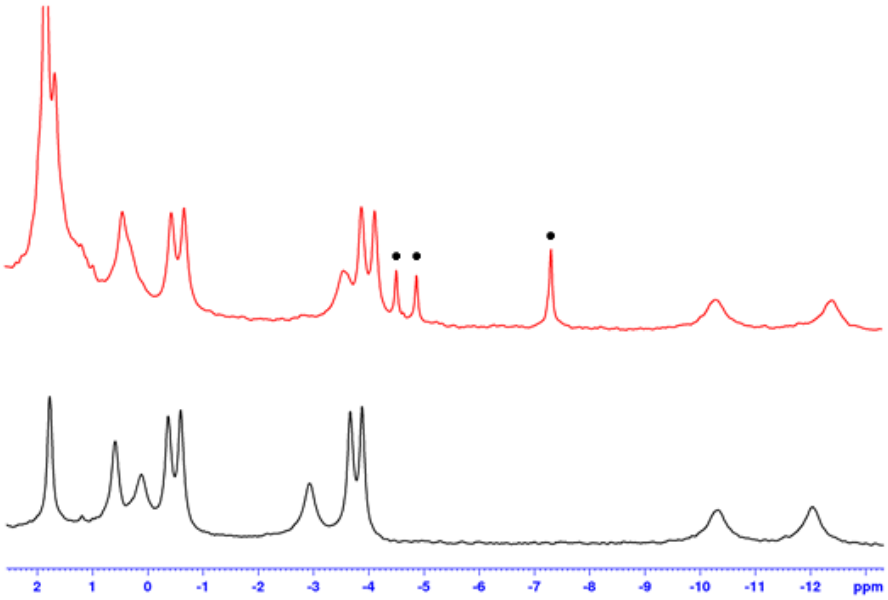

Figure 3.2.2 – Partial (400 MHz, D_2O) ^{1}H NMR spectrum of 0.2 mM $\mathbf{H_{Co}}$ (black) and $\mathbf{H_{Co}}$ after the addition of 2 equivalents **G20** (red), the peaks labelled with • correspond to bound **G20.**

Titration of an aqueous solution of $[Re(CO)_5Cl]$ (**G21**) into a solution of **H** caused a quenching of **H** fluorescence (fig. A2.1.2 in appendix 2), although – as with **G18** – only partial quenching was observed. This suggests again the quenching is purely vibrational and that no energy or electron processes are occurring which would be expected to cause stronger quenching. Fitting of the luminescence intensity data to a 1:1 binding isotherm yielded a binding constant of $1.1 \times 10^7\ M^{-1}$ (Fig. 3.2.3).

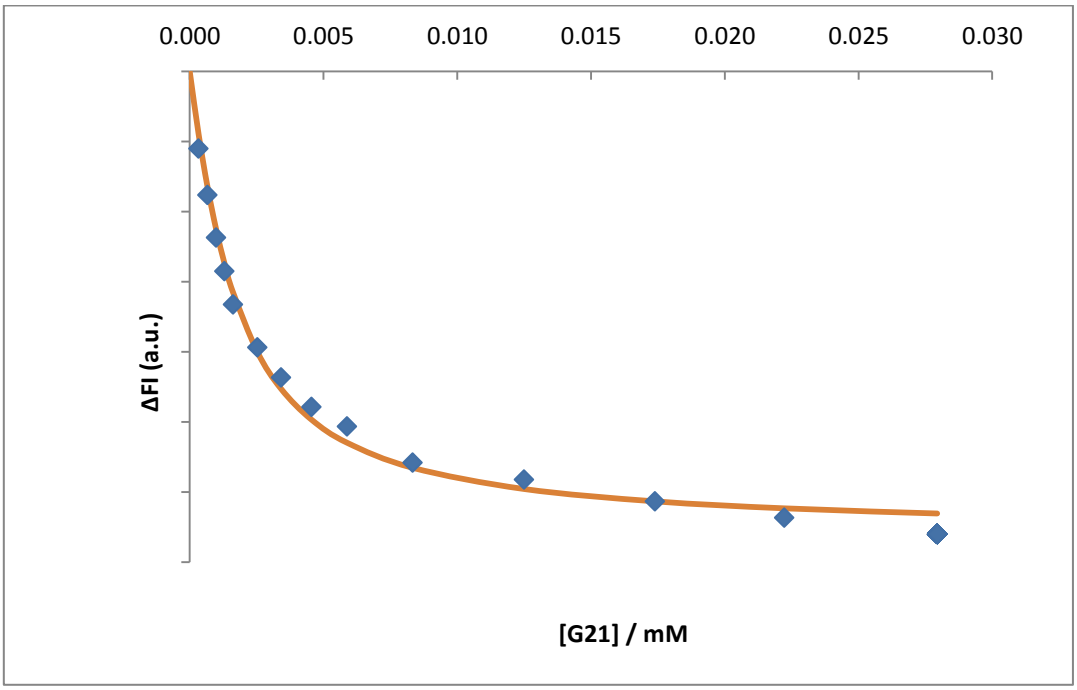

Figure 3.2.3 – 1:1 binding isotherm fit for the uptake of **G21** into **H** in H_2O at room temperature.

Carbonyl groups are a well-known reporter group in infrared spectroscopy. Accordingly we attempted to determine whether it is possible to detect the uptake of a carbonyl-containing guest molecule within the cavity of **H** cavity by infrared spectroscopy. **G21** suits this role well, possessing 5 carbonyl groups and displaying a strong affinity towards binding within the cage cavity.

The experiment was performed by adding 0.8 equivalents of **G21** to a solution of **H** in water; the hydrophobic effect facilitates the uptake of guest into the cavity; and using less than one equivalent we minimise the amount of unbound $Re(CO)_5Cl$ which would complicate the IR spectrum. The water is then removed by evaporation, leaving a powder containing the

H·G21 complex (plus free **H**) in solid form. Measuring the IR spectrum this on an ATR FTIR spectrometer allows for the rapid study of solid samples.

The IR spectrum of free, pure **G21** shows a region of broad, strong absorption between 1900 and 2100 cm^{-1} with some distinct sharp peaks resolved; this is the spectral region characteristic for metal-bound carbonyl stretching frequencies. In the IR spectrum of the host-guest complex **H·G21** these peaks have shifted to higher frequencies by *ca.* 5-20 cm^{-1} (fig. 3.2.3). These small increases in ν(CO) show that the carbonyl bonds have become stronger. This increase can be explained by the presence of hydrogen bonding interactions with the H-bond donor sites on the interior surface of **H**; for example two pockets where several CH protons converge have been shown to act as H-bond donor sites comparable in strength to phenol.[7] Hydrogen bonding to the oxygen lone pairs of metal carbonyl complexes has been shown to result in increased CO stretching frequencies: this is ascribed to an inductive effect resulting in less electron density on the metal, thereby resulting in reduced back-bonding into the CO anti-bonding orbitals and strengthened C-O bonds.[5,8]

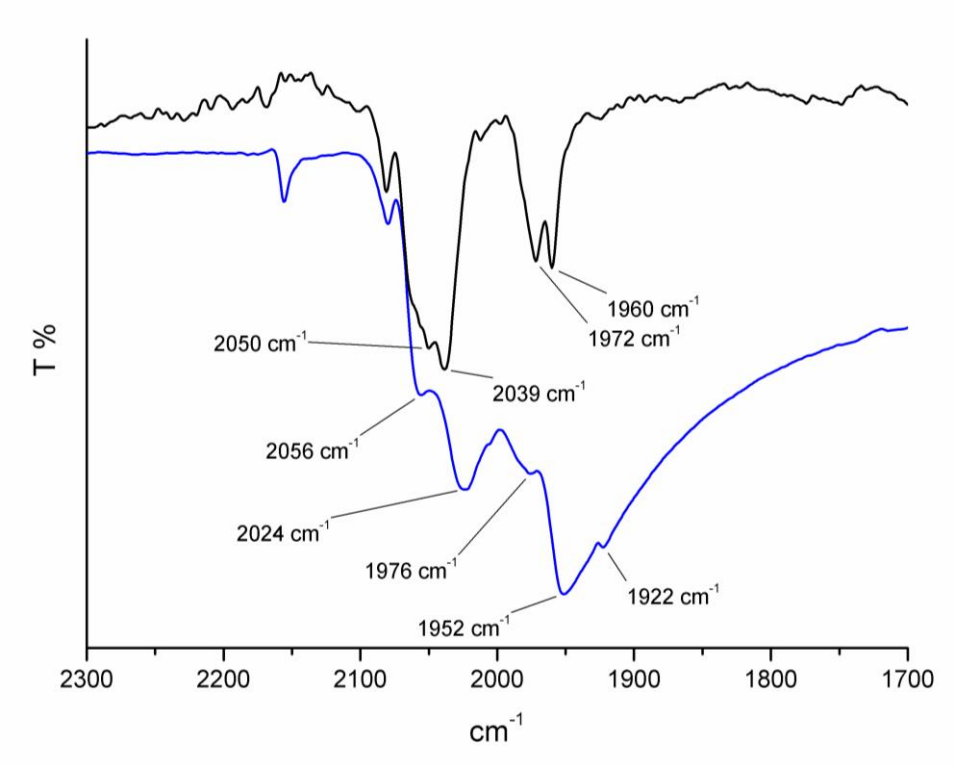

Figure 3.2.3 - ATR Infrared spectra of solid **G21 (Blue)** and **H•G21 (Black).**

A ^{1}H NMR experiment with **G21** provided evidence of the binding of **G21** in $\mathbf{H_{Co}}$. 2 equivalents of **G21** were added to a solution of $\mathbf{H_{Co}}$ in D_2O. NMR spectra were recorded roughly 5 minutes after addition of **G21** and then an hour later. Figure 3.2.4 shows the appearance of new peaks after 5 mins which increased in intensity after an hour – as more **H•G21** is generated. Since **G21** possesses no H atoms there will be no peaks due to bound or free guest.

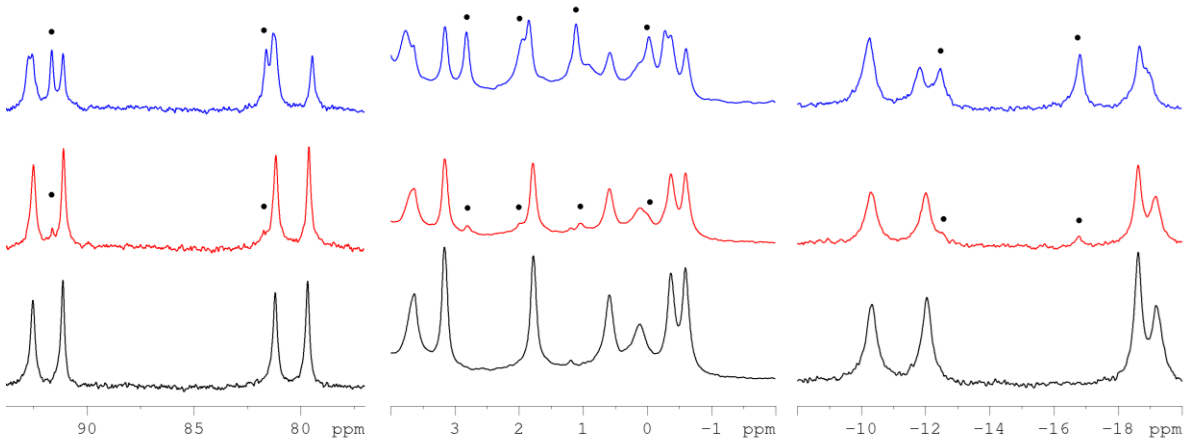

Figure 3.2.4 - Part of the ^{1}H NMR spectra of $\mathbf{H_{Co}}$ (black), 5 minutes after the addition of 2 equivalents of **G21** (red) and 1 hour after the addition of **G21**. New peaks are labelled with •.

The next potential guests that were investigated were the square planar complexes **G22** and **G23**. These metal complexes are both neutral and possess interesting electronic properties. **G22** is a Cu(II)-based bis(thiosemicarbazone) complex; such complexes have been found to be lipophilic and possess a relatively low Cu(II/I) redox potential and also exhibit anti-cancer properties, with the Cu(I) complexes being favoured in the hypoxic environment of tumours.[9–11] The uptake of **G22** into the cavity may potentially facilitate a photoinduced electron transfer from **H** to **G22** resulting in the transient reduction of Cu(II) to Cu(I). **G23** is a bis(dithiolene) metal complex. These have been found to undergo a series of reversible one electron transfers: $[M(S_2C_2R_2)_2] \leftrightarrow [M(S_2C_2R_2)_2]^{1-} \leftrightarrow [M(S_2C_2R_2)_2]^{2-}$.[12] More recent work has discovered that dithiolene complexes exhibit very intense absorptions in the visible and near-infrared regions.[13] Depending on the choice of substituent groups attached to the central core, metal dithiolene complexes can act as either electron donors or acceptors.

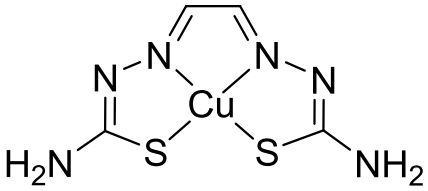

G22

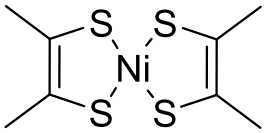

G23

A luminescence titration of **G22** into a solution of **H** afforded the quenching of **H** fluorescence (fig. 3.2.5). Only partial quenching of the cage emission is observed which suggests either: that there is complete quenching of the **H** excited by energy or electron transfer, but a weak binding constant means there is still a significant amount of free cage **H**, or that guest is not in fact binding and that the quenching of fluorescence in afforded collisional quenching.

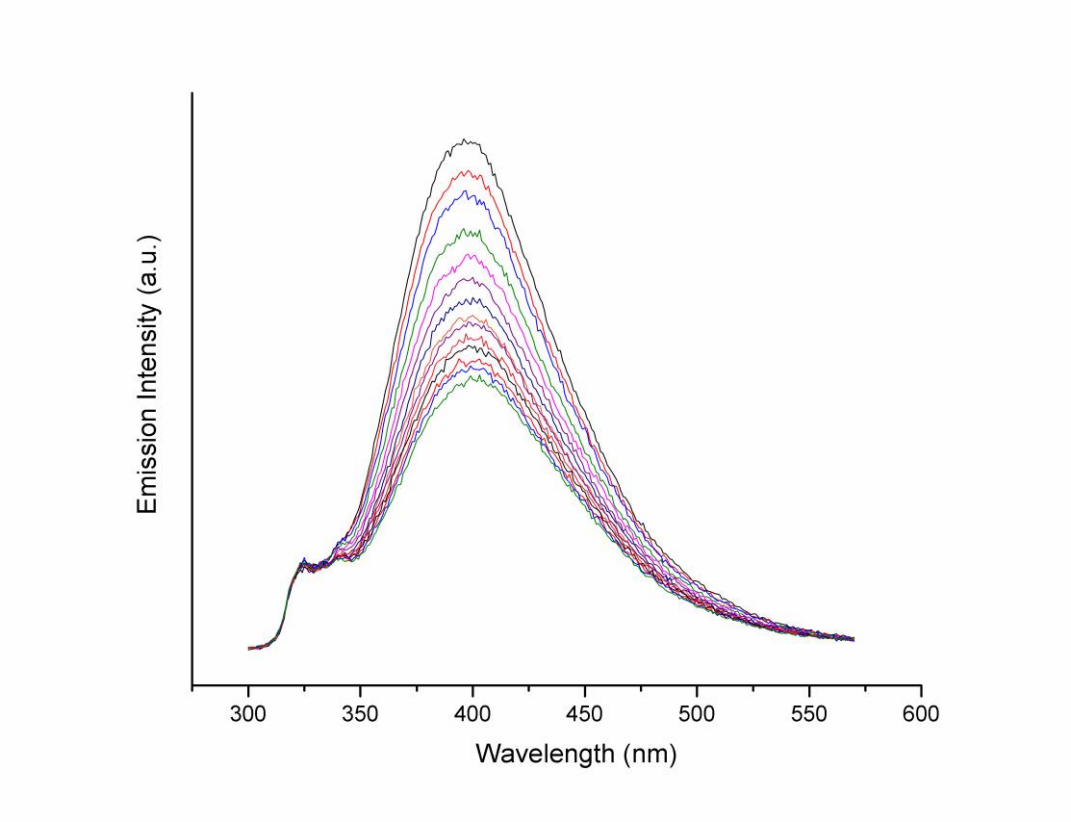

Figure 3.2.5 - Luminsecence spectra recorded during the addition of 0 - 2000 µL **G22** (0.1 mM) into a solution of **H** (1 µM) in H_2O, excitation at 290 nm.

To determine whether or not **G22** is being taken up into the cavity of **H,** a ^{1}H NMR experiment was conducted using $\mathbf{H_{Co}}$ as the host. The addition of **G22** to a solution of $\mathbf{H_{Co}}$ in D_2O showed no change in the NMR spectrum: no shifting of peaks was observed from that of $\mathbf{H_{Co}}$ on its own.

The apparent lack of binding of **G22** is not explained on the basis of molecular volumes: the volume of the cavity is about 407 Å^3 which means that the optimal size of guest for binding is about 224 Å^3**,**[14] and many strongly binding guests are smaller than this. The calculated volume of **G22** is 177 Å^3, so on this basis alone, **G22** would be expected to fit within the cavity. When compared to guests **G18** and **G21**, which do bind within the cage cavity, whose calculated volumes are 199 Å^3 and 175 Å^3 respectively, there seems no reason for **G22** not to bind.

However the cavity is pseudo-spherical in shape, so molecules that bind would be expected to compliment this - guests still need to be able to physically fit inside the cage. Looking at the some of the atom distances in the crystal structure of **G22** (fig. 3.5.6)[15] we see that the size of the molecule in two dimensions is roughly 4.6 x 8.5 Å (larger after taking into account hydrogen atoms) in size.. The Metal···Metal separation in **H** is *ca.* 11 Å, and the cavity has been calculated to have diameter of roughly 7.1 Å so, despite its volume, guest **G22** does not bind due to its eccentric shape which does not match that of the pseudo-spherical cage cavity. In contrast to **G22**, guests **G18** and **G21** are more spherical in shape, better matching the cage cavity which facilitates their uptake.

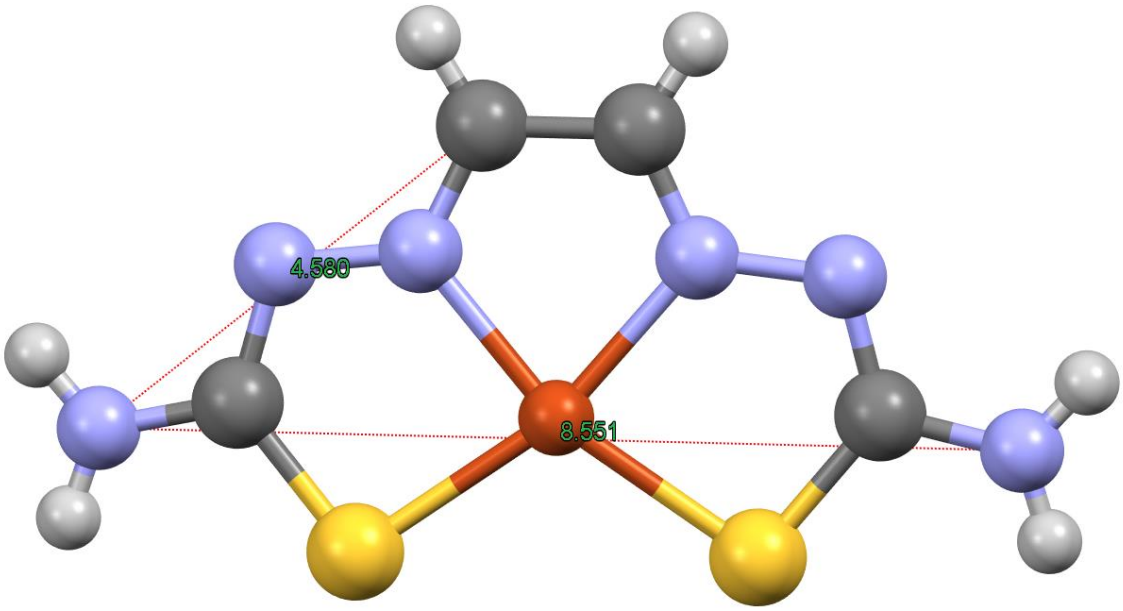

Figure 3.2.6 – Crystal structure of **G22** with two atom-atom distances annotated. [15] Distances are in Å.

As **G22** appears to be too big to bind within the cavity, the observed quenching of luminescence from **H** in Fig. 3.2.5 cannot result from uptake of **G22**. This suggests that the mechanism of quenching is a result of external interaction of **G22** with the cage, possibly by collisional quenching or some type of aggregation.

Titration of **G23** into a solution of **H** again led to partial quenching of **H** fluorescence, however plotting the change in fluorescence intensity against the concentration of **G23** gave a plot that shows a linear relationship between the two (fig. 3.2.7), since a binding curve cannot be accurately fit to this data this suggests that there is no uptake up **G23**. A ^{1}H NMR experiment using $\mathbf{H_{Co}}$ and **G23** also shows no evidence of binding.

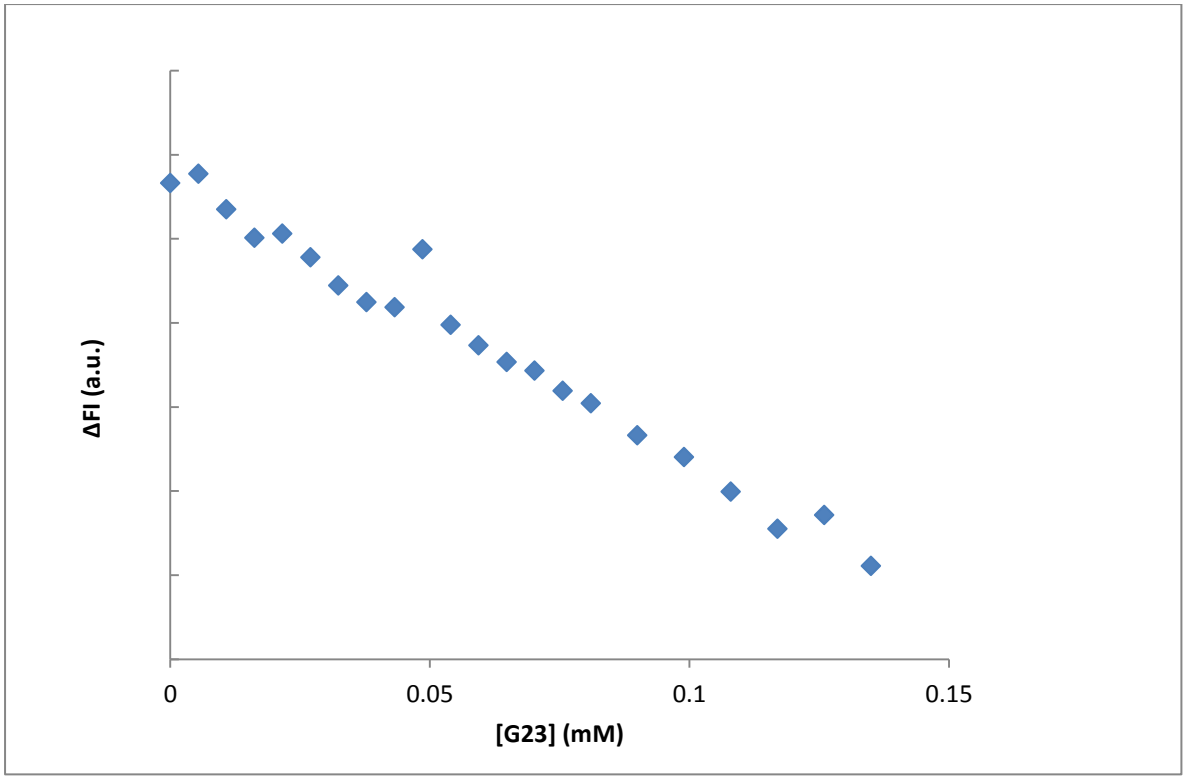

Figure 3.2.7 – Changes of **H** (0.01 mM) fluorescence intensity against concentration of **G23** in H_2O at room temperature.

Using the same size- and shape-based arguments as for **G22**, the calculated volume of **G23** is 228 $Å^3$ which is very close to the ideal guest volume of 224 $Å^3$; so based on volume **G23** should fit within the cavity of **H**. However looking at the atom distances in the crystal structure of **G23** (fig. 3.2.8)[13] the Me···Me distance of opposing ligands is 9.1 Å which, after allowing for H atoms, makes the complex too large to fit inside the cage cavity. Again the issue is the eccentric shape rather than the molecular volume.

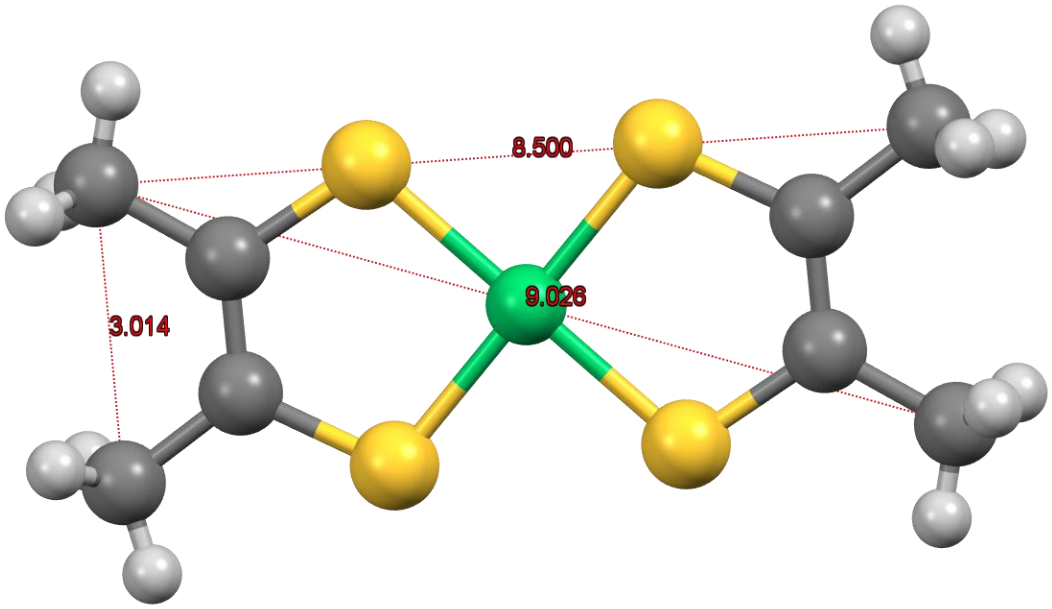

Figure 3.2.8 – Crystal structure of **G23** with three atom-atom distances annotated. Distances are in Å.

Even though there is no evidence for binding of **G23** within the cage cavity we still see a fluorescence quenching effect (Fig. 3.2.7), which is likely due to interaction of **G23** with the exterior of the cage by collisions in solution.

Plotting the fluorescence intensity data as the Stern-Volmer relationship (as given in equation 3.1) produced a non-linear relationship; the shape of the curve suggests that the observed quenching is likely due to a combination of dynamic and static quenching (fig. 3.2.9) mechanisms, for example a combination of collisional quenching (dynamic) and some sort of aggregation of guest and cage in solution (static).

$$\frac{I_0}{I} = 1 + K_{sv}[Q] = 1 + \ k_q \tau_0 [Q]$$

Eq. 3.1: The Stern-Volmer relationship: I = emission intensity; I_0 = emission intensity in absence of quencher; [Q] = quencher concentration; K_{sv} = Stern-Volmer quenching constant; k_q = bimolecular quenching rate constant; τ_0 = lifetime in absence of quencher.

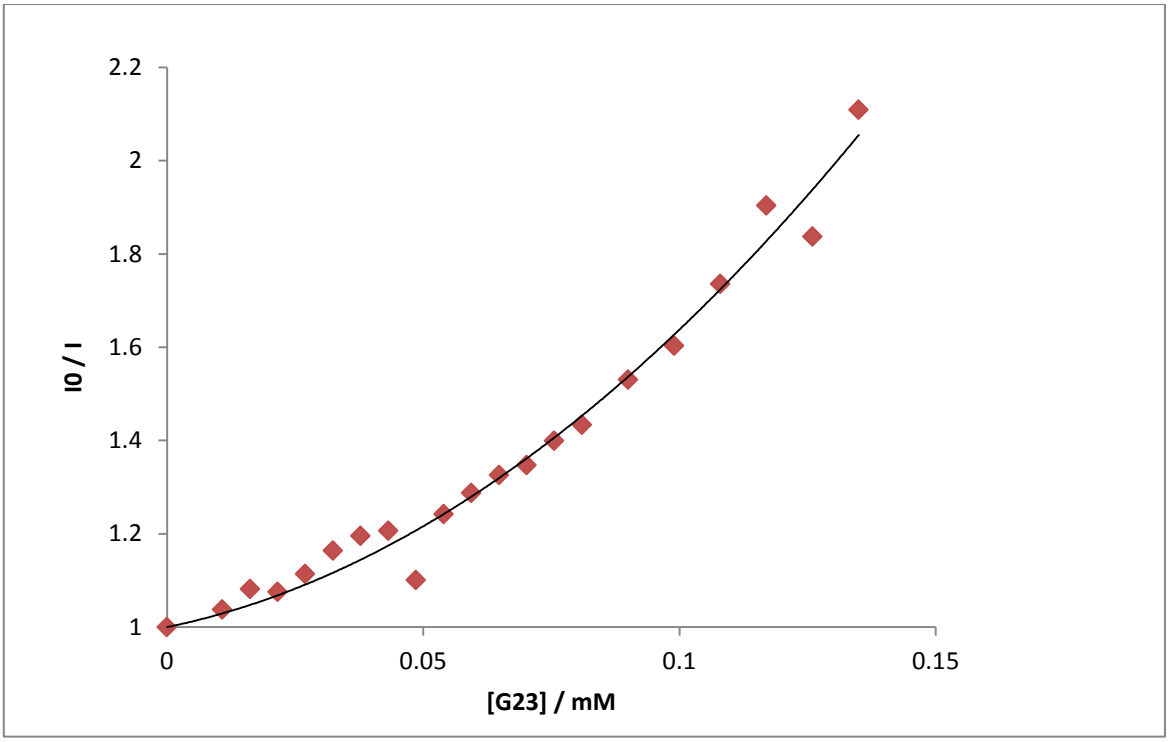

Figure 3.2.9 - Stern-Volmer plot of the change in fluorescence of **H** against the concentration of added **G23**.

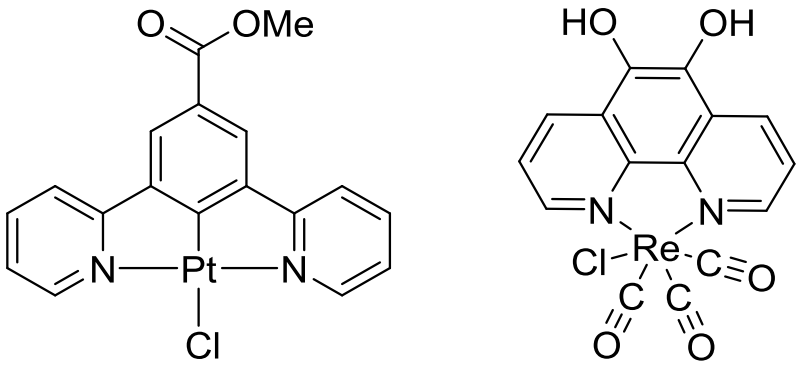

G24 **G25**

The next three metal complexes that were studied as potential guests were deliberately chosen due to them being neutral and also being far too large for the cage cavity to afford binding. These guests (or derivatives of) are known to possess an MLCT absorption band around 400 nm, hopefully overlapping with fluorescence of **H. G24** is planar, similar to guests **G22** and **G23**, whereas the octahedral complex **G25** is more pseudo-spherical in

shape, similar to guests **G1** – **G21.** The titrations of **G24** and **G25** with **H** should provide some insight into whether the quenching of **H** fluorescence observed for some of the other complex guests could be due to interaction of the 'guest' complex with the *exterior* of the cage and not as a result of binding inside the cavity.

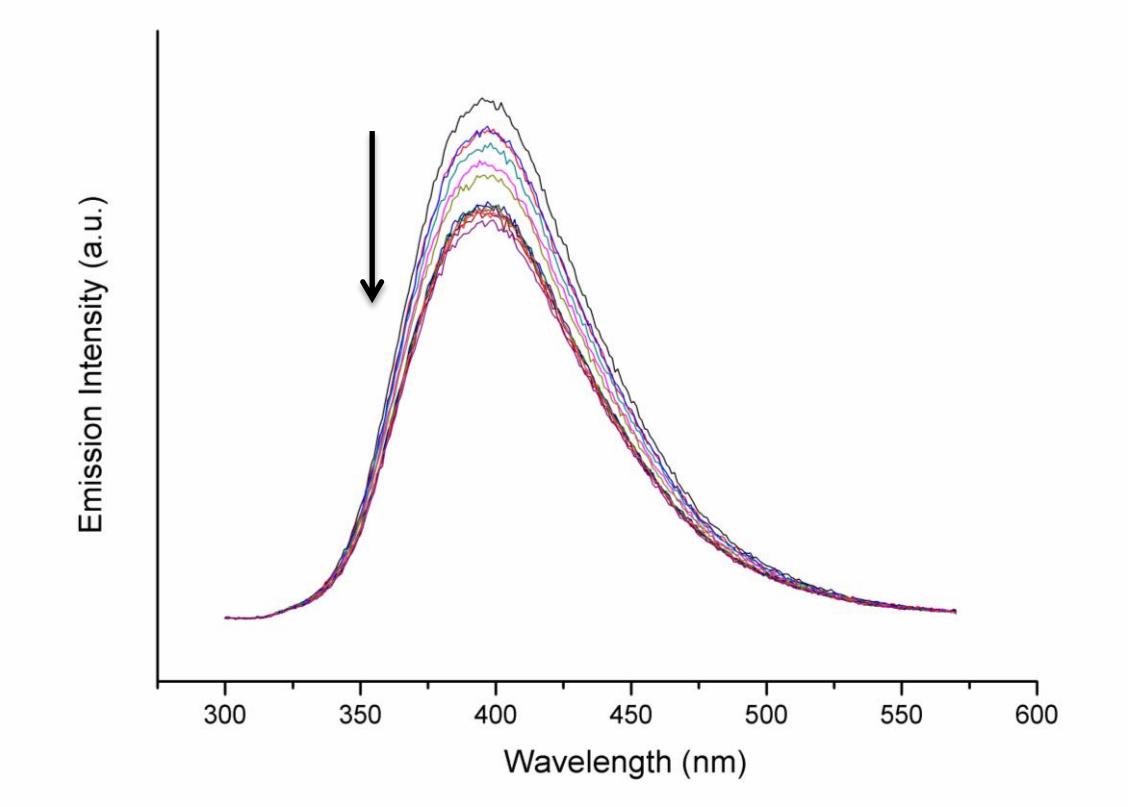

Figure 3.2.10 – Fluorescence spectra recorded during of titration of **G24** (0.1mM) into a solution of **H** (0.01 mM) in water. Excitation at 290 nm.

As expected, due to **G24** being too large for the cavity, the titration of **G24** into a solution of the cage resulted in only a small amount of quenching. Due to the poor solubility of **G24** in aqueous solution it was originally though the lack of quenching was due to solubility limitations. However, plotting the change in fluorescence at 400 nm *vs.* the concentration of **G24** shows that there is no additional quenching of fluorescence after a certain concentration of **G24** (fig. 3.2.11).

This behaviour suggests that the quenching of **H** fluorescence by **G24** may be the result of collisional quenching. The plateau observed in the change in fluorescence resembles that seen for the quenching of tryptophan fluorophores within a protein – one tryptophan is accessible to the quencher while the other is buried within the protein and as such is inaccessible to the quencher.[16]

In the case of **H**, there are 12 naphthyl chromophores within the structure of the cage. The chances of all 12 chromophores being quenched by collision are low, which suggests that a number of napthyl chromophores would remain unquenched, resulting in the plateau.

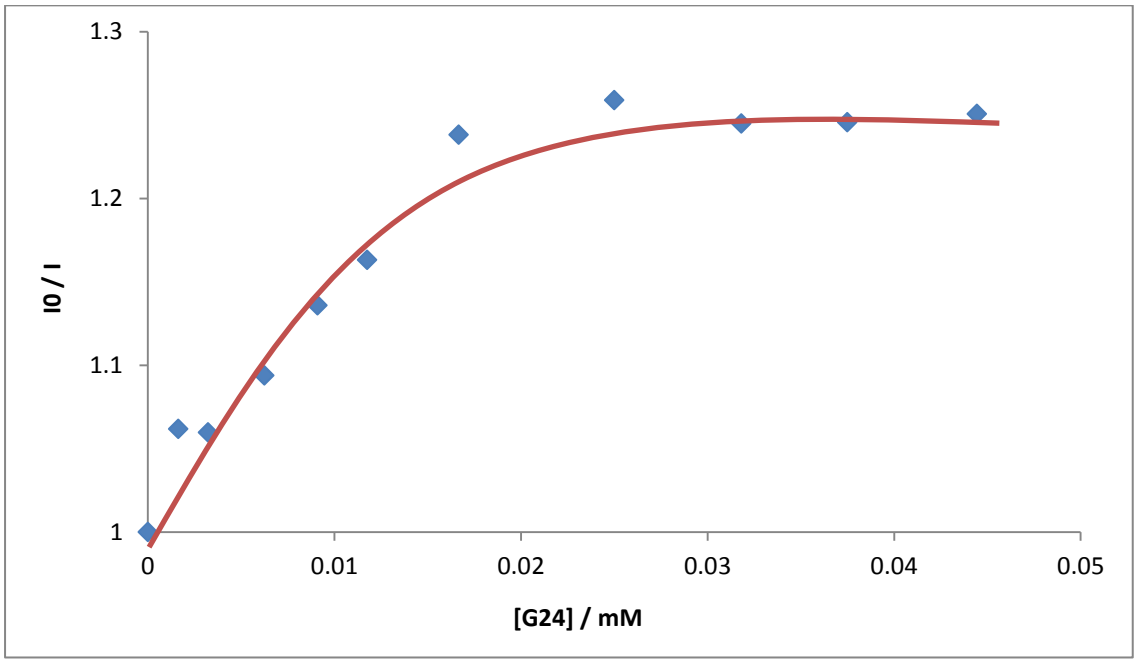

Figure 3.2.11 - Stern-Volmer plot of the change in fluorescence of **H** against the concentration of added **G24**.

The problem with **G24** is its poor solubility in water. Guest **G25** however possesses two hydroxyl groups which imparts superior solubility in water. The titration of **G25** into a solution of **H again** resulted in the quenching of fluorescence: the amount of quenching observed is much more substantial than seen for **G24** but this may simply be due to the better solubility of **G25**, meaning a higher concentration in solution. The quenching of fluorescence by **G25** resulted in a curve (fig. 3.2.12), could not be ascribed to guest binding as **G25,** as with a calculated volume of 323 $Å^3$, this guest is too large to fit within the cage's cavity and there is no ^1H NMR spectroscopic evidence of binding.

A Stern-Volmer plot of luminescence intensity of **H** during titration with **G25** shows a non-linear relationship (fig. 3.2.13), the shape of which is similar to that observed for **G23**, suggesting that the quenching arises from a mixture of dynamic and static quenching mechanisms.

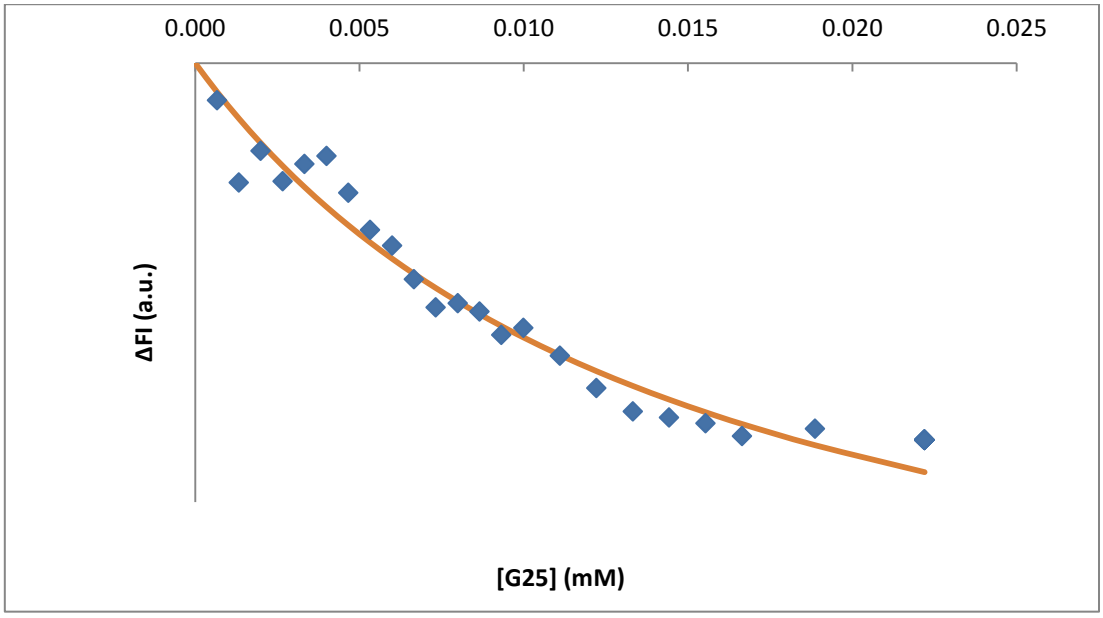

Figure 3.2.12 - 1:1 binding isotherm fit for the uptake of **G25** into **H** in H_2O at room temperature.

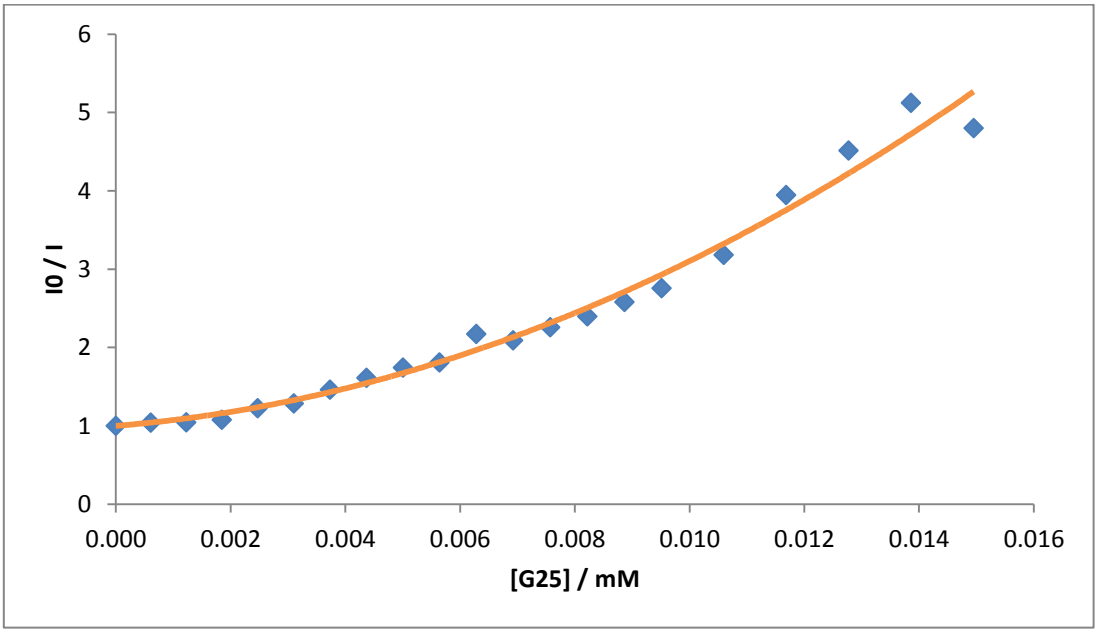

Figure 3.2.13 - Stern-Volmer plot of the change in fluorescence of **H** against the concentration of added **G25**.

3.3 Conclusion

The uptake of neutral metal complexes within the cavity of a $[Cd_8(L_w^{1,5\text{-naph}})_{12}]^{16+}$ cubic cage has been demonstrated. The uptake of guests **G18 – G21** was confirmed by ^{1}H NMR experiments and the binding resulted in partial quenching of the fluorescence of **H.**

Some other neutral metal complexes were found not to bind within the cavity of the cage, while a number of these guests had optimal volumes for binding inside the cage their non-spherical chapes made them larger in one dimension than the cage interior could accommodate, leading to incpatibility between the eccentric shapes of these potential guests and the pseudo-spherical cage cavity.

Guest molecules that not did bind still displayed, however, a quenching effect on the fluorescence of **H**. From applying Stern-Volmer analyses the observed queching could be ascribed to a combination of (i) dynamic collisional quenching with chromophores on the exterior of the cage, and (ii) static quenching involving groundstate aggregation of cage and quencher.

3.4 Experimental techniques and procedures

3.4.1 Materials

G24 was provided by Dr Elizabeth Edwards. Dry solvents were obtained from an in-house Grubbs solvent dispensing system. 5,6-hydroxy-1,10-phenanthroline was synthesised by a previous member of the Ward group.

3.4.2 Volume Calculations

Molecular volumes were calculated by Dr Alex Metherell using the Spartan modelling software, using the molecular mechanics force fields calculation model.

3.4.3 Synthetic Procedures

Glyoxal dithiosemicarbazone

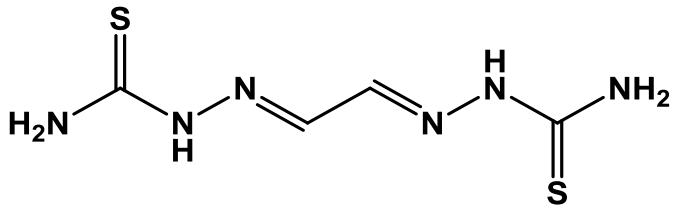

9.8 cm^3 Glyoxal (40% in H_2O, 0.0861 mol) was dissolved in 50 cm^3 ethanol, to this a solution of thiosemicarbazide (15.7 g, 0.172 mol) in 150 cm^3 H2O and 10 cm^3 glacial acetic acid was added. The rection was heated to 100 °C for 30 mins. The reaction was cooled to room temperature and the precipitate was filtered off. The precipitate was washed with 3 x 50 cm^3 hot ethanol and 3 x 50 cm^3 hot acetone to give glyoxal dithiosemicarbazone (15.0 g, 85 %) a yellow solid.

ES-MS: m/z = 205.27 $[M + H]^+$

^{1}H NMR (400 MHz, d_6-DMSO); 7.72 (s, 2H); 7.88 (s, 2H); 8.32 (s, 2H); 11.69 (s, 2H);

Cu(II) glyoxal dithiosemicarbazone (G23)

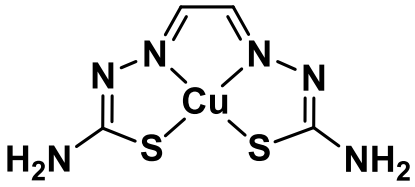

Glyoxal dithiosemicarbazone (2.4 g, 0.012 mol) was suspended in 100 cm^3 DMF, the solution was heated to 150 °C and a solution of $Cu(OAc)_2$ (2.13g, 0.012 mol) in 40 ml 1:1 H2O and ethanol was added. The reaction was stirred at 150 °C for 15 mins, and then cooled to room temperature. The precipitate was filtered off and washed with DMF and ethanol to give **G22** (3.94 g, 94%) a dark red solid.

ES-MS: m/z = 265.94 $[M + H]^+$

Ni(II) $(S_2C_2Me_2)_2$ (G24)

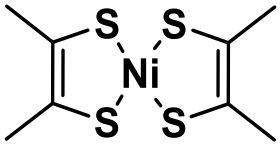

Acetoin (0.11 g, 0.024 mol) and phosphorus pentoxide (1.0 g, 0.023 mol) were dissolved in 35 cm3 1,4-dioxane and refluxed for 2 hours. The reaction was cooled to room temperature and a solution of $NiCl_2.6H_2O$ (1.48 g, 0.062 mol) in 20 cm^3 H_2O was added. The reaction mixture was heated at 100oC for 2 hours and then cooled to room temperature. The resulting black precipitate was filtered and washed with H_2O and recrystallized from toluene to give **G24** (1.50g, 82%) a black/purple solid.

^1H NMR (400 MHz, $CDCl_3$); 7.55 (s, 12H);

5,6-hydroxy-1,10-phenanthroline rhenium tricarbonylchloride (G25)

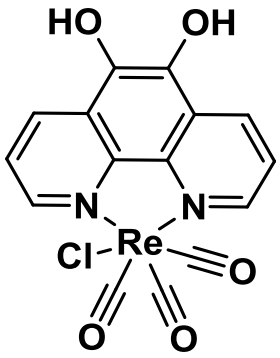

5,6-hydroxy-1,10-phenanthroline (0.1 g, 0.27 mmol) and Rhenium pentacarbonylchloride (0.06 g, 0.27 mmol) were suspended/dissolved in 50 cm^3 toluene. The mixture was refluxed for 3 hours. The resulting precipate was filtered and washed with cold toluene to give **G25** (0.132 g, 94%).

ES MS: m/z= 518.9 $[M + H]^+$, 483.0 $[M - Cl]^+$

3.5 References

1 V. F. Slagt, J. N. H. Reek, P. C. J. Kamer and P. W. N. M. van Leeuwen, *Angew. Chem. Int. Ed.*, 2001, **40**, 4271–4274.

2 M. Kuil, T. Soltner, P. W. N. M. van Leeuwen and J. N. H. Reek, *J. Am. Chem. Soc.*, 2006, **128**, 11344–11345.

3 D. H. Leung, R. G. Bergman and K. N. Raymond, *J. Am. Chem. Soc.*, 2006, **128**, 9781–9797.

4 M. Otte, P. F. Kuijpers, O. Troeppner, I. Ivanović-Burmazović, J. N. H. Reek and B. de Bruin, *Chem. - A Eur. J.*, 2013, **19**, 10170–10178.

5 W. A. G. Graham, *Inorg. Chem.*, 1968, **7**, 315–321.

6 J. E. M. Lewis, E. L. Gavey, S. A. Cameron and J. D. Crowley, *Chem. Sci.*, 2012, **3**, 778–784.

7 S. Turega, M. Whitehead, B. R. Hall, A. J. H. M. Meijer, C. a. Hunter and M. D. Ward, *Inorg. Chem.*, 2013, **52**, 1122–1132.

8 E. Peris, A. Mata and V. Moliner, *J. Chem. Soc.*, Dalton Trans., 1999, **0**, 3893-3898

9 J. L. J. Dearling and P. J. Blower, *Chem. Commun.*, 1998, **0**, 2531–2532.

10 J. L. J. Dearling, J. S. Lewis, G. E. D. Mullen, M. J. Welch and P. J. Blower, *J. Biol. Inorg. Chem.*, 2002, **7**, 249–259.

11 C. Stefani, Z. Al-eisawi, P. J. Jansson, D. S. Kalinowski and D. R. Richardson, *J. Inorg. Biochem.*, 2015, **152**, 20–37.

12 B. S. Lim, D. V. Fomitchev and R. H. Holm, *Inorg. Chem.*, 2001, **40**, 4257–4262.

13 B. Garreau-de Bonneval, K. I. Moineau-Chane Ching, F. Alary, T. T. Bui and L. Valade, *Coord. Chem. Rev.*, 2010, **254**, 1457–1467.

14 S. Turega, W. Cullen, M. Whitehead, C. a. Hunter and M. D. Ward, *J. Am. Chem. Soc.*, 2014, **136**, 8475–8483.

15 P. J. Blower, T. C. Castle, A. R. Cowley, J. R. Dilworth, P. S. Donnelly, E. Labisbal, F. E. Sowrey, S. J. Teat and M. J. Went, *Dalt. Trans.*, 2003, 4416–4425.

16 M. R. Eftink and L. A. Selvidge, *Biochemistry*, 1982, **21**, 117–125.

Chapter 4

Two-step Sensitisation of Eu(III) by Photoinduced Energy-transfer from a Coordination Cage

4.1 Introduction

The drive to find alternative sources of energy has meant that the harvesting of solar energy has been, and still is, a major area of research in chemistry.[1] Nature harvests sunlight through the process of photosynthesis: the endothermic conversion of water and CO_2 to sugars. Many artificial systems are designed to mimic the function of natural light harvesting antennae[2–4] and/or reaction centres[5] as a means to drive chemical reactions or to generate electrical energy. Understanding the role of photoinduced electron- and energy-transfer in these systems helps the creation of various solar energy conversion and storage systems.[6–8]

Porphyrins are highly attractive chromophores, often highly fluorescent and possessing rich redox chemistry – most importantly, both of these properties are easily tuneable. The combination of porphyrins with other photo and redox active species has led to a myriad of multicomponent systems for use in light harvesting applications.[9,10]

One such system from the D'Souza group utilises a two-part system: a carboxylic acid functionalised porphyrin and a 2-aminopydrine functionalised fullerene. The functionalisation of the two components facilitates self-assembly via hydrogen bonding interactions. (Fig. 4.1.1). The self-assembled system was shown to display photoinduced charge separation with slow charge recombination.[11]

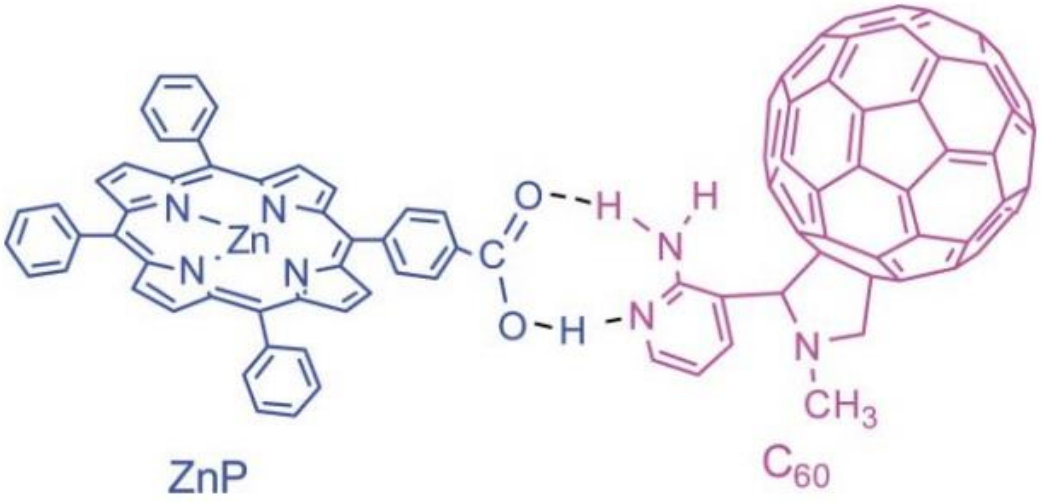

Fig. 4.1.1 - Structure of a porphyrin-fullerene supramolecular adduct held by a hydrogen bonding motif. Reproduced with permission from ref. 11.

Self-assembly has been well studied for its capacity to generate synthetic host molecules which possess a cavity capable of the encapsulation of guest molecules. A number of self-assembled supramolecular systems with redox properties have been reported, these include rings[12,13] and cages.[14,15] A number these host-guest systems have demonstrated the ability to perform photocatalysis on an encapsulated substrate. The photosenstized oxidation of encapsulated adamantane to 1-adamantanol within a Pd_6L_4 tris(pyridyl)triazine-based coordination cage was demonstrated by Fujita and co-workers. Excitation of the host-guest adduct results in the photoinduced electron transfer from adamantane to the photoexcited triazine units in the host structure generating a host-anion guest-cation pair (Fig. 4.1.2), which is then trapped by H_2O or O_2 affording the photooxidised product.[16] The same cage has been also been used in the photodriven anti-Markovnikov hydration of internal alkynes which can occur in the central cavity.[17]

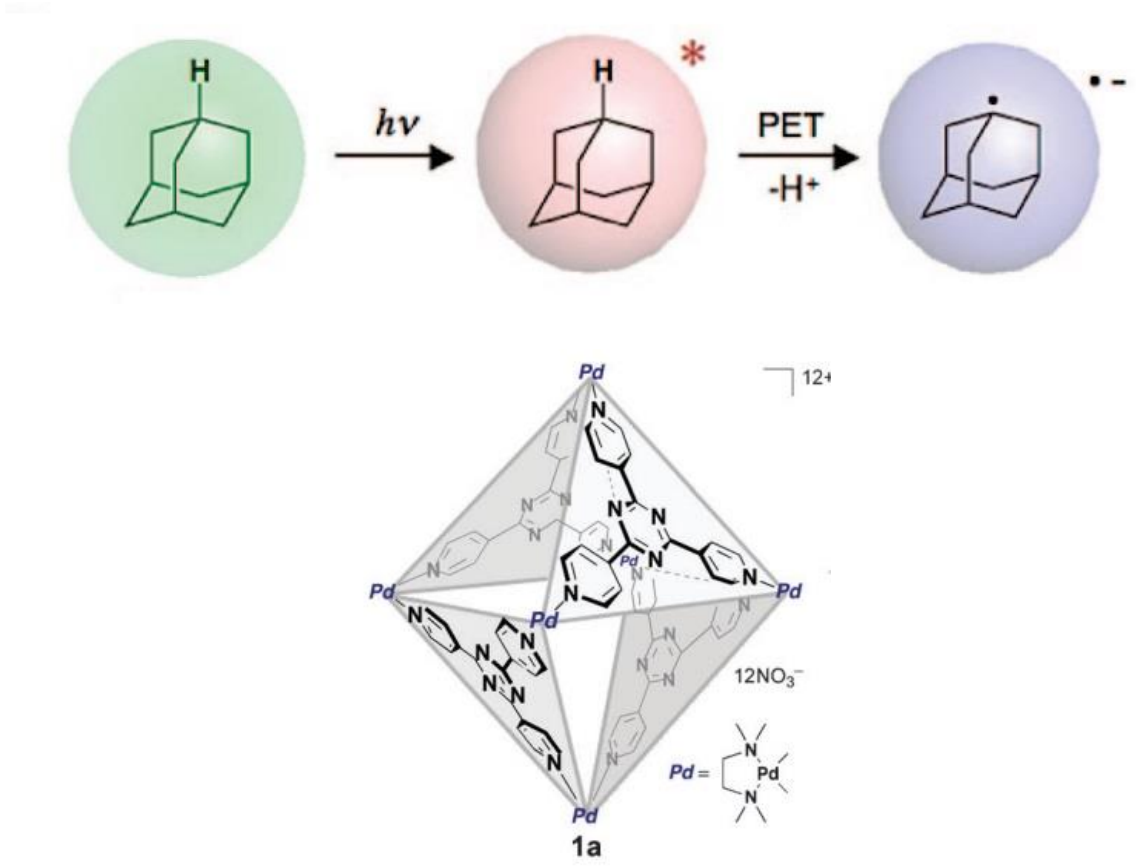

Fig. 4.1.2 – The photogeneration a Pd_6L_4/adamantane radical pair. The used Pd_6L_4 cage is also shown. Reproduced with permission from ref. 16.

Raymond and co-workers have reported an example of photo-induced electron-transfer from a $Ga_4L_6^{12-}$ coordination cage to a bound guest. Encapsulation of cinnamylammonium cation guests followed by irradiation with UV light facilitates the 1,3-rearrangement of the linear guest to a higher energy branched isomer (fig. 4.1.3). The Ga4L612– cage absorbs a photon which then transfers an electron to the encapsulated cinnamylammonium ion: the resulting C–N bond cleavage, followed by back electron transfer to the cage and recombination of the guest fragments form the higher energy isomer. Interestingly, the 1,3-rearrangement does not occur in bulk solution but only in the presence of the cage and light.[18]

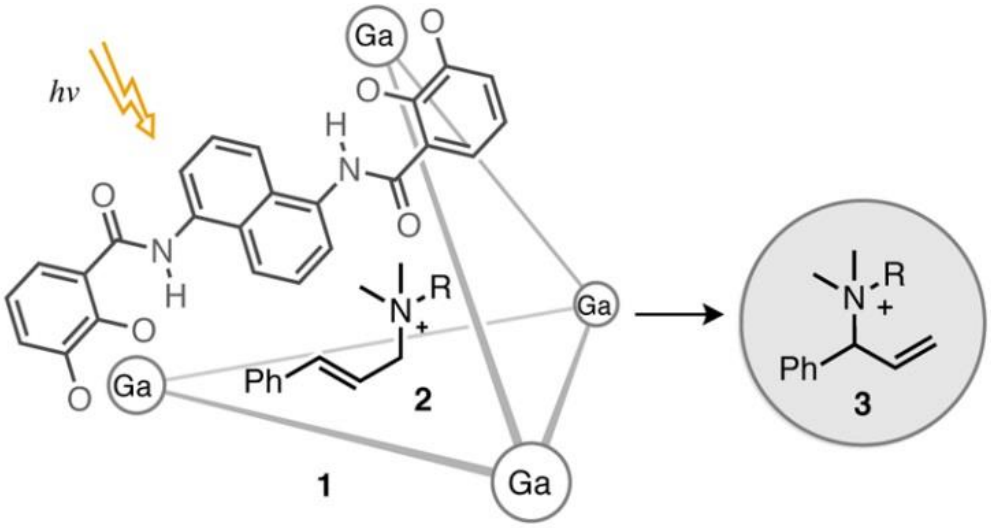

Figure 4.1.3 - 1,3-rearrangement of encapsulated cinnamylammonium ion following photosensitisation by a Ga_4L_6 host. Reproduced with permission from ref. 18.

4.1.2 The Project

The aim of this project were twofold: i) to investigate the possibility of utilising photoinduced energy transfer from the cubic $[Cd_8(L^{w1,5\text{-naph}})_{12}]^{16+}$ cage **H** to an encapsulated guest molecule to sensitise emission from Eu(III) in an indirect two-step process. ii) To design and synthesise a guest molecule that can protrude from within the cage structure into the surrounding aqueous solution.

Lanthanide compounds typically have weak emission intensity when directly excited, owing to the fact that the f-f transitions are Laporte forbidden and possess low molar absorptivity. However, lanthanide emission can be sensitised by an appropriate chromophore acting as an antenna, harvesting photons and transferring the energy to the lanthanide ion. This "antenna-effect" can be performed by both organic[19,20] and d-block transition metal complexes.[21–24] Sensitisation of Eu(III) emission by the antenna-effect has been used as the basis for white light emitting molecules[19,24] and in biological imaging agents.[25–27]

By using a suitable chromophore that can receive energy from the excited state of **H** and which is in turn attached to a lanthanide-binding chelating ligand, it may be possible to create a supramolecular assembly that can act as a two-step energy transfer bridge between **H** and Eu(III) (fig. 4.1.1). Designing the guest to be hydrophobic at one end of the molecule (which binds in the cage cavity) while the other end is hydrophilic and prefers to be in the aqueous solvent outside the cage, using a thin connecting group, will allow for the rod-shaped guest to protrude out from one of the cage windows such that one end is inside the cage and the other end is outside.

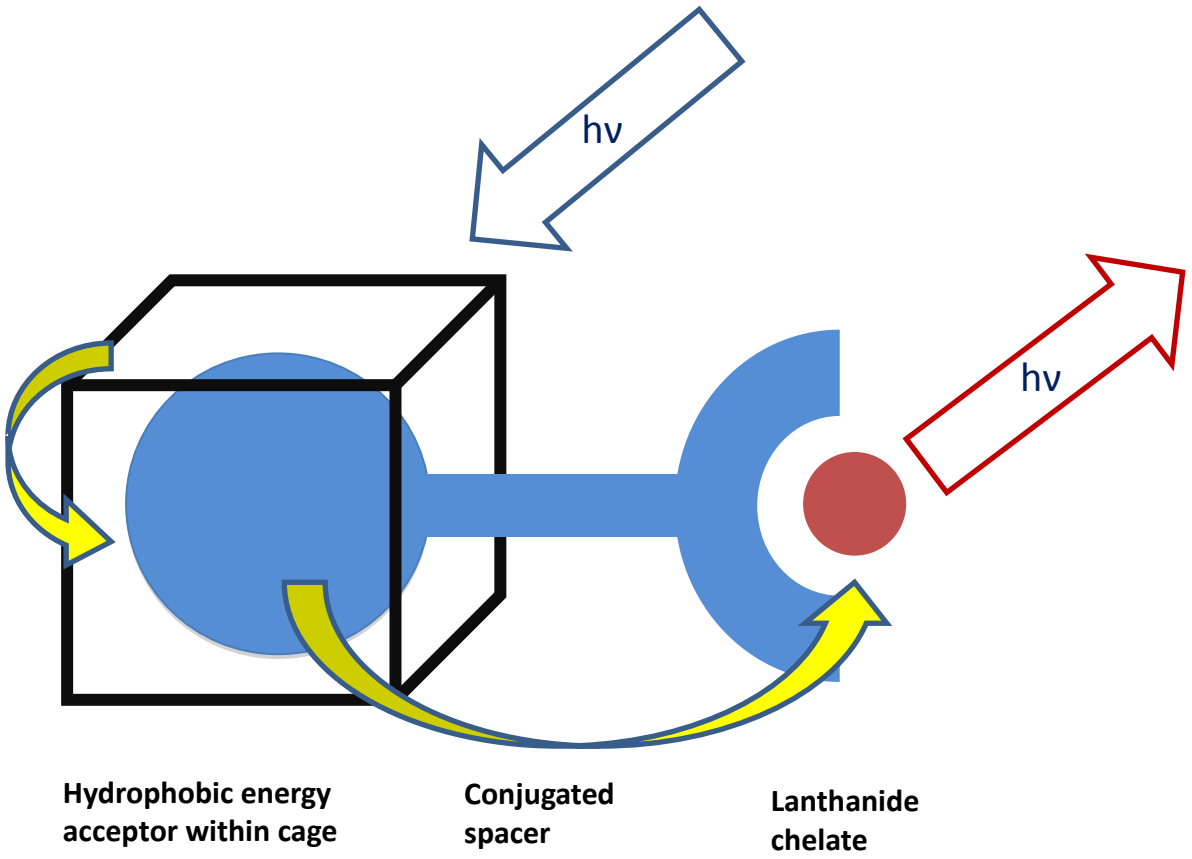

Figure 4.1.1 – Representation of the energy transfer following the excitation of cage, resulting in sensitised emission from Eu(III).

In chapter 2 we saw how the uptake of strongly-binding 1-hydroxypyrene within the cage **H** resulted in photoinduced energy transfer from host to guest. Therefore a pyrene unit was chosen to bind inside the cage cavity where: it binds strongly in the cavity of **H**, is capable of accepting energy from excited naphthyl units and can in turn sensitise the Eu(III) excited state. The coordination of Eu(III) to the pyrene unit will be provided by a heptadentate pyridine-2,6-bis(amino-diacetate) chelating unit, which has an overall charge of 1- and a number of acetate groups, which should provide suitable hydrophilicity for this to be "happy" in aqueous phase outside the cage cavity. These two units are connected together by one or more alkynyl spacers; the target molecule is shown below in fig. 4.1.2.

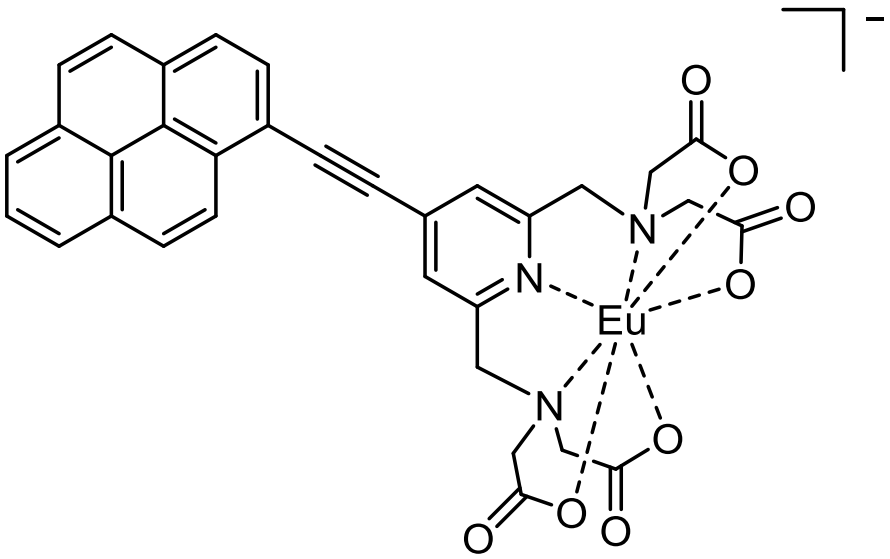

Figure 4.1.2 – The target molecule: **Py-Che-Eu**

4.2 Synthesis of Py-Che-Ln

4.2.1 Synthesis 1-ethynylpyrene

The initial step was the mono-bromination of pyrene following an altered method from the Wu group.[28] The reaction was performed by dissolving the pyrene in DMF and then adding a single equivalent of NBS as the source of bromine. The reaction proceeds at room temperature and is complete by the following day. It was found that the addition of enough H_2O causes the precipitation of the product **1** which, following thorough drying, was found to be pure by ^1H NMR (fig. A3.1.1 in appendix 3) with a yield of 96%.

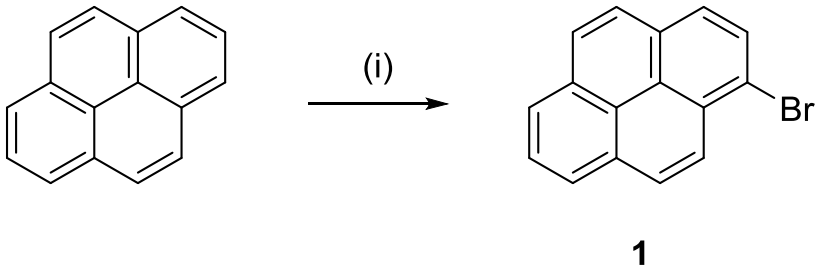

1

Scheme 4.1 – Synthesis of 1-bromopyrene: (i) NBS, DMF, r.t, 16 hours

To connect the conjugated spacer, a Sonogashira coupling reaction was performed between 1-bromopyrene **1** and 1-trimethylsilylacetylene (Scheme 4.2) under an N_2 atmosphere using $Pd(PPh_3)_2Cl_2$ and CuI as the catalysts and triethylamine as base and solvent. Reaction proceeded at R.T. or 60 °C for 16 hours, the reaction mixture was purified by column chromatography on silica eluting with petroleum ether.

The purification presented a few problems: the reaction mixture was not soluble enough in petroleum ether to allow for its addition to the column. The addition of mixtures of dichloromethane and petroleum ether resolved the solubility problem but did not allow for a good separation during elution.

Finally purification was afforded by the solid loading of the reaction mixture to the chromatography column. The reaction mixture was dissolved in the minimum amount of diethyl ether followed by the addition of flash chromatography grade silica; removal of the solvent adsorbed the reaction mixture onto the silica. This allowed for the elution using petroleum ether resulting in good separation of the product, affording the trimethylsilyl protected product **2** with a yield of 78%.

Deprotection of the trimethylsilyl protecting group was afforded by dissolving **2** in a 1:1 mixture of methanol and dichloromethane followed by the addition of K_2CO_3. The suspension was stirred at room temperature overnight. The product was purified by flash chromatography on silica with chloroform.

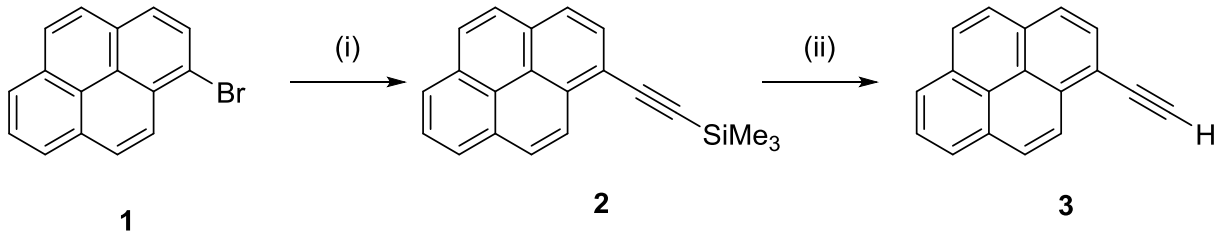

Scheme 4.2 – Synthesis of 1-ethynylpyrene: (i) TMSA, $Pd(PPh_3)_2Cl_2$, CuI, Et_3N, 60 °C, N_2, 24 hours, 78%. (ii) K_2CO_3, $MeOH/CH_2Cl_2$, 16 hours, 99%.

4.2.2 Synthesis of protected lanthanide chelate (4)

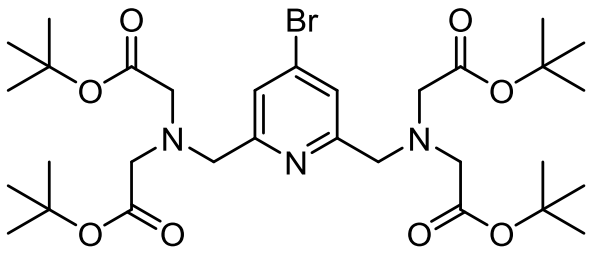

4

The target lanthanide chelating unit had been synthesised and used by the group previously, the protected chelate **4** has a bromine group in the 4 position on the pyridine ring which allows for connection to fragments. The original route to **4** is shown in Scheme 4.3 below; the relatively low overall yield of **4** prompted an attempt to revise the synthetic route to the product.

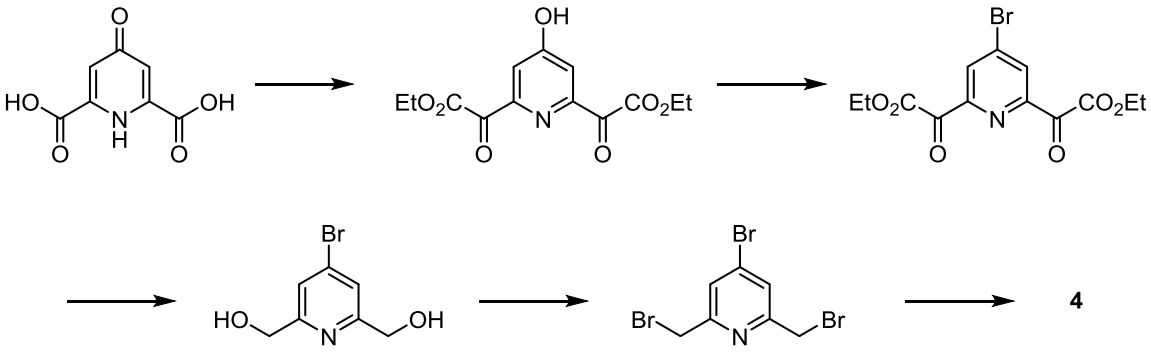

Scheme 4.3 - Original synthetic route to **4**

The first step in the revised synthesis used the commercially available 2,6-dimethyl-4-hydroxypyridine as starting material. The hydroxyl group is substituted by a bromine atom using phosphorus(V) pentabromide in chloroform (scheme 4.4) to give **5** with a yield of 76%.

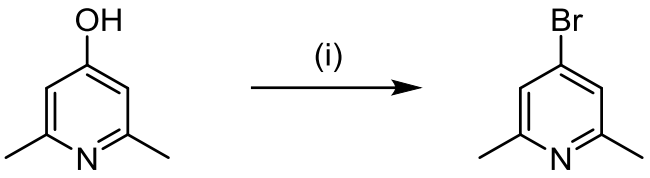

5

Scheme 4.4 – Synthesis of 4-bromo-2,6-dimethylpyridine: (i) PBr_5, $CHCl_3$, Reflux, 16 hours.

Next, 2,6-dimethyl-4-bromopyridine **5** was converted to **6** via a radical bromination reaction utilising N-bromosuccinimde (NBS) as the source of bromine radicals. However, the initial attempts to synthesise **6** from **5** via this method resulted in low and inconsistent yields; using two equivalents of NBS lead to large amount of unreacted starting material, some desired product, and some partially reacted material in which one methyl group of **5** was singly or doubly brominated. Increasing the number of equivalents of NBS resulted in an increased yield of **6**, but also increased the complexity in number of side products with over-bromination and uneven bromination of the two methyl groups of **5** occurring.

The solution to this problem came from the adapting a preparation of benzylic bromides by Liu *et. al.*[29] By reacting **5** with a large excess of NBS, in refluxing chloroform, under UV irradiation with benzoyl peroxide as the radical initiator, an over brominated product **5a** was obtained. This was followed by a partial debromination to the desired mono-brominated product by the addition of 4 equivalents of both N,N-diisopropylethylamine and diethylphosphite at 0 °C in dry THF under an inert atmosphere (Scheme 4.5). After purification by column chromatography the synthesis of the product was confirmed by ^1H NMR (fig. A3.1.2 in appendix 3) obtained with a yield of 63%.

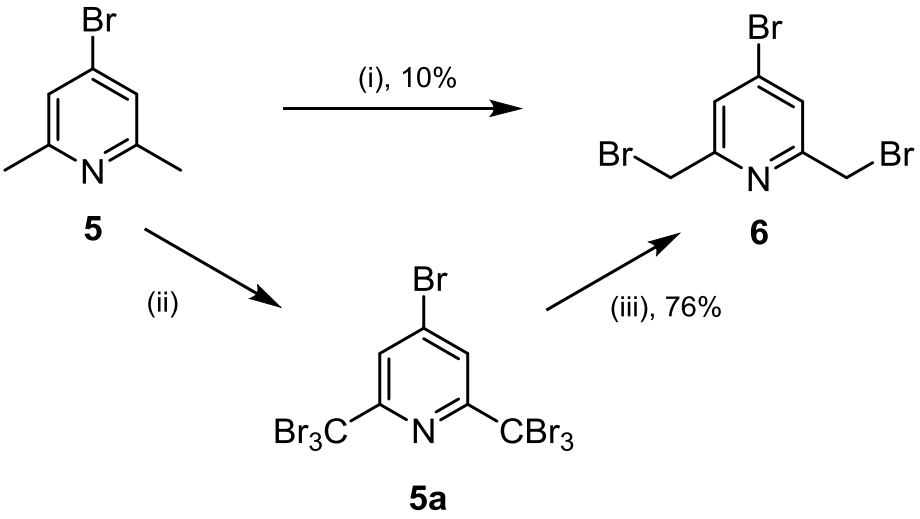

Scheme 4.5 – Two routes towards the synthesis of 4-bromo-2,6-dimethylpyridine: (i) 2 equiv. NBS, AIBN, $CHCl_3$, reflux, 6 hours. (ii) 3 x 2 eq equiv. NBS, $CHCl_3$, benzoyl peroxide, reflux, 6 hours.

The final step remained unaltered from the original route: reaction of **6** with di-tert-butyl iminodiacetate and potassium carbonate in MeCN gave the target compound **4** with a good yield of 90% (Scheme 4.6).

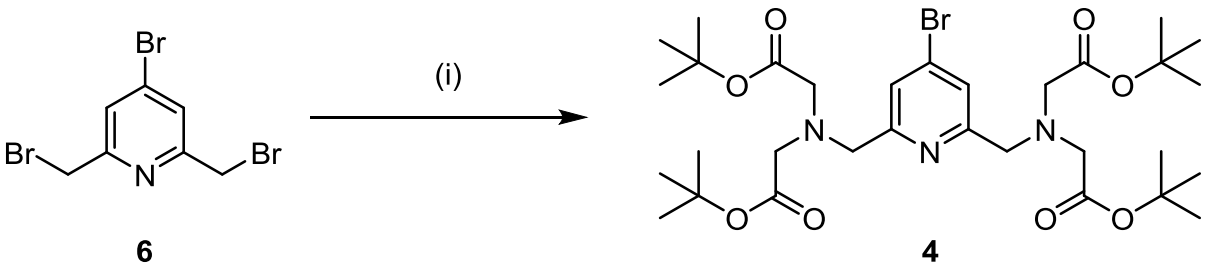

Scheme 4.6 – Synthesis of **4**: (i) di-*t*-butyl-iminodiacetate, K_2CO_3, MeCN, 16 hours.

4.2.3 Synthesis of Py-Che-Eu

Compounds **3** and **4** were then coupled together via the use of a Sonogashira coupling reaction. While Sonogashira couplings typically utilise a Cu(I) co-catalyst for the transmetalation step, the use of such a catalyst led to a large amount of alkyne homocoupling (the Glaser reaction, Scheme 4.7); for which Cu(II) – presumably arising from partial oxidation of the Cu(I) ions present – is a well-known catalyst. Attempts to remove as much oxygen from the system, by means of a more thorough deaerating of solvent and the use of Ar in place of N_2 as the inert gas, resulted in a decrease in the amount of homocoupled product but there still was a significant amount.

This lead to an attempt of a copper-free Sonogashira-type coupling, this method utilised tetrabutylammonium fluoride instead of copper;[30] the lack of Cu(I) should result in a significant decrease in homocoupled product. The suggested mechanism involves the reaction of the alkyne with TBAF to generate a small amount of alkynyl anion which then then goes on to react with the Pd catalyst in place of the standard transmetallation step. The reaction of **3** with **4** in the presence of the Pd catalyst and tetrabutylammonium fluoride did indeed significantly reduce the amount of alkyne homocoupling and after purification the desired product **7** was obtained with a yield of 60% and confirmed by NMR (Figure A3.1.3 in appendix 3). This method could also be used for the one-pot desilylation and copper-free coupling of **2** with **4.**[31]

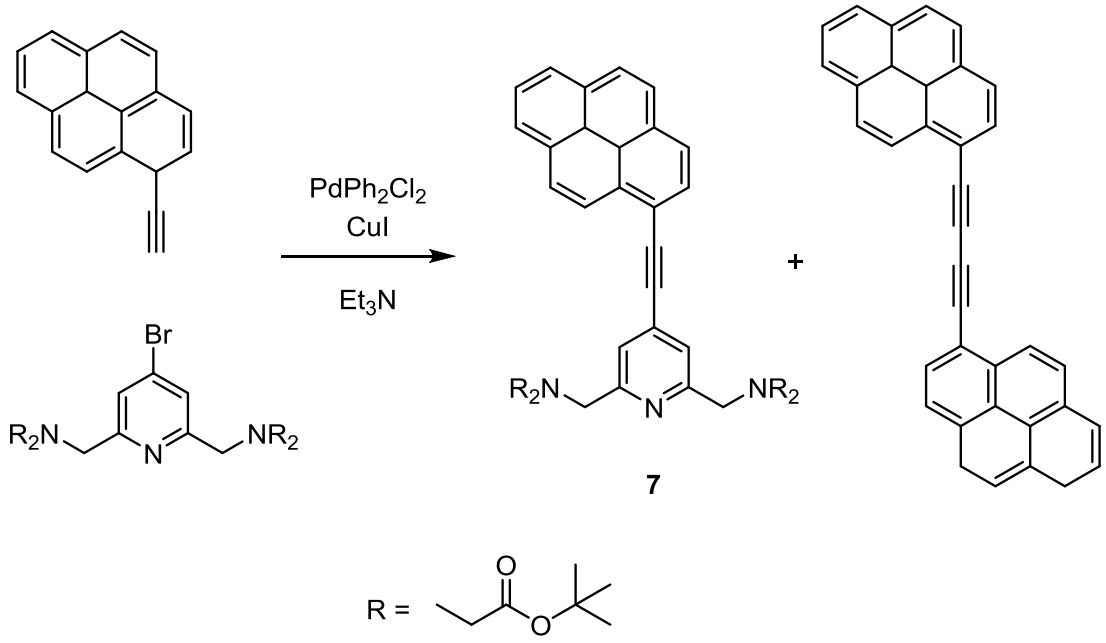

Scheme 4.7 – Sonogashira coupling of **3** and **4** resulting in a mixture of **7** and the homo-coupling of **3**.

Removal of the tert-butoxy groups of **7** was afforded by reaction with trifluoroacetic acid in dichloromethane, to yield the tetra-acid **8**. The solid tetra-acid was orange-red in colour and a solution of **8** gives a weak pink coloured emission under irradiation from a handheld UV visualizer. The luminescence spectrum in water showed the presence two broad peaks centred at 460 nm and 620 nm (Fig. 4.2.1); the balance of blue and red light emission components explains the white light observed.

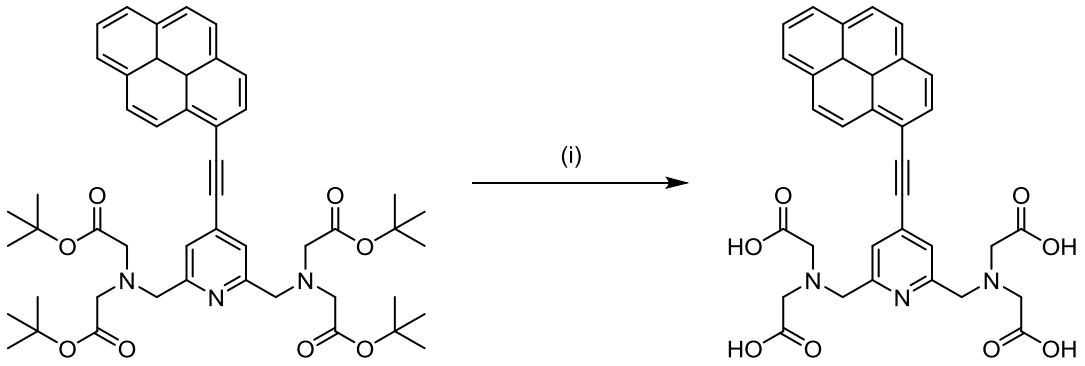

7 **8**

Scheme 4.8 – Synthesis of **8** from **7:** (i) TFA, CH_2Cl_2, 2 hours.

The addition of base to the solution of **8** caused to the solution to change colour from orange to yellow; the luminescence spectrum now showed a single broad peak centred at about 470 nm plus an additional feature appearing at 450 nm. This is about what would be expected for the emission of a substituted pyrene such as **8**: pyrene emission is at about 400 nm and the extended conjugated structure provided by the ethynyl-pyridine substituent would be expected to cause a red-shift in the emission wavelength.

The peak at 620 nm in the luminescence spectrum of **8** before the addition of base is likely an excimer emission – caused by the aggregation and π-stacking of the pyrene groups in solution. The addition of base led to the generation of a tetracetate anion with an overall charge of 4-, electrostatic repulsion prevents the aggregation of **8** in solution and as such no excimer emission was observed.

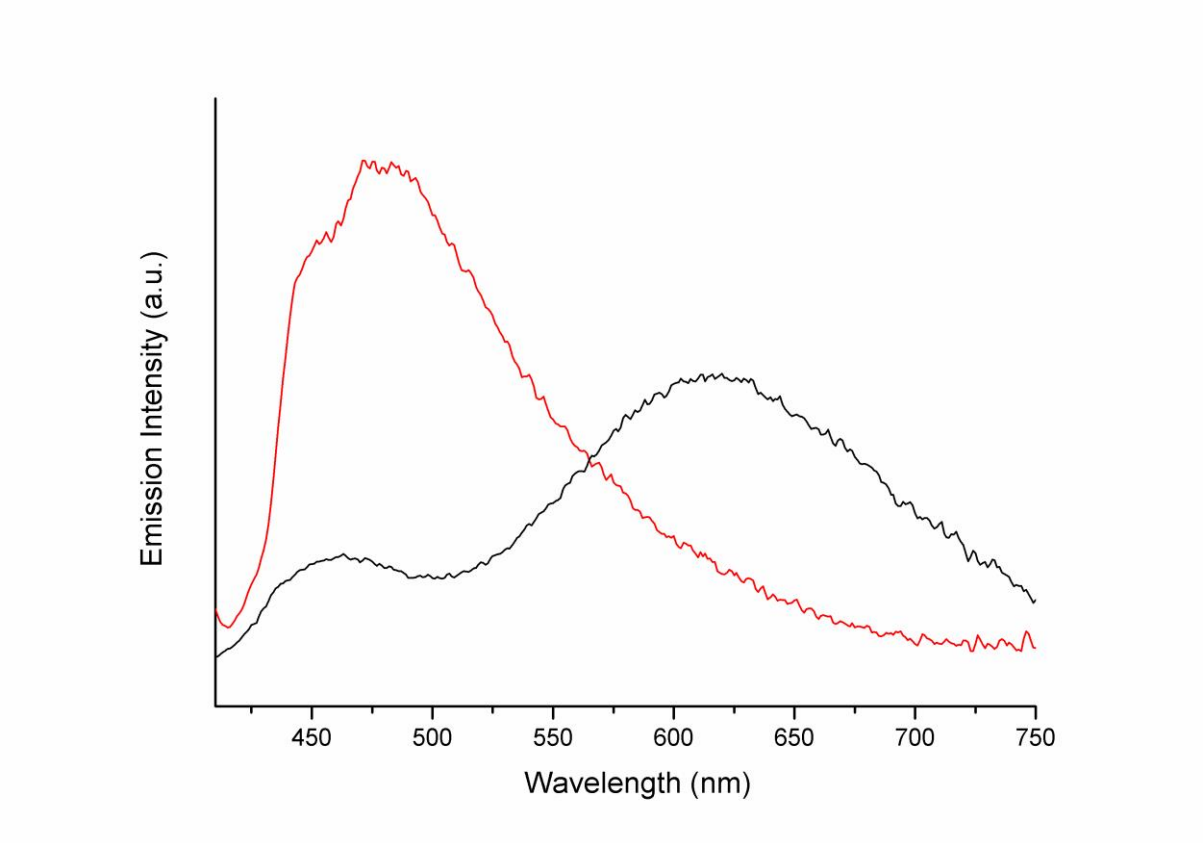

Figure 4.2.1 - Luminescence spectra of the tetraacid **8** (black), and after adjustment of the pH to 6.5 (red). Both spectra were recorded in H_2O with excitation at 400 nm.

The final lanthanide complexes, **Py-Che-Eu** and **Py-Che-Gd,** were synthesised by dissolving/suspending **8** in water and then adjusting the pH to 6.5 - 7 with 0.1M NaOH followed by addition of either $Eu(OTf)_3$ or $GdCl_3$. Following stirring overnight, the product was precipitated by addition of acetone.

The maxima in the luminescence spectrum lie in the region of 450 - 470 nm indicating an excited state energy of 22200 cm^{-1} which is high enough in energy for sensitisation of Eu(III) emission. The emissive $^5D_0$ level of Eu(III) lies at 17500 cm^{-1} meaning the gradient for energy transfer from the pyrene unit to the Eu(III) chelate is 4700 cm^{-1}; a gradient of roughly 2000 cm^{-1} is deemed necessary to prevent the occurrence of back-energy transfer.[32]

The luminescence spectrum of **Py-Che-Eu** below (fig. 4.2.2) shows the characteristic peaks for the emission of Eu(III) . This confirms two important things: firstly that the Eu(III) was successfully incorporated into the chelating ligand; and secondly that there is sensitisation of Eu(III) emission via the antenna effect from the pyrene antenna.

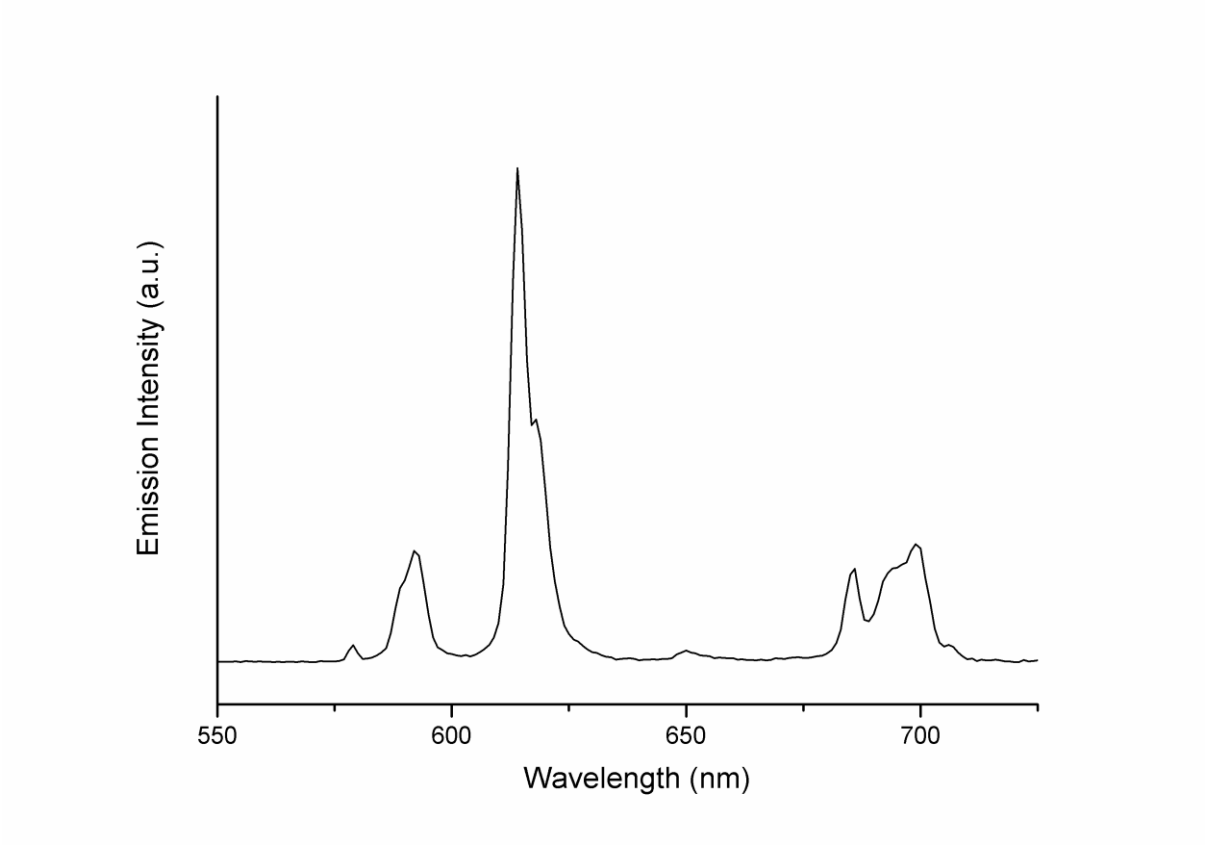

Figure 4.2.2 - Luminescence spectrum of **Py-Che-Eu** in H_2O, excitation at 260 nm.

A ^{1}H NMR spectrum of **Py-Che-Eu** was recorded in D_2O (fig. 4.2.3). The spectrum showed a number of broad peaks which is a result of Eu(III) being paramagnetic; the broad peaks made assigning intregrals difficult but a rough fitting suggests the number of protons present is roughly consistent with the 23 protons expected. The paramagnetism of Eu(III) caused a number of peaks to shift to different ppm - the closer the proximity of a H to the paramagnetic centre the larger the shift that is observed. The peak centred about 8-9 ppm is in the region expected of pyrene, in **Py-Che-Eu** these are the furthest from the Eu(III) ion so are expected to be least shifted. The peaks at roughly 3 and 4 ppm may be the singlets associated with the two protons on the pyridine ring, the broad peak at 1.5 ppm is ascribed to the four protons alpha to the ring, and the remaining peak/s which has been shifted the most to *ca.* -4 ppm may be ascribed to the protons on the chlating arms of **Py-Che-Eu.**

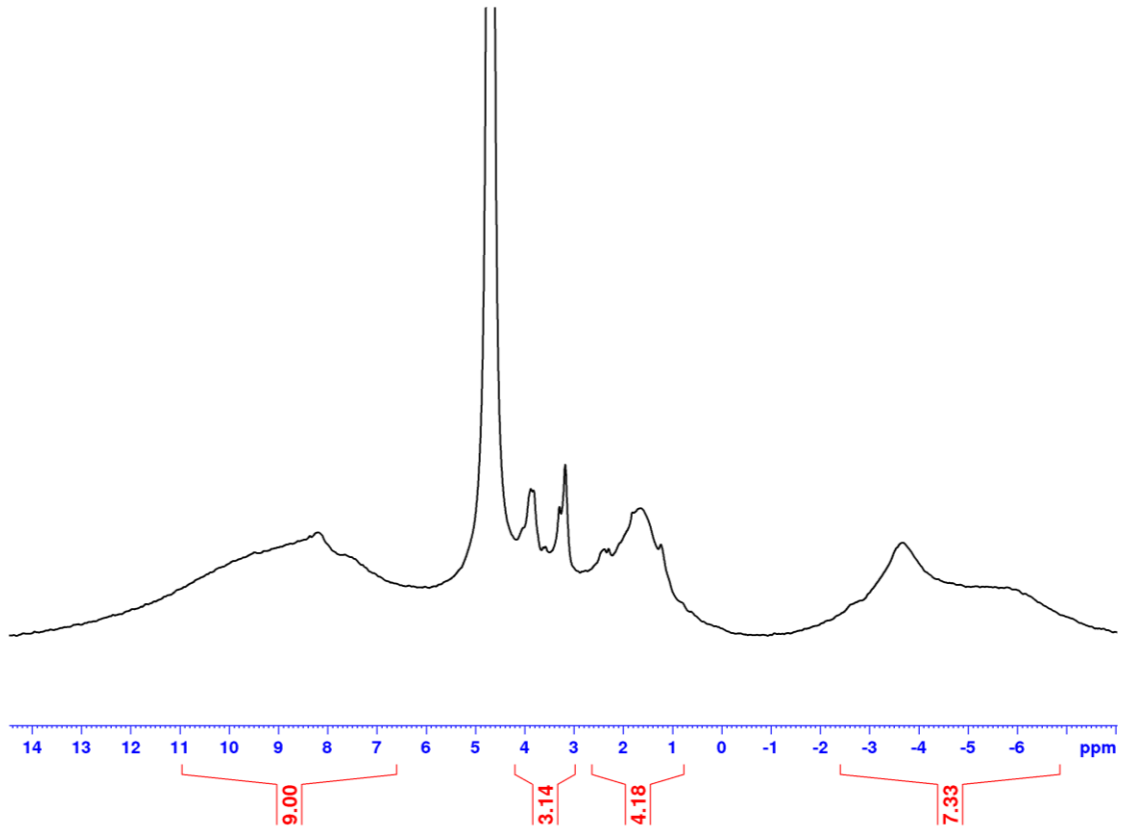

Figure 4.2.2 – ^{1}H NMR spectrum of **Py-Che-Eu** in D_2O.

4.3 Binding Study of Py-Che-Eu with the cage H

Upon titration of **Py-Che-Eu** into a solution of cage **H,** quenching of the cage fluorescence (arising from the naphthyl groups) was observed (Fig. 4.3.1). Fitting the change in fluorescence intensity to a 1:1 binding isotherm yielded a binding constant of 1.2 x 10^5 M^{-1}. This binding constant is an order of magnitude lower than that measured for 1-hydroxypyrene (1.3 x 10^6 M^{-1}). This could be explained by the differing sizes and shapes of **Py-Che-Eu** and 1-hydroxypyrene, in addition to the superior solubility of **Py-Che-Eu** in aqueous solution.

In addition to the quenching of cage fluorescence, the growth of an emission at 615 nm was also observed. This can be ascribed to emission from the excited Eu(III) $^5D_0$ energy level. Fitting the growth of Eu emission to the binding isotherm afforded a binding constant of 2.2 x 10^5 M^{-1} which is comparable to that calculated by measuring the quenching of cage fluorescence. This suggests that the observed growth of Eu emission is a consequence of the binding of **Py-Che-Eu** into the cavity of **H**.

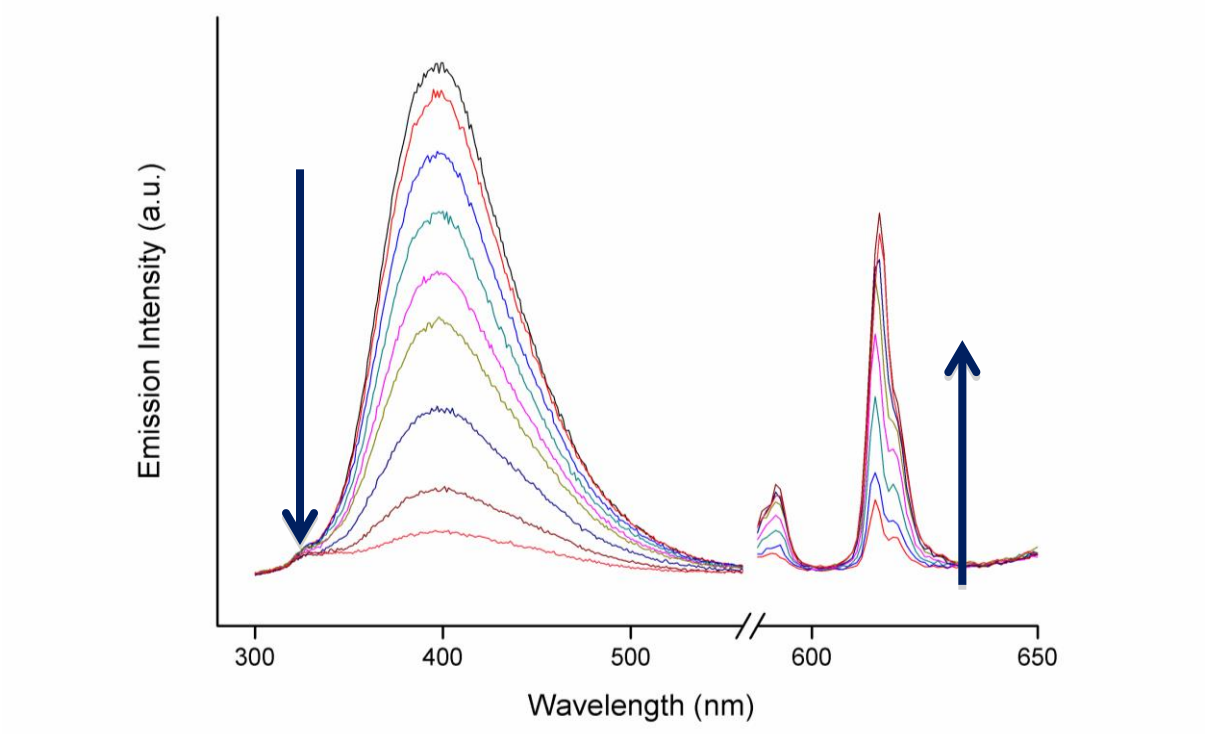

Figure 4.3.1 – Luminescence spectra recorded during the addition of portions of **Py-Che-Eu** (0.2 mM, 0 – 500 µL) into a solution of **H** (0.01 mM) in H_2O. Excitation was at 290 nm.

To determine whether the sensitised Eu(III)-based emission is a result of energy transfer from cage to bound guest, a competition experiment was conducted. Addition of cycloundecanone (a competing, photophysically innocent guest) to a solution of the **H** / **Py-Che-Eu** host-guest complex resulted in loss of Eu-based emission (fig. 4.3.2), which indicates that **Py-Che-Eu** bound within the host has been displaced by the cycloundecanone. Additional amounts of cycloundecanone had no further effect on the emission spectrum of the sample, which suggests that the residual weak Eu-based emission in Fig. 4.3.2 after addition of cycloundecanone arises from direct excitation of **Py-Che-Eu** at 290 nm.

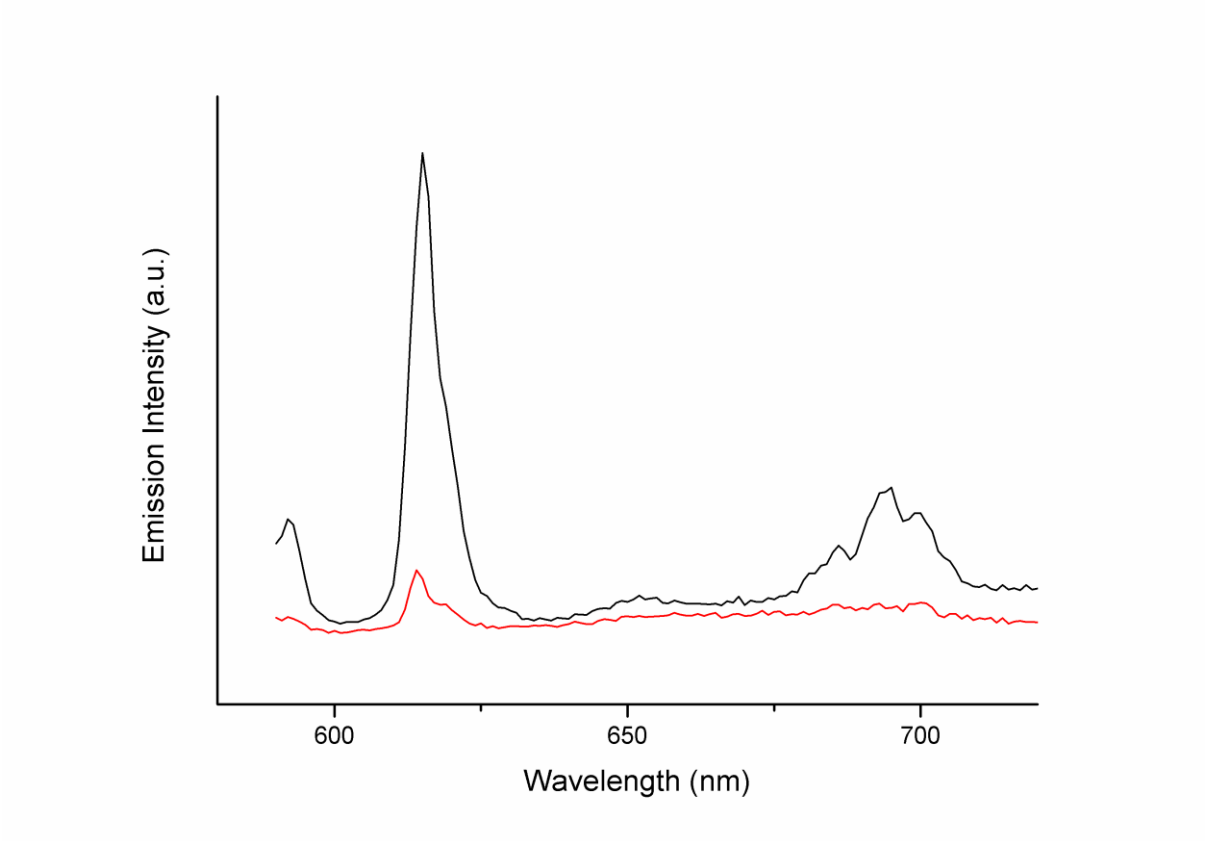

Figure 4.3.2 – Luminescence spectra of the host/guest complex **H·Py-Che-Eu** before(black) and after (red) the addition of 1 equivalent of cycloundecanone in H_2O. Excitation at 290 nm.

Exchanging Eu(III) for Gd(III) in the pyrene-based chelate generates a new complex which can be used as a control due to the excited energy levels of Gd(III) being too high in energy for energy transfer to occur into them from the pyrene unit. As such, **Py-Che-Gd** can be used to see the effect of a 3+ lanthanide ion on the emission of the pyrene-chelate and be representitive of the lanthanide (III) pyrene-chelate complexes in the absence of energy transfer. Fig. 4.2.3 shows a comparison of **Py-Che-Eu** and the Gd(III) analogue **Py-Che-Gd**, luminescence spectra; ligand fluorescence is basically quenched by the Eu(III), which is what you would expect for energy transfer to Eu(III). The lack of quenching for **Py-Che-Gd**, is the result of Gd(III) not participating in energy transfer.

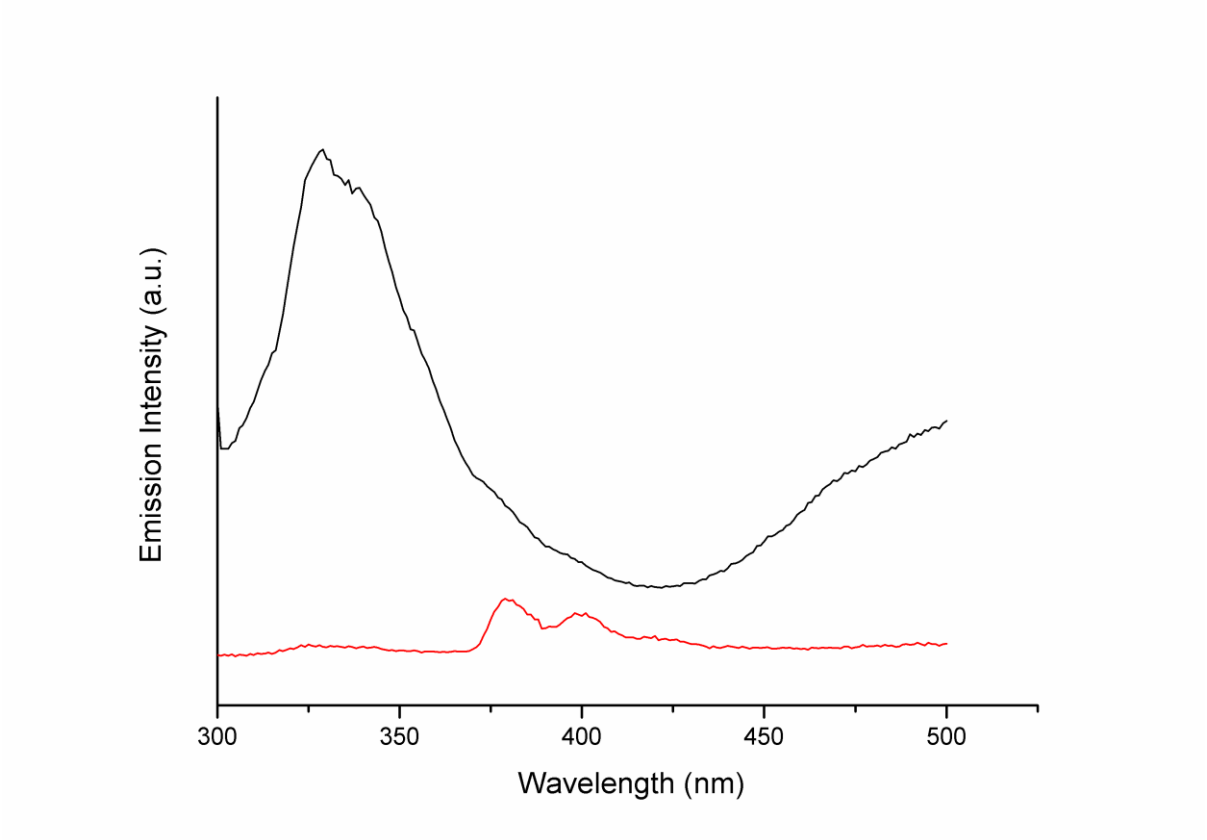

Figure 4.2.3 - Luminescence spectra of Py-Che-Eu (red) and the Gd(III) analogue Py-Che-Eu (black) in H_2O, excitation at 260 nm.

These results suggest that **Py-Che-Eu** binds within the cage, which due to the structure of the guest suggests that the one end of the guest (the pyrene) is bound in the cage due to the hydrophobic effect, while the charged Eu(III) chelate at the other end of the rod-shaped ligand sticks out into the bulk water. This is further reinforced by the failed attempts by the group, to bind charged speces of any kind with the cage cavity due to their hydrophilicity. Another possiblity that may help explain the binding of **Py-Che-Eu,** is due the known binding of anions to the surface and within the windows of the cage; the anionic end of **Py-Che-Eu** may be interacting with the cationic cage surface in a similar fashion.

To provide additional evidence for the uptake of the guest into the cage, an amount of **Py-Che-Eu** was added to a solution of $[Co_8(Lw^{1,5\text{-naph}})_{12}][BF_4]_{16}$ ($\mathbf{H_{Co}}$) in D_2O for a qualitative NMR binding experiment. The paramagnetism of the Co(II)-based cage makes it easy to see if a guest is bound in the cage cavity: the ^1H signals are substantially shifted to lower frequencies and are typically visible in the region -5 to -10. Comparing the spectra of "empty" $\mathbf{H_{Co}}$ with that in which **Py-Che-Eu** has been added (fig. 4.3.4) one can see how peaks corresponding to the cage $\mathbf{H_{Co}}$ have been shifted upon addition of the guest, consistent with binding of a guest molecule.

The appearance of a new peak in the -5 to -10 ppm range is typically ascribed to that of the of the bound guest. However the integration of this peak does not match what is expected for **Py-Che-Eu**. This may be the result of not all of the cage being occupied by **Py-Che-Eu** meaning that more free host than host-guest adduct is present; or this peak may be due to unbound guest in solution as the paramagnetism of Eu(III) causes shifts to about the -5 ppm area, see the ^1H NMR spectrum of **Py-Che-Eu** (figure. 4.2.2).

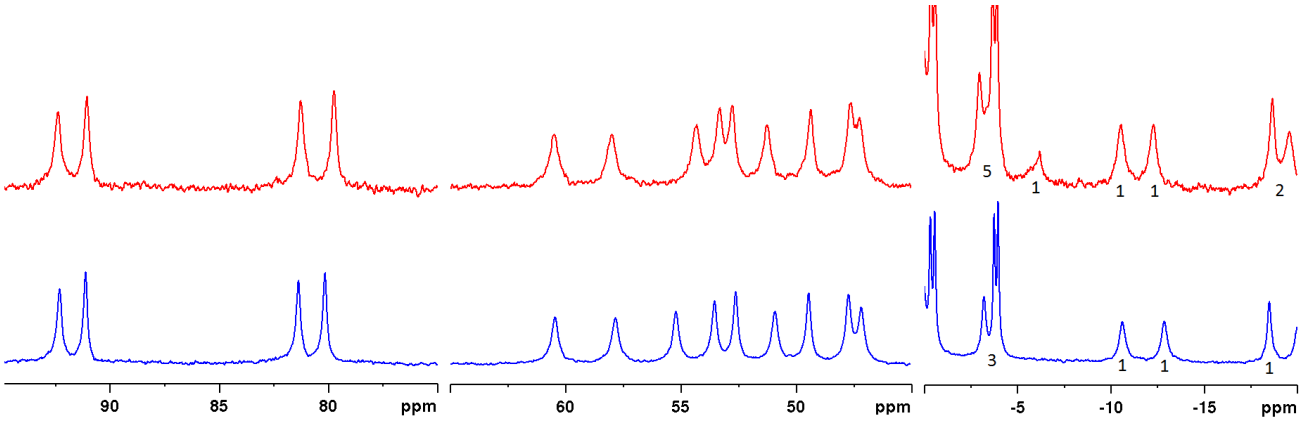

Figure 4.3.4 – Different chemical shift ranges in the ^{1}H NMR spectra of free $\mathbf{H_{Co}}$ (Blue) and after the addition of **Py-Che-Eu** (Red) in D_2O showing the regions of significant shifting of peaks is suggesting the binding of **Py-Che-Eu** in the cage cavity**.** The new signal at -5.5 ppm is ascribed to **Py-Che-Eu**, a number of integrals have been added for comparison.

4.4 Conclusion

The synthesis of **Py-Che-Eu** appeared successful with sensitised emission from Eu(III) observed. This was then used to create a host-guest system between **Py-Che-Eu** and **the** $[Cd_8Lw^{1,5\text{-naph}})_{12}]^{16+}$ cubic coordination cage (**H**); the **H/Py-Che-Eu** host-guest assembly successfully afforded the two-step energy transfer from cage to pyrene, and then pyrene to Eu(III). Evidence was provided by addition of a competing guest which resulted in the disprution the sensitisation of Eu(III).

^{1}H NMR and fluorescence binding studies suggested evidence of the binding of **Py-Che-Eu** within $[(Cd_8Lw^{1,5\text{-naph}})_{12}]^{16+}$ and $[(Co_8Lw^{1,5\text{-naph}})_{12}]^{16+}$ cages; demonstrating the possibility for guest molecules to protrude from the cage cavity via windows in the cage structure.

The attempt to develop an alternative route to **4** proved successful, leading to improved overall yield and a fewer number of steps. The starting material 2,6-methyl-4-hydroxypyridine also was cheaper than the previously used chelidamic acid.

4.5 Experimental techniques and procedures

4.5.1 Synthetic Procedures

1-bromopyrene (1)

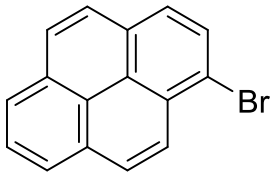

Pyrene (15 g, 0.074 mol) was dissolved in 150 cm^3 N,N'-dimethylformamide. N-bromosuccinimide (13.2 g, 0.074 mol) was added and the reaction was stirred at room temperature for 24 hours. 150 ml water was added and an off-white precipitate formed, the precipitated was filtered and washed with water and thgen dried to give 1-bromopyrene (20.1 g, 96.6%) an off-white solid.

MS-EI: m/z = 280.0 [M^+]

^{1}H NMR (400 MHz, $CDCl_3$) δH 8.03-8.13 (m, 4H); 8.18-8.28 (m, 4H); 8.47 (d, 9.2 Hz, 1H);

1-(trimethylsilylethynyl)pyrene (2)

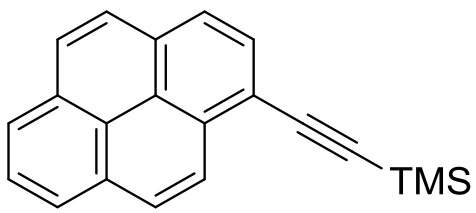

1-bromopyrene (2.0 g, 7.11 mmol) was dissolved in 80 cm^3 triethylamine under N_2. $Pd(PPh_3)_2Cl_2$ (0.50 g, 0.71 mmol), Copper Iodide (0.14 g, 0.71 mmol) were added and the mixture was bubbled with N_2 for 15 minutes. Trimethylsilylacetylene (2.54 cm^3, 18.0 mmol)

was added and the reaction was heated to 60 ^{o}C for 24 hours. The reaction was allowed to cool to room temperature and the solvent was removed under reduced pressure. 50 cm^3 of diethylether was added and the solution was filtered through celite. The solvent was removed under reduced pressure and purification was afforded by column chromatography, silica, petroleum ether. To give 1-(trimethylsilylethynyl)pyrene (1.65 g, 78%) a pale yellow solid.

MS-EI: m/z = 298.1 [M^+]

^{1}H NMR (400 MHz, $CDCl_3$) δH 1.57 (s, 9H); 8.03-8.33 (m, 8H); 8.47 (d, 9.7 Hz, 1H);

1-ethynylpyrene (3)

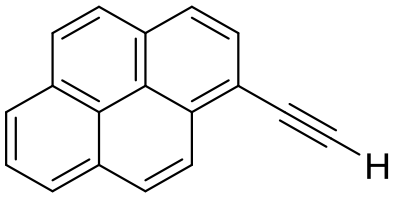

1-(trimethylsilylethynyl)pyrene (3.80 g, 13 mmol) was dissolved in 50 cm^3 methanol and 50 cm^3 dichloromethane. K_2CO_3 (8.70 g, 63 mmol) was added and the reaction was stirred at room temperature for 24 hours. The reaction mixture was filtered and solvent removed under reduced pressure. 50 cm3 H_2O was added and the product was extracted with 3 x 50 cm^3 Et_2O. The organic phase was dried with $MgSO_4$ and the solvent removed under reduced pressure. Purification was afforded by column chromatography, silica, petroleum ether to give 1-ethynylpyrene (2. 82 g, 99%) a white solid.

MS-EI: m/z = 226.1 [M^+]

^{1}H NMR (400 MHz, $CDCl_3$) δH 3.67 (s, 1H); 8.04-8.27 (m, 8H); 8.62 (d, 9.3 Hz, 1H);

2,6-dimethyl-4-bromopyridine (5)

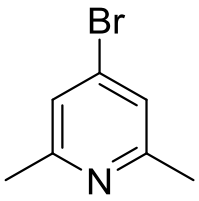

2,6-dimethyl-4-hydroxypyridine (7.25 g, 59 mmol) was dissolved in 150 cm^3 $CHCl_3$. Phosphorus pentabromide (25.0 g, 58 mmol) was added and the reaction was heated to 60 ^oC for 3 hours. The reaction was concentrated under reduced pressure and the residue was heat at 120 ^oC for 16 hours. 200 cm^3 of 10 M $NaOH_{(aq)}$ was added and the product was extracted with EtOAc (3 x 100 cm^3). The organic phase was dried with $MgSO_4$, filtered and solvent was removed under reduced pressure to give 2,6-dimethyl-4-bromopyridine (8.25 g, 76%) a yellow oil that solidified upon standing.

MS-ES: m/z = 186.0 $[M+H]^+$

^1H NMR (400 MHz, $CDCl_3$) δH 1.27 (t, EtOAc); 2.06 (s, EtOAc); 2.51 (s, 6H); 4.14(q, EtOAc) 7.17 (s, 2H); 7.26 (s, $CHCl_3$);

13C NMR

2,6-bis(bromomethyl)-4-hydroxypyridine (6)

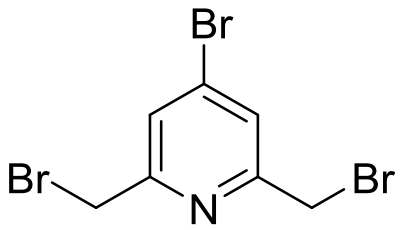

2,6-dimethyl-4-bromopyridine (6.23 g, 3.4 mmol), n-bromosuccinimide (36.2 g, 20.3 mmol) dissolved in 100 cm^3 $CHCl_3$. A spatula of benzoyl peroxide was added and the reaction was heated to reflux under UV irradiation from a tungsten lamp, reaction progress was monitored via TLC (10:1 petroleum ether - ethyl acetate). Every 2 hours another 2 equivalents of NBS were added followed by more benzoyl peroxide. After completion (no

change on TLC, approx. 6-8 hours) the solvent was removed under reduced pressure and 25 ml of dry thf was added under nitrogen atmosphere. The solution was cooled to 0 ^{o}C, diethylphosphite (17.4 cm^3, 13.6 mmol) and diisopropylethylamine (23.7 cm^3, 13.6 mmol) were then added. The reaction mixture was allowed to warm to room temperature and left to stir for 24 hours. The reaction was poured into 100 cm^3 ice water and extracted with diethyl ether (3 x 100 cm^3), The organic phase was dried with $MgSO_4$, filtered and solvent was removed under reduced pressure. Purification was afforded by column chromatography, silica, 4:1 petroleum ether - ethyl acetate. The product 2,6-bis(bromomethyl)-4-bromopyridine (7.37 g, 63%) was afforded as a white solid.

MS-ES: m/z = 343.8 $[M + H]^+$; 262.0 $[M - Br]^+$; 185.0 $[M - 2Br]^+$

^{1}H NMR (400 MHz, d_6-DMSO) δH 2.5 (DMSO); 3.33 (s, H_2O) 4.67 (s, 4H); 7.82 (s, 2H);

4-bromo -2,6-[di(*tert*-butyl)iminodiacetate]methylpyridine (7)

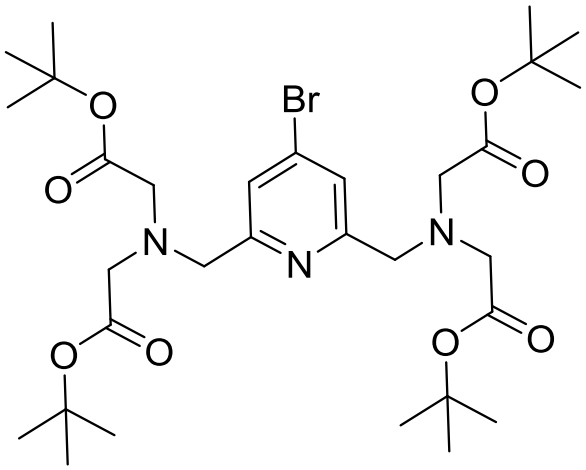

2,6-bis(bromomethyl)-4-bromopyridine (2.11 g, 6.0 mmol), di(*tert*-butyl)iminodiacetate (2.94 g, 12.0 mmol) and sodium carbonate (6.46 g, 61.0 mmol) were added to 100 cm^3 dry acetonitrile. The reaction was stirred at room temperature for 24 hours. The reaction was filter and the solvent removed *in vacuo*. 50 cm^3 dichloromethane was then added and

washed with 3 x 20 cm^3 water. The organic phase was dried with $MgSO_4$ and solvent was removed in vacuo to afford **7** (7.26 g, 90%) a yellow oil.

MS-ES: m/z = 671.28 $[M + H]^+$; 614.2 $[M - C_4H_6]^+$; 569.1 $[M – 2(C_4H_6)]^+$

^1H NMR (400 MHz, $CDCl_3$) δH 1.48 (s, 36H); 3.48 (s, 8H); 4.67 (s, 4H); 7.74 (s, 2H);

4-(1-ethynylpyrene) -2,6-[di(*tert*-butyl)iminodiacetate]methylpyridine (8)

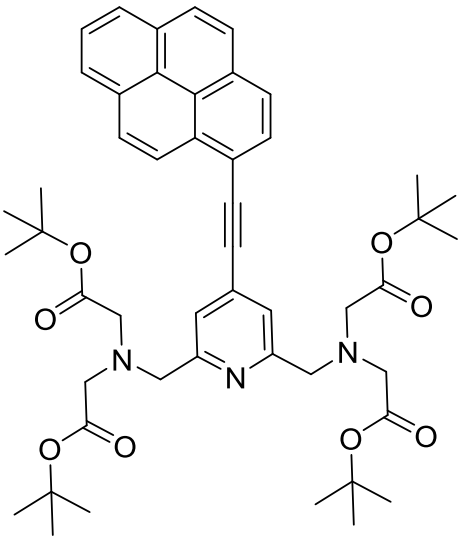

3 (0.58 g, 2.2 mmol), **7** (1.0 g, 1.4 mmol) and tetrabutylammonium fluoride (1.3 g, 4.2 mmol) were dissolved in 25 cm^3 THF under N_2 and the mixture was bubbled with N_2 for 15 minutes. $Pd(PPh_3)_2Cl_2$ (0.50 g, 0.71 mmol) was added and the reaction was heated to 60 ^oC for 24 hours. The reaction was cooled to room temperature and the solvent removed under reduced pressure. 50 cm^3 of dichloromethane was added and washed with H_2O and brine. The organic phase dried with $MgSO_4$ and solvent removed under reduced pressure. Purification was afforded by column chromatography, silica, petroleum ether : ethyl acetate 70:30. To give **8** (0.2 g, 18%) a yellow solid.

MS-ES: m/z = 818.18 $[M + H]^+$; 761.36 $[MH - (C_3H_9)]^+$; 704.30 $[MH - 2(C_3H_9)]^+$

^{1}H NMR (400 MHz, $CDCl_3$) δH 1.51 (s, 36H); 3.58 (s, 8H); 4.15 (s, 4H); 7.86 (s, 2H); 8.06 - 8.30 (m, 8H); (d, J = 8.67 Hz, 1H).

4-(1-ethynylpyrene) -2,6-[(iminodiacetic acid)methyl]pyridine (9)

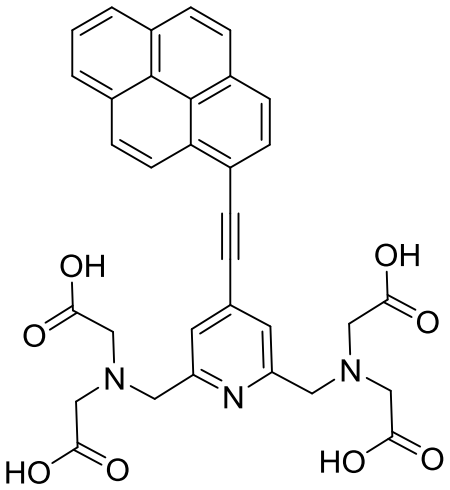

8 (0.2 g, 0.24 mmol) was added to 10 cm^3 dichloromethane and 10 cm^3 trifluoroacetic acid stirred at room temperature for 2 hours. The solvent was removed under reduced pressure and the residue was triturated with diethyl ether to give **9** (0.15 g, 71%) a red solid.

MS-ES: m/z = 147.3 $[M - 4H]^{4-}$

^{1}H NMR (400 MHz, $CDCl_3$) δH 3.60 (s, 8H); 4.15 (s, 4H); 7.81 (s, 2H); 8.10 - 8.35 (m, 8H); (d, J = 8.67 Hz, 1H)

Py-Che-Eu (10)

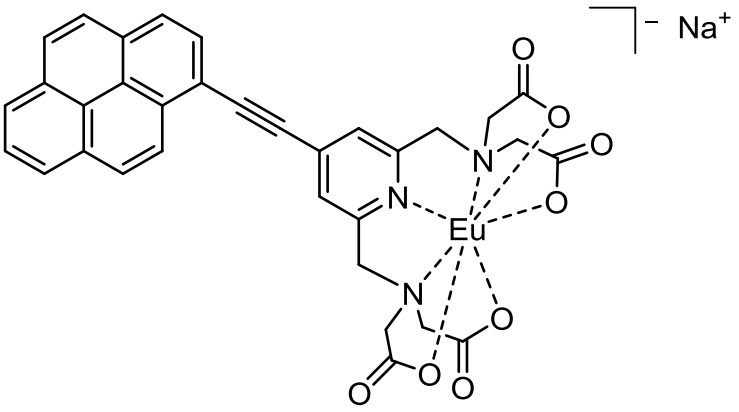

9 (50 mg, 0.084 mmol) was suspended in 20 cm^3 of H_2O. The pH of the solution was adjusted to 7-8 with 0.1 M NaOH solution after which **9** dissolved and the solution became yellow. $Eu(OTf)_3$ (51 mg, 0.084 mmol) was added and the reaction mixture was stirred at room temperature overnight. 30 ml of acetone was added and a yellow precipitate formed which was filtered off and washed with acetone to give the target molecule **10** (62 mg, 91%)

Py-Che-Eu (11)

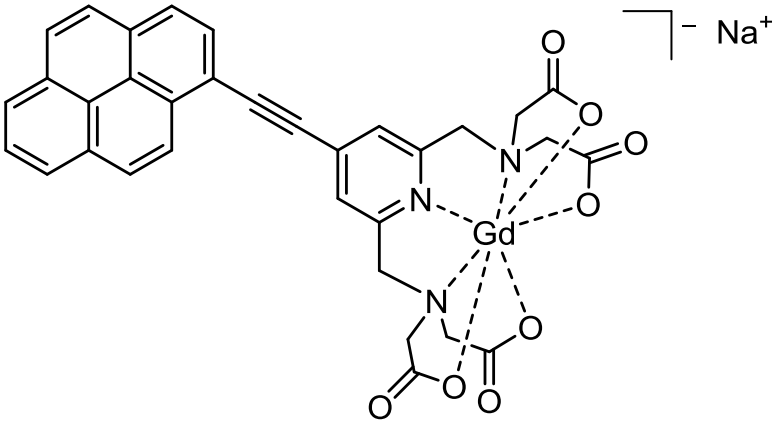

11 was prepared in the same way as **10** but using $GdCl_3.6H_2O$ (0.31 g 0.084 mmol) yielding 6.0 mg, 9.2 %.

4.5 References

1 N. S. Lewis and D. G. Nocera, *Proc. Natl. Acad. Sci.*, 2006, **103**, 15729–15735.

2 M.-S. Choi, T. Yamazaki, I. Yamazaki and T. Aida, *Angew. Chem. Int. Ed.*, 2004, **43**, 150–158.

3 N. Aratani, D. Kim and A. Osuka, *Acc. Chem. Res.*, 2009, **42**, 1922–1934.

4 J. Yang, M.-C. Yoon, H. Yoo, P. Kim and D. Kim, *Chem. Soc. Rev.*, 2012, **41**, 4808.

5 M. R. Wasielewski, *Chem. Rev.*, 1992, **92**, 435–461.

6 C. Luo, D. M. Guldi, H. Imahori, K. Tamaki and Y. Sakata, *J. Am. Chem. Soc.*, 2000, **122**, 6535–6551.

7 M. R. Wasielewski, *Acc. Chem. Res.*, 2009, **42**, 1910–1921.

8 M. R. Wasielewski, *J. Org. Chem.*, 2006, **71**, 5051–5066.

9 M. D. Ward, *Chem. Soc. Rev.*, 1997, **26**, 365.

10 F. D'Souza and O. Ito, *Chem. Commun.*, 2009, 4913.

11 F. D'Souza, G. M. Venukadasula, K. Yamanaka, N. K. Subbaiyan, M. E. Zandler and O. Ito, *Org. Biomol. Chem.*, 2009, **7**, 1076.

12 C. You and F. Würthner, *J. Am. Chem. Soc.*, 2003, **125**, 9716–9725.

13 H.-B. Yang, K. Ghosh, Y. Zhao, B. H. Northrop, M. M. Lyndon, D. C. Muddiman, H. S. White and P. J. Stang, *J. Am. Chem. Soc.*, 2008, **130**, 839–841.

14 K. Ghosh, J. Hu, H. S. White and P. J. Stang, *J. Am. Chem. Soc.*, 2009, **131**, 6695–6697.

15 K. Mahata, P. D. Frischmann and F. Würthner, *J. Am. Chem. Soc.*, 2013, **135**, 15656–15661.

16 Y. Furutani, H. Kandori, M. Kawano, K. Nakabayashi, M. Yoshizawa and M. Fujita, *J. Am. Chem. Soc.*, 2009, **131**, 4764–4768.

17 T. Murase, H. Takezawa and M. Fujita, *Chem. Commun.*, 2011, **47**, 10960.

18 D. M. Dalton, S. R. Ellis, E. M. Nichols, R. A. Mathies, F. D. Toste, R. G. Bergman and K. N. Raymond, *J. Am. Chem. Soc.*, 2015, **137**, 10128–10131.

19 V. F. Plyusnin, A. S. Kupryakov, V. P. Grivin, A. H. Shelton, I. V. Sazanovich, A. J. H. M. Meijer, J. A. Weinstein and M. D. Ward, *Photochem. Photobiol. Sci.*, 2013, **12**, 1666.

20 L. F. Smith, B. A. Blight, H. J. Park and S. Wang, *Inorg. Chem.*, 2014, **53**, 8036–8044.

21 S. Faulkner, L. S. Natrajan, W. S. Perry and D. Sykes, *Dalton Trans.*, 2009, 3890.

22 D. Sykes and M. D. Ward, *Chem. Commun.*, 2011, **47**, 2279–81.

23 P. Lian, H. Wei, C. Zheng, Y. Nie, J. Bian, Z. Bian and C. Huang, *Dalton Trans.*, 2011, **40**, 5476.

24 D. Sykes, A. J. Cankut, N. M. Ali, A. Stephenson, S. J. P. Spall, S. C. Parker, J. A. Weinstein and M. D. Ward, *Dalton Trans.*, 2014, **43**, 6414.

25 E. Baggaley, D. K. Cao, D. Sykes, S. W. Botchway, J. a. Weinstein and M. D. Ward, *Chem. - A Eur. J.*, 2014, **20**, 8898–8903.

26 A. Jana, E. Baggaley, A. Amoroso and M. D. Ward, *Chem. Commun.*, 2015, **51**, 8833–8836.

27 A. T. Bui, M. Beyler, Y. Y. Liao, A. Grichine, A. Duperray, J. C. Mulatier, B. Le Guennic, C. Andraud, O. Maury and R. Tripier, *Inorg. Chem.*, 2016, **55**, 7020–7025.

28 W. Wu, X. Wu, J. Zhao and M. Wu, *J. Mater. Chem. C*, 2015, **3**, 2291–2301.

29 P. Liu, Y. Chen, J. Deng and Y. Tu, *Synthesis (Stuttg).*, 2001, **2001**, 2078–2080.

30 Y. Liang, Y.-X. Xie and J.-H. Li, *J. Org. Chem.*, 2006, **71**, 379–381.

31 A. Jiblaoui, C. Baudequin, V. Chaleix, G. Ducourthial, F. Louradour, Y. Ramondenc, V. Sol and S. Leroy-Lhez, *Tetrahedron*, 2013, **69**, 5098–5103.

32 S. Sato and M. Wada, *Bull. Chem. Soc. Jpn.*, 1970, **43**, 1955–1962.

Chapter 5

General Experimental Techniques and Procedures

5.1. Materials

All starting materials were purchased from the following commercial sources: Sigma-Aldrich, Fisher Scientific, Alfa Aesar and Fluorochem; which were used without purification. All solvents were of HPLC grade quality and obtained from Fisher, excluding the deuterated solvents which were obtained from Sigma-Aldrich; $CDCl_3$ was stored over molecular sieves. Dry solvents (toluene and THF) were obtained from the Grubbs dry solvent system at the University of Sheffield.

$[Co_8(Lw^{1,5naph})_{12}](BF_4)$, **$H_{Co}$**, was provided by Dr William Cullen and/or Dr Alex Metherell.

5.2 Nuclear magnetic resonance spectra

All NMR data was collected on a Bruker AV-3HD 400 MHz, Bruker Avance III 400 MHz or Bruker AV-3 500 MHz spectrometer at 298 K. 500 MHz spectra were recorded by the University of Sheffield Chemistry Department NMR service.
Samples were prepared by adding 0.7 – 1.0 cm^3 of deuterated solvent to 5-15 mg of sample, the solution was then filtered through a cotton wool plug into a NMR tube.

5.3 Mass Spectrometry

All ES mass spectra were recorded with a Waters LCT mass spectrometer, EI mass spectra were recorded by a VG AutoSpec mass spectrometer. Spectra were recorded by the University of Sheffield Mass Spectrometry Service.

Mobile phase was either 0.1% formic acid or acetonitrile/0.1% formic acid, with a flow rate of 0.4 cm^3 min^{-1} down a Agilent Extended C18 2.1mm x 50mm column.

5.4 Photophysical measurements

All UV-vis, emission, excitation-emission and lifetime measurements were recorded from room temperature solutions (298 K), unless stated otherwise, using a quartz fluorescence cell, with a path length of 1 cm.

5.4.1 Uv-visible absorption

UV/Vis spectra were recorded on a Cary 50 Bio spectrometer. Extinction coefficients were calculated in accordance with the Beer Lambert law (Equation 5.1). Spectra were baselined internally the instrument by utilising an appropriate sample of blank solvent.

$$A = \varepsilon l c$$

Equation 5.1 - The Beer Lambert Law; A = absorbance, ε = extinction coefficient (dm^3 Mol^{-1} cm^{-1}), l = path length (cm), c = concentration (Mol dm^{-3}).

5.4.2 Emission / excitation

Emission and excitation-emission spectra were recorded on a Horiba Jobin Yvon Fluoromax-4 spectrofluorometer. Integration time of each reading was 0.5 s, with a spectral resolution of 1 nm. Typical slit widths used were 3 nm / 3 nm for excitation / emission gratings.

5.4.3 Quantum yield

Quantum yield values were calculated using Equation 5.#, where ϕ_s and ϕ_r is the quantum yield of the sample under investigation and reference solution, respectively. I is emission intensity (integrated area under the emission profile) of sample (I_s) and reference (I_r), and A is the absorbance of sample (A_s) and reference (A_r) at a particular excitation wavelength. η is the refractive index of the solvent used for the sample (η_s) and the reference (η_r).

Quantum yields quoted were calculated using the reference standard $[Ru(bipy)_3]Cl_2$ in aerated water.

$$\Phi_s = \Phi_r \left(\frac{I_s}{(1-10^{-A})_s}\right)\left(\frac{(1-10^{-A})_r}{I_r}\right)\left(\frac{\eta_s^2}{\eta_r^2}\right)$$

Equation 5.2 - Quantum Yield. ϕ = quantum yield, A = optical density (absorbance) at excitation wavelength, I = integrated emission intensity, η = solvent refractive index.

5.4.4 Emission lifetimes

Lifetime measurements were recorded using Edinburgh Instruments Mini τ, with a 1 ns pulse LED laser (260 nm excitation). Decay curves generated by single photon counting were fitted using the mini τ software supplied by Edinburgh Instruments.

5.5 Binding Constants

Binding constants were determined by the fitting of a 1:1 binding isotherm using equations 5.3, 5.4 and 5.5. Curve fitting was performed using the simplex method.

$$K_a = \frac{[HG]}{[H][G]}$$

Equation 5.3 - General expression for equilibrium binding constant. Ka = Binding (association) constant; [HG] = concentration of host-guest complex; [H] = concentration of host; [G] = concentration of guest.

$$[HG] = \frac{1}{2}\left(\left(G_0 - H_0 - \frac{1}{K_a}\right) - \sqrt{\left(G_0 + H_0 + \frac{1}{K_a}\right)^2 + 4[H_0][G_0]}\right)$$

Equation 5.4 - Expression for host-guest concentration. G_0 = total concentration of guest; H_0 = total concentration of host; K_a = association constant.

$$\Delta F = k_{\Delta HG}([HG])$$

Equation 5.5 - Change in fluorescence of host upon titration. ΔF = change in fluorescence, k = proportionality constant.

5.6 Fluorescence Titrations

Fluorescence titrations were carried out by preparing a stock solution of $[Cd_8(Lw^{1,5\text{-}naph})_{12}][NO_3]_{16}$ at a concentration of 0.1 or 0.01 mM in de-ionised water. Guest solutions (typically 0.05 – 5 mM) were made up using the stock solution of host to avoid dilution of host as guest is added during the titration. 1500 µL of host solution was added to a standard 1 cm quartz fluorescence cuvette, to which sequential portions of guest solution were then added, leaving 15 minutes after each addition to allow the host / guest mixture to equilibrate.

For fluorescence assays, aliquots of the stock cage solution (0−100 µL) and the guest solution (0−100 µL) were added to 24 wells of a Griener Bio-one µClear black 384-well plate in different proportions to a total volume of 100 µL in each well. The plates were heated to and maintained at 308 K for 1 hour to assist mixing of solutions, followed by cooling to 298 K and maintained for 20 mins to equilibrate. The fluorescence emission at 420 nm, using an excitation wavelength of 280 nm, was measured for each well using a BMG FLUOstar Omega plate reader. Binding constants given are the average of at least three repeat measurements for each guest.

Appendix 1

Additional Chapter 2 Data

Appendix 1.1 – Chapter 2 ^{1}H NMR Spectra

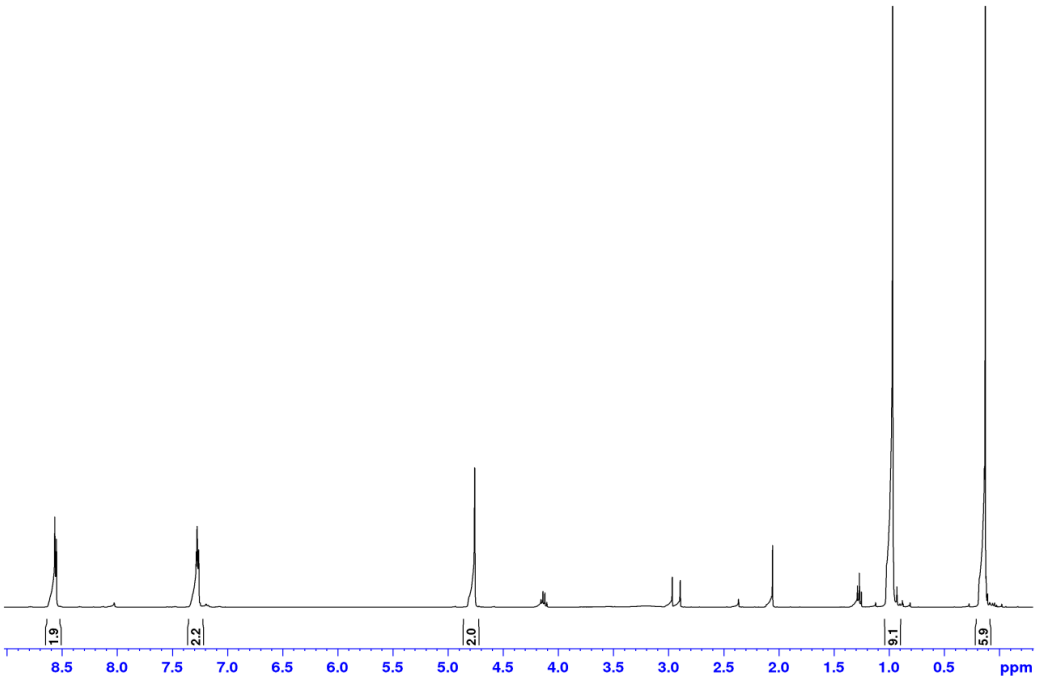

Figure A1.1.1 – ^{1}H NMR spectrum of 4-[(*tert*-butyldimethylsilyl)hydroxymethyl]pyridine (**1**) in $CDCl_3$.

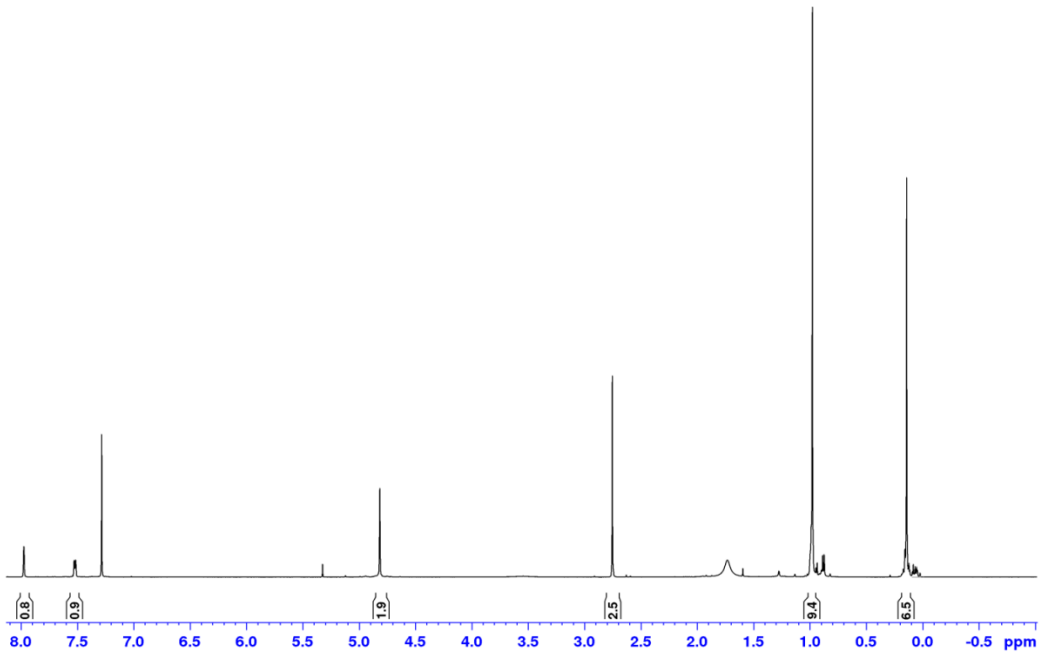

Figure A1.1.2 – ^{1}H NMR spectrum of 2-(acetyl)-4-[(*tert*butyldimethylsilyl)oxymethyl] pyridine (**2**) in $CDCl_3$.

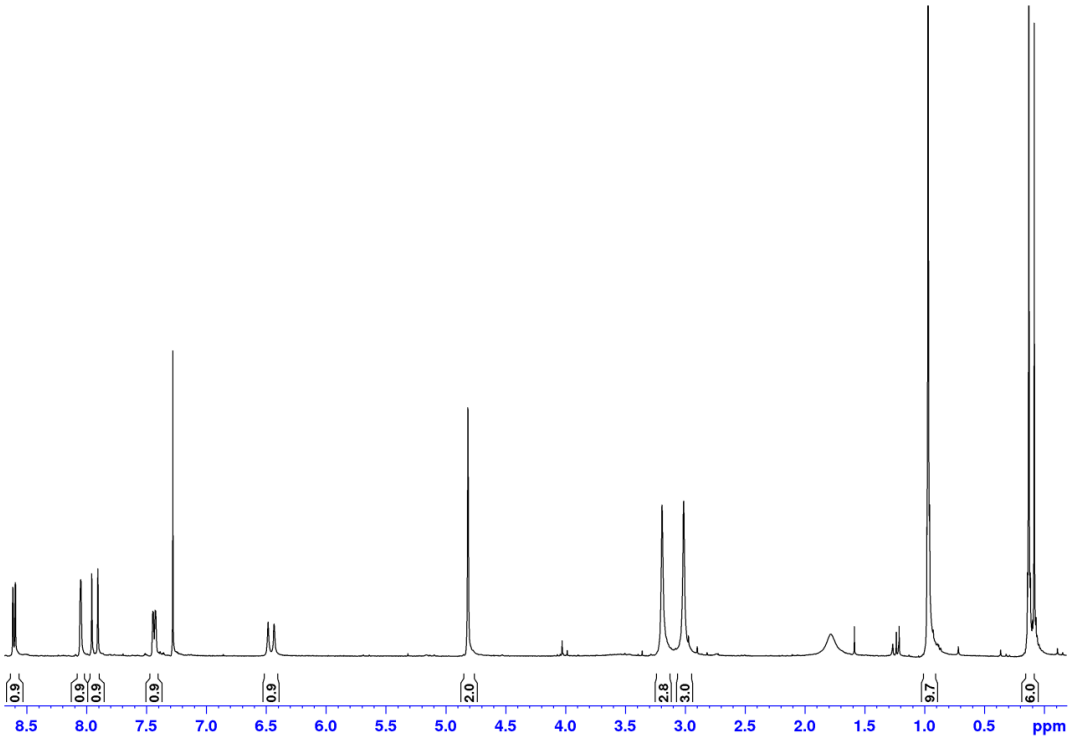

Figure A1.1.3 – ^{1}H NMR spectrum of of 2-(acetyl-dimethylenamine)-4-[(tert-butyldimethylsilyl) oxymethyl] pyridine (**3**) in $CDCl_3$.

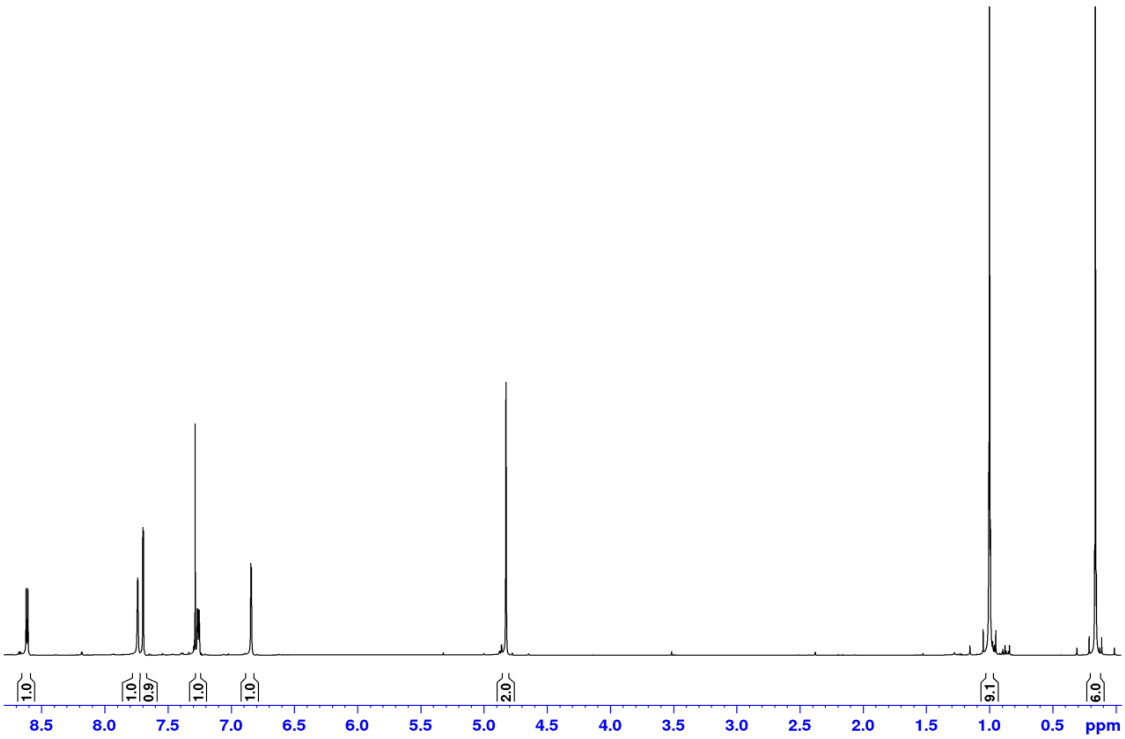

Figure A1.1.4 – ^{1}H NMR spectrum of 4-[(*tert*-butyldimethylsilyl)oxymethyl]-PyPz (**4**) in $CDCl_3$.

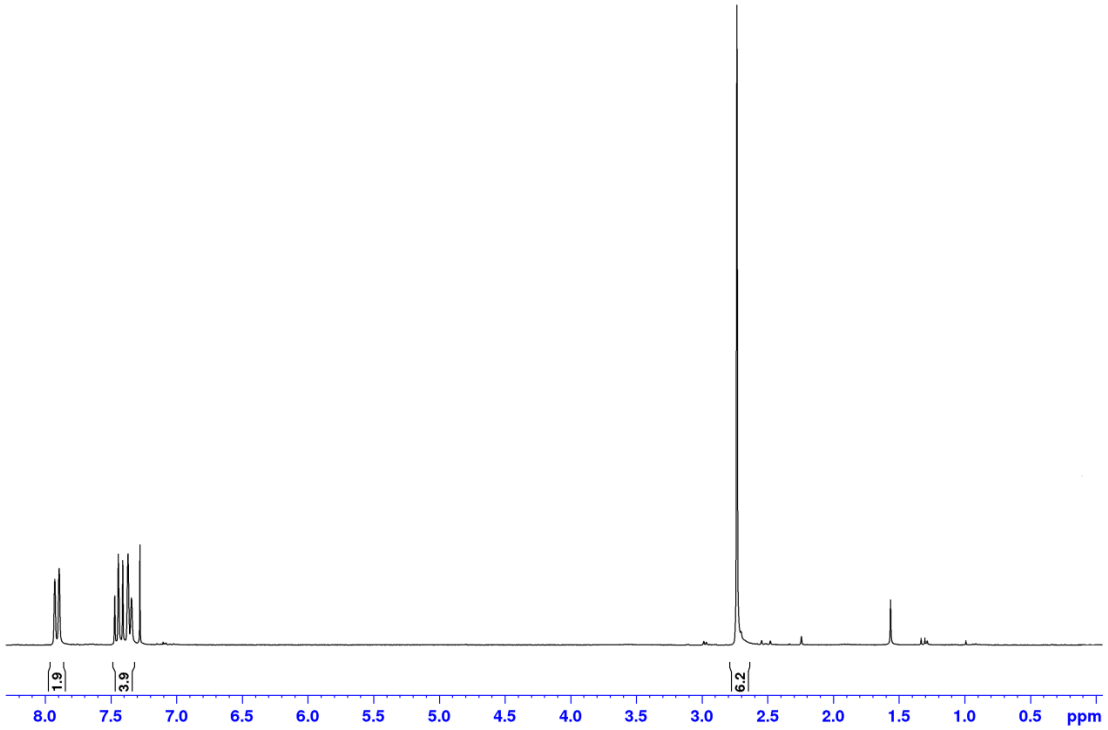

Figure A1.1.5 – ^{1}H NMR spectrum of 1,5-dimethylnaphthalene **(5)** in $CDCl_3$.

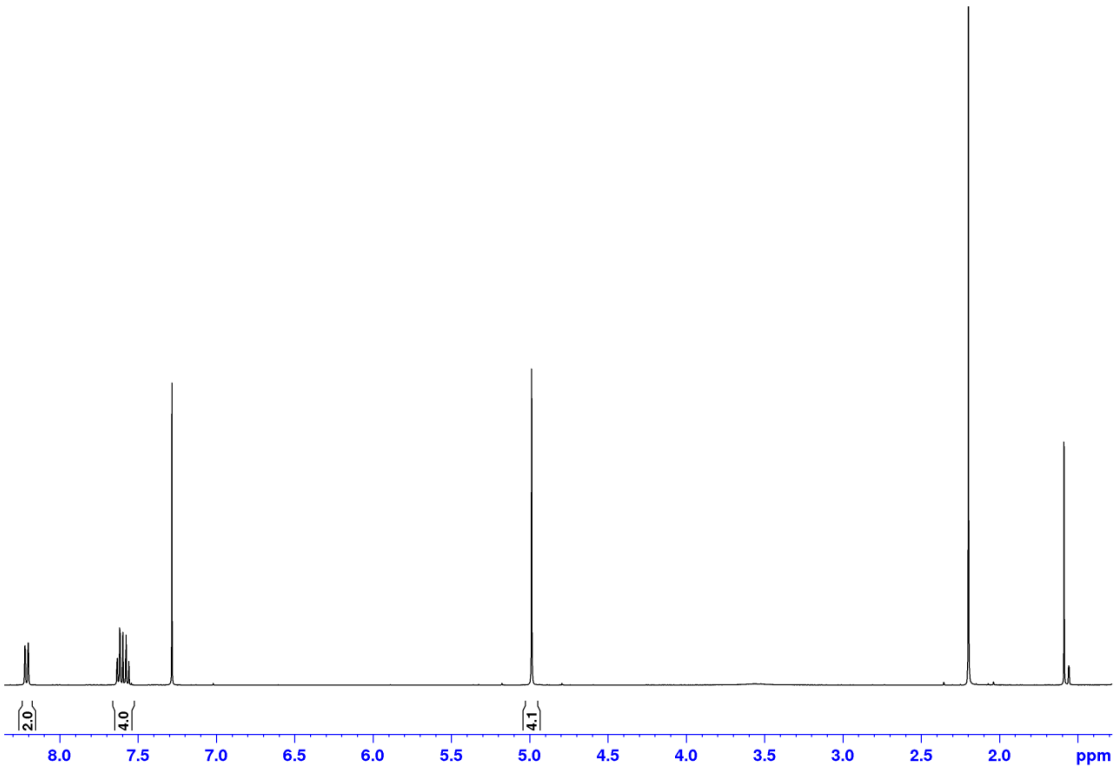

Figure A1.1.6 – ^{1}H NMR spectrum of 1,5-bis(bromomethyl)naphthalene **(6)** in $CDCl_3$.

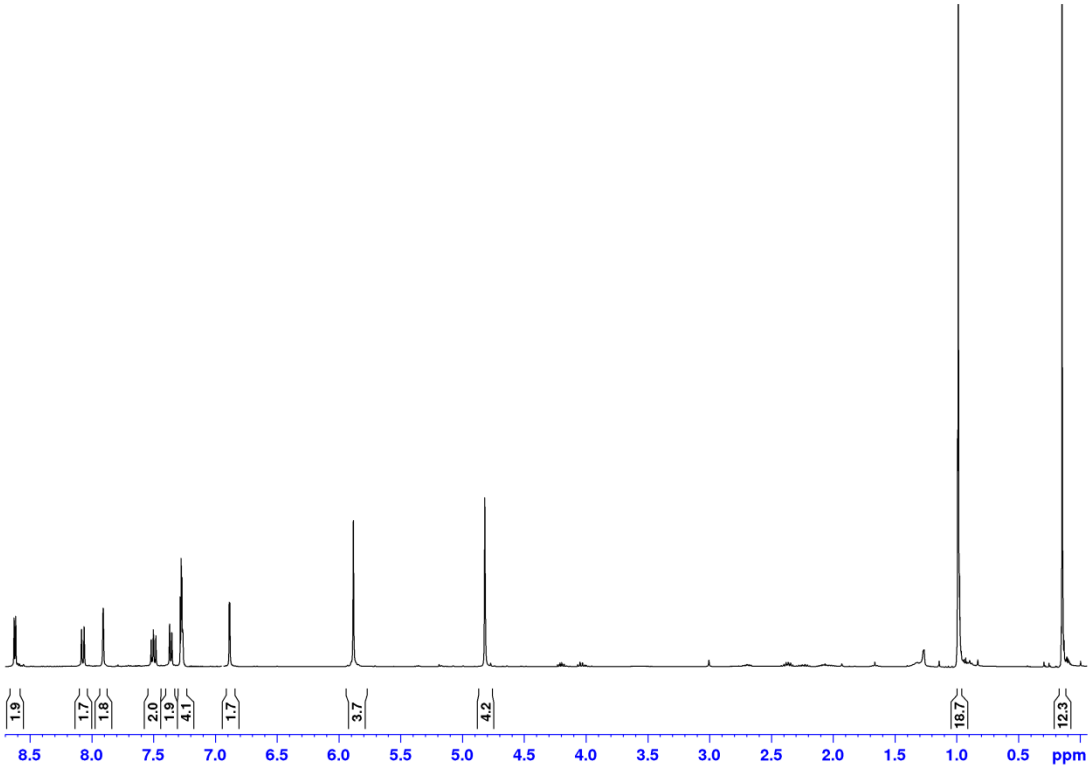

Figure A1.1.7 – ^{1}H NMR spectrum of OTBDMS-$L_w^{1,5naph}$ **(7)** in $CDCl_3$.

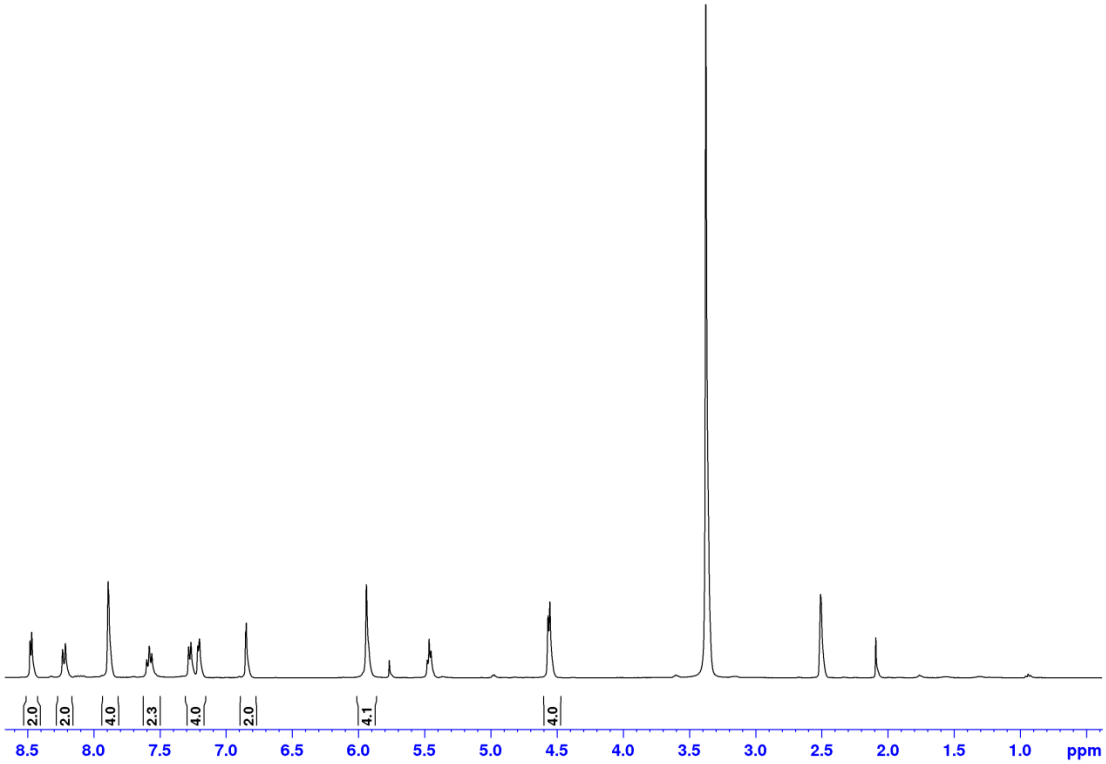

Figure A1.1.8 – ^{1}H NMR spectrum of $\mathbf{L_w^{1,5naph}}$ **(8)** in d^6-DMSO.

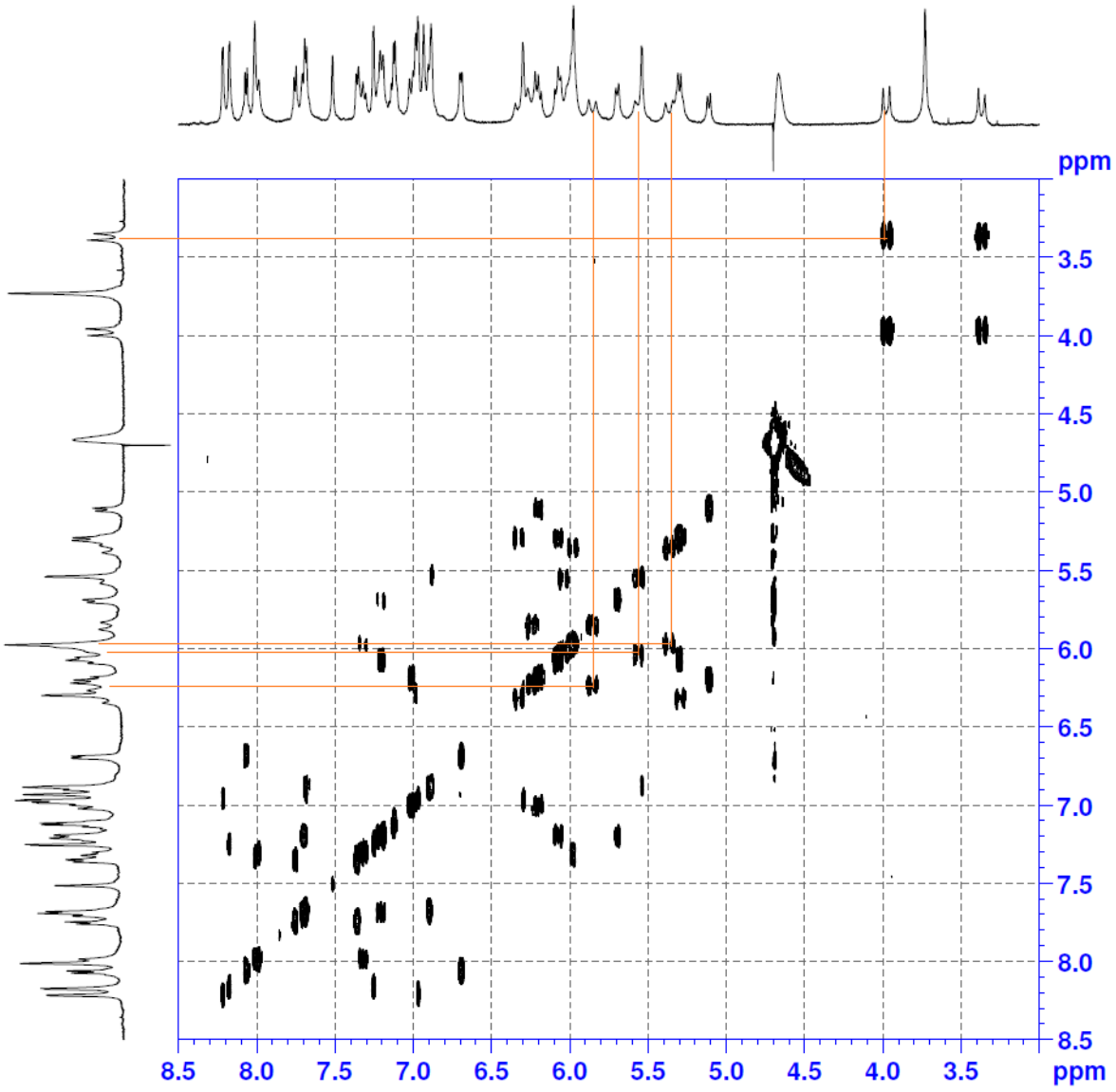

Figure A1.1.9 – Annotated ^{1}H COSY NMR spectrum of $[Cd_8Lw^{1,5naph}{}_{12}](NO_3)_{16}$ in D_2O at 298 K.

A1.2 Chapter 2 fluorescence titration spectra

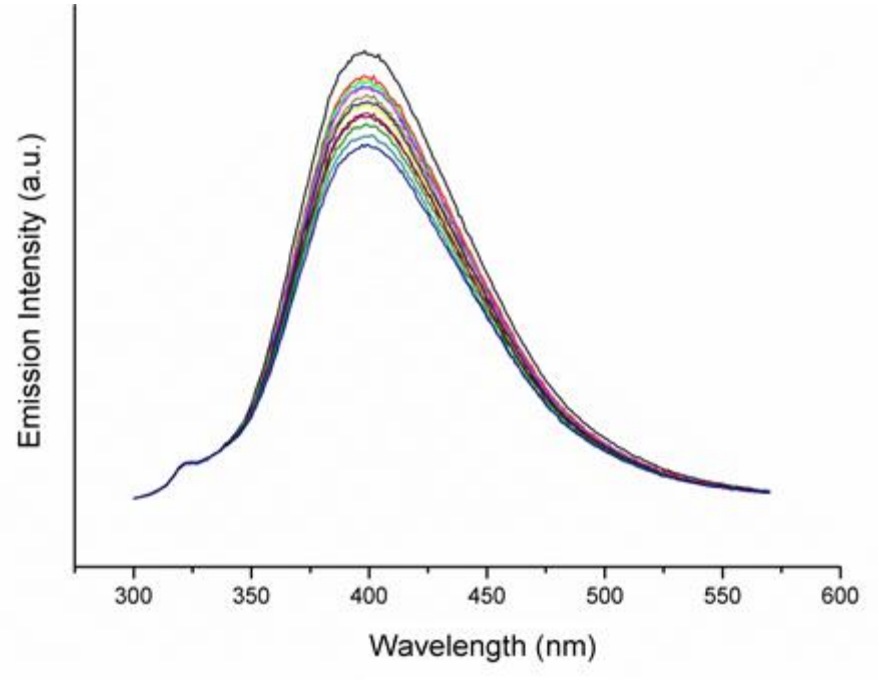

Figure A1.2.1 - Luminsecence spectra recorded during the addition of 0 - 2000 µL **G2** (0.1 mM) into a solution of **H** (0.01 mM) in H_2O, excitation at 290 nm.

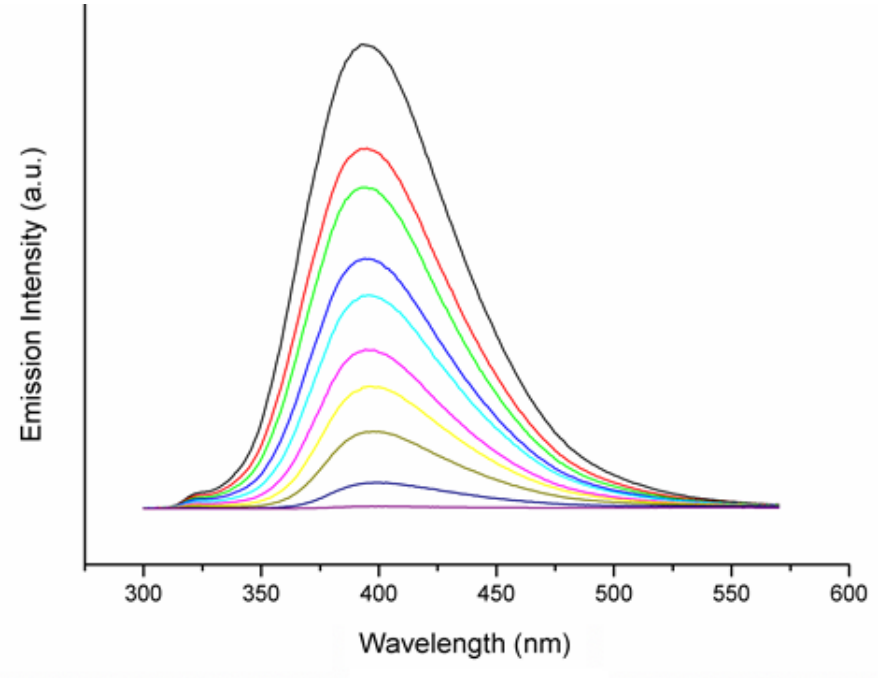

Figure A1.2.2 - Luminsecence spectra recorded during the addition of 0 - 2000 µL **G5** (0.1 mM) into a solution of **H** (0.01 mM) in H_2O, excitation at 290 nm.

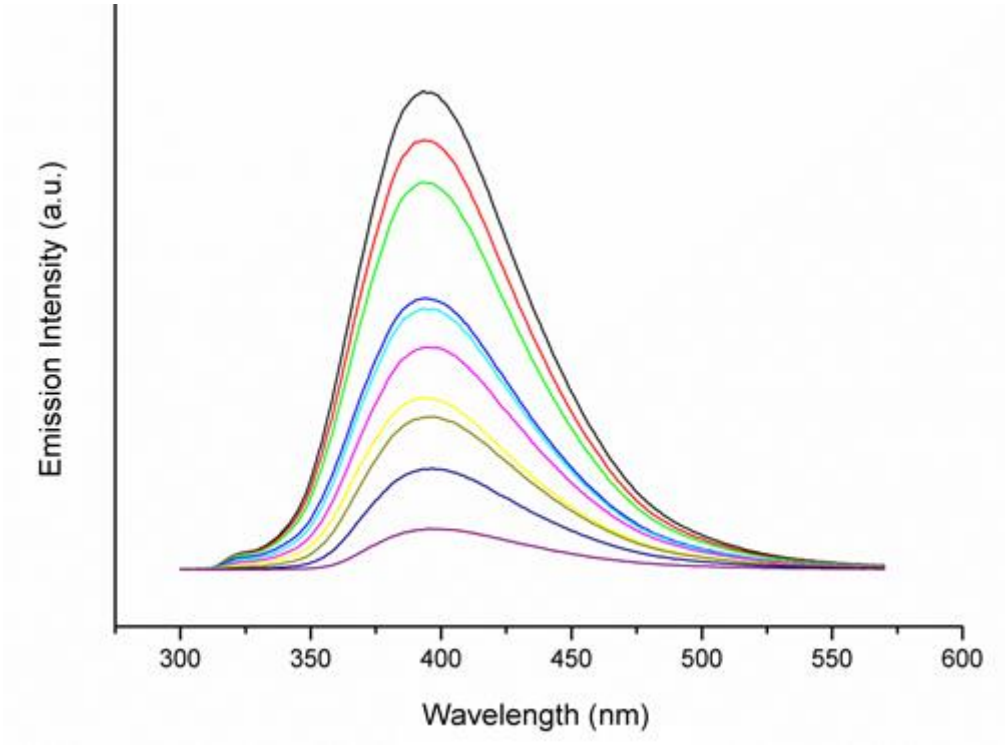

Figure A1.2.3 - Luminsecence spectra recorded during the addition of 0 - 2000 µL **G8** (0.1 mM) into a solution of **H** (0.01 mM) in H_2O, excitation at 290 nm.

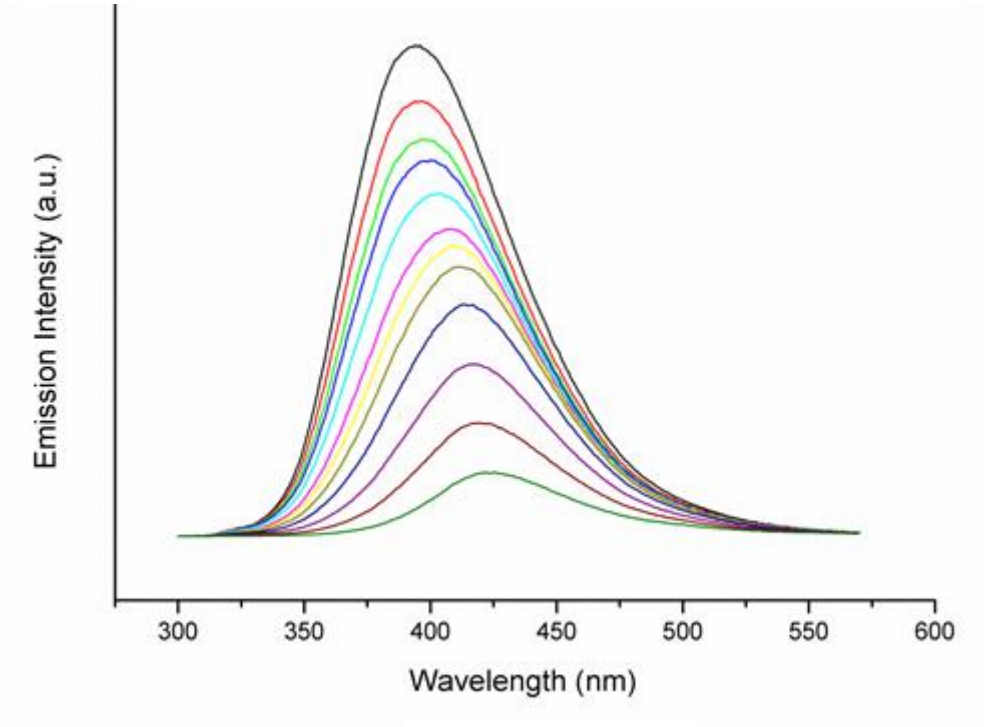

Figure A1.2.4 - Luminsecence spectra recorded during the addition of 0 - 2000 µL **G9** (0.1 mM) into a solution of **H** (0.01 mM) in H_2O, excitation at 290 nm.

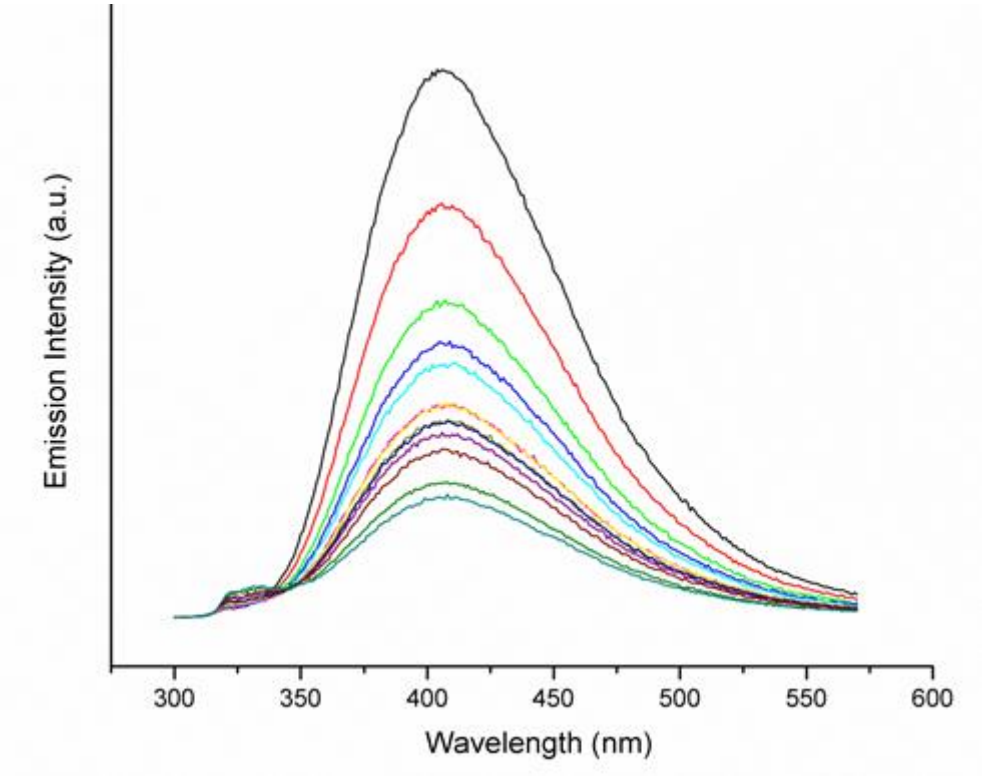

Figure A1.2.6 - Luminsecence spectra recorded during the addition of 0 - 2000 µL **G10** (0.11 mM) into a solution of **H** (0.01 mM) in H_2O, excitation at 290 nm.

A1.3 Chapter 2 Binding Isotherm Curve Fits

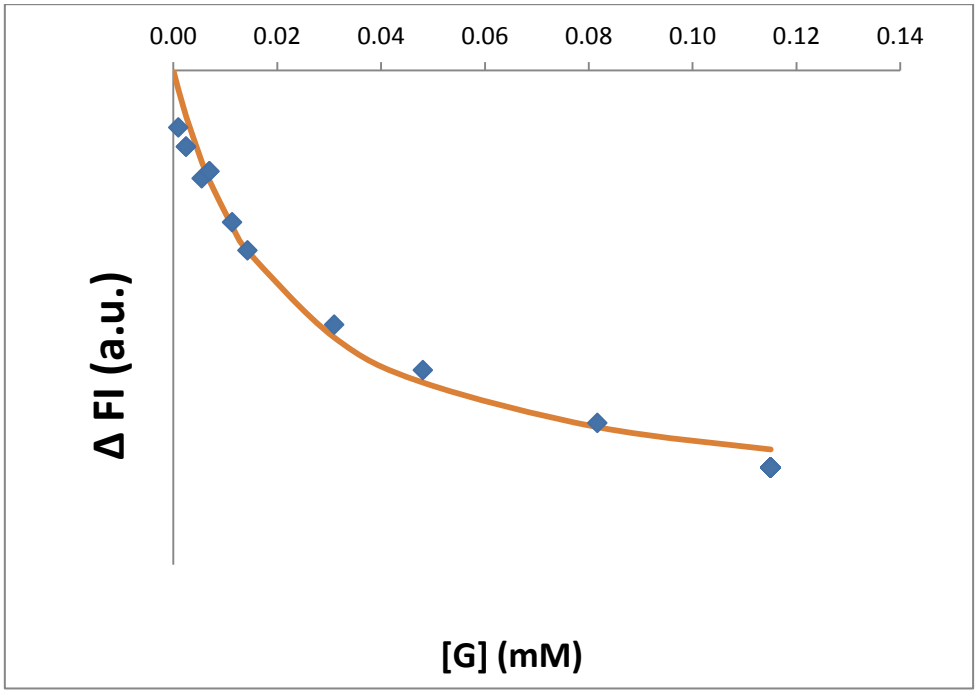

Figure A1.3.1 - Binding isotherm fit for **G2** in a solution of **H** in H_2O at 298 K.

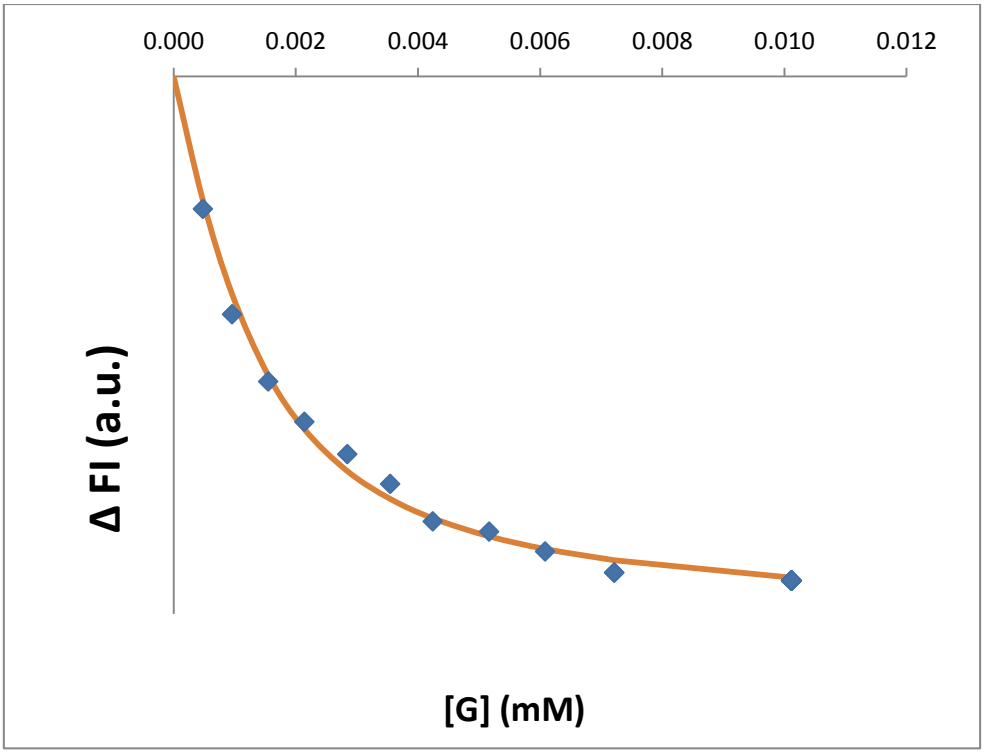

Figure A1.3.2 - Binding isotherm fits for **G4** in a solution of **H** in H_2O at 298 K.

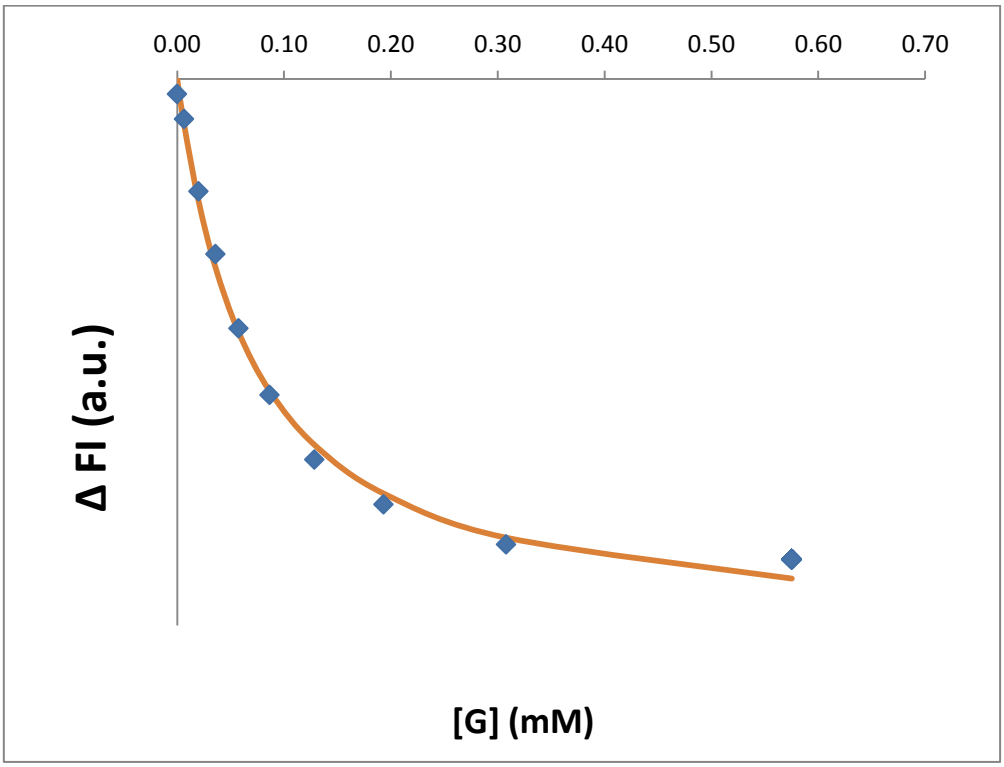

Figure A1.3.3 - Binding isotherm fit for **G5** in a solution of **H** in H_2O at 298 K.

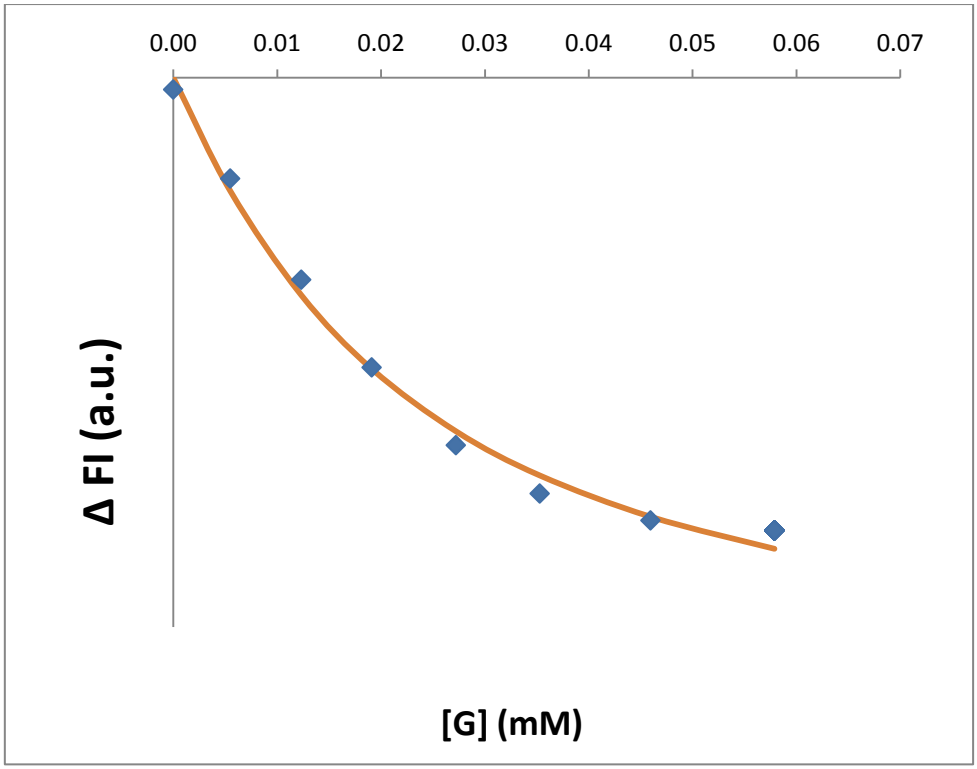

Figure A1.3.4 - Binding isotherm fits for **G6** in a solution of **H** in H_2O at 298 K.

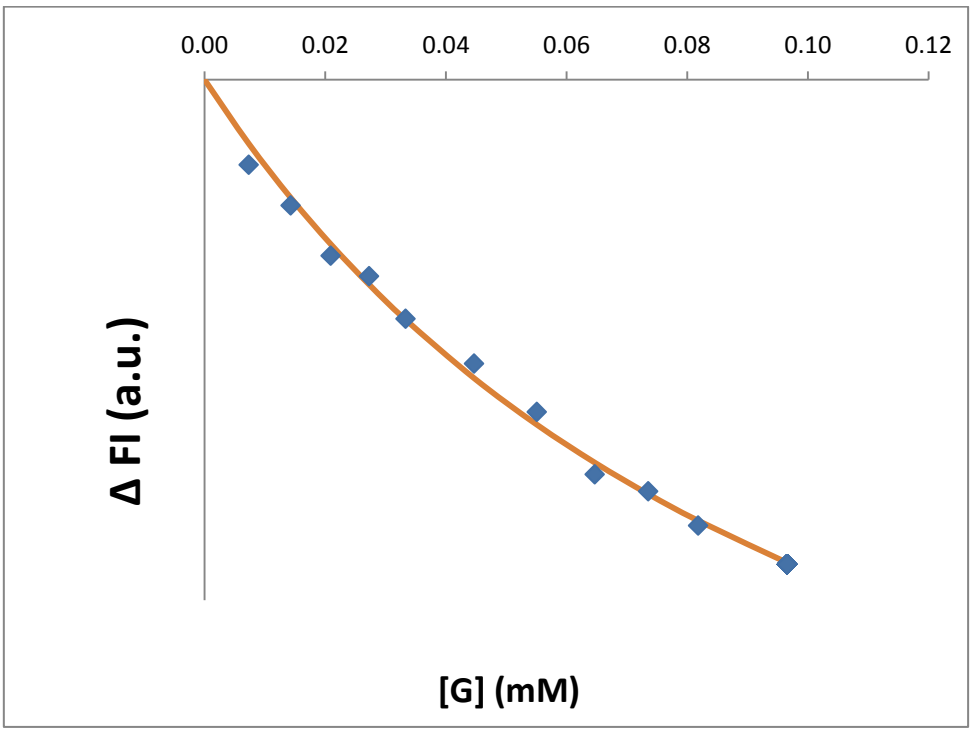

Figure A1.3.5 - Binding isotherm fit for **G7** in a solution of **H** in H_2O at 298 K.

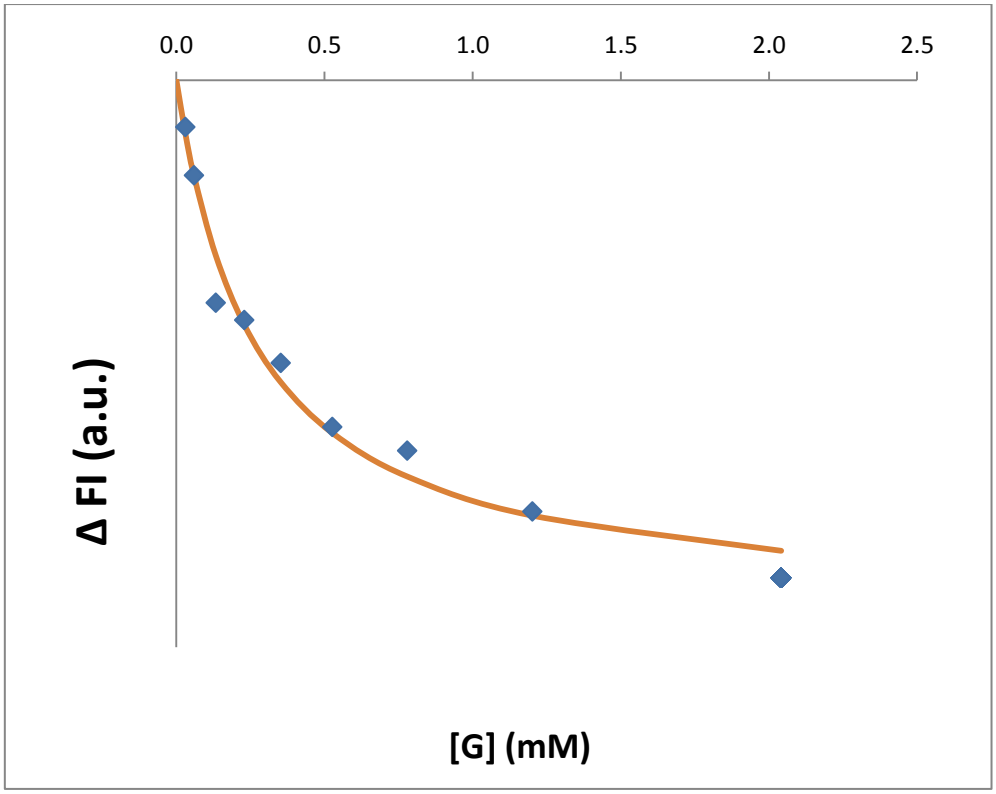

Figure A1.3.6 - Binding isotherm fit for **G8** in a solution of **H** in H_2O at 298 K.

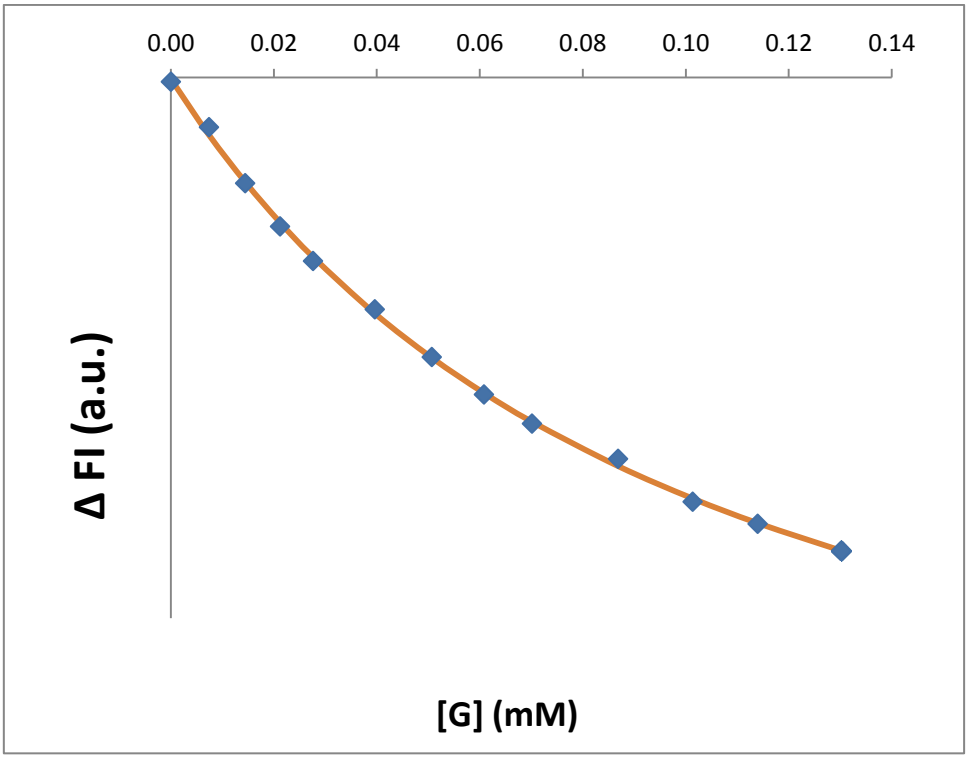

Figure A1.3.7 - Binding isotherm fits for **G10** in a solution of **H** in H_2O at 298 K.

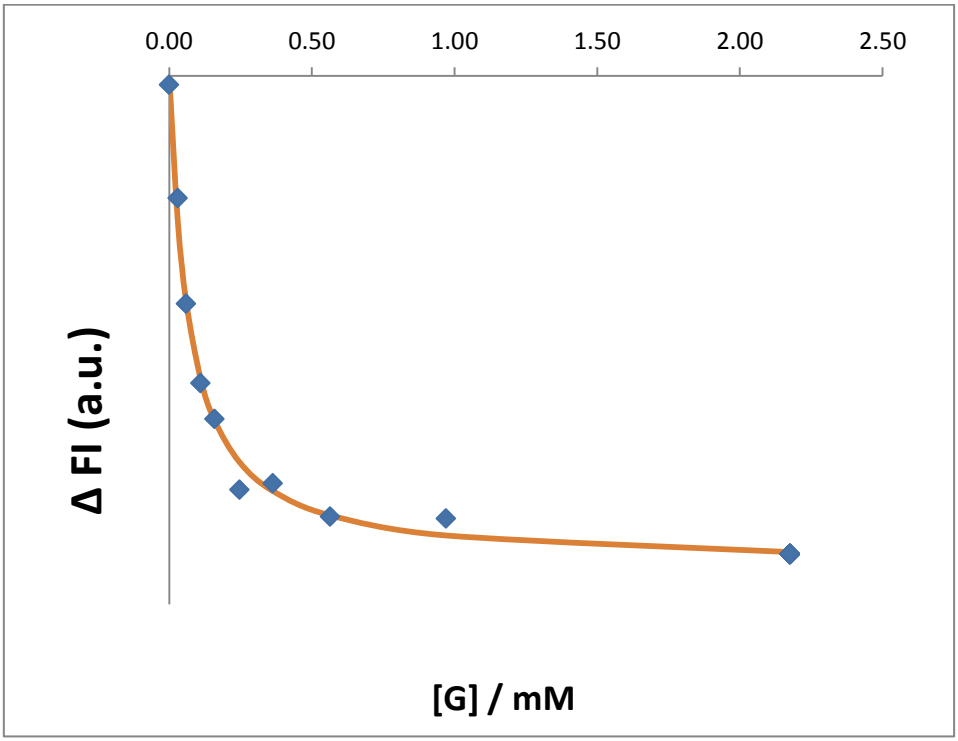

Figure A1.3.8 - Binding isotherm fit for **G11** in a solution of **H** in H_2O at 298 K.

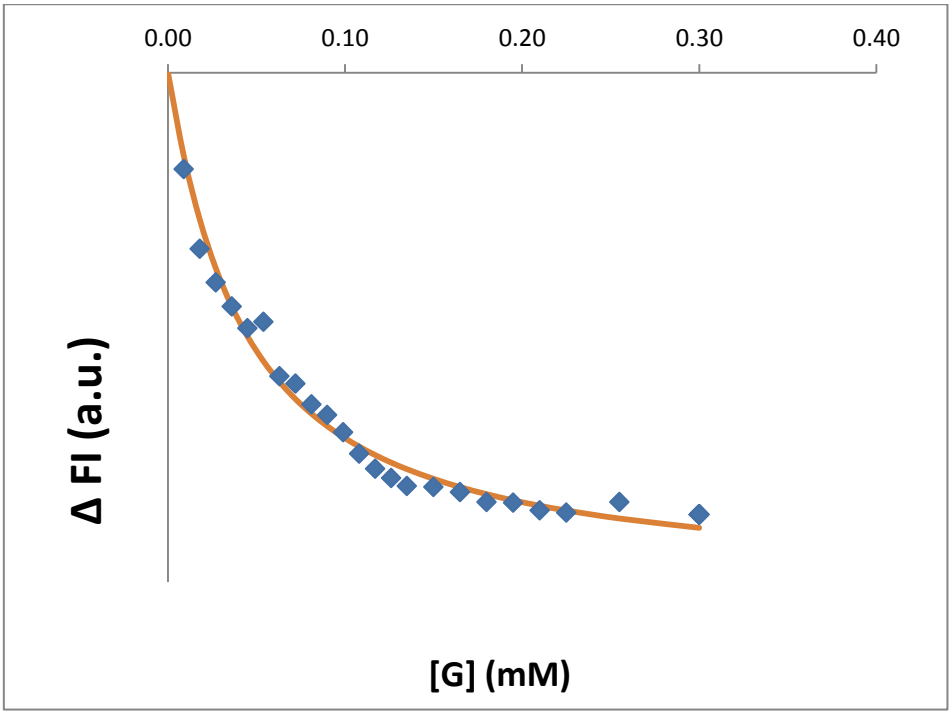

Figure A1.3.9 - Binding isotherm fit for **G12** in a solution of **H** in H_2O at 298 K.

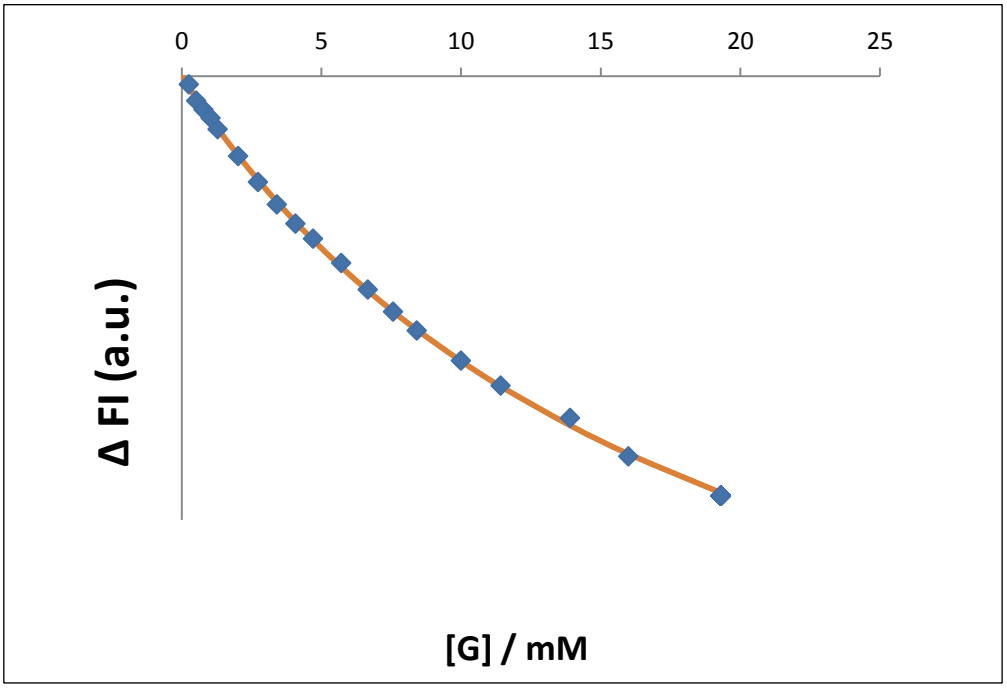

Figure A1.3.10 - Binding isotherm fit for **G14** in a solution of **H** in H_2O at 298 K.

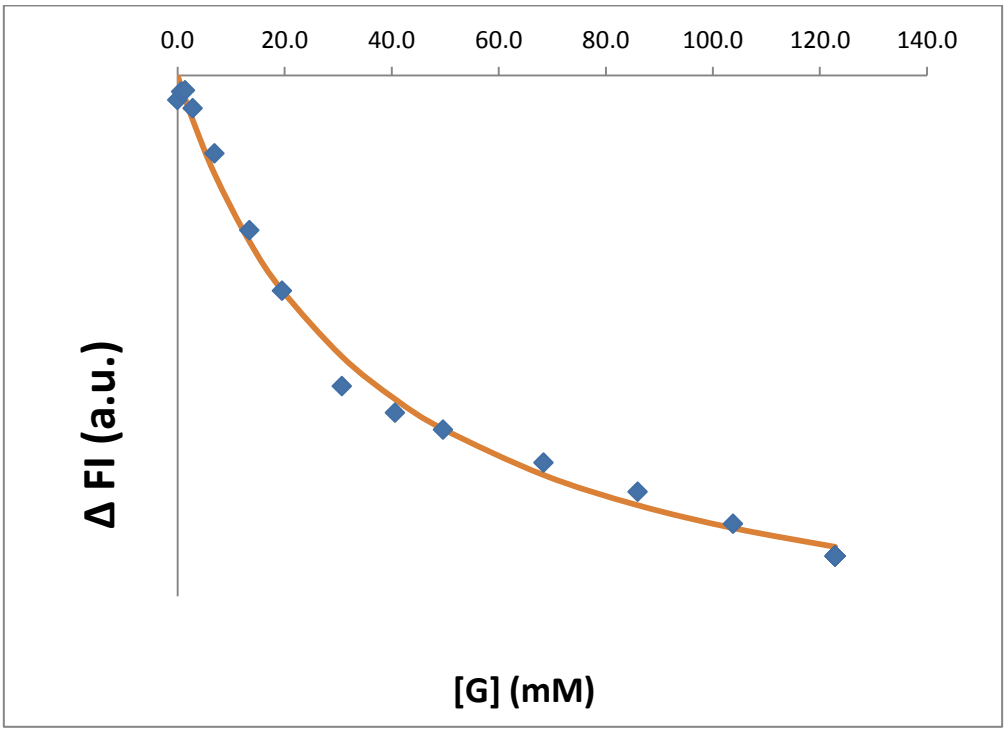

Figure A1.3.11 - Binding isotherm fit for **G15** in a solution of **H** in H_2O at 298 K.

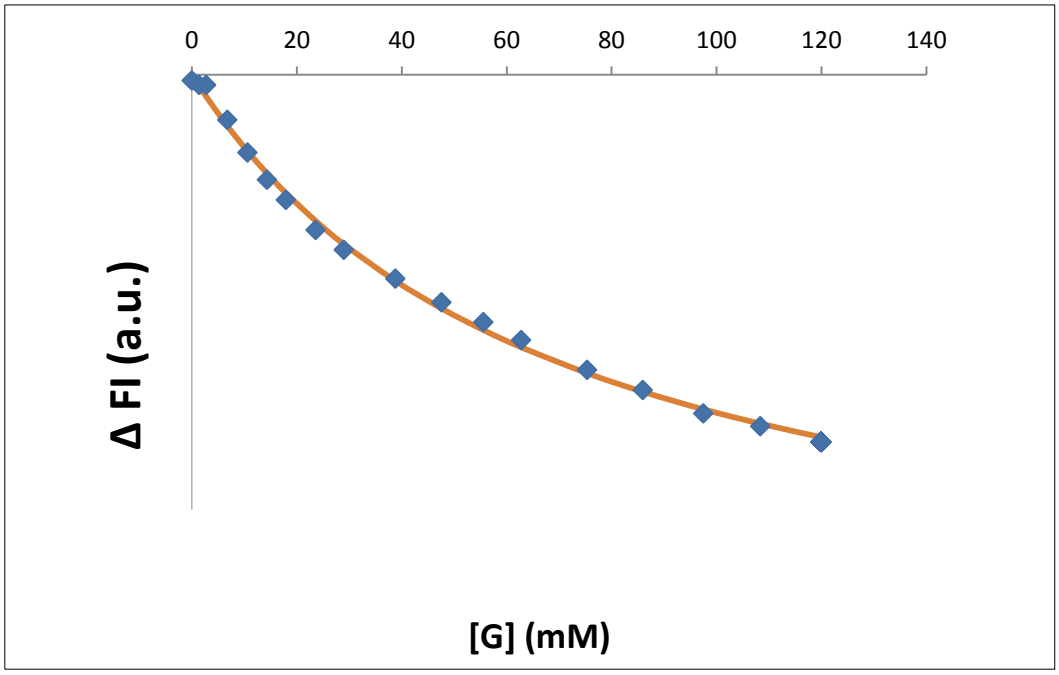

Figure A1.3.12 - Binding isotherm fit for **G16** in a solution of **H** in H_2O at 298 K.

Appendix 2

Additional Chapter 3 Data

A2.1 Fluorescence Titration Spectra

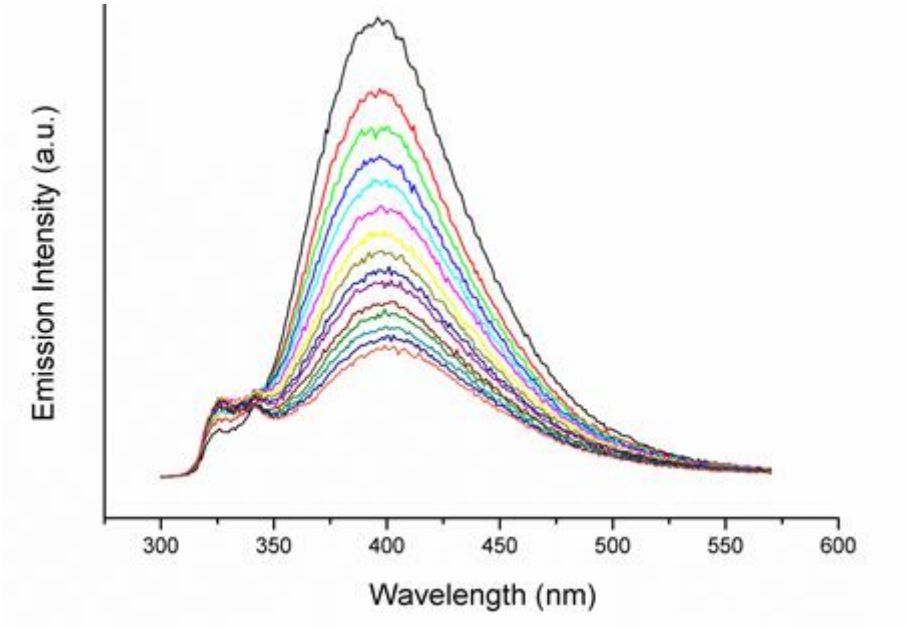

Figure A2.1.1 - Luminsecence spectra recorded during the addition of 0 - 2000 µL **G19** (0.1 mM) into a solution of **H** (10 µM) in H_2O, excitation at 290 nm.

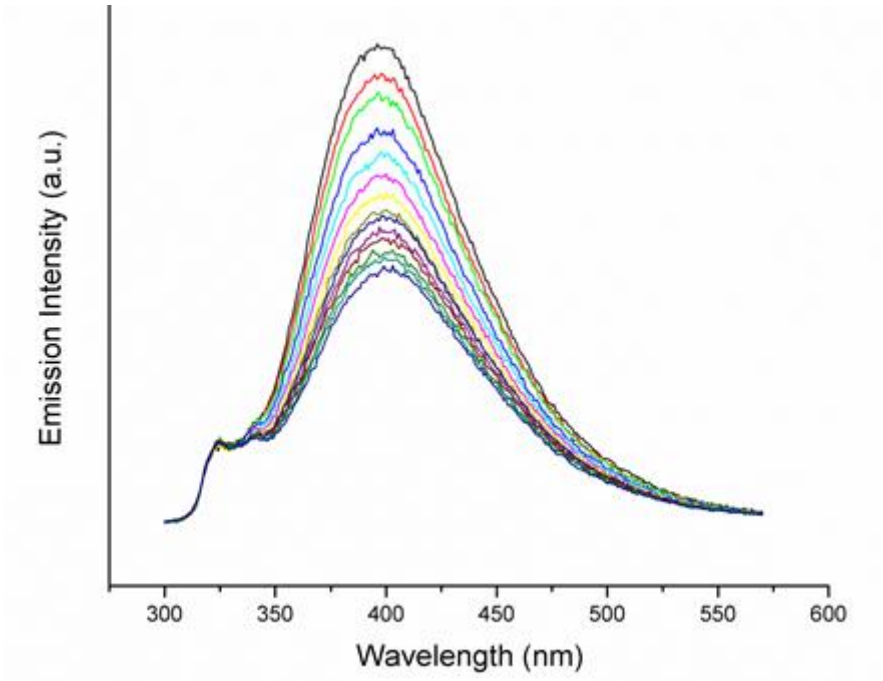

Figure A2.1.2 - Luminsecence spectra recorded during the addition of 0 - 1500 µL **G21** (0.01 mM) into a solution of **H** (1 µM) in H_2O, excitation at 290 nm.

Appendix 3

Additional Chapter 4 Data

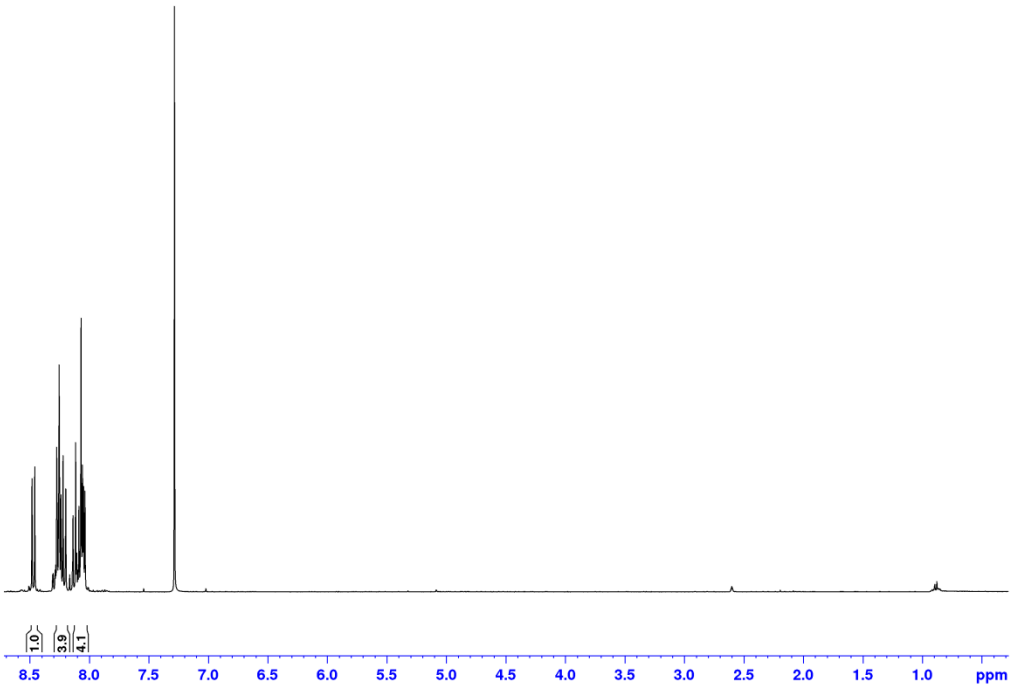

Figure A3.1.1 – ^{1}H NMR spectrum of 1-bromopyrene in $CDCl_3$.

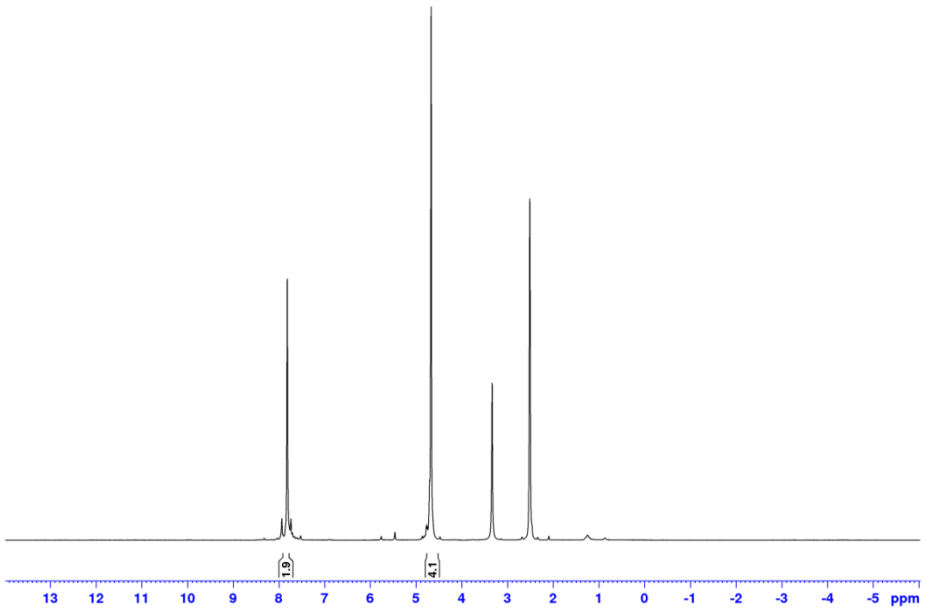

Figure A3.1.2 – ^{1}H NMR spectrum of 2,6-bis(bromomethyl)-4-bromopyridine (**1**) in d^{6}-DMSO.

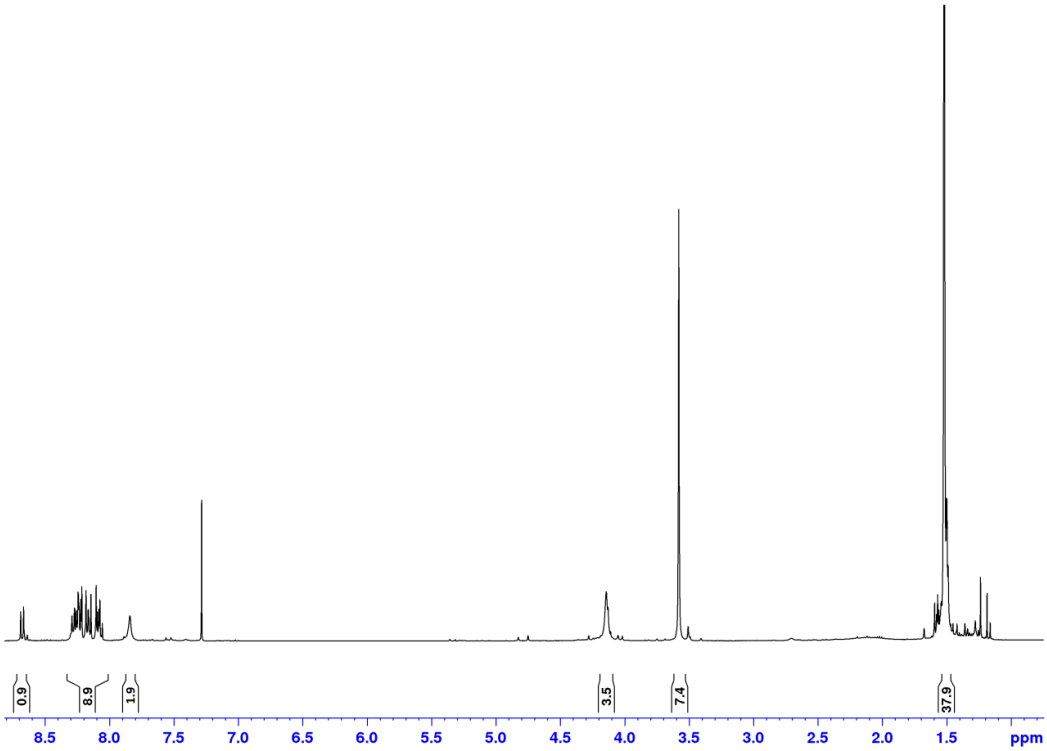

Figure A1.1.3 – ^{1}H NMR spectrum of the Protected Pyrene-Chelate in $CDCl_3$.